The nuanced effects of redox-active metabolites on bacterial physiology and antibiotic susceptibility

Thesis by

Lucas Andrade Meirelles

In Partial Fulfillment of the Requirements for the Degree of

Doctor of Philosophy in Biology

CALIFORNIA INSTITUTE OF TECHNOLOGY

Pasadena, California

2022

(Defended December 17, 2021)

Lucas Andrade Meirelles
ORCID: 0000-0003-3194-7136

ACKNOWLEDGMENTS

Finishing this thesis is a very, very special moment for me. Over the last ~2 years, the world has been living in this weird, mostly chaotic, new reality of a global pandemic that poses uncertainty to everyone's life in a way that we can't predict when this all will be done and when (if) we'll be back to "normal" one day. Yet, this hasn't affected the overall way I feel about the last ~6 years of my life. The graduate school period, although stressful in many situations, has been altogether extremely joyful and fun, where I could explore scientific questions I was interested in, learn and grow **a lot** as a scientist and as a person, meet very interesting people, and make friends I will take with me for the rest of my life. Before moving to California from Brazil, I remember myself thinking that this was a unique opportunity that could change my life forever, and I really think it did exactly that. There's a lot of people I want to thank and mention here who have played an essential role in building the person I am today. Without them, I would not be here celebrating this special and fun moment writing this section for my thesis.

To my family/para minha família. To my parents, ***Adriana*** and ***José Roberto Meirelles***, thank you for the unconditional love and support throughout my life. I told you this before, but I think it's worth mentioning again: if I ever become a parent one day, matching at least partially your educational skills would make me feel very proud of myself. Now, I get the "why" for many of the decisions you made for us when we were children and the implications they had in our life. I also know how hard you had to work to support our education and how much of your comfort you needed to give up for that. You are the main reason I am here today, and I'll be forever grateful. Aos meus pais, ***Adriana*** e ***José Roberto Meirelles***, muito obrigado pelo amor incondicional e todo o suporte que vocês me deram durante toda a minha vida. Eu já disse isso antes pra vocês, mas é sempre bom repetir: se algum dia eu for pai, alcançar pelo menos um pouco da capacidade de vocês como educadores já me deixaria extremamente feliz comigo mesmo. Hoje eu consigo entender o porquê de muitas das decisões e ensinamentos que vocês tomaram em relação à gente, e como elas acabaram sendo importantes para a nossa vida. Eu nunca vou me esquecer de uma frase que lembro de vocês falarem quando éramos criança, bem pequenos. Era algo como: "o mundo não se resume à isso que vocês estão vivendo aqui hoje, à cidade que vocês moram, e às pessoas que vocês conhecem; o mundo é muito maior, e vocês devem ir explorar."

Não sei se acabamos levando isso muito literalmente, mas sei que mesmo sendo tão difícil estar tão longe, posso contar com o apoio incondicional de vocês. Amo vocês, e sinto muitas saudades! To my siblings, ***Matheus***, ***Esther***, and ***João Marcos***, thank you for all the fun that has been to be your "old brother." I miss you guys so much, and I wish we could spend more time together. Hopefully, soon you will all be able to visit. Saudades demais de vocês, molecada! To my grandparents, ***Vera*** and ***Orney Andrade***, and my uncle, ***Angelo Andrade***, thank you for being so kind every time I have the chance to visit. I grew up seeing you every day, and it is still weird to be far away for so long. Talking to you on video makes my weekends much happier. I miss you! I'm also forever thankful to my grandparents, ***Elza*** and ***Paulo Meirelles***, for all the love and support they gave me while they were alive. I miss them a lot! Aos meus avós, ***Vera*** e ***Orney Andrade***, e meu tio, ***Angelo Andrade***, muito obrigado por todo o carinho toda vez que faço uma visita. Sei que essas são poucas, e gostaria de estar com vocês mais frequentemente. Não acredito que já faz mais de dez anos que saí de casa e que não vejo mais vocês todos os dias. As nossas conversas por vídeo deixam meus fins de semana muito mais felizes. Sinto uma saudade imensa de vocês! Também sempre serei grato aos meus falecidos avós, ***Elza*** e ***Paulo Meirelles***, pelo amor e suporte enquanto estavam conosco. Sinto muitas saudades de vocês! To my aunts, ***Maria Inês***, ***Teresa***, ***Paula*****,** and ***Regina Meirelles***, thank you all for helping me so much at different stages of my life, with important advice, directly and indirectly supporting my education or simply being there for a chat and a hug. The same is true for my aunt ***Eunice*** and uncle ***Pedro Franco***, cousins, and everyone else in the family. It has not been easy to be here, far away from you, for so long. The pandemic made this particular aspect of living abroad very challenging, and I miss you all every day. Às minhas tias, ***Maria Inês***, ***Teresa***, ***Paula*****,** e ***Regina Meirelles***, muito obrigado pela ajuda em diferentes etapas da minha vida. Seja dando um conselho importante, me ajudando direta ou indiretamente com meus estudos, ou simplesmente com uma conversa ou um abraço. O mesmo é válido para os tios, ***Eunice*** e ***Pedro Franco*** (o qual infelizmente não está mais conosco), primos, e todo mundo na família. Não tem sido nada fácil estar aqui longe de vocês por tanto tempo. Essa pandemia fez esse aspecto de morar em outro país extremamente difícil, e meu sinto falta de vocês todos os dias. Amo todos vocês! To my parents-in-law, ***Alcilene*** and ***Anísio Baccaro***, thank you for raising the love of my life and for making her into the fantastic person she is. Also, thank you for welcoming me so well into your family and for trusting me since the first day I met you. Aos

meus sogros, ***Alcilene*** e ***Anísio Baccaro***, muito obrigado por educarem e criarem o amor da minha vida, e por fazer dela a pessoa fantástica que ela é. Além disso, muito obrigado por me acolherem tão bem na família, e por confiarem em mim desde a primeira vez que os conheci.

To my wife, ***Fernanda Baccaro***, thank you for being my partner in life and my best friend. I can't believe it's been almost seven years since our first date! We've been through a lot, including moments that have made our relationship much stronger. I admire you so, so much. I admire your ability to handle multiple problems at the same time. I admire you as the amazing engineer you are; talented, smart, hard-working. You speak three (almost four) languages! But more than that, I admire the **amazing person** you are; (extremely) humble, brave, kind, generous, empathetic, and always trying to help everyone. I know you have always been the one managing and intermediating conflicts among your friends and co-workers, and maybe that's a reason why it's so easy to share a life with you. You're just so conscious about everything around you. Your humbleness is always an inspiration for me. You're the person who does the job with real-world implications every day. And I lost count of how many times when asked about your job, you just said, "Oh, I work with poop water!" This will sound cliché, but it's the truth. I never really thought the saying "when you find the one, you will know" made much sense. I still think this is not always the case, and people can learn to live with each other and be perfectly happy, even without having the certainty, at least initially, if the other person is the "perfect partner" for life. But with you, I felt something different as soon as we met and had our first few conversations. That lasted for years until it was finally the right moment for us to be with each other. And I just knew you were the one. We got engaged, we got married, and I'm grateful for every single day I'm by your side. "In the vastness of space and the immensity of time, it is…" just so fun to have the chance to share a life with you. Eu te amo, e pra sempre vou te amar.

To my advisor, ***Dianne Newman***, thank you for being so supportive and making my time in graduate school so fun and joyful; I will remember these years with happiness for the rest of my life. Thank you for giving me the opportunity to work in your lab, to learn from you, and for trusting me. You inspire me as a scientist and as a person. For me, you're the proof that one can succeed professionally and still be a kind and understanding person, something that is very important and inspiring in the world we live in today. It has been so fun to interact with you over

these years, and I will miss you and the lab a lot. I feel like just by being around and observing you, I could learn so much about science and how to understand and be approachable to different people. You're a fantastic manager, a very brilliant advisor, and I consider you a good friend. Thank you for giving me the freedom to explore my ideas, empowering me to take ownership of my work, but also to guide me through the process of scientific research with your unique talent for seeing the "big picture." Working in your lab has been the greatest professional honor of my life. Accordingly, I also took it as the greatest professional opportunity of my life, and it has been so much fun. I also had a great time first taking and then teaching the microbial metabolic diversity course with you, where I learned a lot. I will miss my days in the Newman Lab, but I hope we'll still do some work together in the future. And importantly, you don't need to worry; I forgive you for not going to my wedding in Brazil ☺. But I still think you should visit someday. Thank you for everything; you're the best!

To my committee members, ***Jared Leadbetter***, ***Marianne Bronner***, and ***Michael Elowitz***, thank you for the feedback and discussions during the committee meetings I had during graduate school. I want to highlight and thank ***Jared*** for all the support over the years, even before I started in the program. You were the first person I contacted at Caltech, and you were patient and kind to answer all my questions about the application process and Caltech. You were also the one who put me in contact with Dianne. Without your help, I would not be here today finishing this thesis, and I'm forever grateful for that. It was also a lot of fun to be in Woods Hole with you for the Microbial Diversity course and watch your unmatchable microbiology skills in action. Thank you for everything!

To the ***Marine Biological Laboratory and everyone involved in the 2016 Microbial Diversity course***: thank you for giving me one of the best summers of my life! Taking the course was a landmark experience during my PhD, and something I will never forget. It also gave me the opportunity to spend two weeks in Switzerland with a post-course research fellowship. This was my first time in Europe, and this opportunity played an essential role in the decisions I'm making for my future career steps. On that note, I need to thank ***Alex Persat*** for inviting me to visit his lab at EPFL on that occasion, and for all the support ever since, especially during this last year with fellowship applications. Alex, I was lucky to meet you during my first rotation here at Caltech

more than six years ago, and it has been fun to interact with you since then. Thank you! I'm excited to work together soon. And to all the ***Persat Lab members***, thank you for being so lovely and welcoming when I visited the lab many years ago. A special thanks to *Tamara Rossy* for all the help with experiments on that occasion.

To my former advisors, ***Ulrich Mueller*** and ***Andre Rodrigues***, thank you for providing me with the opportunities that ultimately led me to Caltech and for being my first mentors in science. ***Ulrich***, the six months I spent in Austin working with you at the UT were a turning point in my life. It was only for that reason that I applied to graduate school in the US, and you helped me so much during that process. More than seven years later, you're still helping me with letters of recommendation for fellowships and future applications. Thank you very much! ***Andre***, your mentorship during my undergraduate and Master's degree at UNESP started shaping the scientist I am today. With your help, I was able to go to Texas for my internship, which started this chain of events that changed my life. Thank you for everything you have done for me! Finally, I would like to thank my co-advisors at UNESP, ***Fernando Pagnocca*** and ***Mauricio Bacci Jr.*** for all the support when I was in the department.

To ***Justin Bois***, thank you for the transformative work you have been doing at Caltech over the last years with your classes. It's something really special. I took the first version of your data analysis boot camp during my first week at Caltech. I confess that, at first, it got me quite scared. But you showed me that going out of the comfort zone is essential for the learning process, and even a biologist with zero experience can learn some coding! It took me many years to prepare myself and get the courage to take your full course. But taking it was one of my best decisions in graduate school. It's incredible to see your enthusiasm and effort in preparing outstanding courses for Caltech. Moreover, besides teaching and scientific skills, I recently found out what a fantastic goalkeeper you are. Thank you for inviting me to play soccer in your team and also for taking me to see the LAFC. It has been a really fun semester!

The Newman lab. To ***all the Newman lab members*** (current and past), thank you for providing such an inclusive and fun environment for work. I learned a great deal from all of you over these years, and it has been an honor to be part of this group. Here are the people who made

my day-to-day work experience during graduate school so pleasant: *Rei Alcalde, David Basta, Brittany Belin, Megan Bergkessel, John Ciemniecki, Kyle Costa, Kurt Dahlstrom, Daniel Dar, Will DePas, Hazel Dilmore, Avi Flamholz, Nate Glasser, Richard Horak, Peter Jorth, Gargi Kulkarni, Elin Larsson, Ruth Lee, Jadzia Livingston, Zach Lonergan, Shivansh Mahajan, Darcy McRose, Caj Neubauer, Kristy Nguyen, Shannon Park, Elena Perry, Lisa Racki, Scott Saunders, Melanie Spero, Georgia Squyres, Korbi Thalhammer, Elise Tookmanian, Lev Tsypin, Chelsey VanDrisse, Renee Wang,* and *Steven Wilbert*. Moreover, to ***Kyle***, thank you for your guidance during my rotation and the free rides to Vegas. To ***David***, thank you for a great time at the GRC at Mount Holyoke/Boston and for being so fun in the lab. To ***John***, thank you for the beers (and drinks!) and the exciting conversations and brainstorming, especially over this last year. To ***Lisa***, thank you for introducing me to the cloning world and for teaching me some of your rigorous organizational skills. To ***Daniel***, thank you for the multiple interesting chats and bits of advice about science and life. To ***Will***, thank you for organizing the best game nights (I miss them!) and always being so nice, calm, and chill. I feel like you automatically made me less stressed just by being around you. To ***Kristy*** and ***Shannon***, thank you so much for all your effort to keep our lab working every day. And to ***Elena*** and ***Elise***, thank you for being the best cohort I could have asked for when we all started in the lab together.

I also met some people in the lab that I need to highlight in more detail. To my co-authors, ***Elena Perry*** and ***Megan Bergkessel***, thank you for being scientific role models and friends to me. ***Elena***, I had the honor to work with you for ~2 years, and this was the most inspiring and fun research time for me during my PhD. You're the most rigorous scientist I know and the best collaborator I could have ever asked. We spent two years talking almost every day about the science and the experiments we were doing for our paper, and later about our review, and I learned a ton from you. In addition, you're a great friend! It was so much fun for Fernanda and me to spend many Thanksgivings with you and Shashank, be at your wedding, and show you both the best places in São Paulo. I'm sure you'll do amazingly well in future endeavors, and I'm looking forward to seeing the fun things you'll discover in your research! ***Megan***, I consider you my second mentor during graduate school. I also admire you as a scientist and as a person. You know so (so!) much, and still, you're so kind and always open to helping everyone around you. I probably discussed every experiment from my first PhD paper with you, and your feedback and help on the

second one were essential to make it much better. And now, long after you have left the lab, you still find the time to chat and help me, even with your busy professor schedule. You're an inspiration for me, and I'm looking forward to reading the future works from the Bergkessel lab. I also hope I can visit you in Scotland in a not so distant future.

And to ***Scott Saunders***, thank you for being a great friend over all these years and for helping me since my first few days at Caltech. When I met you during recruitment, I could already tell you were a good person. But getting to know you better over these ~6 years has been one of the best parts of graduate school. Our friendship made my adaptation to life in the US much easier. Thank you for all the conversations, soccer games, game nights, and for making it all the way to São Paulo. Also, thank you for making me one of your groomsmen; it was an honor to be there by your side.

More friends. I have been fortunate to meet many interesting and kind people during my time here in LA. To ***all my friends***, who have brought joy to my life, thank you! I need to highlight some of them. To ***Tomás Aquino*** and ***Giovani Tomaleri***, thank you for being the best Brazilian crew I could have ever asked for. Having friends who share my culture and struggles made the process of living abroad much better. ***Tomás***, sharing a friend in common that put us in contact with each other before we started was pure luck, but I'm so grateful for that. You're certainly one of the smartest people I know. You're also one of the humblest. I loved being your roommate for all those early years here at Caltech, and I feel like I found a friend for the rest of my life. ***Giovani***, I wish you had started at Caltech a few years before you did, and I wish I had met you earlier. It would have been amazing to spend more time here with you. It has been great to be your friend, and I also think it's just the beginning of a friendship that will last to rest of our lives. Seu único defeito é ser palmeirense, mas ninguém é perfeito. To ***Shashank Gandhi***, thank you for being a great friend over all these years. You were the first person from our cohort I talked to when I arrived in Pasadena, and I will never forget that first dinner at Pie'n Burger. It was an honor to be a groomsman at your wedding and share many Thanksgiving dinners with you and Elena. Hopefully, we can cross paths and live close to each other again. Regardless, we'll always keep in touch, and I'm looking forward to seeing your future scientific discoveries. To ***Alicia Rogers***, thank you for being a great friend to Fernanda and me, going all the way to Brazil for our wedding, and

always helping us with our cats. You and Scott always took such good care of Houdini and Dory. I'll never forget the multiple hangouts at your place. Also, I'm sure you'll rock as a professor at UT Arlington! To ***Lola Carda*** and ***Guillem Camps***, thank you for being the best Spanish friends Fernanda and I could have ever asked for! Thank you for the multiple long and interesting conversations until late in the night, the countless beers at King's Row, and thanks for going multiple times from Paris to Berlin with us ♪♫. I will always be impressed with how fast you can eat grapes during the New Year's Eve countdown. We'll miss you immensely, but I'm sure we'll all visit each other soon. To the remaining members of ***The Dirrty Thirrty crew*** (*Rebecca Orr*, *Riley Connors*, *Annelise* and *Rob Reny*, and *Gullo Mostroserio*), thank you for giving Fernanda and I the opportunity to be your friends over this last year; it has been a blast. We'll miss you all! ***Rebecca***, you are a very special person, and thank you for always organizing the parties so well! ***Riley***, it has been great to get to know you better this last year and playing soccer with you and Guillem will always be a pleasure. To the ***FC Monrovia team***, thank you for sharing the pitch with me for all these years. Soccer (I need to get back to saying Football now) has always been my escape from stress, and that it has been incredibly fun to play with you in so many leagues. ***To all my other friends from near*** (*Porfirio Quintero, Manuel Razo, Sharan Prakash, Bryan Rodriguez*, the Cambrian Explosion team, and others) ***or from far*** (*Leonardo Beraldo, Jorge Evangelista, Marcel Prataviera, Quimi Montoya*, *Lucas A. Costa*, and others), thank you very much for being part of my life.

To ***Liz Ayala***, ***Raina Beaven***, and ***Lauren Breeyear***, thank you for the support over all these years here at Caltech. Your availability for always helping with administrative issues is much appreciated. The same is true for all the employees that keep the institute working every day. Thank you!

Finally, I wanted to thank all the teachers who have inspired me with their lessons and advice over the years. These include teachers from my early days in school in Conceição do Rio Verde, my hometown in Brazil (e.g., *Profs. Jussara, Maria, Genésia, Maria Faraco, Tânia, Cidinha, Aparecida, Fabinho, Goretti, Bebel, Neila, Helena Maria, Izildinha, Ana Lídia, Eliane, Tina, Márcia, Marina, Tereza, Sandra, Marcilene, Beth, Lucília, Vânia*, and others that might have escaped my memory), and from high school (a special thanks to my literature teacher *Margareth*

de Godoi). There is one name I will never forget when I think about my education. To my sciences teacher, ***Néia Mury***, thank you for igniting my curiosity and interest in science during your classes. Your classes are one of the main reasons I became a biologist. I still remember the bread decomposition experiment using plastic and paper bags. Thinking about it, it was my first experiment (and it was a microbiology one!). I'm forever grateful to you and all who directly or indirectly participated in my education. Thank you! Por fim, eu gostaria de agradecer aos professores que me inspiraram ao longo dos anos com muitos ensinamentos e conselhos. Entre eles, estão professores e educadores envolvidos nos meus primeiros anos escolares. Vários de vocês foram chave durante minha educação básica (*Profs. Jussara, Maria, Genésia, Maria Faraco, Tânia, Cidinha, Aparecida, Fabinho, Goretti, Bebel, Neila, Helena Maria, Izildinha, Ana Lídia, Eliane, Tina, Márcia, Marina, Tereza, Sandra, Marcilene, Beth, Lucília, Vânia*, entre outros; todos vocês fazem parte da minha história). Gostaria de agradecer também aos meus professores do ensino médio, em especial à *Margareth de Godoi*. Por fim, não tem como eu não agradecer especificamente à professora ***Néia Mury*.** Dona Néia, suas aulas são um dos principais motivos pelo qual eu me tornei um biólogo. Eu ainda me lembro do experimento de decomposição de pão dentro do saco plástico e saco de papel. Acredito que tenha sido um meu primeiro experimento (e foi um experimento de microbiologia!) Vou ser eternamente grato por você e por todos que participaram direta ou indiretamente da minha educação. Muito obrigado!

And yeah, I'm not going to forget the furry little ones. To my cats, ***Dory*** and ***Houdini***, thank you for giving us company and love (with some hissing/scratches) over all these years. Houdini was my first "real" pet, and I'll always miss her. I hope we can have Dory with us for many years to come.

ABSTRACT

The production of secondary metabolites is widespread throughout the tree of life. Bacteria, including many relevant opportunistic pathogens, can make redox-active secondary metabolites, both in the environment and while causing infections. Yet, their physiological consequences for the microbial communities exposed to them are much less understood. This thesis investigates the multifaceted and nuanced effects that such metabolites can have on their producers and other bacteria found in the producer's vicinity, focusing on the role these molecules play as modulators of antibiotic susceptibility. I start by presenting a literature review addressing the link between secondary metabolite production and resilience to clinical antibiotics in diverse opportunistic and enteric bacterial pathogens.

Next, using *Pseudomonas aeruginosa* (a widespread opportunistic pathogen) and its endogenously produced metabolite called pyocyanin, I explore the nuanced effects of the metabolite's production throughout the producer's lifecycle. Pyocyanin is part of a class of redox-active molecules made by *P. aeruginosa* called phenazines. I show that the production of pyocyanin, due to its self-poisoning effects, is a "double-edged sword," where the ultimate consequences for the producer are directly dependent on the physiological and environmental conditions. Carbon source limitation plays a major role in the self-poisoning effect of pyocyanin, a process responsible for killing a subpopulation of cells that, through extracellular DNA release, seems critical for proper biofilm development.

Despite pyocyanin's toxicity, *P. aeruginosa* is remarkably tolerant to its harmful effects. For this reason, I then explore how *P. aeruginosa* handles the stress caused by the metabolite. I present results using a functional genomics approach (transposon-sequencing) to screen for genes involved in *P. aeruginosa* tolerance to pyocyanin. Defenses involved in pyocyanin tolerance are similar to ones involved in tolerance to clinical antibiotics. These shared mechanisms lead to testing the hypothesis that defenses induced by the production of or exposure to "natural antibiotics" (such as pyocyanin) may affect the efficacy of treatments with clinical antibiotics. Supporting this hypothesis, exposure to pyocyanin significantly induces tolerance and resistance to certain clinical drugs, both in *P. aeruginosa* and other opportunistic pathogens within

the *Burkholderia cepacia* complex (Bcc). Pyocyanin and the drugs affected, such as fluoroquinolones, share molecular structure similarities, which is likely responsible for the shared protection.

Finally, based on these results, I explore the broader role of redox-active metabolites as modulators of antibiotic resilience in opportunistic pathogens. I show that pyocyanin, another phenazine called phenazine-1-carboxylic acid, and a non-phenazine redox-active molecule called toxoflavin can all modulate antibiotic susceptibility in Bcc species. Depending on the antibiotic's class, the metabolites' presence can either antagonize or potentiate the drug's efficacy. All the studied metabolites are produced by clinical isolates that infect cystic fibrosis and other immunocompromised patients. I demonstrate that the modulator effect of redox-active molecules in the pathogens is dependent on the transcription factor SoxR, which senses the presence of the metabolites and induces specific redox-regulated efflux systems that are effective in transporting both the metabolites and the structurally related drugs. To end, I provide a proof-of-principle that including such metabolites during clinical drug susceptibility tests may lead to a more accurate assessment of pathogens' resistance profile.

Taken together, the findings presented in this thesis demonstrate that redox-active secondary metabolites have profound effects on the physiology and antibiotic sensitivity levels of opportunistic pathogens. Their modulator effect on antibiotic susceptibility is likely a widespread phenomenon in polymicrobial communities that has been overlooked and may have direct consequences for the evolution of antibiotic resistance. Understanding the physiological roles of these metabolites at the molecular level is essential for accurate predictions of the drugs and pathogens affected, which may lead to more effective treatment strategies.

PUBLISHED CONTENT AND CONTRIBUTIONS

1. Perry, E.K.*, **Meirelles, L.A.***, and Newman, D.K (2021). From the soil to the clinic: the impact of microbial secondary metabolites on antibiotic tolerance and resistance. *Nat Rev Microbiol.* https://doi.org/10.1038/s41579-021-00620-w

* Equal contribution

L.A.M. participated in the conceptualization of the topic and structure of the review, literature collection, and manuscript writing.

2. **Meirelles, L.A.**, and Newman, D.K. (2018). Both toxic and beneficial effects of pyocyanin contribute to the lifecycle of *Pseudomonas aeruginosa*. *Mol Microbiol* **110**: 995-1010. https://doi.org/10.1111/mmi.14132

L.A.M. conceptualized the project, designed and performed the experiments, analyzed the data, and wrote the manuscript, all with input from D.K.N.

3. **Meirelles, L.A.***, Perry, E.K.*, Bergkessel, M., and Newman, D.K. (2021) Bacterial defenses against a natural antibiotic promote collateral resilience to clinical antibiotics. *PLoS Biol* **19**: e3001093. https://doi.org/10.1371/journal.pbio.3001093

* Equal contribution

L.A.M. conceptualized the project together with E.K.P, designed and performed the experiments involving the Tn-seq and antibiotic tolerance, analyzed the resulting data, and wrote the manuscript together with E.K.P, all with input from M.B and D.K.N.

4. **Meirelles, L.A.**, and Newman, D.K (2021). Redox-active secondary metabolites act as interspecies modulators of antibiotic resilience. *bioRxiv*. https://doi.org/10.1101/2021.12.01.470848

L.A.M. conceptualized the project, designed and performed the experiments, analyzed the data, and wrote the manuscript, all with input from D.K.N.

TABLE OF CONTENTS

C h a p t e r 1

INTRODUCTION

> *''One can designate as ~~by products~~* ***secondary products*** *of metabolism such compounds which are formed during metabolism, but which are no longer used in the formation of new cells. .... Any importance of these compounds for the ~~inner economy~~* ***primary metabolism*** *of the plant* ***<u>is so far unknown.</u>*** *''*
>
> Quote from Sachs [1], translated to English and presented (including the term substitutions) by Hartmann [2].

The study of what we call "secondary metabolites" likely started in plant research in the early 1800s with the isolation of morphine from opium poppy by Friedrich Wilhelm Sertürner [2]. Over the years, researchers began isolating and later synthesizing various compounds for which their relevance during growth was unknown, as highlighted in the quote above. The production of secondary metabolites is not unique to plants: microbes make them too, including some of the most well-known: penicillin (made by a fungus), streptomycin (made by a bacterium), and many other antibiotics. In bacteria, these molecules are also generally made under slow or non-growth stages (also called "stationary phase" in planktonic cultures), and the name "secondary" comes from the fact that such metabolites are not directly involved in "primary" growth-related metabolism [3]. Therefore, we can define secondary metabolites as *small organic molecules not directly involved in their producers' primary (central) metabolism*. For some time around the middle of the 20th century, it was thought that such metabolites were simply waste or detoxification products of growth-derived metabolism [2]. However, it is now broadly accepted that secondary metabolites play important ecological roles for their producers [4]. This is the context I want to explore with the reader in my thesis. *<u>The effects that these molecules can have on bacterial cells are dynamic, complex, and important!</u>* Because the nomenclature could still, at least unintentionally, be interpreted as if these metabolites are "secondary" and less important, the name has been put to debate, with alternative suggestions for its replacement [3]. Although I absolutely agree that the functions of secondary metabolites are not secondary at all, I still decided

to use the "secondary metabolites" term in this thesis due to (i) its widespread acceptance/recognition and (ii) the lack of a better term, since all the ones I could come up with also had significant caveats, probably because these metabolites represent such a broad class of molecules that it is very hard to find a term generalizable enough.

However, except for Chapter 2, this thesis is not about several different classes of secondary metabolites, at least not experimentally. Although I believe many of the reflections presented here are applicable for distinct secondary metabolites categories, experimentally, I focus on a specific group that, in my opinion, is among the most curious and interesting: *redox-active secondary metabolites*. These redox-active molecules can undergo redox reactions, giving them interesting properties. Their reactivity has been linked to multiple physiological roles, from "natural antibiotics" that are toxic and used to kill competitor species or host cells (when made during infections) to extracellular electron shuttles that promote energy conservation and sustain metabolism under anoxic conditions. The toxicity of redox-active secondary metabolites is (i) mainly indirect and caused through the generation of superoxide radicals when ambient oxygen is present, but (ii) there is also evidence that these metabolites may directly damage proteins inside the cell through unwanted oxidations. At the same time, in nature, bacterial cells primarily exist as aggregates called biofilms, and redox-active secondary metabolites play crucial roles in promoting biofilm formation and sustaining metabolism within its anoxic/hypoxic zones. This creates a dilemma for the cells that are constantly exposed to these metabolites: *to benefit from their dynamic properties and functions, cells need to adapt to their toxic effects and find ways to not die in their presence*. However, the story gets even more complicated because bacterial populations are heterogeneous, and in fact, killing a subpopulation of cells is an essential developmental process during biofilm formation.

This dynamic and complex, sometimes subtle and even apparently contradictory, range of physiological effects of redox-active secondary metabolites motivated the selection of the title for this thesis. Early in my PhD, I wanted to understand the contexts in which one particular redox-active metabolite, the phenazine pyocyanin, is toxic to its producer, the opportunistic pathogen *Pseudomonas aeruginosa*. Even though *P. aeruginosa* infections are very relevant

medically, I did not start my Ph.D. with the goal of studying clinical antibiotics. I was simply curious about how *P. aeruginosa* manages the stress caused by its self-produced toxin. However, while investigating the mechanisms *P. aeruginosa* uses to defend itself from pyocyanin, I realized that these two topics are deeply connected. Like many other redox-active secondary metabolites, pyocyanin is a (natural) antibiotic. Soil-borne opportunistic pathogens, such as *P. aeruginosa* and the other species studied in this thesis, are constantly producing and/or being exposed to natural antibiotics in the environment. At the same time, the soil has been extensively explored as a source of antibiotics we use in the clinic. With this realization, the connection between the production of redox-active metabolites by opportunistic pathogens and recalcitrance to antibiotic treatment due to shared defense mechanisms became the main topic of my thesis. I hope that by the end of this thesis, the reader will appreciate how intriguing redox-active metabolites physiology is. As a bonus, hopefully the reader will share my view about the urgency of looking for additional examples of metabolite-triggered antibiotic resilience in the context of infectious disease.

Overview

In Chapter 2, in collaboration with Elena Perry, a former graduate student and my years-long collaborator in the Newman Lab, I discuss the evidence linking secondary metabolites to the modulation of antibiotic susceptibility in multiple opportunistic and enteric pathogens. We present numerous metabolites and the antibiotics affected, discuss the molecular mechanisms involved in the modulation, provide guidelines on finding new examples and how to account for their effects in the clinic, and speculate on their consequences for the evolution of antibiotic resistance.

In Chapter 3, I focus on the physiological consequences of redox-active metabolites, using one example (pyocyanin) and its producer (*P. aeruginosa*). I explore the beneficial and detrimental aspects of pyocyanin production during *the P. aeruginosa* lifecycle and discuss their consequences for biofilm development. Specifically, I identify the conditions under which pyocyanin becomes toxic to its producer and reveal that distinct subpopulations of cells can be sensitive or extremely tolerant to pyocyanin toxicity. The susceptible subpopulation is killed and releases extracellular DNA in the environment, a process essential for biofilm formation. The highly tolerant population

resembles a "persister-like" state, a state analogous to the persistence phenomenon used to describe how tolerant subpopulations of bacterial cells can escape antibiotic treatment in the clinic.

In Chapter 4, building on the conditions identified in Chapter 3, I start by performing a genetic screen to identify mechanisms used by the "persister-like" population to tolerate pyocyanin toxicity. I discovered that multiple of these mechanisms are related to how pathogens tolerate antibiotic treatment in the clinic. This then turned into a years-long collaboration with Elena, where we investigated the consequences of pyocyanin production on antibiotic tolerance (i.e., the ability of a pathogen to *survive* drug treatment) and resistance (i.e., the ability of a pathogen to *grow* in the presence of the drug). Specifically, in this chapter, we use pyocyanin as a model to test the hypothesis that the production of "natural antibiotics" by pathogens may increase recalcitrance to clinical antibiotic treatment, where defenses evolved to cope with the metabolite's toxicity cause collateral protection against the drug. We show specific efflux systems used by *P. aeruginosa* to handle pyocyanin toxicity also induce tolerance against fluoroquinolones, a broadly used class of clinical antibiotics. We reveal that defenses induced by pyocyanin in *P. aeruginosa* can also increase the rates at which resistant mutants pass through antibiotic selection, showing that pyocyanin can increase resistance levels against these drugs. Finally, because *P. aeruginosa* is not found alone during infections, we finish by expanding the effect of pyocyanin to other opportunistic pathogens found in polymicrobial infections with *P. aeruginosa*. We find that pyocyanin can increase tolerance and resistance to fluoroquinolones in pathogens within the *Burkholderia cepacia* complex (Bcc) group, with effect sizes dramatically higher than in *P. aeruginosa*.

The surprisingly high effect sizes found for Bcc species in Chapter 4 motivated the hypotheses I test in Chapter 5. This chapter explores the phenomenon of redox-active metabolites acting as modulators of antibiotic susceptibility more broadly, focusing on interspecies interactions. The opportunist pathogens studied in this thesis are relevant during chronic lung infections, a context in which they are often found in multi-species communities within the same patient. In Chapter 5, I investigate the role of two redox-active metabolites (pyocyanin and toxoflavin) made by two opportunist pathogens (*P. aeruginosa* and *B. gladioli*) on antibiotic

susceptibility levels of Bcc species. I show that both of these metabolites can increase resilience against fluoroquinolones and reveal the molecular mechanism involved in this process. Moreover, following the guidelines we describe in Chapter 1, I provide a proof of principle for how antibiotic susceptibility testing used in the clinic can, with simple modifications, be adapted to account for the modulator effect of secondary metabolites. This is relevant because such assays are used to determine which drug is prescribed to a patient, but they are currently blind to the changes in antibiotic resilience caused by secondary metabolites. Together with the results presented throughout this thesis, this chapter suggests that alterations on antibiotic sensitivity caused by interspecies exchange of secondary metabolites is likely a widespread phenomenon in polymicrobial communities. However, it is also one that remains overlooked, with potential consequences on treatment efficacy and the evolution of antibiotic resistance.

Finally, in Chapter 6, I provide some concluding remarks and suggestions for future directions I see as natural expansions for the findings presented in this thesis.

References

1. Sachs, J. Lehrbuch der Botanik. W. Engelmann, Leipzig. 1873.
2. Hartmann T. From waste products to ecochemicals: fifty years research of plant secondary metabolism. Phytochemistry. 2007;68: 2831–2846.
3. Davies J. Specialized microbial metabolites: functions and origins. J Antibiot. 2013;66: 361–364.
4. Tyc O, Song C, Dickschat JS, Vos M, Garbeva P. The ecological role of volatile and soluble secondary metabolites produced by soil bacteria. Trends Microbiol. 2017;25: 280–292.

Chapter 2

SECONDARY METABOLITES AND ANTIBIOTIC SUSCEPTIBILITY

This chapter is adapted from:

Perry, E.K.*, Meirelles, L.A.*, and Newman, D.K (2021). From the soil to the clinic: the impact of microbial secondary metabolites on antibiotic tolerance and resistance. *Nat Rev Microbiol*. https://doi.org/10.1038/s41579-021-00620-w

Abstract

Secondary metabolites profoundly affect microbial physiology, metabolism, and stress responses. Increasing evidence suggests that these molecules can modulate microbial susceptibility to commonly used antibiotics; however, secondary metabolites are typically excluded from standard antimicrobial susceptibility assays. This may in part account for why infections by diverse opportunistic bacteria that produce secondary metabolites often exhibit discrepancies between clinical antimicrobial susceptibility testing results and clinical treatment outcomes. In this chapter, we explore which types of secondary metabolites alter antimicrobial susceptibility, as well as how and why this phenomenon occurs. We discuss examples of molecules that opportunistic and enteric pathogens either generate themselves or are exposed to from their neighbors, and the nuanced impacts these molecules can have on tolerance and resistance to certain antibiotics.

Introduction

A vast number of organisms, many of which hail from the soil, produce a wide range of molecules classified as 'secondary metabolites' [1,2]. They can be generated by Eukarya (for example, plants and fungi), Bacteria and Archaea, and are usually defined as organic compounds that do not directly support the producer's growth or development [3–5]. In microbial planktonic cultures, they are typically produced during stationary phase, once doubling times have slowed [6,7]. As a result, these compounds were for many years assumed to be waste products of metabolism [8]. However, a more nuanced view of the biological functions of microbial secondary metabolites has emerged over the past two decades. Indeed, the moniker 'secondary' is something of a misnomer, as these molecules have been shown to have key roles in multiple physiological processes that are critical for microbial survival [6,7], including but not limited to the acquisition of nutrients (such as iron or phosphate), cell–cell signaling and energy conservation in the absence of oxygen [2,9–12].

In addition to conferring such pleiotropic benefits, many microbial secondary metabolites are also toxic, both to their producers and to neighboring organisms [1,2,8]. It is therefore not surprising that antibiotic development pipelines have driven the majority of secondary metabolite characterization and purification efforts, dating back to the discoveries of penicillin and streptomycin in the early 20th century. Most modern clinical antibiotics are derivatives of natural products that originated from soil microorganisms, and the soil-to-clinic axis continues to inspire natural product chemists in their search for and design of new drugs [13]. Yet, microbiologists have neglected to consider the potential for unintended consequences of this pipeline, particularly with respect to antibiotic efficacy against opportunistic pathogens that evolved in the same environment. Microorganisms are rarely, if ever, found in isolation, and therefore the presence of secondary metabolites in a microbial community exerts evolutionary pressure both on secondary metabolite-producing and non-producing members to develop means to withstand them. These defenses can in turn have collateral activity against clinical antibiotics.

In this chapter, we highlight the growing body of evidence connecting bacterial secondary metabolites to the phenomena of antibiotic **tolerance** (that is, the ability to survive transient

antibiotic exposure) and **resistance** (that is, the ability to grow in the presence of antibiotics at a given concentration) [14–16]. We also use the more generic term '**antibiotic resilience**' to refer to the ability of a bacterial population to be refractory to antibiotic treatment, which can arise from an increase in tolerance and/or resistance. Emphasizing examples of secondary metabolites produced by opportunistic or enteric pathogens (Table 1), we discuss common modes of action through which these molecules can alter antibiotic efficacy in both single-species and polymicrobial communities. Specifically, we draw attention to secondary metabolites that regulate multidrug resistance efflux systems, secondary metabolites that modulate the toxicity of antibiotics through interactions with reactive oxygen species, and the potential for secondary metabolite-induced antibiotic tolerance to provide an overlooked route for the evolution of antibiotic resistance. Although the impact of bacterial secondary metabolites on infection treatment outcomes has yet to be addressed in clinical studies, *in vitro* data indicating changes in antimicrobial susceptibility in the presence of diverse secondary metabolites strongly suggest that these molecules may represent an underappreciated factor in the recalcitrance of many opportunistic and chronic infections. We offer recommendations for future experiments to explore the breadth of relevance of these observations (Box 1) and discuss the implications that secondary metabolite production can have for the diagnosis of antibiotic resistance (Box 2). Finally, we consider how knowledge of interactions between secondary metabolites and antibiotic efficacy could be applied to optimize the use of existing antimicrobial drugs and generate targets for novel therapeutic strategies.

Induction of efflux systems

Activation of **efflux pumps** that export toxins out of the cell is one mechanism used by diverse bacteria to thrive during clinical antibiotic treatment [17,18]. However, efflux pumps long predate human use of synthetic antibiotics, and therefore are presumed to have originally evolved to transport other, naturally occurring substrates, such as secondary metabolites [19,20]. The types and components of efflux pumps have been extensively reviewed [21,22]. In this chapter, we focus on how the induction of efflux systems in response to self-produced secondary metabolites can affect antibiotic tolerance and resistance in pathogenic bacteria (Fig. 1A). The examples we

discuss fall mostly within the resistance-nodulation-division (RND) efflux systems, but the same principles could, in theory, be applicable to other types of efflux systems that are regulated by secondary metabolites. Importantly, efflux pumps vary in their specificity, with regard to both their regulation and their substrate affinity [22]. Therefore, to predict whether a secondary metabolite will increase antibiotic resilience in its producer through the induction of a particular efflux system, it is essential to understand how the secondary metabolite interacts with the transcriptional regulation of the system, as well as which classes of drugs the system can transport. Many known efflux-regulating secondary metabolites have at least one aromatic or heterocyclic ring (Fig. 1B), possibly suggesting that secondary metabolites with this structural motif are particularly likely to affect antibiotic resilience through the induction of multidrug efflux systems.

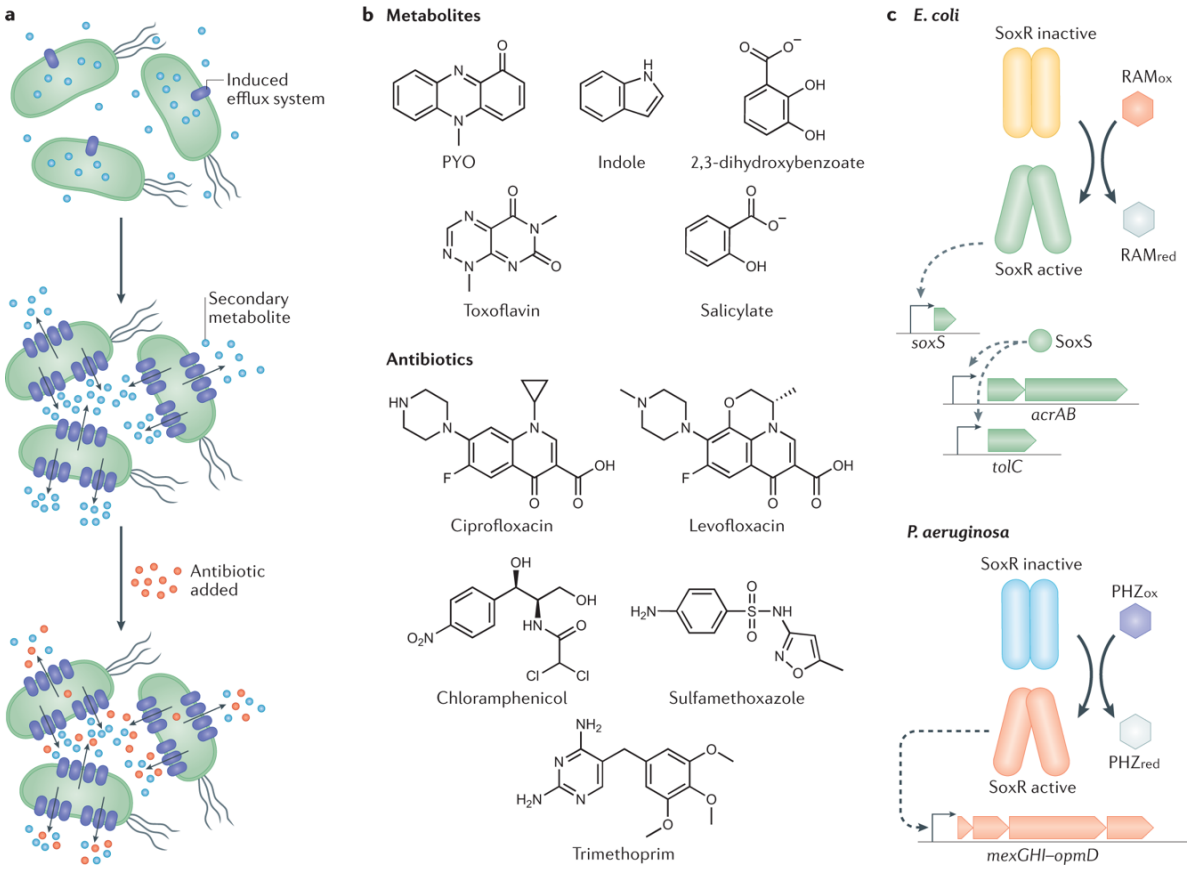

Figure 1. Secondary metabolite-mediated regulation of multidrug resistance efflux pumps. A. Secondary metabolites induce the expression of efflux systems, which export the metabolite. The increased expression of efflux pumps can provide collateral resilience to antibiotics used in the clinic by expelling the drugs out of the microbial cells. **B.** Structures of known efflux pump-regulating secondary metabolites and selected clinical antibiotics, showing

the shared prevalence of aromatic and/or heterocyclic ring motifs. **C.** SoxR-regulated efflux systems in *Escherichia coli* and *Pseudomonas aeruginosa*. Each SoxR monomer contains a Fe–S cluster that can be directly oxidized by redox-active molecules, which leads to its activation and transcriptional induction of efflux systems [23,24]. In *E. coli* (top), several molecules can induce transcription of the efflux system AcrAB–TolC through the activation of SoxR [23,25,26]. Note that *acrAB* and *tolC* are transcribed separately, and this is a simplified version of a very complex regulatory system [22]. Importantly, TolC can assemble with efflux systems from different classes, such as AcrAB–TolC and several others from the resistance-nodulation-division (RND) efflux systems superfamily, EmrAB–TolC (major facilitator superfamily), and MacAB–TolC (ABC superfamily) [27–29]. When studying how additional secondary metabolites might affect *E. coli* susceptibility to antibiotics, it will be important to determine which specific efflux system TolC is part of, the regulation involved in the induction of the system, and its substrate-specificity. In *P. aeruginosa* (bottom), the activation of SoxR is mediated by two endogenous phenazines, 5-Me-PCA (not shown) and PYO, and leads to the induction of the efflux system MexGHI–OpmD [9,24,30,31]. PYO, pyocyanin; PHZ_{ox}, phenazine in the oxidized state; PHZ_{red}, phenazine in the reduced state; RAM_{ox}, redox-active molecule in oxidized state, RAM_{red}, redox-active molecule in reduced state.

In the enteric bacterium *Escherichia coli*, one of the best-studied multidrug resistance efflux systems is AcrAB–TolC, which has a complex regulatory system and an extensive substrate range, being part of a general stress response [22,27]. Although AcrAB–TolC is generally expressed at high intrinsic levels [22,32], numerous molecules have been shown to further upregulate its transcription, including self-produced secondary metabolites such as the compound 2,3-dihydroxybenzoate, an intermediate in the biosynthesis of the siderophore enterobactin [33]. In fact, 2,3-dihydroxybenzoate directly binds to MarR [34], a transcriptional repressor that modulates the expression of AcrAB–-TolC alongside the redox-sensing SoxRS regulatory system [22] (Fig. 1C). Although it has not been directly tested whether the production of enterobactin or 2,3-dihydroxybenzoate *per se* increases antibiotic resilience, it is well established that AcrAB–TolC provides protection against many classes of clinical antibiotics [27]. The signaling molecule indole is another example of a self-produced secondary metabolite in *E. coli* with an efflux-mediated effect on antibiotic susceptibility. Indole triggers the expression of certain multidrug efflux pumps in enteric bacteria [35–38]. Indeed, the production of high levels of indole by a subpopulation of mutants has been characterized as a 'charity' mechanism that induces population-level resistance against norfloxacin and gentamicin in *E. coli*, with the MdtEF–TolC efflux system being upregulated by this secondary metabolite [39]. Intriguingly, a *tolC* mutant of *Shewanella oneidensis*, an environmental isolate related to opportunistic pathogens of fish [40], was sensitive to anthraquinone-2,6-disulfonate (an analog of naturally occurring redox-active humic substances in soils and sediments that resembles quinone-containing synthetic antibiotics) [41], further

suggesting that functional relationships between structurally similar natural and synthetic molecules may be common.

Efflux pumps can also provide protection against secondary metabolites that are toxic to their producers, an effect that might confer resilience to clinical antibiotics. For example, in the opportunistic pathogen *Pseudomonas aeruginosa*, the redox-sensing transcription factor SoxR (Fig. 1C) activates expression of the MexGHI–OpmD efflux system in response to phenazines, which are toxic, redox-active self-produced secondary metabolites [9,30,31,42]. Phenazines have important roles both in natural environments (for example, by protecting plants against fungal pathogens) as well as in infections (for example, by increasing *P. aeruginosa* virulence in the lungs of patients with cystic fibrosis) [43,44]. The phenazine pyocyanin (PYO) also induces a second efflux operon in *P. aeruginosa*, *mexEF–oprN* [31,42], which is clinically relevant [45,46]. Experiments with a broad-spectrum efflux pump inhibitor that reduces the activity of various RND efflux systems [47,48], as well as a knockout mutant lacking the *mexGHI–opmD* operon, have confirmed that efflux is a major mechanism underlying the tolerance and resistance of *P. aeruginosa* to its own phenazines [30,31,49]. Importantly, both phenazine-regulated efflux pumps are also known to transport fluoroquinolones, and multiple studies have reported a strong antagonistic effect of phenazines on fluoroquinolone efficacy [31,49–51]. For example, *P. aeruginosa* cells exposed to PYO (either self-produced or exogenously added) display increased tolerance against the fluoroquinolones ciprofloxacin and levofloxacin [31]. This phenotype was recapitulated in one study by artificially overexpressing MexGHI–OpmD in a phenazine-null mutant to a level similar to that achieved in the presence of PYO, which suggests that drug efflux drives PYO-mediated increases in fluoroquinolone tolerance [31]. Interestingly, besides fluoroquinolones and chloramphenicol, MexEF–OprN is also thought to transport trimethoprim and sulfamethoxazole, to which *P. aeruginosa* is intrinsically resistant [52], but not aminoglycosides [52], against which phenazines have demonstrated mixed effects on tolerance [31,50,51]. Like phenazines, but unlike aminoglycosides, all of the known antibiotic substrates for MexEF–OprN have at least one aromatic ring (Fig. 1B), which suggests that analysis of shared structural motifs may enable prediction of which clinical antibiotics will be most affected. Such structural comparisons would only be appropriate for efflux systems that are relatively specific in

substrate recognition, and would not apply to efflux systems that export a wide range of antibiotics [52].

In addition to MexGHI–OpmD and MexEF–OprN, *P. aeruginosa* possesses at least nine other efflux systems that belong to the RND family, many of which have been studied in detail with respect to their structures and biochemistry [22,52–54]. Whether any *P. aeruginosa*-produced secondary metabolites regulate these other efflux systems under clinically relevant circumstances remains to be determined. Notably, however, phenazines are not the only secondary metabolites produced by *P. aeruginosa* that promote increased resilience against antibiotics by inducing efflux. Recent work showed that production of the secondary metabolite paerucumarin also stimulates transcription of the MexEF–OprN efflux system in *P. aeruginosa*, with consequent increases in resistance to both chloramphenicol and ciprofloxacin [55,56]. These findings underscore the potential for self-produced secondary metabolites to promote resilience to clinical antibiotics in opportunistic pathogens by triggering the upregulation of efflux pumps.

Other bacterial opportunistic pathogens inhabiting soils or plant roots also produce secondary metabolites that promote efflux and decrease antibiotic susceptibility. For example, several strains of '*Burkholderia cepacia* complex' species isolated from patients with cystic fibrosis can produce salicylate [57,58]. Salicylate has Fe-chelating properties and is used as a siderophore by the producing cells [59,60]. It also induces specific efflux systems in *Burkholderia* species (for example, CeoAB–OpcM in *B. cenocepacia*), which leads to increased antibiotic resistance [61]. The salicylate-derived antibiotic resistance effect is not limited to the *Burkholderia* genus; for example, in enterobacteria, salicylate binds to and inactivates MarR, which leads to upregulation of efflux pump expression and increased resistance to multiple clinical antibiotics [62,63]. *Burkholderia* species also produce several other secondary metabolites that could affect antibiotic resilience, including many natural antibiotics with strong inhibitory capacities relevant during plant host colonization [64–67]. One intriguing example is toxoflavin, which is produced by several *Burkholderia* species, including *Burkholderia gladioli*, a common species found in patients with cystic fibrosis [68,69]. Although it is still unknown whether toxoflavin poisons producing cells, it is redox-active [70–72], presumably causing oxidative stress through the

generation of H_2O_2 [71], and it is toxic to other bacteria and fungi [71,73]. More importantly, like PYO, toxoflavin induces a specific RND efflux system, ToxFGHI, which is used for its export [74]. It is not yet known if *B. gladioli* or other opportunistic pathogens within the *Burkholderia* genus produce toxoflavin during infections, or if the toxoflavin-induced RND efflux system ToxFGHI can transport any of the currently used clinical antibiotics; however, this is a possibility, given that toxoflavin, like PYO, bears structural similarity to fluoroquinolones.

Finally, we note that the above examples of efflux system induction due to the presence of secondary metabolites are all from Gram-negative bacteria, which are traditionally the organisms in which drug efflux has been studied in more detail. However, a related phenomenon has been demonstrated in the non-pathogenic Gram-positive bacterium *Streptomyces coelicolor*, which produces a natural antibiotic, actinorhodin, that stimulates expression of a transporter similar to those that export tetracycline [75,76]. Future work should investigate the extent to which secondary metabolite-mediated induction of multidrug efflux pumps might occur in pathogenic Gram-positive bacteria and its consequences for antibiotic resilience. Taken together, the examples discussed highlight the rich diversity of bacterial secondary metabolites that induce efflux activity in their producers, potentially compromising the efficacy of clinical antibiotics.

Modulation of oxidative stress

More than a decade ago, it was proposed that bactericidal antibiotics exert their lethal effects in part by inducing oxidative stress, regardless of the specific cellular targets of different antibiotic classes [77]. Although this hypothesis has engendered controversy [78,79], evidence reviewed elsewhere [80] suggests that bactericidal antibiotics have an impact on cellular redox states, and that the resulting increases in reactive oxygen species (ROS) and oxidative stress can contribute to cell death. Importantly, many secondary metabolites also interface with cellular redox homeostasis and oxidative stress responses. In this section, we discuss three different modes of action by which these metabolites can potentially antagonize or potentiate the toxicity of clinical antibiotics (Fig. 2A): upregulation of oxidative stress response genes; direct detoxification of ROS; and increased endogenous ROS generation.

Upregulation of defenses against oxidative stress

Secondary metabolites that upregulate the expression of oxidative stress responses can prime bacterial cells for tolerance and/or resistance to clinical antibiotics, analogous to the protective effects of exposure to sub-lethal concentrations of oxidants like H_2O_2. Among this class of metabolites, indole is perhaps the best-studied. As mentioned above, indole can also influence antibiotic susceptibility by upregulating efflux pump expression. However, this effect is thought to happen primarily at high concentrations of indole (>1 mM) [35,37]; indole concentrations in human feces tend to be lower [81], though measurements up to the equivalent of 1100 μM have been recorded [82]. At these lower concentrations, indole is non-toxic to its producer, *E. coli*, but still induces oxidative stress response genes regulated by OxyR, including alkyl hydroperoxide reductases, thioredoxin reductase, and the DNA-binding protein Dps [83]. Exposure to indole increases the frequency of *E. coli* **persisters** to antibiotics that belong to three different classes (fluoroquinolones, aminoglycosides and β-lactams) by at least an order of magnitude, and deletion of *oxyR* substantially diminishes this effect, which demonstrates that upregulation of oxidative stress responses by a secondary metabolite can contribute to bacterial persistence [83]. The molecular pathway through which indole activates OxyR remains unclear, but indole readily undergoes one-electron reduction to a radical form in the presence of hydroxyl radicals or other strong oxidants [84], which suggests that it might interact with and potentially amplify endogenous ROS generated as a byproduct of respiration. Indole has also been proposed to disrupt the arrangement of membrane lipids, which would enable the direct interaction of respiratory quinones with dioxygen and thereby lead to the generation of superoxide [85].

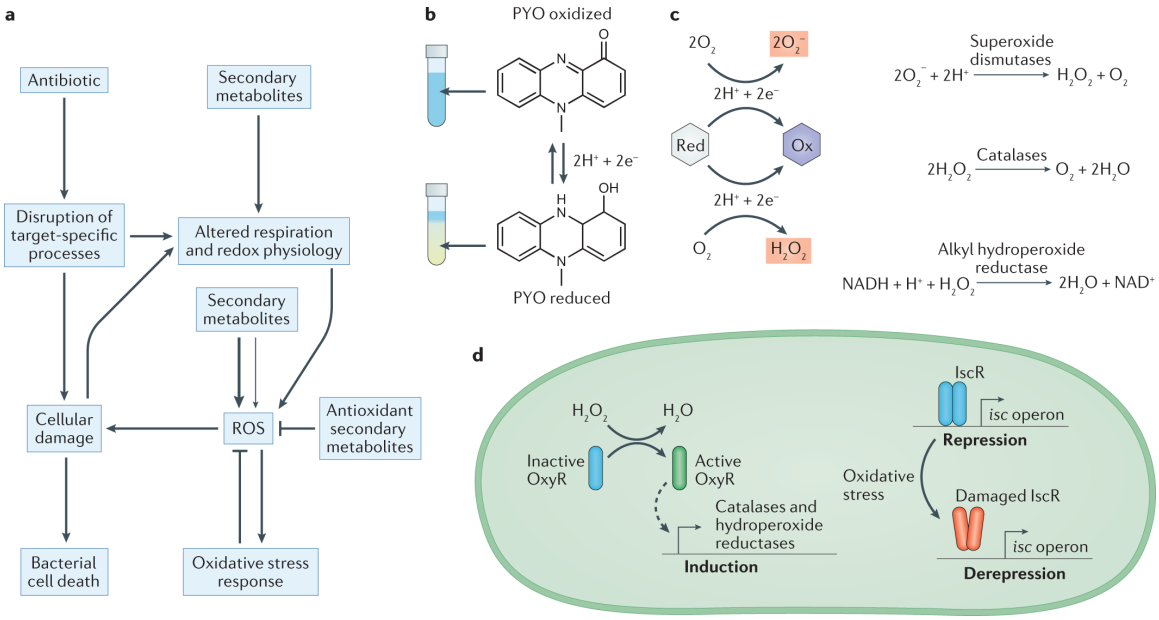

Figure 2. Secondary metabolite interactions with oxidative stress. A. Schematic depicting how bactericidal antibiotics can cause cell death both by directly disrupting target-specific processes, and by indirectly promoting the formation of reactive oxygen species (ROS) as a consequence of altered respiration and cellular damage. Secondary metabolites can interface with these pathways at multiple points, including by interfering with respiration and redox homeostasis, directly generating ROS through redox-cycling, and detoxifying ROS via one-electron reactions. Secondary metabolites that promote oxidative stress can either antagonize or potentiate antibiotic toxicity, which is likely to depend on whether the resulting increases in ROS are moderate (thin arrow) or severe (thick arrow). Moderate increases in ROS may induce protective oxidative stress responses that can counteract antibiotic toxicity, whereas severe increases in ROS may overwhelm the defenses of the cell, which leads to synergistic effects with bactericidal antibiotics. **B.** The redox-active nature of pyocyanin (PYO) is visually apparent as it undergoes a color change from blue (oxidized) to colorless (reduced) upon gaining two electrons and two protons from cellular reductants. This reaction is reversible under physiological conditions. **C.** Many redox-active secondary metabolites can donate electrons to molecular oxygen in the process of cycling from a reduced (Red) to an oxidized (Ox) state, which leads to the formation of superoxide or hydrogen peroxide. Cells can detoxify these forms of ROS through enzymatic reactions catalyzed by superoxide dismutase, catalase, and alkyl hydroperoxide reductase [23]. **D.** Bacterial oxidative stress responses are typically regulated through multiple pathways. For example, in *Pseudomonas aeruginosa*, the H_2O_2-sensing transcription factor OxyR controls the expression of catalases and alkyl hydroperoxide reductases (AHPs) [86,87] (left). In addition, the transcription factor iron-sulfur cluster regulator (IscR) upregulates the biosynthesis of iron–sulfur cluster (*isc*) operons in response to oxidative stress caused by ROS such as superoxide or H_2O_2, which can directly damage the iron–sulfur cluster in IscR itself and thereby lead to depression of its regulon [88].

PYO is another example of a bacterial secondary metabolite that induces oxidative stress responses. As a redox-active metabolite that can gain and lose electrons reversibly under physiological conditions (Fig. 2B), PYO can generate ROS under aerobic conditions through direct reduction of oxygen to superoxide (Fig. 2C), in addition to interfering with respiration [89,90]. In its producer, *P. aeruginosa*, PYO increases superoxide dismutase activity [91] and upregulates the

transcription of several other oxidative stress response genes, including those encoding alkyl hydroperoxide reductases, thioredoxin reductase, catalase and iron-sulfur cluster biogenesis machinery [42] (Fig. 2C-D). Intriguingly, PYO has been shown to increase the frequency of gentamicin-resistant mutants in *P. aeruginosa* cultures in a manner that is independent of drug efflux, as PYO does not upregulate aminoglycoside-transporting efflux pumps [31]. Given that gentamicin is known to promote increased intracellular ROS levels through the formation of complexes with iron [92,93], and that pre-treating cells with oxidants can prime them to tolerate antibiotics [94], a plausible explanation for this phenomenon is that PYO-induced oxidative stress responses counteract ROS-related gentamicin toxicity. This in turn could decrease the rate at which spontaneous mutants are stochastically lost from the population [95], which would lead to the observed increase in the frequency of resistant mutants. PYO can also promote the growth of *P. aeruginosa* in the presence of other aminoglycosides (kanamycin, streptomycin and tobramycin) and a β-lactam antibiotic (carbenicillin) [51]. Like gentamicin, these antibiotics are not known to be substrates for PYO-regulated efflux systems [31,52], but they belong to classes of drugs that have been shown to perturb cellular redox states [96,97], which again suggests that the observed decreases in antibiotic efficacy could be related to PYO-induced oxidative stress responses.

Detoxification of ROS

In contrast to ROS-generating redox-active secondary metabolites that induce enzymatic oxidative stress responses, secondary metabolites that possess **antioxidant activity** can protect against antibiotic assaults by directly detoxifying antibiotic-derived ROS. One example is ergothioneine, which is one of two major sulfur-containing redox buffers in mycobacteria, along with mycothiol. Loss of ergothioneine biosynthesis genes in *Mycobacterium tuberculosis* decreases minimum inhibitory concentrations (MICs) for rifampicin, isoniazid, bedaquiline and clofazimine, in addition to decreasing survival under treatment at the wildtype MICs by at least 30-60% [98]. Other secondary metabolites with antioxidant activity have been shown to be important for resistance to ROS generated by host immune cells, including macrophages and neutrophils. One such metabolite is staphyloxanthin, a membrane-embedded carotenoid pigment that protects *Staphylococcus aureus* against ROS [99,100] and consequently decreases killing by

neutrophils [100]. Likewise, carotenoids produced by group B *Streptococcus* [101] and the dental pathogen *Streptococcus mutans* [102] have been implicated in resistance to ROS. The antioxidant capacity of these pigments has been attributed to their highly conjugated polyene backbones [103], though the exact mechanisms by which different carotenoids scavenge ROS remain unclear [104]. Importantly, antioxidant agents need not necessarily be located in the cytoplasm to protect against antibiotic-induced ROS accumulation, as exogenous catalase has been shown to increase bacterial survival following exposure to trimethoprim [105]. Thus, although most studies on membrane-embedded carotenoids have focused on interactions with extracellular sources of ROS, these pigments might also be able to dampen oxidative stress that originates inside the cell during treatment with bactericidal antibiotics. Considering the growing body of evidence that redox imbalance and oxidative stress are downstream effects of many antimicrobial drugs [80], the possibility that staphyloxanthin or other membrane-associated pigments promote resilience to clinical antibiotics is worthy of further investigation.

In addition to the above examples, certain microbially produced compounds that are not classic secondary metabolites, either because they are inorganic or are not always dispensable for normal growth, also contribute to antibiotic tolerance or resistance by enhancing the antioxidant capacity of bacterial cells. For example, endogenously generated H_2S protects a diverse range of bacteria, including *E. coli*, *P. aeruginosa*, and *S. aureus*, against the toxicity of antibiotics known to exert oxidative stress, such as gentamicin [106]. This phenomenon has been proposed to stem from a dual-action mechanism whereby H_2S both inhibits the Fenton reaction and stimulates the activities of catalase and superoxide dismutase [106]. Polyamines have also been shown to protect bacteria from antibiotic toxicity by counteracting oxidative stress. This is thought to be due in part to their capacity to neutralize free radicals [107,108], though physical protection of cellular components and indirect upregulation of other oxidative stress responses may also be involved [107,109]. *E. coli* upregulates production of putrescine and spermidine upon exposure to antibiotics under aerobic conditions, and these polyamines in turn statistically significantly increase viability under antibiotic treatment by decreasing ROS production and oxidative damage [110]. Similarly, putrescine secreted by *Burkholderia cenocepacia* protects its producer against oxidative stress arising from treatment with polymyxin B, norfloxacin, or rifampicin [108].

Finally, in *P. aeruginosa*, the BqsRS regulatory system drives increased polyamine production upon sensing ferrous iron, which is prevalent in the lungs of patients with cystic fibrosis, thereby promoting survival in the presence of cationic antibiotics such as polymyxins and aminoglycosides [111]. Together, these examples demonstrate how interactions between diverse bacterial metabolites and oxidative stress can lead to increased resilience against clinical antibiotics.

Synergistic interactions between secondary metabolites and antibiotics

Besides the examples in which secondary metabolites decrease antibiotic efficacy by attenuating oxidative stress, it is also important to note that in some cases, secondary metabolites that increase ROS generation can amplify the toxicity of clinical antibiotics. One example is 2-heptyl-3-hydroxy-4-quinolone, also known as the *Pseudomonas* quinolone signal (PQS), which is produced by *P. aeruginosa*. PQS is a redox-active molecule that can reduce not only free radicals but also metal ions, and consequently possesses both antioxidant properties and **pro-oxidant activity**, as reduction of iron promotes ROS formation through the Fenton reaction [112]. The pro-oxidant activity seems to dominate in cells, as PQS induces oxidative stress responses and increases sensitivity to hydrogen peroxide and ciprofloxacin [112,113]. The pro-oxidant activity of PQS is also evidenced by the fact that overproduction of PQS acts synergistically with impairment of superoxide dismutase and catalase activity to increase endogenous oxidative stress and antibiotic susceptibility [114]. Notably, abolishment of PQS production increases tolerance to ciprofloxacin, imipenem and gentamicin [112]. Another redox-active secondary metabolite that increases antibiotic susceptibility under certain conditions is PYO. Although pre-exposure of *P. aeruginosa* to PYO increases tolerance to fluoroquinolones and promotes the establishment of gentamicin-resistant mutants, PYO and other phenazines have also been shown to increase the sensitivity of *P. aeruginosa* to cationic antimicrobial peptides, including colistin [31,50] and polymyxin B [51]. The underlying mechanism of this synergistic interaction has yet to be determined, but it is notable that polymyxin B precipitates severe oxidative stress in *P. aeruginosa* and other Gram-negative opportunistic pathogens [115,116]. Moreover, unlike fluoroquinolones or aminoglycosides, cationic antimicrobial peptides also permeabilize the outer membrane [117] and consequently might increase phenazine uptake, which would accelerate ROS generation even

further. Thus, the synergy between phenazines and cationic antimicrobial peptides may ultimately be driven by an overwhelming cascade of oxidative stress. Given that ROS-generating secondary metabolites can both potentiate and diminish antibiotic efficacy depending on the circumstances, future studies focused on revealing which of these effects take precedence during infections will be critical to better understand how such secondary metabolites may affect clinical treatment outcomes.

Interspecies antibiotic resilience

So far, we have discussed examples of secondary metabolites that either are known to affect their producer's susceptibility to clinical antibiotics, or have the potential to do so based on their interactions with established mechanisms of antibiotic tolerance and resistance. However, equally important is the fact that many secondary metabolites, in particular those that are secreted, can also modulate interspecies antibiotic resilience (Fig. 3). Indeed, how interactions among members of a **polymicrobial infection** might affect antibiotic treatment outcomes has recently received much attention [118,119].

Although our understanding of how exchangeable secondary metabolites affect community-level antibiotic resilience is still in its infancy, there have been several reports on this subject. For example, indole has been identified as an interspecies modulator of antibiotic tolerance between *E. coli* and *Salmonella enterica* subsp. *enterica* serovar Typhimurium [37,120]. *S.* Typhimurium, which is likely to interact with commensal *E. coli* during infection, does not produce indole, yet its tolerance to ciprofloxacin increased by greater than threefold in the presence of exogenously added indole, as well as in co-cultures with indole-producing *E. coli* [120]. Similar to its effect in *E. coli*, indole induces OxyR-regulated oxidative stress responses in *S.* Typhimurium, and deletion of *oxyR* abolished the indole-mediated increase in ciprofloxacin tolerance [120]. Interestingly, indole has also been reported to increase resistance to ampicillin in the indole non-producer *P. aeruginosa*, not by inducing oxidative stress responses, but rather by stimulating the expression of efflux pumps and a chromosomal β-lactamase [121]. These examples highlight the potential for secreted secondary metabolites to have both conserved and mechanistically divergent effects on antibiotic resilience in neighboring species.

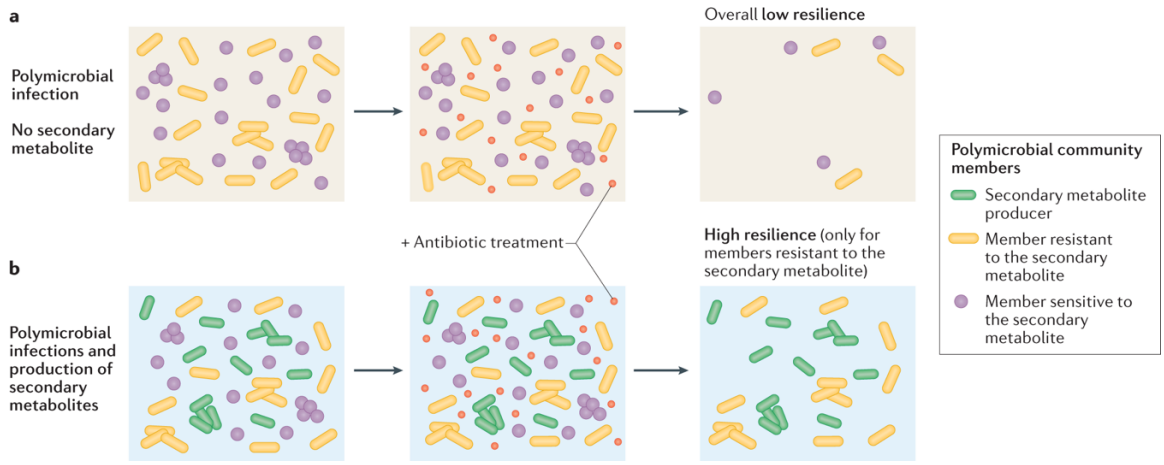

Figure 3. Secondary metabolites as interspecies modulators of antibiotic resilience. The presence of secondary metabolite producers in polymicrobial infections can alter the community susceptibility profile to antibiotic treatment. When the producer is not present (part a), overall resilience levels upon antibiotic treatment are low. However, through the secretion of the secondary metabolite, the producer's presence (part b; blue cells) can have distinct effects on different community members. For members intrinsically resistant to the secondary metabolite (yellow cells), the molecule's presence can increase resilience to antibiotic treatment. However, if a member is sensitive to the secondary metabolite (green cells), the added toxicity can overwhelm cellular defenses, potentiating the killing by the clinical drug.

Other secondary metabolites besides indole have shown potential as interspecies modulators of antibiotic resilience. For example, the protective effect against polymyxin B of putrescine secreted by *B. cenocepacia* extends not only to the producer, but also to neighboring species in co-cultures, including *E. coli* and *P. aeruginosa* [109]. Similarly, PYO produced by *P. aeruginosa* considerably increases the tolerance of multiple clinically relevant *Burkholderia* species to ciprofloxacin in co-cultures [31]. In yet another opportunistic pathogen, *Acinetobacter baumannii*, exposure to PYO increases the frequency of persisters to amikacin and carbenicillin by three- to four-fold [122], possibly through the upregulation of superoxide dismutase and catalase [122,123]. Finally, quorum sensing signals produced by *P. aeruginosa* induce fluconazole resistance in the yeast *Candida albicans* [124], which indicates that bacterial secondary metabolites can mediate not only interspecies but also interkingdom effects on antimicrobial efficacy. So far, these interactions have only been demonstrated *in vitro*. However, given that *Burkholderia* species, *Acinetobacter* species and fungal pathogens can all be found together with *P. aeruginosa* in chronic infections [68,125,126], these findings suggest that valuable insights could be gained from future studies focused on the *in vivo* relevance of secondary metabolite-mediated interspecies induction of antibiotic resilience.

Importantly, although the above examples suggest that certain secreted secondary metabolites have the potential to raise the community-wide level of antibiotic resilience in polymicrobial infections, a secondary metabolite that promotes antibiotic resilience in one species will not always do so in others. One key consideration is that in order for a secondary metabolite to trigger cross-species induction of resilience to clinical antibiotics, the non-producing species must be able to tolerate any stress caused by the secondary metabolite. If toxicity outweighs benefits from defense induction or antibiotic detoxification, the non-producing species would not gain a benefit. In fact, the secondary metabolite might even act synergistically with the clinical antibiotic [127]. Examples of this type of interaction have been found between *S. aureus* and *P. aeruginosa*, two species that often co-occur in patients with cystic fibrosis [128–130]. *S. aureus* is sensitive to several secondary metabolites secreted by *P. aeruginosa* [131,132], and some of these can increase the susceptibility of *S. aureus* to clinical antibiotics. For example, *P. aeruginosa*-produced rhamnolipids potentiate tobramycin toxicity in *S. aureus* by increasing membrane permeability [131]. Another *P. aeruginosa*-produced secondary metabolite, 2-n-heptyl-4-hydroxyquinoline N oxide (HQNO), was recently shown to increase the sensitivity of *S. aureus* biofilms to fluoroquinolones and membrane-targeting antibiotics via a similar mechanism [133]. However, the toxic effects of *P. aeruginosa* secondary metabolites on *S. aureus* are not always synergistic with clinical antibiotics. By inhibiting growth, HQNO promotes tolerance in *S. aureus* biofilms specifically to antibiotics targeting cell wall synthesis and protein synthesis [134], contrary to its effect on other classes of antibiotics. By contrast, in planktonic cultures of *S. aureus*, HQNO can induce multidrug tolerance by inhibiting respiration and depleting intracellular ATP [131]. The interference of PYO with respiration in *S. aureus* similarly selects for non-respiring small colony variants [132,135], which are often resistant to antibiotic treatment [136]. In such cases where different secondary metabolites produced by one species seem to have conflicting and condition-dependent effects on a neighboring species, *in vivo* studies and co-culture experiments are particularly necessary to determine the overall impact on clinical antibiotic efficacy.

The potential for *P. aeruginosa*-produced secondary metabolites to have complex effects on antibiotic resilience has also been observed in another opportunistic pathogen, *Stenotrophomonas maltophilia*. Compared to members of the *Burkholderia cepacia* complex,

which strongly benefit from exposure to PYO during treatment with ciprofloxacin, *S. maltophilia* is more sensitive to PYO toxicity, exhibiting growth inhibition at concentrations as low as 50 μM [31]. At a low but still lethal dose of ciprofloxacin, PYO at concentrations up to 50 μM statistically significantly increased survival of *S. maltophilia*, which suggests that defenses against fluoroquinolones are indeed induced by PYO in this species [31]. Yet at a ten-fold higher dose of ciprofloxacin, even 10 μM PYO was detrimental [31]. Notably, although *in situ* levels of PYO can vary greatly across patients infected with *P. aeruginosa*, PYO has been detected in infected sputum and wound exudates at concentrations up to 130 μM or 0.31 mg/g, respectively [137,138]. Thus, the example of PYO and *S. maltophilia* suggests that to predict how a secondary metabolite will affect community-wide levels of resilience to clinical antibiotics during a polymicrobial infection, it is imperative to characterize the directionality and magnitude of interspecies effects over a range of clinically relevant concentrations of both the secondary metabolite and the clinical antibiotic.

Implications for resistance evolution

In recent years, it has increasingly become appreciated that antibiotic tolerance cannot only directly contribute to infection treatment failure, but also promote the establishment of heritable resistance mutations [139–143]. Exploration of the connection between antibiotic tolerance and the evolution of resistance has largely focused on tolerance resulting from spontaneous mutations that are selected by treatment with clinical antibiotics [139,140,142,143]. However, effects on the establishment of heritable resistance mutations have also been demonstrated for at least one secondary metabolite produced by an opportunistic pathogen, namely, PYO. Experiments based on classic fluctuation tests revealed that PYO increases the rate of mutation to antibiotic resistance not only in the producing species, *P. aeruginosa*, but also in a clinical isolate of a co-occurring opportunist, *Burkholderia multivorans* [31]. Notably, the impact of PYO on the acquisition of heritable resistance varied across different classes of antibiotics. In particular, strong effects were observed for drugs against which PYO-induced defenses confer increased tolerance, which suggests that this phenomenon is indeed driven by tolerance as opposed to a mutagenic effect of PYO. Remarkably, in *B. multivorans*, treatment with PYO increased mutation rates for ciprofloxacin resistance to a level rivaling clinical hypermutator strains [31,144]. In addition, in

both *P. aeruginosa* and *B. multivorans*, pre-treatment with PYO prior to antibiotic treatment was sufficient to increase the rate at which resistant mutants became established, even without continued exposure to high levels of PYO [31]. These findings collectively reveal the potential for tolerance-inducing secondary metabolites to have a substantial impact on the evolution of antibiotic resistance. However, future experiments will be necessary to investigate the clinical relevance of these observations, and whether the link between tolerance and resistance triggered by PYO exposure can be generalized to other secondary metabolites remains to be determined.

Concluding remarks and future directions

Although direct connections between bacterial secondary metabolite production or exposure and resilience to clinical antibiotics have only been pursued in a small number of studies, many more secondary metabolites are known to interface with cellular functions that are relevant to antibiotic tolerance and resistance, especially drug efflux and oxidative stress responses. We hope the examples discussed in this chapter stimulate further investigation into the conditions under which these and related secondary metabolites alter the efficacy of clinical antibiotics, particularly during treatment of infections. Currently, PYO represents the secondary metabolite for which the most detailed evidence on this topic is available, likely due to the extensive research attention that its producer, *P. aeruginosa*, has received. However, we expect that deliberately searching for such molecules across a broad range of opportunistic pathogens (Box 1) will reveal additional as-yet-uncharacterized secondary metabolites that have the potential to affect antibiotic treatment outcomes. Soil-borne opportunistic pathogens in particular often possess the biosynthetic capacity to produce a great variety of secondary metabolites [66,145–147], perhaps because they have to cope with the extraordinary complexity and heterogeneity that typifies the soil environment [148]. In most cases, the biological functions of these secondary metabolites, as well as whether they are produced during infections, remain unknown. However, biosynthetic gene clusters for secondary metabolites are often located near or co-transcribed with genes encoding efflux pumps [149–151], and numerous microbial secondary metabolites are redox-active and therefore have the potential to generate or detoxify ROS [12,152], which suggests that interactions with clinical antibiotic efficacy are likely to be far more common than is currently appreciated.

Importantly, understanding the molecular mechanisms involved in the cellular responses triggered by a secondary metabolite, as well as the chemical properties of the secondary metabolite itself, can provide practical insights regarding which clinical antibiotics are likely to be affected. With this knowledge in hand, combined with an understanding of other environmental and physiological factors that affect antibiotic susceptibility [153,154], we posit that it will be possible to optimize the use of existing antibiotics so as to better minimize the risk of treatment failure and prevent the evolution of resistance *in vivo*. For example, if a pathogen produces a secondary metabolite that upregulates efflux pumps specific to fluoroquinolones and other aromatic molecules, the chances of successful treatment would likely be higher with another class of antibiotics that is not susceptible to this defense, such as aminoglycosides. The biosynthetic pathways for these secondary metabolites, or even the molecules themselves, could also be targets for the development of new adjuvants for antimicrobial drugs. Such efforts are already underway for secondary metabolites such as PYO and staphyloxanthin [155–158], which are also known to act as virulence factors [159]. For example, enzymatic removal of PYO increased antibiotic killing of *P. aeruginosa* biofilms *in vitro* [158]. In addition, inhibiting a bacterial enzyme that generates H_2S increased the potency of bactericidal antibiotics both *in vitro* and in mouse infection models [160]. These results encourage further exploration of whether targeting the production or presence of specific bacterial metabolites could optimize the clinical efficacy of treatments for infections. Finally, retooling clinical antimicrobial susceptibility testing protocols to account for the impact of secondary metabolites on antibiotic efficacy (Box 2) could potentially improve the predictive value of these assays, especially in the case of secondary metabolite-producing opportunistic pathogens, such as members of the *Burkholderia cepacia* complex, that often exhibit discrepancies between *in vitro* minimum inhibitory concentration measurements and clinical treatment outcomes [161].

In conclusion, our ability to address the vexing challenges posed by antibiotic tolerance and resistance in the future has much to gain by reflecting on the past. The evolutionary and ecological history of natural antibiotics intersects directly with the history of clinical antibiotic discovery. While the soil has continued to provide a rich reservoir for natural product mining efforts, what has gotten lost is the fact that alongside the evolution of pathways that synthesize

these molecules, other pathways have co-evolved that respond to them. Remembering this shared historical context is important for predicting how secondary metabolites might affect the response of polymicrobial communities to conventional antibiotics, and compels creative thinking about novel ways to manage such responses.

Box 1: Guidelines for establishing causal links between secondary metabolite production and increased antibiotic tolerance or resistance

We propose a few steps for the investigation of secondary metabolite-mediated changes in antibiotic susceptibility.

1. *Identifying the candidate secondary metabolite.* This can be achieved in multiple ways, including based on molecular structure or its physiological effects on the cells. Genomic analysis could also reveal potentially relevant secondary metabolites produced by pathogens [162]. Researchers should investigate whether the putative secondary metabolite of interest shows any toxicity to the producer, as well as the molecular responses induced upon exposure to it. For example, the fact that pyocyanin (PYO) is toxic to producing cells [42], shares structural similarities to fluoroquinolones (Fig. 1B), and induces efflux systems [9,42], led to predictions about how this metabolite could decrease susceptibility to these drugs [31]. Transcriptomics approaches can be used to reveal responses caused by the specific secondary metabolite [9,31,35,37,42]. Importantly, it will often be necessary to construct a mutant strain lacking the biosynthetic genes for production of the secondary metabolite as a negative control.

2. *Detecting the secondary metabolite*. It is essential to use an accurate and quantitative detection method because the secondary metabolite concentration might affect antibiotic susceptibility. Possible detection methods may include ultraviolet or visible light spectroscopy or mass spectrometry, both of which can be coupled to high-performance liquid chromatography in the case of analyzing complex samples (for example, extracts of microbial cultures or clinical samples). Investigators should attempt to detect the secondary metabolite in the relevant clinical context (for example, in infected sputum, wound exudates or stool samples)

[81,82,137,138]. Importantly, concentrations of the secondary metabolite *in vivo* might vary greatly among patients, depending on a variety of infection parameters (for example, infection stage, the strain causing the infection, the number of bacterial cells present). For this reason, the guidelines provided will, at least initially, likely be most useful for cases of chronic infections, where longitudinal monitoring of patients coupled with repeated measurements of the *in vivo* concentrations of secondary metabolites can be used to constrain *in vitro* experiments (see below; and Box 2).

3. *Considering the effects on nearby species.* It is also critical to account for the effect of secondary metabolites on the entire microbial community in the case of polymicrobial infections. Thus, investigators should consider which species are most commonly found together with the secondary metabolite producer in the type of infection being studied. Then, investigators should perform experiments in which the producer and non-producers are co-cultured, or the non-producers are separately exposed to controlled concentrations of the secondary metabolite. Understanding how the non-producers are affected, including the molecular mechanisms involved, is essential for predicting how the secondary metabolite might change the overall antibiotic susceptibility profile of a microbial community.

4. *Testing the secondary metabolite-mediated effects on antibiotic susceptibility*. Tolerance and resistance are two different modes of antibiotic resilience that should be tested separately [14–16] (see the figure, part a); the former can be measured by determining the percentage of surviving cells following a temporary exposure to the antibiotic, whereas the latter calls for assessing the ability to grow in the presence of the antibiotic. There are also various assays available for testing secondary metabolite-mediated effects on drug susceptibility in multispecies communities (see the figure, part b). In liquid co-cultures, the species can be grown with or without separation by a permeable membrane that restricts interactions to those mediated by diffusible small molecules. For biofilms, experiments can be performed in macroscopic assays (for example, colony biofilms, with species mixed or separated), or microscopic assays (for example, microfluidics [163,164] or alternative assays like the agar block biofilm assay (ABBA) [157,165], to which concomitant measurements of

microenvironment variables such as pH or O_2 levels have been applied (see the figure, part b)). Importantly, the decision to perform experiments on liquid cultures versus biofilms can influence the results, as some secondary metabolite-mediated tolerance mechanisms are specific to biofilms. For example, the increased release of extracellular DNA mediated by secondary metabolites can stimulate biofilm formation, which results in increased tolerance levels [166]. In addition, redox-active secondary metabolites, such as phenazines, greatly affect metabolism within biofilms [50,167], which in turn modulates antimicrobial drug efficacy [50,80]. By contrast, planktonic cultures provide better control for testing specific secondary metabolite-mediated responses and are amenable to more sophisticated methods when evaluating resistance, such as fluctuation tests, in which a large number of parallel cultures are plated on a selective medium and the number of spontaneous resistant mutants from each culture serves as the input into a mathematical formula for inferring mutation rates [168,169]. The investigators should therefore decide what is more appropriate for their particular questions.

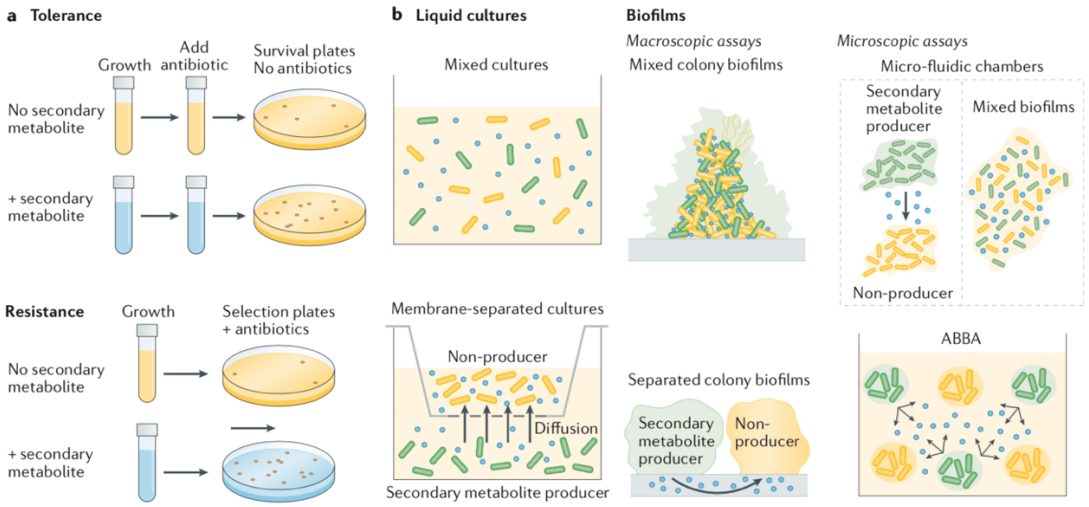

Box Figure. The blue color in tubes or plates (in part A) or the blue dots (in part B) represent the secondary metabolite.

Box 2: Accounting for secondary metabolite production during AST

As the traditional basis for determining appropriate courses of treatment for infections, antimicrobial susceptibility testing (AST) is a cornerstone of clinical microbiology. However, in many clinical contexts, there is little to no correlation between AST results and treatment outcomes

[170,171], which may stem in some cases from the fact that standard AST conditions generally preclude detection of interactions between secondary metabolites and antimicrobial drugs. Clinical AST relies on a readout of absence of growth in cultures that are inoculated at low cell densities [172], whereas secondary metabolites are typically not produced until at least late log-phase or early stationary phase [7]. Moreover, AST is routinely performed on single-species cultures even in the case of polymicrobial infections, eliminating the possibility of detecting secondary metabolite-mediated interspecies interactions that could affect antimicrobial efficacy.

We suggest a few speculative but testable modifications to clinical AST protocols that could help account for the effects of microbial secondary metabolites produced during infections. Our intent is to inspire concrete discussion of how a better understanding of interactions between secondary metabolites and clinical antibiotic efficacy could eventually be applied to improve treatment outcomes, while also recognizing the probable complexity of such endeavors. Given that secondary metabolites can substantially affect antimicrobial efficacy, the proposed modifications might improve the empirical correlation between *in vitro* AST results and the success of clinical treatments. However, many factors beyond secondary metabolite production (for example, biofilm formation, nutritional conditions and/or host-derived molecules) are likely to also affect antibiotic susceptibility *in situ* during infections. The approaches proposed below would need to be refined and validated in animal models of infection, and ultimately tested in clinical trials comparing patient outcomes against the use of traditional AST for antimicrobial drug selection. In addition, if studies indicate that secondary metabolite-related modifications improve the predictive value of AST, scalability in terms of cost and throughput will need to be further optimized before widespread implementation becomes possible in clinical microbiology laboratories.

1. *Use filtered supernatants from overnight cultures of the infective microorganism or microorganisms).* By setting up AST assays using a mixture of fresh growth media and filtered supernatant from an overnight culture of the infective agent, the effects of any secondary metabolites produced during late log phase or stationary phase could be accounted for without needing to modify other aspects of standard AST protocols (for example, visible growth as a readout). A key advantage of this approach is that it is agnostic to which secondary metabolite

is produced, avoiding the need for prior knowledge of the biosynthetic capabilities of the infective agent, as well as accounting for the combined effects of multiple secondary metabolites. However, this approach would significantly increase the time to result. In addition, mixing spent supernatant with fresh growth media might dilute the concentrations of the secondary metabolites below clinically relevant levels. The concentrations of different nutrients in the media would also be affected, possibly in unpredictable ways across different strains, which in turn could also impact antibiotic susceptibility; indeed, the choice of growth medium in general can significantly influence MIC measurements [173].

2. *Add purified secondary metabolites exogenously to cultures.* If it is known that the infective species produces specific secondary metabolites that have been validated as clinically relevant (for example, pyocyanin (PYO) in *Pseudomonas aeruginosa* or indole in *Escherichia coli*), purified forms of the secondary metabolites could be added to traditional AST assays. An advantage of this approach is the ability to control the level of exposure to the secondary metabolites, which would make it possible to ensure that the concentrations in the AST assay are similar to those detected in clinical samples. However, this approach requires that the secondary metabolites be commercially available or otherwise economically viable to synthesize or purify from cultures. In addition, prior knowledge of the biosynthetic capabilities of the infective agent would be necessary. An important caveat in this regard is that microbial secondary metabolite production can vary greatly from strain to strain within the same species. Thus, basing the working concentration of a secondary metabolite on an average across strains or patient samples may lead to over- or underestimation of the effects of the secondary metabolite in individual cases.

3. *Adjust antibiotic 'breakpoint' guidelines according to* in situ *levels of secondary metabolites.* For secondary metabolites that are commonly found in infections and can be procured in purified form, *in vitro* testing could lead to the development of mathematical models that quantitatively relate the concentration of the secondary metabolite to the change in the producing species' resistance to different antimicrobial drugs. Once validated across a range of different strains, such models could potentially enable secondary metabolite-based

adjustments to the standard ‘breakpoint’ antibiotic concentrations used by clinicians to classify microorganisms as susceptible or resistant. Assays for the quantification of the secondary metabolite in patient samples could then be combined with traditional AST testing. Such an approach would enable taking into account strain variability in secondary metabolite production and avoid necessitating modifications to existing AST protocols. However, this approach might also lead to underestimation of secondary metabolite effects in some cases, as bulk measurements of a secondary metabolite in a patient sample may obscure heterogeneity at the micron scale.

4. *Grow multiple species together if they are co-isolated from a polymicrobial infection*. Secreted secondary metabolites produced by one species can affect antimicrobial efficacy in neighboring species. Thus, in the case of polymicrobial infections, inoculating multiple species together in AST assays may improve prediction of the overall community response to antimicrobial drugs. To account for the production of secondary metabolites, this approach would still need to be combined with other modifications, such as those proposed above (points 1-3). In addition, the optimal ratios at which to inoculate different species would need to be investigated and standardized. Alternatively, it may be possible to perform AST using mixed cultures derived directly from patient samples, either bypassing or in parallel to the step in which individual isolates are obtained and identified.

Glossary

Tolerance: The ability to survive transient antibiotic exposure.

Resistance: The ability to grow in the presence of antibiotics at a given concentration.

Antibiotic resilience: The ability of a bacterial population to be refractory to antibiotic treatment via tolerance and/or resistance.

Efflux pumps: Membrane-associated transport proteins that are responsible for the extrusion of various compounds out of the cell.

Persisters: A subpopulation of bacteria that is killed by a given antibiotic at a much slower rate than the rest of the population, in a manner that is non-heritable.

Antioxidant activity: The ability to neutralize highly reactive free radicals.

Pro-oxidant activity: The ability to induce oxidative stress.

Polymicrobial infection: An infection that is caused by more than one species of microorganism.

Acknowledgements

Work in the corresponding author's laboratory was supported by grants to D.K.N. from the NIH (1R01AI127850-01A1, 1R01HL152190-01) and the Doren Family Foundation. E.K.P. was supported by a National Science Foundation Graduate Research Fellowship under Grant No. DGE-1745301.

Table 1. Secondary metabolites produced by opportunistic or enteric pathogens and their impacts on antibiotic efficacy.

Metabolite	Producer	Antibiotic affected	Mechanism	Refs
PYO	*Pseudomonas aeruginosa*	Fluoroquinolones, aminoglycosides*, chloramphenicol, carbenicillin	Efflux induction, oxidative stress response induction	[31,50,51]
PCA, PCN	*P. aeruginosa*	Ciprofloxacin, tobramycin, carbenicillin	Metabolic changes	[50]
Paerucumarin	*P. aeruginosa*	Chloramphenicol, ciprofloxacin	Efflux induction	[56]
Indole	*Escherichia coli*	Fluoroquinolones, gentamicin, ampicillin, carbenicillin	Efflux induction, oxidative stress response induction	[35,39,83,120]
Salicylate	*Burkholderia* spp.	Chloramphenicol, trimethoprim, ciprofloxacin	Efflux induction	[61]
HQNO	*P. aeruginosa*	Meropenem	Increased extracellular DNA release and biofilm formation	[166]
Ergothioneine	*Mycobacterium tuberculosis*	Rifampicin, isoniazid, bedaquiline, clofazimine	Direct ROS detoxification, redox buffering	[98]
Polyamines (putrescine, spermidine)	*E. coli, Burkholderia cenocepacia, P. aeruginosa*	Levofloxacin, amikacin, cefotaxime, polymyxin B, norfloxacin, rifampicin, tobramycin	Direct ROS detoxification, decreased drug penetration	[108,110]
PQS	*P. aeruginosa*	Ciprofloxacin, oxofloxacin, imipenem, meropenem, gentamicin, colistin	Increased ROS generation	[112,114]
H_2S	Diverse microorganisms	Gentamicin, amikacin, nalidixic acid, ciprofloxacin, ampicillin	Oxidative stress response induction, Fe^{2+} sequestration, redox buffering	[106,174]
Staphyloxanthin	*Staphylococcus aureus*	ND	Direct ROS detoxification	[99,100]
Carotenoids	*Streptococcus* spp.	ND	Direct ROS detoxification	[101,102]
2,3-dihydroxybenzoate	*E. coli*	ND	Efflux induction	[33]
Toxoflavin	*Burkholderia* spp.	ND	Efflux induction**, oxidative stress response induction**	[71,74]
Phthiocol	*M. tuberculosis*	ND	Oxidative stress response induction**	[175,176]
D-alanylgriseoluteic acid	*Pantoea agglomerans*	ND	Oxidative stress response induction**	[177,178]
β-3H-indolydenopyruvate	*Achromobacter* sp.	ND	ND	[179]
Anthraquinones (for example, emodin, endocrocin)	*Aspergillus* spp.	ND	ND	[180,181]

HQNO, 2-n-heptyl-4-hydroxyquinoline N oxide; PCA, phenazine 1-carboxylic acid; PCN, phenazine 1-carboxamide; PQS, *Pseudomonas* quinolone signal; PYO, pyocyanin, ROS, reactive oxygen species.
ND, not determined; these are molecules whose effects on antibiotics have not been directly tested.
* For aminoglycosides, PYO has been shown to increase or decrease antibiotic resilience, depending on the studied conditions.
** Hypothesized mechanisms by which the molecule might affect susceptibility.

References

1. Maplestone RA, Stone MJ, Williams DH. The evolutionary role of secondary metabolites--a review. Gene. 1992;115: 151–157.
2. Demain AL, Fang A. The natural functions of secondary metabolites. Adv Biochem Eng Biotechnol. 2000;69: 1–39.
3. Keller NP, Turner G, Bennett JW. Fungal secondary metabolism - from biochemistry to genomics. Nat Rev Microbiol. 2005;3: 937–947.
4. Tyc O, Song C, Dickschat JS, Vos M, Garbeva P. The ecological role of volatile and soluble secondary metabolites produced by soil bacteria. Trends Microbiol. 2017;25: 280–292.
5. Wang S, Lu Z. Secondary metabolites in archaea and extreme environments. In: Witzany G, editor. Biocommunication of Archaea. Cham: Springer International Publishing; 2017. pp. 235–239.
6. Price-Whelan A, Dietrich LEP, Newman DK. Rethinking "secondary" metabolism: physiological roles for phenazine antibiotics. Nat Chem Biol. 2006;2: 71–78.
7. Davies J. Specialized microbial metabolites: functions and origins. J Antibiot. 2013;66: 361–364.
8. Haslam E. Secondary metabolism - fact and fiction. Nat Prod Rep. 1986;3: 217.
9. Dietrich LE, Price-Whelan A, Petersen A, Whiteley M, Newman DK. The phenazine pyocyanin is a terminal signalling factor in the quorum sensing network of *Pseudomonas aeruginosa*. Mol Microbiol. 2006;61: 1308–1321.
10. Glasser NR, Kern SE, Newman DK. Phenazine redox cycling enhances anaerobic survival in *Pseudomonas aeruginosa* by facilitating generation of ATP and a proton-motive force. Mol Microbiol. 2014;92: 399–412.
11. Wang Y, Wilks JC, Danhorn T, Ramos I, Croal L, Newman DK. Phenazine-1-carboxylic acid promotes bacterial biofilm development via ferrous iron acquisition. J Bacteriol. 2011;193: 3606–3617.
12. McRose DL, Newman DK. Redox-active antibiotics enhance phosphorus bioavailability. Science. 2021;371: 1033–1037.
13. Ling LL, Schneider T, Peoples AJ, Spoering AL, Engels I, Conlon BP, et al. A new antibiotic kills pathogens without detectable resistance. Nature. 2015;517: 455–459.
14. Kester JC, Fortune SM. Persisters and beyond: mechanisms of phenotypic drug resistance and drug tolerance in bacteria. Crit Rev Biochem Mol Biol. 2014;49: 91–101.
15. Brauner A, Fridman O, Gefen O, Balaban NQ. Distinguishing between resistance, tolerance and persistence to antibiotic treatment. Nat Rev Microbiol. 2016;14: 320–330.
16. Balaban NQ, Helaine S, Lewis K, Ackermann M, Aldridge B, Andersson DI, et al. Definitions and guidelines for research on antibiotic persistence. Nat Rev Microbiol. 2019;17: 441–448.
17. Piddock LJV. Clinically relevant chromosomally encoded multidrug resistance efflux pumps in bacteria. Clin Microbiol Rev. 2006;19: 382–402.
18. Li X-Z, Plésiat P, Nikaido H. The challenge of efflux-mediated antibiotic resistance in Gram-negative bacteria. Clin Microbiol Rev. 2015;28: 337–418.
19. Piddock LJV. Multidrug-resistance efflux pumps - not just for resistance. Nat Rev Microbiol. 2006;4: 629–636.

20. Martinez JL, Sánchez MB, Martínez-Solano L, Hernandez A, Garmendia L, Fajardo A, et al. Functional role of bacterial multidrug efflux pumps in microbial natural ecosystems. FEMS Microbiol Rev. 2009;33: 430–449.
21. Mousa JJ, Bruner SD. Structural and mechanistic diversity of multidrug transporters. Nat Prod Rep. 2016;33: 1255–1267.
22. Du D, Wang-Kan X, Neuberger A, van Veen HW, Pos KM, Piddock LJV, et al. Multidrug efflux pumps: structure, function and regulation. Nat Rev Microbiol. 2018;16: 523–539.
23. Imlay JA. The molecular mechanisms and physiological consequences of oxidative stress: lessons from a model bacterium. Nat Rev Microbiol. 2013;11: 443–454.
24. Dietrich LEP, Teal TK, Price-Whelan A, Newman DK. Redox-active antibiotics control gene expression and community behavior in divergent bacteria. Science. 2008;321: 1203–1206.
25. Gu M, Imlay JA. The SoxRS response of *Escherichia coli* is directly activated by redox-cycling drugs rather than by superoxide. Mol Microbiol. 2011;79: 1136–1150.
26. Singh AK, Shin J-H, Lee K-L, Imlay JA, Roe J-H. Comparative study of SoxR activation by redox-active compounds. Mol Microbiol. 2013;90: 983–996.
27. Anes J, McCusker MP, Fanning S, Martins M. The ins and outs of RND efflux pumps in *Escherichia coli*. Front Microbiol. 2015;6: 587.
28. Tanabe M, Szakonyi G, Brown KA, Henderson PJF, Nield J, Byrne B. The multidrug resistance efflux complex, EmrAB from *Escherichia coli* forms a dimer *in vitro*. Biochem Biophys Res Commun. 2009;380: 338–342.
29. Lu S, Zgurskaya HI. Role of ATP binding and hydrolysis in assembly of MacAB-TolC macrolide transporter. Mol Microbiol. 2012;86: 1132–1143.
30. Sakhtah H, Koyama L, Zhang Y, Morales DK, Fields BL, Price-Whelan A, et al. The *Pseudomonas aeruginosa* efflux pump MexGHI-OpmD transports a natural phenazine that controls gene expression and biofilm development. Proc Natl Acad Sci USA. 2016;113: E3538-47.
31. Meirelles LA, Perry EK, Bergkessel M, Newman DK. Bacterial defenses against a natural antibiotic promote collateral resilience to clinical antibiotics. PLoS Biol. 2021;19: e3001093.
32. Li X-Z, Nikaido H. Antimicrobial drug efflux pumps in *Escherichia coli*. In: Li X-Z, Elkins CA, Zgurskaya HI, editors. Efflux-mediated antimicrobial resistance in Bacteria. Cham: Springer International Publishing; 2016. pp. 219–259.
33. Ruiz C, Levy SB. Regulation of *acrAB* expression by cellular metabolites in *Escherichia coli*. J Antimicrob Chemother. 2014;69: 390–399.
34. Chubiz LM, Rao CV. Aromatic acid metabolites of *Escherichia coli* K-12 can induce the *marRAB* operon. J Bacteriol. 2010;192: 4786–4789.
35. Hirakawa H, Inazumi Y, Masaki T, Hirata T, Yamaguchi A. Indole induces the expression of multidrug exporter genes in *Escherichia coli*. Mol Microbiol. 2005;55: 1113–1126.
36. Nishino K, Honda T, Yamaguchi A. Genome-wide analyses of *Escherichia coli* gene expression responsive to the BaeSR two-component regulatory system. J Bacteriol. 2005;187: 1763–1772.
37. Nikaido E, Giraud E, Baucheron S, Yamasaki S, Wiedemann A, Okamoto K, et al. Effects of indole on drug resistance and virulence of *Salmonella enterica* serovar Typhimurium revealed by genome-wide analyses. Gut Pathog. 2012;4: 5.

38. Nishino K, Nikaido E, Yamaguchi A. Regulation of multidrug efflux systems involved in multidrug and metal resistance of *Salmonella enterica* serovar Typhimurium. J Bacteriol. 2007;189: 9066–9075.
39. Lee HH, Molla MN, Cantor CR, Collins JJ. Bacterial charity work leads to population-wide resistance. Nature. 2010;467: 82–85.
40. Paździor E, Pękala-Safińska A, Wasyl D. Phenotypic diversity and potential virulence factors of the *Shewanella putrefaciens* group isolated from freshwater fish. J Vet Res. 2019;63: 321–332.
41. Shyu JBH, Lies DP, Newman DK. Protective role of *tolC* in efflux of the electron shuttle anthraquinone-2,6-disulfonate. J Bacteriol. 2002;184: 1806–1810.
42. Meirelles LA, Newman DK. Both toxic and beneficial effects of pyocyanin contribute to the lifecycle of *Pseudomonas aeruginosa*. Mol Microbiol. 2018;110: 995–1010.
43. Lau GW, Hassett DJ, Ran H, Kong F. The role of pyocyanin in *Pseudomonas aeruginosa* infection. Trends Mol Med. 2004;10: 599–606.
44. Mavrodi DV, Blankenfeldt W, Thomashow LS. Phenazine compounds in fluorescent *Pseudomonas* spp. biosynthesis and regulation. Annu Rev Phytopathol. 2006;44: 417–445.
45. Llanes C, Köhler T, Patry I, Dehecq B, van Delden C, Plésiat P. Role of the MexEF-OprN efflux system in low-level resistance of *Pseudomonas aeruginosa* to ciprofloxacin. Antimicrob Agents Chemother. 2011;55: 5676–5684.
46. Richardot C, Juarez P, Jeannot K, Patry I, Plésiat P, Llanes C. Amino acid substitutions account for most MexS alterations in clinical *nfxC* mutants of *Pseudomonas aeruginosa*. Antimicrob Agents Chemother. 2016;60: 2302–2310.
47. Lomovskaya O, Bostian KA. Practical applications and feasibility of efflux pump inhibitors in the clinic--a vision for applied use. Biochem Pharmacol. 2006;71: 910–918.
48. Jamshidi S, Sutton JM, Rahman KM. Computational study reveals the molecular mechanism of the interaction between the efflux inhibitor PAβN and the AdeB transporter from *Acinetobacter baumannii*. ACS Omega. 2017;2: 3002–3016.
49. Wolloscheck D, Krishnamoorthy G, Nguyen J, Zgurskaya HI. Kinetic control of quorum sensing in *Pseudomonas aeruginosa* by multidrug efflux pumps. ACS Infect Dis. 2018;4: 185–195.
50. Schiessl KT, Hu F, Jo J, Nazia SZ, Wang B, Price-Whelan A, et al. Phenazine production promotes antibiotic tolerance and metabolic heterogeneity in *Pseudomonas aeruginosa* biofilms. Nat Commun. 2019;10: 762.
51. Zhu K, Chen S, Sysoeva TA, You L. Universal antibiotic tolerance arising from antibiotic-triggered accumulation of pyocyanin in *Pseudomonas aeruginosa.* PLoS Biol. 2019;17: e3000573.
52. Lister PD, Wolter DJ, Hanson ND. Antibacterial-resistant *Pseudomonas aeruginosa*: Clinical impact and complex regulation of chromosomally encoded resistance mechanisms. Clin Microbiol Rev. 2009;22: 582–610.
53. Yonehara R, Yamashita E, Nakagawa A. Crystal structures of OprN and OprJ, outer membrane factors of multidrug tripartite efflux pumps of *Pseudomonas aeruginosa*. Proteins. 2016;84: 759–769.
54. Glavier M, Puvanendran D, Salvador D, Decossas M, Phan G, Garnier C, et al. Antibiotic export by MexB multidrug efflux transporter is allosterically controlled by a MexA-OprM chaperone-like complex. Nat Commun. 2020;11: 4948.

55. Clarke-Pearson MF, Brady SF. Paerucumarin, a new metabolite produced by the *pvc* gene cluster from *Pseudomonas aeruginosa*. J Bacteriol. 2008;190: 6927–6930.
56. Iftikhar A, Asif A, Manzoor A, Azeem M, Sarwar G, Rashid N, et al. Mutation in *pvcABCD* operon of *Pseudomonas aeruginosa* modulates MexEF-OprN efflux system and hence resistance to chloramphenicol and ciprofloxacin. Microb Pathog. 2020; 104491.
57. Sokol PA, Lewis CJ, Dennis JJ. Isolation of a novel siderophore from *Pseudomonas cepacia*. J Med Microbiol. 1992;36: 184–189.
58. Darling P, Chan M, Cox AD, Sokol PA. Siderophore production by cystic fibrosis isolates of *Burkholderia cepacia*. Infect Immun. 1998;66: 874–877.
59. Visca P, Ciervo A, Sanfilippo V, Orsi N. Iron-regulated salicylate synthesis by *Pseudomonas* spp. J Gen Microbiol. 1993;139: 1995–2001.
60. Bakker PAHM, Ran L, Mercado-Blanco J. Rhizobacterial salicylate production provokes headaches! Plant Soil. 2014;382: 1–16.
61. Nair BM, Cheung K-J, Griffith A, Burns JL. Salicylate induces an antibiotic efflux pump in *Burkholderia cepacia* complex genomovar III (*B. cenocepacia*). J Clin Invest. 2004;113: 464–473.
62. Cohen SP, Levy SB, Foulds J, Rosner JL. Salicylate induction of antibiotic resistance in *Escherichia coli*: Activation of the mar operon and a mar-independent pathway. J Bacteriol. 1993;175: 7856–7862.
63. Brochado AR, Telzerow A, Bobonis J, Banzhaf M, Mateus A, Selkrig J, et al. Species-specific activity of antibacterial drug combinations. Nature. 2018;559: 259–263.
64. Burkhead KD, Schisler DA, Slininger PJ. Pyrrolnitrin production by biological control agent *Pseudomonas cepacia* B37w in culture and in colonized wounds of potatoes. Appl Environ Microbiol. 1994;60: 2031–2039.
65. Jeong Y, Kim J, Kim S, Kang Y, Nagamatsu T, Hwang I. Toxoflavin produced by *Burkholderia glumae* causing rice grain rot is responsible for inducing bacterial wilt in many field crops. Plant Dis. 2003;87: 890–895.
66. Depoorter E, Bull MJ, Peeters C, Coenye T, Vandamme P, Mahenthiralingam E. *Burkholderia*: an update on taxonomy and biotechnological potential as antibiotic producers. Appl Microbiol Biotechnol. 2016;100: 5215–5229.
67. Depoorter E, De Canck E, Coenye T, Vandamme P. *Burkholderia* bacteria produce multiple potentially novel molecules that inhibit carbapenem-resistant gram-negative bacterial pathogens. Antibiotics (Basel). 2021;10.
68. Lipuma JJ. The changing microbial epidemiology in cystic fibrosis. Clin Microbiol Rev. 2010;23: 299–323.
69. Jones C, Webster G, Mullins AJ, Jenner M, Bull MJ, Dashti Y, et al. Kill and cure: genomic phylogeny and bioactivity of *Burkholderia gladioli* bacteria capable of pathogenic and beneficial lifestyles. Microb Genom. 2021;7.
70. Stern KG. Oxidation-reduction potentials of toxoflavin. Biochem J. 1935;29: 500–508.
71. Latuasan HE, Berends W. On the origin of the toxicity of toxoflavin. Biochim Biophys Acta. 1961;52: 502–508.
72. Gencheva R, Cheng Q, Arnér ESJ. Efficient selenocysteine-dependent reduction of toxoflavin by mammalian thioredoxin reductase. Biochim Biophys Acta Gen Subj. 2018.
73. Li X, Li Y, Wang R, Wang Q, Lu L. Toxoflavin produced by *Burkholderia gladioli* from *Lycoris aurea* is a new broad-spectrum fungicide. Appl Environ Microbiol. 2019;85.

74. Kim J, Kim J-G, Kang Y, Jang JY, Jog GJ, Lim JY, et al. Quorum sensing and the LysR-type transcriptional activator ToxR regulate toxoflavin biosynthesis and transport in Burkholderia glumae. Mol Microbiol. 2004;54: 921–934.
75. Tahlan K, Ahn SK, Sing A, Bodnaruk TD, Willems AR, Davidson AR, et al. Initiation of actinorhodin export in *Streptomyces coelicolor*. Mol Microbiol. 2007;63: 951–961.
76. Willems AR, Tahlan K, Taguchi T, Zhang K, Lee ZZ, Ichinose K, et al. Crystal structures of the *Streptomyces coelicolor* TetR-like protein ActR alone and in complex with actinorhodin or the actinorhodin biosynthetic precursor (S)-DNPA. J Mol Biol. 2008;376: 1377–1387.
77. Kohanski MA, Dwyer DJ, Hayete B, Lawrence CA, Collins JJ. A common mechanism of cellular death induced by bactericidal antibiotics. Cell. 2007;130: 797–810.
78. Keren I, Wu Y, Inocencio J, Mulcahy LR, Lewis K. Killing by bactericidal antibiotics does not depend on reactive oxygen species. Science. 2013;339: 1213–1216.
79. Liu Y, Imlay JA. Cell death from antibiotics without the involvement of reactive oxygen species. Science. 2013;339: 1210–1213.
80. Dwyer DJ, Collins JJ, Walker GC. Unraveling the physiological complexities of antibiotic lethality. Annu Rev Pharmacol Toxicol. 2015;55: 313–332.
81. Zuccato E, Venturi M, Di Leo G, Colombo L, Bertolo C, Doldi SB, et al. Role of bile acids and metabolic activity of colonic bacteria in increased risk of colon cancer after cholecystectomy. Dig Dis Sci. 1993;38: 514–519.
82. Karlin DA, Mastromarino AJ, Jones RD, Stroehlein JR, Lorentz O. Fecal skatole and indole and breath methane and hydrogen in patients with large bowel polyps or cancer. J Cancer Res Clin Oncol. 1985;109: 135–141.
83. Vega NM, Allison KR, Khalil AS, Collins JJ. Signaling-mediated bacterial persister formation. Nat Chem Biol. 2012;8: 431–433.
84. Shen X, Lind J, Merenyi G. One-electron oxidation of indoles and acid-base properties of the indolyl radicals. J Phys Chem. 1987;91: 4403–4406.
85. Garbe TR, Kobayashi M, Yukawa H. Indole-inducible proteins in bacteria suggest membrane and oxidant toxicity. Arch Microbiol. 2000;173: 78–82.
86. Wei Q, Minh PNL, Dötsch A, Hildebrand F, Panmanee W, Elfarash A, et al. Global regulation of gene expression by OxyR in an important human opportunistic pathogen. Nucleic Acids Res. 2012;40: 4320–4333.
87. Ochsner UA, Vasil ML, Alsabbagh E, Parvatiyar K, Hassett DJ. Role of the *Pseudomonas aeruginosa oxyR-recG* operon in oxidative stress defense and DNA repair: OxyR-dependent regulation of *katB-ankB*, *ahpB*, and *ahpC-ahpF*. J Bacteriol. 2000;182: 4533–4544.
88. Romsang A, Dubbs JM, Mongkolsuk S. The iron-sulfur cluster biosynthesis regulator IscR contributes to iron homeostasis and resistance to oxidants in *Pseudomonas Aeruginosa*. In: de Bruijn FJ, editor. Stress and environmental regulation of gene expression and adaptation in bacteria. Hoboken, NJ, USA: John Wiley & Sons, Inc.; 2016. pp. 1090–1102.
89. Perry EK, Newman DK. The transcription factors ActR and SoxR differentially affect the phenazine tolerance of *Agrobacterium tumefaciens*. Mol Microbiol. 2019;112: 199–218.
90. Voggu L, Schlag S, Biswas R, Rosenstein R, Rausch C, Götz F. Microevolution of cytochrome *bd* oxidase in Staphylococci and its implication in resistance to respiratory toxins released by *Pseudomonas*. J Bacteriol. 2006;188: 8079–8086.

91. Hassett DJ, Charniga L, Bean K, Ohman DE, Cohen MS. Response of *Pseudomonas aeruginosa* to pyocyanin: mechanisms of resistance, antioxidant defenses, and demonstration of a manganese-cofactored superoxide dismutase. Infect Immun. 1992;60: 328–336.
92. Priuska EM, Schacht J. Formation of free radicals by gentamicin and iron and evidence for an iron/gentamicin complex. Biochem Pharmacol. 1995;50: 1749–1752.
93. Prayle A, Watson A, Fortnum H, Smyth A. Side effects of aminoglycosides on the kidney, ear and balance in cystic fibrosis. Thorax. 2010;65: 654–658.
94. Mosel M, Li L, Drlica K, Zhao X. Superoxide-mediated protection of *Escherichia coli* from antimicrobials. Antimicrob Agents Chemother. 2013;57: 5755–5759.
95. Alexander HK, MacLean RC. Stochastic bacterial population dynamics restrict the establishment of antibiotic resistance from single cells. Proc Natl Acad Sci USA. 2020;117: 19455–19464.
96. Dwyer DJ, Belenky PA, Yang JH, MacDonald IC, Martell JD, Takahashi N, et al. Antibiotics induce redox-related physiological alterations as part of their lethality. Proc Natl Acad Sci USA. 2014;111: E2100-9.
97. Belenky P, Ye JD, Porter CBM, Cohen NR, Lobritz MA, Ferrante T, et al. Bactericidal antibiotics induce toxic metabolic perturbations that lead to cellular damage. Cell Rep. 2015;13: 968–980.
98. Saini V, Cumming BM, Guidry L, Lamprecht DA, Adamson JH, Reddy VP, et al. Ergothioneine maintains redox and bioenergetic homeostasis essential for drug susceptibility and virulence of *Mycobacterium tuberculosis*. Cell Rep. 2016;14: 572–585.
99. Hall JW, Yang J, Guo H, Ji Y. The *Staphylococcus aureus* AirSR two-component system mediates reactive oxygen species resistance via transcriptional regulation of staphyloxanthin production. Infect Immun. 2017;85.
100. Clauditz A, Resch A, Wieland K-P, Peschel A, Götz F. Staphyloxanthin plays a role in the fitness of *Staphylococcus aureus* and its ability to cope with oxidative stress. Infect Immun. 2006;74: 4950–4953.
101. Liu GY, Doran KS, Lawrence T, Turkson N, Puliti M, Tissi L, et al. Sword and shield: linked group B streptococcal beta-hemolysin/cytolysin and carotenoid pigment function to subvert host phagocyte defense. Proc Natl Acad Sci USA. 2004;101: 14491–14496.
102. Wu C, Cichewicz R, Li Y, Liu J, Roe B, Ferretti J, et al. Genomic island TnSmu2 of *Streptococcus mutans* harbors a nonribosomal peptide synthetase-polyketide synthase gene cluster responsible for the biosynthesis of pigments involved in oxygen and H_2O_2 tolerance. Appl Environ Microbiol. 2010;76: 5815–5826.
103. Edge R, Truscott TG. Singlet oxygen and free radical reactions of retinoids and carotenoids-A Review. Antioxidants (Basel). 2018;7.
104. Young AJ, Lowe GL. Carotenoids-antioxidant properties. Antioxidants (Basel). 2018;7.
105. Hong Y, Zeng J, Wang X, Drlica K, Zhao X. Post-stress bacterial cell death mediated by reactive oxygen species. Proc Natl Acad Sci USA. 2019;116: 10064–10071.
106. Shatalin K, Shatalina E, Mironov A, Nudler E. H_2S: a universal defense against antibiotics in bacteria. Science. 2011;334: 986–990.
107. Tkachenko AG, Fedotova MV. Dependence of protective functions of *Escherichia coli* polyamines on strength of stress caused by superoxide radicals. Biochemistry (Mosc). 2007;72: 109–116.

108. El-Halfawy OM, Valvano MA. Putrescine reduces antibiotic-induced oxidative stress as a mechanism of modulation of antibiotic resistance in *Burkholderia cenocepacia*. Antimicrob Agents Chemother. 2014;58: 4162–4171.
109. El-Halfawy OM, Valvano MA. Chemical communication of antibiotic resistance by a highly resistant subpopulation of bacterial cells. PLoS One. 2013;8: e68874.
110. Tkachenko AG, Akhova AV, Shumkov MS, Nesterova LY. Polyamines reduce oxidative stress in *Escherichia coli* cells exposed to bactericidal antibiotics. Res Microbiol. 2012;163: 83–91.
111. Kreamer NN, Costa F, Newman DK. The ferrous iron-responsive BqsRS two-component system activates genes that promote cationic stress tolerance. MBio. 2015;6: e02549.
112. Häussler S, Becker T. The pseudomonas quinolone signal (PQS) balances life and death in *Pseudomonas aeruginosa* populations. PLoS Pathog. 2008;4: e1000166.
113. Bredenbruch F, Geffers R, Nimtz M, Buer J, Häussler S. The *Pseudomonas aeruginosa* quinolone signal (PQS) has an iron-chelating activity. Environ Microbiol. 2006;8: 1318–1329.
114. Nguyen D, Joshi-Datar A, Lepine F, Bauerle E, Olakanmi O, Beer K, et al. Active starvation responses mediate antibiotic tolerance in biofilms and nutrient-limited bacteria. Science. 2011;334: 982–986.
115. Han M-L, Zhu Y, Creek DJ, Lin Y-W, Gutu AD, Hertzog P, et al. Comparative metabolomics and transcriptomics reveal multiple pathways associated with polymyxin killing in *Pseudomonas aeruginosa*. mSystems. 2019;4.
116. Sampson TR, Liu X, Schroeder MR, Kraft CS, Burd EM, Weiss DS. Rapid killing of *Acinetobacter baumannii* by polymyxins is mediated by a hydroxyl radical death pathway. Antimicrob Agents Chemother. 2012;56: 5642–5649.
117. Trimble MJ, Mlynárčik P, Kolář M, Hancock REW. Polymyxin: alternative mechanisms of action and resistance. Cold Spring Harb Perspect Med. 2016;6.
118. Bottery MJ, Pitchford JW, Friman V-P. Ecology and evolution of antimicrobial resistance in bacterial communities. ISME J. 2021;15: 939–948.
119. Welp AL, Bomberger JM. Bacterial community interactions during chronic respiratory disease. Front Cell Infect Microbiol. 2020;10: 213.
120. Vega NM, Allison KR, Samuels AN, Klempner MS, Collins JJ. *Salmonella typhimurium* intercepts *Escherichia coli* signaling to enhance antibiotic tolerance. Proc Natl Acad Sci USA. 2013;110: 14420–14425.
121. Kim J, Shin B, Park C, Park W. Indole-induced activities of β-lactamase and efflux pump confer ampicillin resistance in *Pseudomonas putida* KT2440. Front Microbiol. 2017;8: 433.
122. Bhargava N, Sharma P, Capalash N. Pyocyanin stimulates quorum sensing-mediated tolerance to oxidative stress and increases persister cell populations in *Acinetobacter baumannii*. Infect Immun. 2014;82: 3417–3425.
123. Heindorf M, Kadari M, Heider C, Skiebe E, Wilharm G. Impact of *Acinetobacter baumannii* superoxide dismutase on motility, virulence, oxidative stress resistance and susceptibility to antibiotics. PLoS One. 2014;9: e101033.
124. Bandara HMHN, Wood DLA, Vanwonterghem I, Hugenholtz P, Cheung BPK, Samaranayake LP. Fluconazole resistance in *Candida albicans* is induced by *Pseudomonas aeruginosa* quorum sensing. Sci Rep. 2020;10: 7769.

125. Chmiel JF, Aksamit TR, Chotirmall SH, Dasenbrook EC, Elborn JS, LiPuma JJ, et al. Antibiotic management of lung infections in cystic fibrosis. I. The microbiome, methicillin-resistant *Staphylococcus aureus*, gram-negative bacteria, and multiple infections. Annals of the American Thoracic Society. 2014;11: 1120–1129.
126. Schwab U, Abdullah LH, Perlmutt OS, Albert D, Davis CW, Arnold RR, et al. Localization of *Burkholderia cepacia* complex bacteria in cystic fibrosis lungs and interactions with *Pseudomonas aeruginosa* in hypoxic mucus. Infect Immun. 2014;82: 4729–4745.
127. Wood KB, Cluzel P. Trade-offs between drug toxicity and benefit in the multi-antibiotic resistance system underlie optimal growth of *E. coli*. BMC Syst Biol. 2012;6: 48.
128. Yung DBY, Sircombe KJ, Pletzer D. Friends or enemies? The complicated relationship between *Pseudomonas aeruginosa* and *Staphylococcus aureus*. Mol Microbiol. 2021;116: 1–15.
129. Camus L, Briaud P, Vandenesch F, Moreau K. How bacterial adaptation to cystic fibrosis environment shapes interactions between *Pseudomonas aeruginosa* and *Staphylococcus aureus*. Front Microbiol. 2021;12: 617784.
130. Briaud P, Bastien S, Camus L, Boyadjian M, Reix P, Mainguy C, et al. Impact of coexistence phenotype between *Staphylococcus aureus* and *Pseudomonas aeruginosa* isolates on clinical outcomes among cystic fibrosis patients. Front Cell Infect Microbiol. 2020;10: 266.
131. Radlinski L, Rowe SE, Kartchner LB, Maile R, Cairns BA, Vitko NP, et al. *Pseudomonas aeruginosa* exoproducts determine antibiotic efficacy against *Staphylococcus aureus*. PLoS Biol. 2017;15: e2003981.
132. Noto MJ, Burns WJ, Beavers WN, Skaar EP. Mechanisms of pyocyanin toxicity and genetic determinants of resistance in *Staphylococcus aureus*. J Bacteriol. 2017;199.
133. Orazi G, Ruoff KL, O'Toole GA. *Pseudomonas aeruginosa* increases the sensitivity of biofilm-grown *Staphylococcus aureus* to membrane-targeting antiseptics and antibiotics. MBio. 2019;10.
134. Orazi G, O'Toole GA. *Pseudomonas aeruginosa* alters *Staphylococcus aureus* sensitivity to vancomycin in a biofilm model of cystic fibrosis infection. MBio. 2017;8.
135. Biswas L, Biswas R, Schlag M, Bertram R, Götz F. Small-colony variant selection as a survival strategy for *Staphylococcus aureus* in the presence of *Pseudomonas aeruginosa*. Appl Environ Microbiol. 2009;75: 6910–6912.
136. McNamara PJ, Proctor RA. *Staphylococcus aureus* small colony variants, electron transport and persistent infections. Int J Antimicrob Agents. 2000;14: 117–122.
137. Wilson R, Sykes DA, Watson D, Rutman A, Taylor GW, Cole PJ. Measurement of *Pseudomonas aeruginosa* phenazine pigments in sputum and assessment of their contribution to sputum sol toxicity for respiratory epithelium. Infect Immun. 1988;56: 2515–2517.
138. Cruickshank CN, Lowbury EJ. The effect of pyocyanin on human skin cells and leucocytes. Br J Exp Pathol. 1953;34: 583–587.
139. Levin-Reisman I, Brauner A, Ronin I, Balaban NQ. Epistasis between antibiotic tolerance, persistence, and resistance mutations. Proc Natl Acad Sci USA. 2019;116: 14734–14739.
140. Santi I, Manfredi P, Maffei E, Egli A, Jenal U. Evolution of antibiotic tolerance shapes resistance development in chronic *Pseudomonas aeruginosa* infections. MBio. 2021;12.

141. Windels EM, Michiels JE, Fauvart M, Wenseleers T, Van den Bergh B, Michiels J. Bacterial persistence promotes the evolution of antibiotic resistance by increasing survival and mutation rates. ISME J. 2019;13: 1239–1251.
142. Levin-Reisman I, Ronin I, Gefen O, Braniss I, Shoresh N, Balaban NQ. Antibiotic tolerance facilitates the evolution of resistance. Science. 2017;355: 826–830.
143. Liu J, Gefen O, Ronin I, Bar-Meir M, Balaban NQ. Effect of tolerance on the evolution of antibiotic resistance under drug combinations. Science. 2020;367: 200–204.
144. Martina P, Feliziani S, Juan C, Bettiol M, Gatti B, Yantorno O, et al. Hypermutation in *Burkholderia cepacia* complex is mediated by DNA mismatch repair inactivation and is highly prevalent in cystic fibrosis chronic respiratory infection. Int J Med Microbiol. 2014;304: 1182–1191.
145. Ryan RP, Monchy S, Cardinale M, Taghavi S, Crossman L, Avison MB, et al. The versatility and adaptation of bacteria from the genus *Stenotrophomonas*. Nat Rev Microbiol. 2009;7: 514–525.
146. Walterson AM, Stavrinides J. *Pantoea*: insights into a highly versatile and diverse genus within the Enterobacteriaceae. FEMS Microbiol Rev. 2015;39: 968–984.
147. Smith DDN, Kirzinger MWB, Stavrinides J. Draft genome sequence of the antibiotic-producing cystic fibrosis isolate *Pantoea agglomerans* Tx10. Genome Announc. 2013;1.
148. König S, Vogel H-J, Harms H, Worrich A. Physical, chemical and biological effects on soil bacterial dynamics in microscale models. Front Ecol Evol. 2020;8.
149. Severi E, Thomas GH. Antibiotic export: transporters involved in the final step of natural product production. Microbiology (Reading, Engl). 2019;165: 805–818.
150. Martín JF, Casqueiro J, Liras P. Secretion systems for secondary metabolites: how producer cells send out messages of intercellular communication. Curr Opin Microbiol. 2005;8: 282–293.
151. Crits-Christoph A, Bhattacharya N, Olm MR, Song YS, Banfield JF. Transporter genes in biosynthetic gene clusters predict metabolite characteristics and siderophore activity. Genome Res. 2020;
152. Glasser NR, Saunders SH, Newman DK. The colorful world of extracellular electron shuttles. Annu Rev Microbiol. 2017;71: 731–751.
153. Yan J, Bassler BL. Surviving as a community: antibiotic tolerance and persistence in bacterial biofilms. Cell Host Microbe. 2019;26: 15–21.
154. Ersoy SC, Heithoff DM, Barnes L, Tripp GK, House JK, Marth JD, et al. Correcting a fundamental flaw in the paradigm for antimicrobial susceptibility testing. EBioMedicine. 2017;20: 173–181.
155. Song Y, Liu C-I, Lin F-Y, No JH, Hensler M, Liu Y-L, et al. Inhibition of staphyloxanthin virulence factor biosynthesis in *Staphylococcus aureus*: *in vitro*, *in vivo*, and crystallographic results. J Med Chem. 2009;52: 3869–3880.
156. Liu C-I, Liu GY, Song Y, Yin F, Hensler ME, Jeng W-Y, et al. A cholesterol biosynthesis inhibitor blocks *Staphylococcus aureus* virulence. Science. 2008;319: 1391–1394.
157. Costa KC, Glasser NR, Conway SJ, Newman DK. Pyocyanin degradation by a tautomerizing demethylase inhibits *Pseudomonas aeruginosa* biofilms. Science. 2017;355: 170–173.

158. VanDrisse CM, Lipsh-Sokolik R, Khersonsky O, Fleishman SJ, Newman DK. Computationally designed pyocyanin demethylase acts synergistically with tobramycin to kill recalcitrant *Pseudomonas aeruginosa* biofilms. Proc Natl Acad Sci USA. 2021;118.
159. Liu GY, Nizet V. Color me bad: microbial pigments as virulence factors. Trends Microbiol. 2009;17: 406–413.
160. Shatalin K, Nuthanakanti A, Kaushik A, Shishov D, Peselis A, Shamovsky I, et al. Inhibitors of bacterial H_2S biogenesis targeting antibiotic resistance and tolerance. Science. 2021;372: 1169–1175.
161. Abbott IJ, Peleg AY. *Stenotrophomonas*, *Achromobacter*, and nonmelioid *Burkholderia* species: antimicrobial resistance and therapeutic strategies. Semin Respir Crit Care Med. 2015;36: 99–110.
162. Blin K, Shaw S, Steinke K, Villebro R, Ziemert N, Lee SY, et al. antiSMASH 5.0: updates to the secondary metabolite genome mining pipeline. Nucleic Acids Res. 2019;47: W81–W87.
163. Liu J, Prindle A, Humphries J, Gabalda-Sagarra M, Asally M, Lee DD, et al. Metabolic co-dependence gives rise to collective oscillations within biofilms. Nature. 2015;523: 550–554.
164. Liu J, Martinez-Corral R, Prindle A, Lee D-YD, Larkin J, Gabalda-Sagarra M, et al. Coupling between distant biofilms and emergence of nutrient time-sharing. Science. 2017;356: 638–642.
165. Spero MA, Newman DK. Chlorate specifically targets oxidant-starved, antibiotic-tolerant populations of *Pseudomonas aeruginosa* biofilms. MBio. 2018;9.
166. Hazan R, Que YA, Maura D, Strobel B, Majcherczyk PA, Hopper LR, et al. Auto poisoning of the respiratory chain by a quorum-sensing-regulated molecule favors biofilm formation and antibiotic tolerance. Curr Biol. 2016;26: 195–206.
167. Saunders SH, Tse ECM, Yates MD, Otero FJ, Trammell SA, Stemp EDA, et al. Extracellular DNA promotes efficient extracellular electron transfer by pyocyanin in *Pseudomonas aeruginosa* biofilms. Cell. 2020;182: 919–932.e19.
168. Rosche WA, Foster PL. Determining mutation rates in bacterial populations. Methods. 2000;20: 4–17.
169. Zheng Q. A new practical guide to the Luria-Delbrück protocol. Mutat Res. 2015;781: 7–13.
170. Somayaji R, Parkins MD, Shah A, Martiniano SL, Tunney MM, Kahle JS, et al. Antimicrobial susceptibility testing (AST) and associated clinical outcomes in individuals with cystic fibrosis: A systematic review. J Cyst Fibros. 2019;18: 236–243.
171. Hurley MN, Ariff AHA, Bertenshaw C, Bhatt J, Smyth AR. Results of antibiotic susceptibility testing do not influence clinical outcome in children with cystic fibrosis. J Cyst Fibros. 2012;11: 288–292.
172. Jorgensen JH, Ferraro MJ. Antimicrobial susceptibility testing: a review of general principles and contemporary practices. Clin Infect Dis. 2009;49: 1749–1755.
173. Brown MR. Nutrient depletion and antibiotic susceptibility. J Antimicrob Chemother. 1977;3: 198–201.
174. Shukla P, Khodade VS, SharathChandra M, Chauhan P, Mishra S, Siddaramappa S, et al. “On demand” redox buffering by H_2S contributes to antibiotic resistance revealed by a bacteria-specific H_2S donor. Chem Sci. 2017;8: 4967–4972.

175. Anderson RJ, Newman MS. The chemistry of the lipids of tubercle bacilli. J Bio Chem. 1933;103: 405–412.
176. Gardner PR. Superoxide production by the mycobacterial and pseudomonad quinoid pigments phthiocol and pyocyanine in human lung cells. Arch Biochem Biophys. 1996;333: 267–274.
177. Giddens SR, Feng Y, Mahanty HK. Characterization of a novel phenazine antibiotic gene cluster in *Erwinia herbicola* Eh1087. Mol Microbiol. 2002;45: 769–783.
178. Giddens SR, Bean DC. Investigations into the *in vitro* antimicrobial activity and mode of action of the phenazine antibiotic D-alanylgriseoluteic acid. Int J Antimicrob Agents. 2007;29: 93–97.
179. Krishnamurthi VS, Buckley PJ, Duerre JA. Pigment formation from l-tryptophan by a particulate fraction from an *Achromobacter* species. Arch Biochem Biophys. 1969;130: 636–645.
180. Wells JM, Cole RJ, Kirksey JW. Emodin, a toxic metabolite of *Aspergillus wentii* isolated from weevil-damaged chestnuts. Appl Microbiol. 1975;30: 26–28.
181. Lim FY, Hou Y, Chen Y, Oh J-H, Lee I, Bugni TS, et al. Genome-based cluster deletion reveals an endocrocin biosynthetic pathway in *Aspergillus fumigatus*. Appl Environ Microbiol. 2012;78: 4117–4125.

C h a p t e r 3

PHENAZINE PRODUCTION IS A "DOUBLE-EDGED SWORD": The nuanced physiological effects of pyocyanin on *Pseudomonas aeruginosa*

This chapter is adapted from:

Meirelles, L.A., and Newman, D.K. (2018). Both toxic and beneficial effects of pyocyanin contribute to the lifecycle of *Pseudomonas aeruginosa*. *Mol Microbiol* **110**: 995-1010. https://doi.org/10.1111/mmi.14132

Abstract

Pseudomonas aeruginosa, an opportunistic pathogen, produces redox-active pigments called phenazines. Pyocyanin (PYO, the blue phenazine) plays an important role during biofilm development. Paradoxically, PYO auto-poisoning can stimulate cell death and release of extracellular DNA (eDNA), yet PYO can also promote survival within biofilms when cells are oxidant-limited. Here we identify the environmental and physiological conditions in planktonic culture that promote PYO-mediated cell death. We demonstrate that PYO auto-poisoning is enhanced when cells are starved for carbon. In the presence of PYO, cells activate a set of genes involved in energy-dependent defenses, including: (i) the oxidative stress response, (ii) RND efflux systems and (iii) iron-sulfur cluster biogenesis factors. *P. aeruginosa* can avoid PYO poisoning when reduced carbon is available, but blockage of adenosine triphosphate (ATP) synthesis either through carbon limitation or direct inhibition of the F_0F_1-ATP synthase triggers death and eDNA release. Finally, even though PYO is toxic to the majority of the population when cells are nutrient limited, a subset of cells is intrinsically PYO resistant. The effect of PYO on the producer population thus appears to be dynamic, playing dramatically different yet predictable roles throughout distinct stages of growth, helping rationalize its multifaceted contributions to biofilm development.

Introduction

In nature, bacteria rarely grow alone and mostly live in microbial communities called biofilms. The term "biofilm" refers to aggregates of microorganisms embedded in a self-produced, extracellular matrix [1]. Biofilms are important in many contexts, not the least of which is human health, as diverse pathogens become significantly more drug-tolerant when they adopt a biofilm lifestyle rather than a free-growing state [2]. Among the different bacteria that can form biofilms, *Pseudomonas aeruginosa* is one of the most notorious: a globally-significant, opportunistic pathogen that contributes to many types of infections [3].

The biofilm extracellular matrix comprises diverse extracellular polymeric substances (EPS), including polysaccharides, proteins, lipids and extracellular DNA (eDNA) [4]. Extracellular DNA is an important building component of the matrix and has become a target in biofilm-control approaches [5]. The importance of eDNA during biofilm formation has been established for several bacterial species, as recently reviewed by [6]. In the *P. aeruginosa* biofilm matrix, eDNA is the most abundant polymer, often accounting for more than 50% of the extracellular matrix; its removal can significantly disrupt biofilm structure [7–9]. It is well known that most of the eDNA important for biofilm formation in *P. aeruginosa* biofilms comes from lysis of a subpopulation of the cells [10]. A few different mechanisms for cell lysis have been described for *P. aeruginosa*, including activation of prophage endolysins that disrupt the cell wall and release DNA and other cytoplasmic contents to the environment [11–13]. This type of eDNA release is stimulated under stressful conditions. Auto-poisoning through production of the small molecule 2-n-heptyl-4-hydroxyquinoline-N-oxide (HQNO) also leads to eDNA release and has a direct impact on biofilm formation [14]. We use the terms "auto-poisoning," "cell death," and "cell lysis" as follows: auto-poisoning is the toxic effect caused by a molecule that eventually can kill the producing cells; after auto-poisoning, different cell death processes can be activated, which may or may not lead to cell lysis (breaking down of the cell membrane) and eDNA release [15,16].

In addition to being a model biofilm-forming organism, *P. aeruginosa* is also known for its production of colorful, redox-active molecules called phenazines—dibenzo annulated pyrazines, containing two nitrogen atoms in the center ring that mediate proton-coupled electron

transfer [17–19]. Over the last decade, a variety of beneficial physiological functions have been attributed to phenazines, for example, cell signaling, electron shuttling to diverse oxidants and promotion of survival under electron acceptor limitation [20–23], with different functions attributed to different phenazines. One of the best studied phenazines is pyocyanin (PYO), which has medical importance and has long been considered a virulence factor that is toxic to host cells [24]. This toxicity is mainly due to its capacity to quickly reduce molecular oxygen, thereby generating superoxide, which by enzymatic or abiotic dismutation generates hydrogen peroxide [25,26].

Even though PYO production can enhance biofilm formation in *P. aeruginosa* [27,28], at which stages of biofilm development and precisely how it acts, are not fully understood. Previous studies suggest that PYO might mediate biofilm development in at least three different, complementary ways: (i) causing auto-poisoning and eDNA release during early stages of biofilm formation, mostly due to generation of oxidative stress [29,30], which we expand upon in this study; (ii) indirectly modulating levels of the second messenger bis-(3′,5′)-cyclic-dimeric-guanosine (c-di-GMP) and EPS production [31]; and (iii) stimulating expansion of biofilms/aggregates under anoxic/hypoxic conditions, where PYO can function as an alternative electron acceptor and alleviate reducing stress [30,32,33]. In all cases, PYO-modulated effects—be they beneficial or deleterious, at the level of the single cell—seem to be tightly linked to environmental and physiological conditions. Accordingly, we set out to determine how different conditions commonly encountered by cellular populations at distinct growth stages result in PYO-dependent cellular effects, focusing primarily on cell death. We demonstrate that PYO production has predictable, distinct and dramatic cellular consequences, according to the physiological state of the producer.

Results

Phenazine production stimulates a morphologically-distinct type of cell death early in biofilm development

We started by imaging early-stage biofilms attached to glass, when cells settle on the surface and form microcolonies. eDNA is known to play an important structural role at this stage of biofilm development [8]. We performed a standard biofilm development assay and quantified phenazine auto-poisoning using the wild-type (WT) strain of *P. aeruginosa* PA14 (*Pa* PA14) that produces different phenazines, including PYO, and a Δ*phz* strain that cannot make phenazines (both *phz1* and *phz2* operons are deleted in this strain [20]). We grew WT and Δ*phz Pa* PA14 cells in 8-well chambers for 6 hours. In this assay, cells attach to the coverslip on the bottom of the chamber to initiate biofilm formation (Fig. 1A). We noticed significant amounts of cell death in these young biofilms (Fig. 1A). In addition, we found that the WT attached cells died more than Δ*phz* cells (Fig. 1B), consistent with the observation that phenazine production increases cell death in biofilms.

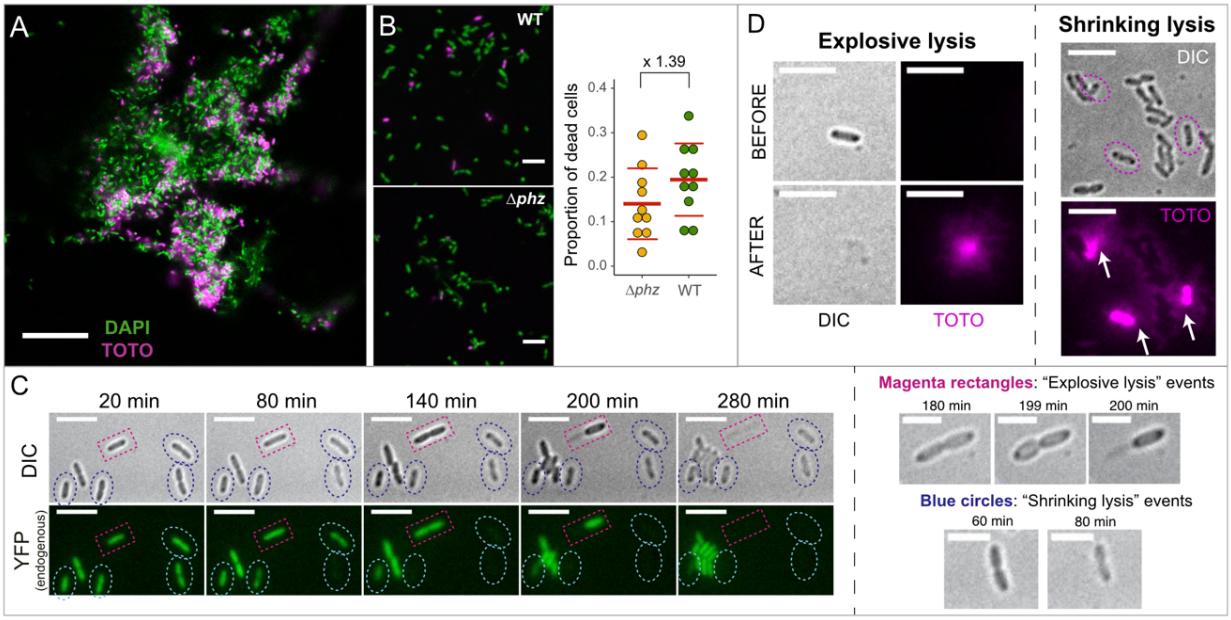

Figure 1. Phenazine production increases cell death early in biofilm development, and cell death happens in two morphologically-distinct ways. **A.** Picture of a 6-hour WT biofilm showing dead cells stained with TOTO-1 iodide (magenta), which does not penetrate live cells; scale bar: 20 μm. **B**. WT strain shows higher levels of cell death when compared to the Δ*phz* strain that cannot produce phenazines. *Left*: representative pictures of attached live (green-

DAPI) and dead (magenta-TOTO) cells – scale bars: 5 μm; *right*: quantification of cell death for WT and Δ*phz*. Red lines show the average + standard deviation of the proportion of dead cells for both treatments. Ratio of cell death WT/Δ*phz* = 1.39. **C**. Time-lapse of cells growing on agar pads showing the two morphologically-distinct cell death events: "shrinking" (blue circles) and "explosive" lysis (magenta rectangles); scale bars: 5 μm. Zoomed in pictures for both are shown on the right (scale bars: 3 μm). Cells were constitutively expressing yellow fluorescent protein (YFP), and fluorescence loss combined with morphology change (DIC) can be seen during cell death. **D**. Both explosive and shrinking lysis release DNA and other cellular contents into the environment. Explosive lysis quickly spreads eDNA extracellularly (left), but eDNA also leaks out of dead cells after shrinkage events (right: note the cloud of fluorescence [white arrows] leaking from the three dead cells [circles, DIC]). Scale bars: 5 μm. Brightness was increased for better visualization of the TOTO signal.

Next, we visualized cell death at the single-cell level. Because previous studies suggested that PYO production can cause eDNA release [29], we used this phenazine for these experiments. Cells in mid-exponential phase were washed and re-suspended on top of agarose pads containing 100 μM PYO and imaged using fluorescence microscopy. When looking at the cells, we observed at least two morphologically-distinct death events that we refer to as "explosive" and "shrinking lysis" (Fig. 1C). Explosive cell lysis in *P. aeruginosa* occurs in different strains (including PA14, PAO1, PAK, PA103 and others), stimulating eDNA release and biofilm formation [13]. It is caused by the activation of a prophage endolysin (*lys*) present in the R- and F-pyocin gene cluster in the *P. aeruginosa* genome, and is activated under stressful conditions [13]. We observed a very similar phenomenon happening during our experiments (Fig. 1C). Yet we also noticed a different cell death phenotype, "shrinking lysis," where cells contract in size at the moment of death (Fig. 1C); in contrast to explosive lysis, these cells remain visible under the microscope after death (Fig. 1C). Phenazine production increases shrinking lysis during early biofilm development (Fig. 1B); to our knowledge, this cell death phenotype has not been previously characterized. It was previously shown that after explosive lysis, all the cytoplasmic contents (including DNA) are expelled to the environment (Fig. 1D-left, [13]). To test if shrinking lysis events can also release eDNA in the medium, we used TOTO-1 iodide, a nucleic acid stain that does not penetrate living cells [34]. We observed that eDNA slowly leaks out of shrunken cells, indicating that shrinking lysis provides an alternate route for eDNA release at an early stage in biofilm development (Fig. 1D). Together, these data show that phenazine production stimulates auto-poisoning in *Pa* PA14 biofilms, enhancing eDNA release to the environment by triggering a morphologically-distinct type of cell death.

PYO increases cell death in liquid cultures under stationary phase conditions

Heterogeneity during biofilm development and low efficiency of eDNA quantification in biofilm assays limit the range of conditions we can readily control to study phenazine-mediated eDNA release. Therefore, we switched to experiments using planktonic cultures. First, we checked whether the enhanced cell death we saw in our early stage biofilm experiments could be recapitulated under planktonic growth conditions. We measured the number of colony forming units (CFU) from cultures of WT and Δ*phz* strains over the course of batch growth (Fig. 2A). By the first time point (18h), the WT cultures had already produced considerable amounts of phenazines in the medium, particularly the blue phenazine PYO (see tubes in Fig. 2A). Standard incubator shaking (250 rpm) was sufficient to maintain PYO in its oxidized state (blue color). WT cultures consistently showed lower CFU recovery than Δ*phz* cultures, and this difference increased over time. Adding physiologically relevant amounts of exogenous PYO (100 μM) to the Δ*phz* culture recapitulated poisoning levels present in WT (Fig. 2A).

In addition to PYO, *P. aeruginosa* strains produce and secrete other phenazines, including phenazine-1-carboxylic acid (PCA), phenazine-1-carboxamide (PCN) and 1-hydroxyphenazine (1-OH-PHZ) [18]. Because different phenazines can affect cells in different ways [35], we compared the toxicity of these four phenazines. Δ*phz* cells were re-suspended in phosphate buffer with a given phenazine, and survival was measured after 24 and 48 hours. PYO is the most toxic phenazine (Fig. 2B), followed by 1-OH-PHZ, PCN and PCA. Perhaps not surprisingly, phenazine toxicity under oxic conditions correlates with their oxygen reactivity: the faster a phenazine reduces oxygen abiotically, the higher its toxicity (Fig. 2B, [36]). Because (*i*) *Pa* PA14 produces significant amounts of PYO, (*ii*) PYO causes the highest toxicity, and (*iii*) PYO production is known to be involved in eDNA release [29], we focused specifically on PYO-mediated cell death and eDNA release for the remainder of our experiments.

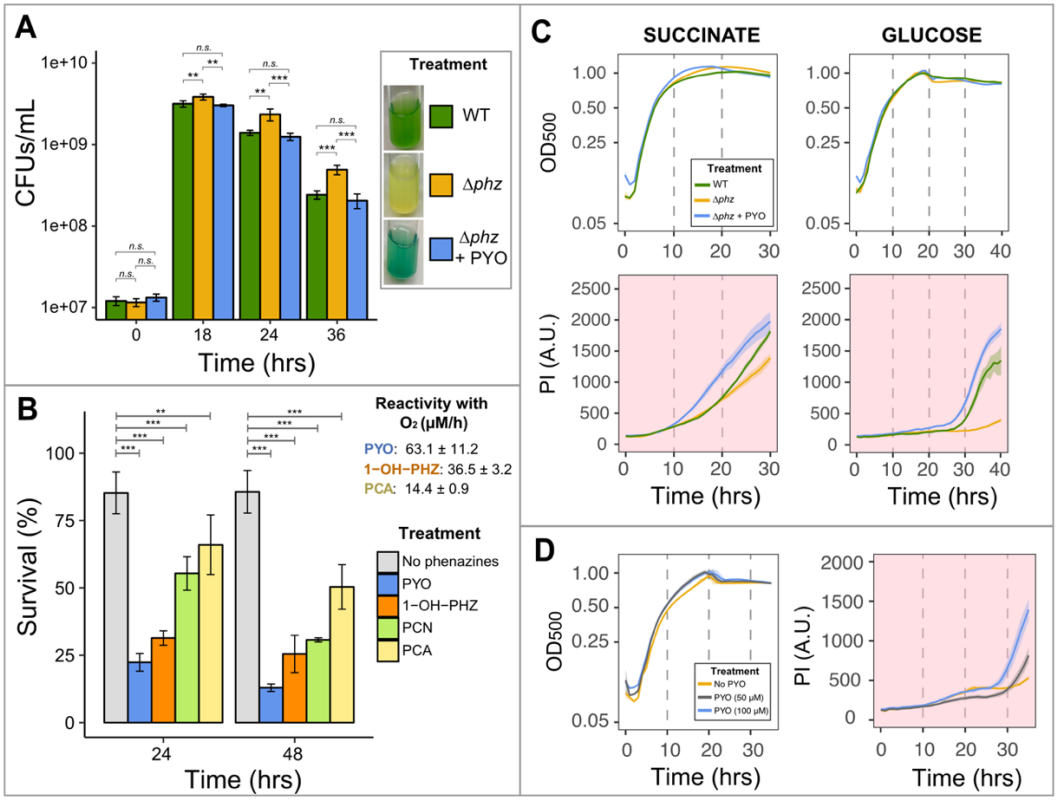

Figure 2. Pyocyanin production causes auto-poisoning and cell death in *Pa* PA14. A. Viability assay shows a faster decrease of CFUs for the WT producing phenazines compared to the Δ*phz* strain; addition of exogenous PYO restores WT poisoning levels. Culture medium used: succinate minimal medium (SMM – see Experimental Procedures), with 40 mM sodium succinate. **B.** Phenazines induce a range of toxicity, with PYO being the most lethal. O_2-reactivity constants previously measured for three of the four used phenazines [36] are also given, showing a correlation between O_2 reactivity and toxicity. For A-B, we performed One-way ANOVA ($p < 0.05$) with Tukey's HSD multiple-comparison test ([*n.s.* = $p > 0.05$ - not a statistically significant difference]; [* = $p < 0.05$]; [** = $p < 0.01$]; [*** = $p < 0.001$]). For p-values of all comparisons between phenazines, see Table S2. Bar graphs represent averages of four replicates and error bars represent standard deviation (SD). **C.** High-throughput plate reader assay confirms higher levels of auto-poisoning due to PYO production. *Top*: optical density at 500nm (OD_{500}) measurements for growth curve; *bottom*: propidium iodide (PI) fluorescence, always presented with background colored in light red, indicating cell death. Minimal medium with different carbon sources were used and showed similar trends, with PYO increasing poisoning (sodium succinate concentration: 40 mM; glucose concentration: 10 mM). **D**. PYO poisoning is concentration dependent (glucose concentration: 10 mM). Plotted lines represent averages of six replicates and shaded areas are SD.

Though CFU counting can reveal the absolute number of viable cells in a culture for a given time point, this method is not conducive to sampling multiple conditions with high temporal resolution. To overcome this limitation, we developed a high-throughput approach using a plate reader assay to quantify cell growth and death simultaneously. Growth was measured by reading optical density (OD_{500}); at the same time, the fluorescence of propidium iodide (PI) dye added to cultures served as a proxy for cell death. Similar to TOTO-1 iodide (used in the biofilm

experiments), PI cannot penetrate live cells and thus has been used as a cell death marker [34]. Because the TOTO fluorescence spectrum overlaps with the background fluorescence of *Pseudomonas* cultures, PI was a better dye for this purpose (see Experimental Procedures). By measuring OD_{500} and PI fluorescence together, we could track the dynamics of auto-poisoning through PYO production at fine temporal resolution.

Confirming results from the CFU experiment, WT *Pa* PA14 consistently had a higher cell death signal when compared to the Δ*phz* mutant (Fig. 2C). In addition, exogenously adding PYO to Δ*phz* increased the death signal (Fig. 2C). The PYO-triggered cell death phenomenon is concentration dependent, with higher concentrations of PYO promoting more cell death (Fig. 2D). The increased cell death of WT in comparison to Δ*phz* is evident regardless of the carbon-source (e.g. succinate or glucose – Fig. 2C). The PI signal increase correlated with cells entering stationary phase (Fig. 2C). This was expected for the WT strain, because PYO production is quorum-sensing regulated [37]. However, PYO was exogenously added to Δ*phz* cultures at the beginning of the experiment. Therefore, even when cells had 100 μM PYO present in their environment prior to exponential growth, cell death was triggered only after cells had entered stationary phase (Fig. 2C). This suggests the existence of specific physiological/environmental conditions during stationary phase that cause PYO-mediated cell death.

Nutrient depletion triggers PYO-mediated cell death

Intrigued by the fact that PYO-triggered cell death only occurred during stationary phase, we hypothesized that a lack of specific nutrients might drive this phenotype. Accordingly, we used our plate reader assay to test the effect of removing each of the main nutritional elements (carbon, nitrogen, phosphorus and sulfur) from the medium on cells in the presence and absence of PYO. Cells were grown to mid-exponential phase, washed, and re-suspended at high cell density in medium lacking each of these nutrients. The absence of nitrogen did not seem to impact the cells with respect to PYO sensitivity (Fig. 3A and Fig. S1). Therefore, we used nitrogen removal as a way to limit growth (cells stopped growing ~5h after the experiment started), enabling us to test the importance of the other nutrients systematically (see Experimental Procedures). Removal of carbon, phosphorus or sulfur significantly stimulated PYO toxicity (Fig. 3B-E), indicating that

these nutrients might support PYO defense mechanisms under oxic conditions. To confirm that cells were indeed dying, we performed viability tests with CFU as a read out; this gave us confidence that the observed PI fluorescence increase could be interpreted as cell death (Fig. S2). The absence of PYO always resulted in lower levels of cell death (Fig. 3).

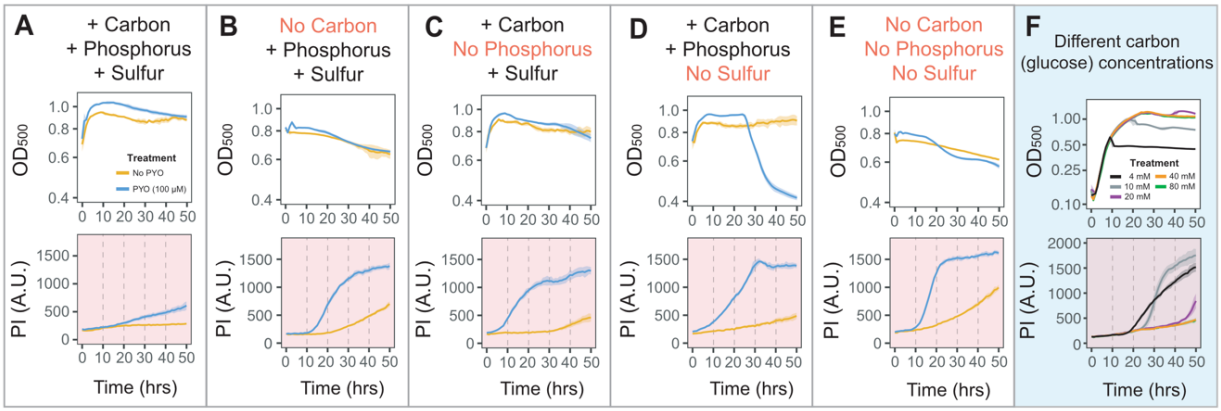

Figure 3. Nutrient depletion triggers PYO-mediated cell death and PYO toxicity is coupled to the available reducing power. A-E. Survival assays under different nutritional conditions. In all experiments, nitrogen was removed to minimize growth (see Experimental Procedures). Starvation for carbon, phosphorus and sulfur causes increased PYO sensitivity. **F**. Carbon starvation in stationary phase results in increased PYO-mediated cell death under normal growth conditions. Cell-death signal increase correlates with carbon limitation, but higher levels of glucose (> 40 mM) inhibit cell death. Concentrations for all other major nutrients (N, P, S) were the standard used for our minimal medium (see Experimental Procedures). Plotted lines represent averages of six replicates and shaded areas are SD.

Even though phosphorus and sulfur seem to be very important for PYO defense, cells usually need significantly lower levels of these nutrients compared to carbon, with S/C and P/C intracellular ratios in bacteria ranging from 0.02 to 0.08 and 0.04 to 0.09, respectively [38]. Therefore, it is likely that carbon depletion would occur first, leading us to speculate that its depletion would be the central driver of the observed stationary phase PYO-stimulated cell death. To test this hypothesis, we grew Δ*phz* cells under different concentrations of carbon (glucose) in the absence or presence of PYO to track poisoning temporally. A clear correlation between glucose availability and cell death in the presence of PYO can be seen in Fig. 3F: lower levels of glucose resulted in increased cell death in a dose-dependent manner. Giving cells 4 mM glucose stimulated earlier PYO poisoning compared to when cells had 10 mM of glucose available. When given 20 mM glucose, cells only started dying after ~ 45 hours, close to the end of the experiment. Further, increasing levels of glucose to 40 mM was sufficient to completely inhibit PYO-mediated cell death (Fig. 3F). In the absence of PYO, cell death was attenuated (Fig. S3), indicating that under

these conditions, PYO was primarily responsible for cell death. Finally, we confirmed that glucose in the medium was completely consumed before PYO-mediated cell death started by measuring bulk glucose levels in cultures at different time points (Fig. S4). These data indicate that PYO's toxic effects on *P. aeruginosa* under oxic conditions are mitigated by available carbon, the source of reducing power.

PYO also poisons cells under anoxic conditions

The most commonly ascribed mechanism for PYO toxicity in *P. aeruginosa* is oxidative stress [25,26,29]. Reduced PYO can partially reduce O_2 to superoxide (O_2^-), which by enzymatic or abiotic dismutation generates hydrogen peroxide (H_2O_2). H_2O_2 can be toxic to cells mainly by participating in the Fenton reaction (step 1: $Fe^{2+} + H_2O_2 \rightarrow [FeO]^{2+} + H_2O$; step 2: $[FeO]^{2+} + H^+ \rightarrow Fe^{3+} + HO^{\bullet}$; [39]) which generates hydroxyl radical ($HO^{\bullet}$). However, in addition to triggering oxidative stress, PYO can also be toxic under anoxic conditions [40]. Accordingly, we sought to determine whether limiting carbon utilization would also impact PYO sensitivity under anoxic conditions using the same survival approach described above. This was done with a plate reader in an anoxic chamber (see Experimental Procedures). In this experiment, no alternative electron acceptor was available (*i.e.* no O_2 or NO_3) and cells should not be able to oxidize the carbon. In addition, there was no extracellular oxidizing potential (e.g. electrode) to re-oxidize PYO in the medium, preventing the anaerobic survival effect caused by the phenazines cycling under anaerobic conditions [21,22]. If energy generation from oxidation of reduced carbon is necessary for PYO defense, incubation of cells with PYO in the absence of an electron acceptor should cause toxicity. In agreement with this hypothesis, we observed that PYO increased cell death anaerobically, even when the medium was carbon-replete (Fig. 4A). We also confirmed that PYO present in the medium was fully reduced by two complementary approaches: (i) measuring absorbance at 310 and (ii) measuring fluorescence (excitation: 360/40, emission: 460/40). Oxidized PYO strongly absorbs at 310 nm [36] and if reduction happens, OD_{310} absorbance drops. In parallel, only the reduced form of the phenazine is fluorescent, leading to an increase in fluorescence emission at ~500 nm if PYO is reduced [36]. As expected, PYO reduction happened very quickly and after one hour PYO was completely reduced (Fig. 4B-C). No detectable re-

oxidation occurred during the experiment. These data reveal that reduced PYO itself can be harmful and cause poisoning in *P. aeruginosa* cultures under anoxic conditions.

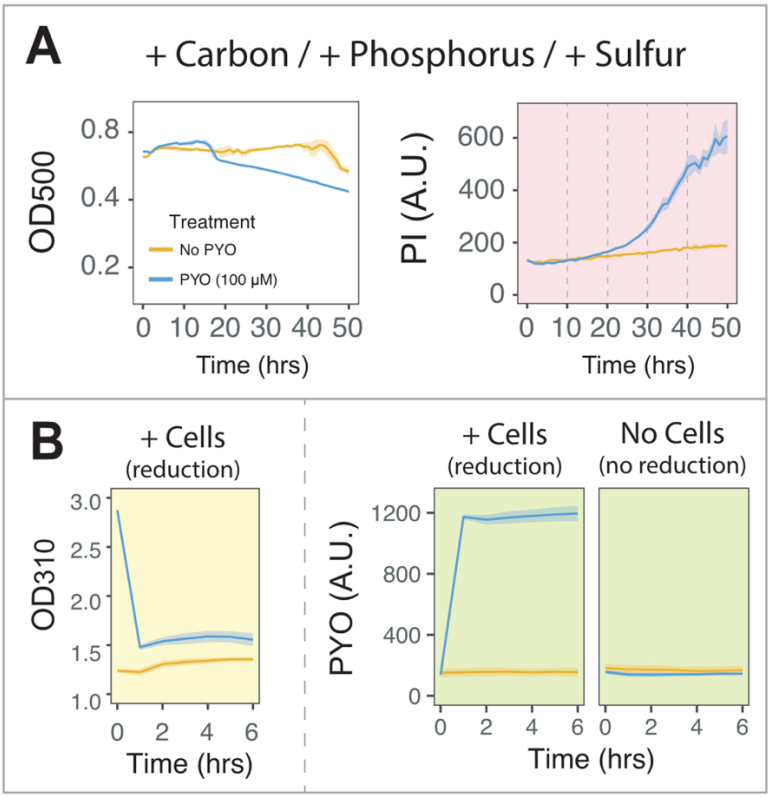

Figure 4. PYO also poisons cells under anoxic conditions. A. Survival experiments as in Fig. 3A, but performed under anoxic conditions also reveal PYO toxicity. Available carbon cannot be used by cells due to the absence of an electron acceptor. **B**. PYO is completely reduced by cells at the beginning of the experiment, as measured by both decrease in OD_{310} absorbance (left) as well as increase in fluorescence (right). Note that PYO stays oxidized (no fluorescence) in the absence of cells. Fluorescence levels reached maximum values before the first hour of the experiment. Plotted lines represent averages of six replicates and shaded areas are SD.

ATP synthesis is required to avoid PYO poisoning

Because (i) under oxic conditions PYO-mediated cell death happens when cells are carbon-limited and (ii) PYO is still toxic under anoxic conditions when cells are carbon replete (but cannot catabolize carbon), we hypothesized that to avoid PYO poisoning, cells must be able to synthesize ATP to power cellular processes involved in PYO resistance. To begin to test this hypothesis, we measured bulk ATP levels in cultures incubated with high and low amounts of carbon under oxic conditions. We found that, in the presence of PYO, ATP levels substantially decreased when cells

were carbon-limited (Fig. 5A-left-top). Confirming our plate reader results, a significant fraction of the population died (Fig. 5A-left-bottom). No substantial decrease in ATP levels or viability happened to the control without PYO. On the other hand, for cells incubated with high levels of glucose, the presence of PYO did not elicit a drop in bulk ATP levels nor a survival decrease (Fig. 5A-right). These data indicate that there is a consistent correlation between ATP depletion and PYO poisoning, with subsequent cell death.

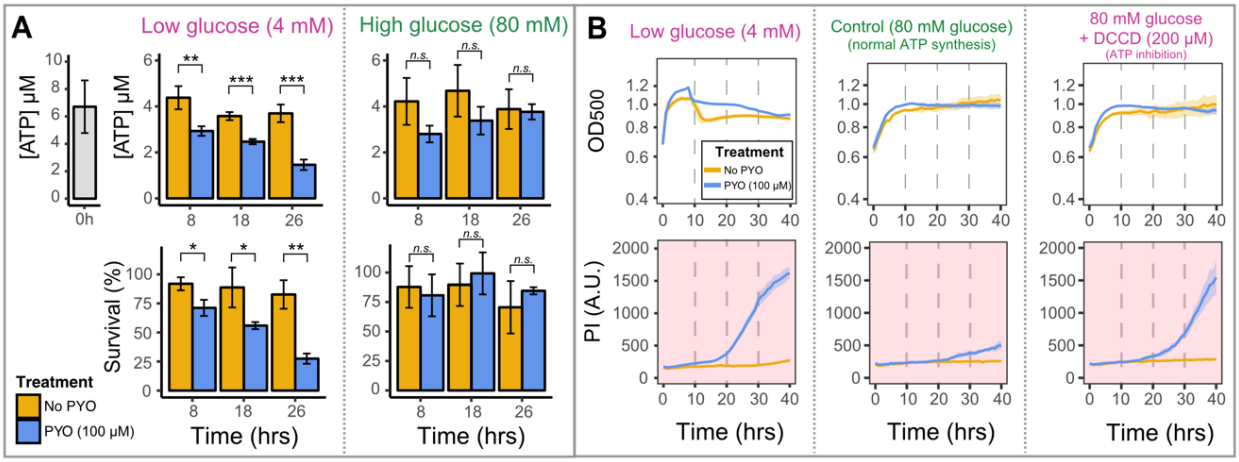

Figure 5. Reduced carbon and ATP synthesis are required to avoid poisoning caused by PYO. A. ATP levels decrease if cells are in the presence of PYO under low carbon (glucose) concentrations (left-top); at the same time, a survival drop can be detected, indicating poisoning and cell death (left-bottom). However, no decrease in ATP levels (right-top) or survival (right-bottom) is detected if cells high levels of glucose are available. Differences were assessed using an unpaired t-test ([*n.s.* = $p > 0.05$ - not a statistically significant difference]; [* = $p < 0.05$]; [** = $p < 0.01$]; [*** = $p < 0.001$]). Bar graphs represent averages of three replicates and error bars are SD. **B.** Inhibition of ATP synthesis using the F_0F_1-ATPase inhibitor DCCD (right) recapitulates the amount of cell death observed when cells are incubated under low carbon concentrations (left). Significantly lower cell death is seen when cells can metabolize the available and abundant reduced carbon (center). Cells survive well in all treatments when PYO is not present (beige lines). Plotted lines represent averages of six replicates and shaded areas are SD.

To further test the necessity of ATP synthesis to avoid PYO poisoning, we exposed cells to N,N-dicyclohexylcarbodiimide (DCCD), a chemical agent that blocks the F_0F_1-ATP synthase and inhibits ATP synthesis [41], and measured their survival under different conditions. We predicted that by inhibiting ATP synthesis, DCCD would increase PYO toxicity even when abundant levels of glucose were available. Indeed, addition of DCCD caused cells to die in the presence of PYO even under high glucose concentrations, indicating that a lack of ATP sensitizes cells to PYO (Fig. 5B-right). Inhibiting ATP synthesis had a similar effect to limiting cells for carbon (Fig. 5B-left), but when ATP synthesis was not inhibited, PYO poisoning was minimal

(Fig. 5B-center). Together, these data indicate that ATP synthesis is necessary for cells to prevent PYO toxicity.

Energy-dependent defense mechanisms are induced when cells are exposed to PYO

Having observed a strong correlation between nutritional conditions (particularly carbon metabolism and ATP synthesis) and PYO toxicity, we sought to explore whether PYO induces particular defense mechanisms that require reduced carbon and ATP synthesis. We performed survival assays under conditions where cells tolerate PYO well (i.e. oxic, nutrient-replete). After exposing cells to PYO for 5 hours, we measured the transcriptional response of genes encoding different categories of energy-dependent defense systems. We separated the tested genes into four main categories: (i) oxidative stress response, (ii) efflux systems, (iii) SOS response and (iv) iron-sulfur (Fe-S) clusters biogenesis (Fig. 6A).

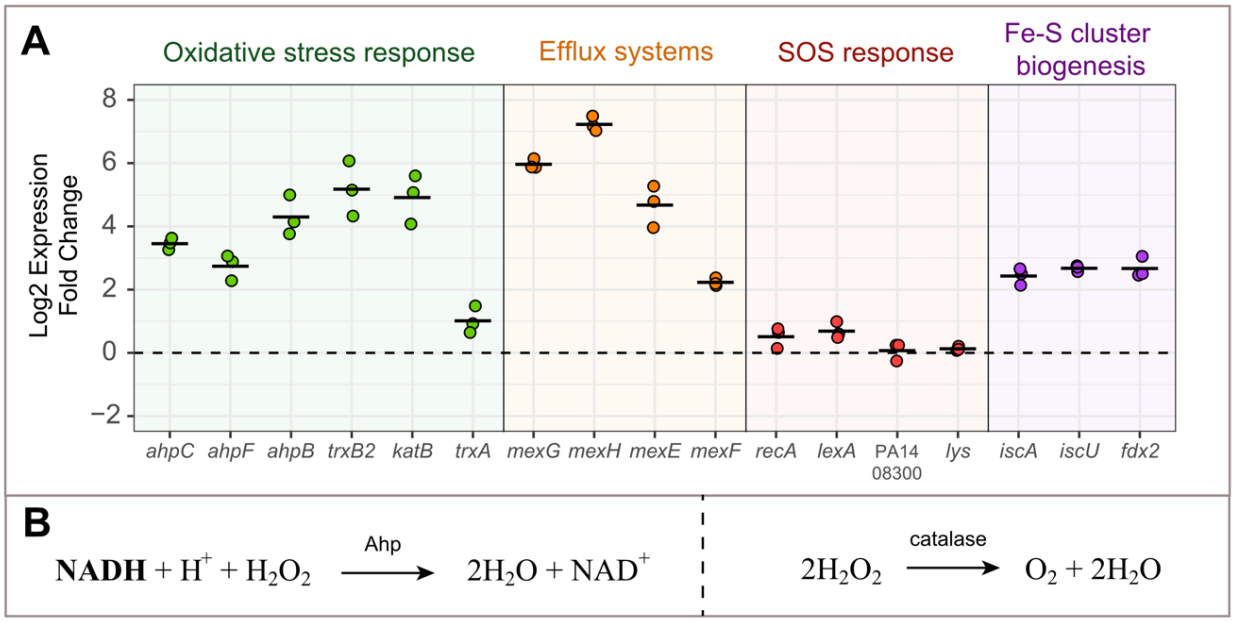

Figure 6. PYO induces energy-dependent defense mechanisms. A. After cells are exposed to PYO under optimal nutritional conditions (i.e. auto-poisoning does not happen), genes involved in the oxidative stress response, RND efflux systems and Fe-S clusters biogenesis are induced. The SOS response is not up-regulated under these conditions, and genes directly related to pyocin clusters/explosive lysis (PA14_08300 and *lys*) are not induced. Black lines show averages of three replicates. **B.** Reactions performed by Ahps and catalases when detoxifying H_2O_2 [39].

A strong induction of oxidative stress-related genes was observed after cells were exposed to PYO. These genes included alkyl hydroperoxide reductases (Ahps: *ahpC*, *ahpF*, *ahpB*), a

thioredoxin reductase (*trxB2*) and a catalase (*katB*) (Fig. 6A). These genes are regulated by the transcription factor OxyR and induced by H_2O_2 [42–44]. A thioredoxin gene (*trxA*) was also mildly upregulated (Fig. 6). The catalytic activity of Ahps depends upon reducing power provided by reduced electron carriers such as nicotinamide adenine dinucleotide (phosphate) (NAD(P)H) to perform the reduction of H_2O_2 to water (Fig. 6B, [39]). Catalases on the other hand, reduce H_2O_2 to water and O_2 in a NAD(P)H-independent manner and do not require stoichiometric reductants (Fig. 6B). That a strong oxidative stress response is part of the PYO defense mechanism under oxic conditions is not surprising [26,45,46]. In addition, at least part of the oxidative stress response is dependent upon reducing power.

Besides the oxidative stress response, we suspected that other cellular processes would be upregulated by PYO and important for defense against it. For example, energy-dependent RND efflux systems such a *mexGHI-opmD* are induced by PYO and involved in phenazine transport [20,35]. We tested two genes in this operon (*mexG* and *mexH*) and both of them were strongly induced by PYO in our survival experiments (Fig. 6A). In addition, we tested another efflux pump system, the *mexEF-oprN* operon, which is a multidrug efflux system in *P. aeruginosa* [47]; its genes were also transcribed more in the presence of PYO (Fig. 6A). We were also curious whether PYO exposure would lead to DNA damage and a subsequent SOS response. Yet the SOS-related genes *recA* and *lexA* were only mildly induced (Fig. 6A). Moreover, we did not detect PYO-upregulation of the endolysin *lys*, known to be responsible for the explosive lysis phenotype in *P. aeruginosa* [13] (Fig. 6A). This suggests that the SOS response and ensuing *lys*-mediated explosive lysis are minimized when cells have sufficient nutrients to power other defense mechanisms.

Finally, we were intrigued that sulfur seemed to significantly affect PYO resistance (Fig. 3D). Fe-S clusters are ubiquitous prosthetic groups that allow proteins to perform several functions, including electron transfer and disulfide reduction [48]. PYO stimulates generation of ROS (O_2^- and H_2O_2), and these species can damage Fe-S clusters [49]. However, phenazines can also directly oxidize Fe-S clusters in proteins [50], which could potentially result in damage. Because (i) Fe-S cluster biogenesis machinery might participate in the replacement/repair of

damaged Fe-S clusters [51], and (ii) the Fe-S cluster biogenesis regulator IscR contributes to resistance to oxidants [52], we tested whether PYO induces genes involved in Fe-S cluster biogenesis. In *P. aeruginosa*, the *isc* operon (iron-sulfur-cluster formation) is the system for Fe-S cluster biogenesis [52,53]. We measured the induction of three different genes in this operon (*iscA*, *iscU*, *fdx2*) and found that all three genes were upregulated in the presence of PYO (Fig. 6A).

A subpopulation of cells resists PYO poisoning even under nutrient-limited conditions

Together, our previous experiments indicated that continuous ATP synthesis through oxidation of reduced carbon helps cells avoid PYO auto-poisoning during the transition from a growth to non-growth state. However, these experiments assessed the bulk response of populations, leading us to wonder whether a subset of the population might respond differently. When exposing cells to PYO under stressful conditions (i.e. oxic, no nutrients), the majority of the population dies (1-3 days after exposure), but a small percentage of the population survives (usually around 5-15% for cells pre-grown in succinate, Fig. 2B). We were interested in understanding what enables this subset of cells to resist PYO, and hypothesized that resistance could occur by two distinct means: (i) the surviving cells are PYO resistant because they are in a distinct physiological state (i.e. "persister-like") due to population heterogeneity; or (ii) they could be surviving based on the nutrients released when the majority of the population dies.

To differentiate between these hypotheses, we performed the experiment shown in Fig. 7. Growing cells were exposed to PYO in the absence of nutrients, causing massive cell death (~5% survival, Fig. 7A). Surviving cells were washed and re-suspended in the same buffer medium (oxic, no nutrients) with or without PYO. If cells were relying on nutrients released from the dead cells to power defense mechanisms against PYO, poisoning and cell death should be high after the wash. However, this was not the case: re-exposure of survivors did not result in any decrease in viability (Fig. 7B). This result suggested that the subpopulation of surviving cells was in a persister-like state [54] that does not require nutrients to survive PYO stress. When we re-grew the survivor cells in fresh medium and re-exposed the population to PYO, the majority of the population was re-sensitized to PYO, with only a small subpopulation again surviving (Fig. 7C).

Such population dynamics indicate that PYO sensitivity is cyclic, dependent upon the environmental conditions.

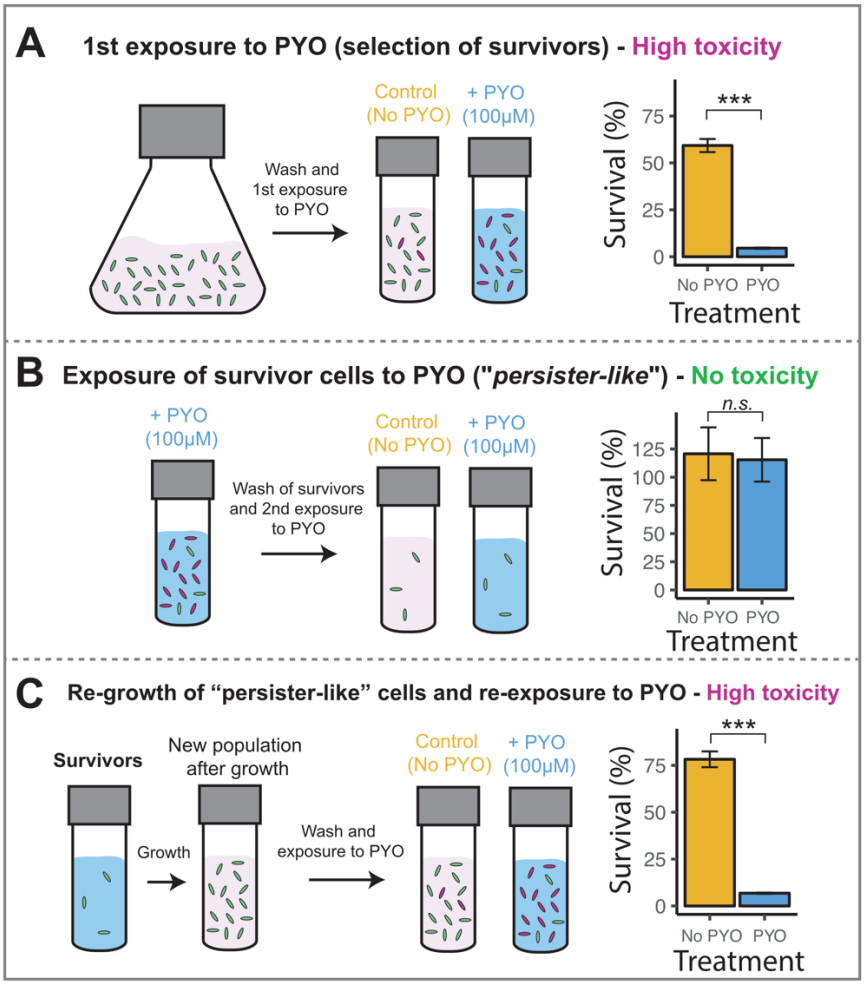

Figure 7. A subpopulation of cells can resist PYO even under nutrient-limited conditions. The experimental protocol is shown on the left with results of survival after exposure to PYO on the right. Survival was quantified by plating and CFU counting. Differences were assessed using an unpaired t-test. Bar graphs represent the average of three replicates and error bars are SD.

Discussion

Over the last decade, a variety of physiological functions for phenazines have been identified [20–23,31,32,55–59]. Phenazines benefit their producers when they are experiencing reducing stress (i.e. cells are electron donor replete but electron acceptor limited). Under these conditions, phenazines can serve as alternative electron acceptors, allowing cells to maintain redox

homeostasis, anoxic energy generation, and survive in regions of biofilms where oxygen is limiting [21,22,33,56]. Even aerobically-grown nutrient replete planktonic cultures achieve significantly greater cell yields when grown in the presence of PYO compared to its absence (Fig. S5), possibly due to oxygen limitation in high-density cultures. Despite these positive effects, phenazines are more commonly considered to be toxic compounds that kill competitors and damage host cells, and can even poison their producers [24,29,60–63]. These opposing functions are striking and paradoxical. The objective of this work was to gain a better understanding of how PYO's "double edged sword" effect impacts *P. aeruginosa* under particular conditions.

Our central hypothesis was that PYO's versatile redox chemistry explains its orthogonal cellular effects in a predictable fashion, depending upon the environment and physiological state of the cells. PYO is only produced at high cell density and when high levels of carbon are available because it is regulated by quorum sensing [20]. Under these conditions, when cells are oxidant-limited, they can thrive by utilizing PYO as an electron acceptor and avoiding toxicity because they are able to power defense mechanisms. However, this benefit to the overall population can quickly change, with PYO becoming dangerous to the majority of the population as it begins to starve for certain nutrients (*e.g.* carbon). Even after cell death due to PYO auto-poisoning, an intrinsically PYO-tolerant subset of the population still survives, resulting in the opportunity for PYO to again become net beneficial to the population when conditions alter. It is also important to consider that even though the toxic effects of PYO can be detrimental at the level of the single cell, in the context of a biofilm, the "altruistic" death of individuals permits eDNA release that provides a structural support for the survivors. Accordingly, PYO's nuanced "double edged sword" effect can be rationalized as net-beneficial for the producer population over its lifecycle (Fig. 8).

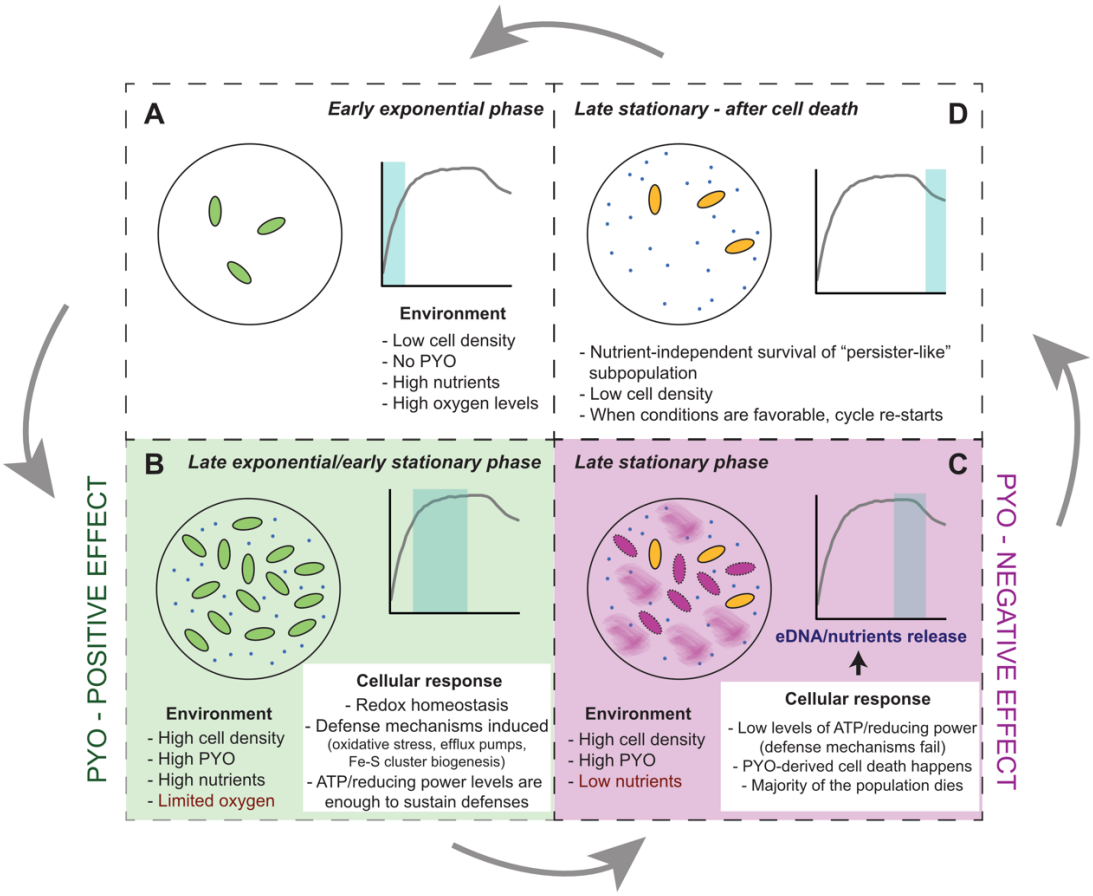

Figure 8. Model of PYO's "double-edged sword" effect throughout the *P. aeruginosa* life cycle. At least four different growth stages where PYO differentially affects *P. aeruginosa* can be distinguished and were tested by our experiments (A-D). **A-B.** Early stages where cells are resistant to PYO. Positive effect of PYO and the ability of cells to turn on energy-dependent mechanisms that result in survival (see Figs. 3A and F, Fig. 5 and Fig. 6). **C.** Negative effects of PYO (poisoning and cell death) when nutritional conditions are unfavorable to power defense mechanisms (see Fig. 1, Figs. 3B-F, Fig. 4 and Fig. 5). **D.** Demonstration of the existence of a "persister-like" subpopulation that is resistant to PYO (see Fig. 7).

Critical to *P. aeruginosa*'s tolerance of PYO is its extensive genetic arsenal to cope with the consequences of PYO's redox activity [45]. This includes catalases, Ahps, multiple thioredoxins and thioredoxins reductases [42]. Thioredoxins reduce disulfide bonds in thiol groups that become oxidized due to oxidative stress [64] and together with Ahps, many thioredoxin systems depend on the availability of reduced carbon provided by (NAD(P)H) [64]. Because PYO is membrane permeable [24,65], its containment (by chaperones and/or efficient transport systems) is also important to minimize unwanted cellular redox reactions, such as reactivity with Fe-S clusters; RND efflux systems powered by the proton-motive force are involved in this task [20,66].

Our results showing a requirement for reducing power (carbon) and sulfur to avoid PYO toxicity (Fig. 3), together with the induction of genes involved in the oxidative stress response, efflux pump and Fe-S cluster systems in the presence of PYO (Fig. 6A), indicate that these defense systems are particularly important for PYO tolerance. Finally, though PYO can also intercalate into DNA [17,27,67], in our experiments, cells seem to avoid extensive DNA damage (at least at the population level) when nutritional conditions are adequate to support other energy-dependent defense mechanisms (only a mild SOS response was detected). However, this does not exclude the possibility that an SOS response might be involved in auto-poisoning and lysis for a subset of the population [13]. Future studies using single-cell tracking will allow this to be determined.

Though we performed the majority of our experiments in this report in planktonic culture for technical reasons, the implications for biofilm development are clear. Biofilms are heterogeneous and dynamic systems, and the ultimate impact of PYO on the different subpopulations would be expected to vary between beneficial and detrimental, depending upon the microenvironment present within the biofilm at different stages of development. Parameters such as nutrient concentrations, availability of electron acceptors and the respective energetic state of the cells should dictate the effect that PYO (and other phenazines) will have on different regions of the biofilm. For example, under nutrient-replete conditions, PYO production can cause beneficial expansion of biofilm aggregates under hypoxic/anoxic conditions [30]. However, in regions of the biofilm where cells are starved for nutrients and PYO is present, PYO-mediated auto-poisoning would contribute to eDNA release, an important structural component of the matrix. Finally, we note that fluctuations of nutrients, which occur in open systems [68,69], would be expected to significantly impact the effect of PYO. These predictions are testable, and going forward, we hope to leverage the findings reported in this work to better understand how versatile, redox-active molecules such as PYO and other phenazines can modulate biofilm development.

Experimental procedures

Biofilm and single-cell experiments

For biofilm experiments, cells of WT and Δ*phz* (both *phz1* and *phz2* operons are deleted in this strain [20]) strains from an overnight culture were washed and diluted (1:50) in succinate minimal medium (SMM, composition: 40 mM sodium succinate, 50 mM KH_2PO_4/K_2HPO_4[pH 7], 42.8 mM NaCl, 1 mM $MgSO_4$, 9.35 mM NH_4Cl, trace elements solution [70]), and grown until OD_{500} = 0.4-0.5. Cells were centrifuged, washed once, and diluted to OD_{500} = 0.25, which was used as the final inoculum. Then, 250 µL of WT or Δ*phz* inoculum were transferred to Nunc Lab-Tek 8-well chambered coverglass (Thermo Scientific) and incubated at 37 ºC in shaking conditions (250 rpm) during six hours for biofilm development. This experiment was repeated 10 times, with two independent wells for WT and Δ*phz* cultures every time. After six hours of incubation, liquid was removed and the chambers were washed twice with PBS (Phosphate buffer saline – 137 mM NaCl, 2.7 mM KCl, 10 mM Na_2HPO_4, 1.8 mM KH_2PO_4, pH 7.2) to remove planktonic cells, leaving only the attached biofilms on the bottom of the chamber. Finally, biofilms were stained with both TOTO-1 Iodide (1 µM) and DAPI (20 µM), and chambers were imaged using confocal microscopy (Leica TCS SPE). For quantification of cell death of attached cells, 10 different fields of view per well were imaged. Images were then analyzed in Oufti [71] using the DAPI channel for total cell counting (live and dead); when checked manually, the software was able to count 80-90% of the total cells for both WT and Δ*phz* treatments. Dead cells were manually counted using the TOTO channel and calculation of the percentage of dead cells was done by dividing the number of dead cells/total number of cells (live and dead). The final proportions of dead cells for each of the 10 replicates for WT and Δ*phz* are plotted in Fig. 1B.

Single-cell experiments were performed using agarose pads (SMM with 2% agarose). Cells were grown from an overnight culture until OD_{500} = 0.4-0.5, spotted on top of the pads and imaged using fluorescence microscopy (Leica TCS SPE). Agarose pads contained 100 µM PYO and we used both WT and WT-YPF (constitutive YFP expression) strains for these experiments. Temperature control was set to 37 ºC. Shrinking and explosive cell lysis were monitored in both

Differential Interference Contrast (DIC) and fluorescence channels under 100x magnification. For eDNA staining, we used agarose pads containing TOTO-1 Iodide (1 μM).

Liquid culture assays and quantification of phenazine toxicity

WT and Δ*phz* cells were grown from overnight cultures to OD_{500} = 0.5 and then diluted into four independent OD_{500} = 0.05 cultures (replicates) using 5 mL glass tubes containing fresh SMM (with and without 100 μM PYO), where the experiment started. Cells were incubated at 37 ºC for 36h, and time-points were taken at 0, 18, 24 and 36 hours for plating and CFU counting. Plating for CFU counting was always done in lysogeny broth (LB) (Difco) plates containing 1.5% agar. PYO final concentration in WT cultures was quantified using high-performance liquid chromatography (HPLC) (Fig. S6). For all experiments shown in this paper, with the exception of the toxicity assay comparing different phenazines (see below), PYO was dissolved in 20 mM HCl, which was always added to PYO-untreated cultures as a control. The PYO used was synthesized and purified using methods previously described [20,72]. Other phenazines were purchased from Princeton Biomolecular Research Inc and TCI America.

Toxicity of different phenazines was assessed by performing shock experiments where cells were shifted from growing conditions to minimal phosphate buffer (MPB, 50 mM KH_2PO_4/ K_2HPO_4[pH 7], 42.8 mM NaCl) containing 100 μM of each of the four phenazines tested: PYO, 1-OH-PHZ, PCN and PCA. Cells were grown in SMM until OD_{500} = 0.7-0.8, washed, and concentrated to final OD_{500} = 2 (which corresponds to ~2-3x10^9 cells) in MPB + phenazines. In this experiment, phenazines needed to be dissolved using a mutual solvent (DMSO), which was used as a negative control. Incubation was done under shaking conditions (250 rpm, 37 ºC) in 1.5 mL Eppendorf tubes containing 1 mL of culture. Cells were plated for CFU counting after 24 and 48 hours of exposure to the phenazines. Four replicates were performed for each treatment.

Plate reader assay for quantification of cell death

The plate reader assay (using a BioTek Synergy 4 plate reader) was developed to efficiently quantify cell death under a variety of environmental conditions. For growth curves presented in

Fig. 1C-D, cells were grown in either SMM or glucose minimal medium (GMM: same composition as SMM, but with glucose instead of succinate as the carbon source) and propidium iodide (PI) at a concentration of 5 μM was added to the cultures. Cells were incubated in the plate reader, with shaking at 37 ºC and monitoring of OD_{500} and fluorescence (xenon lamp, excitation/emission = 535/617 nm). PI was used for cell death monitoring instead of TOTO-1 iodide because cultures displayed auto-fluorescence in the same wavelength as TOTO and the background auto-fluorescence was different for WT and Δ*phz* strains. This is likely due to different amounts of siderophore production, NAD(P)H and/or reduced phenazines present in the culture [73]. This was not observed when using PI (Fig. S7), and therefore this dye was used in all plate reader experiments. Addition of 5 μM PI only mildly impacted cell growth (Fig. S8). For every plate reader experiment reported here, six independent wells were analyzed for each treatment (i.e. six wells with no PYO added, and six wells with 100 μM PYO added), and the averages and standard deviations for the six replicates were plotted. Each plate reader set up was repeated at least twice, with very similar results.

For survival experiments under different nutritional conditions presented in Fig. 3, Δ*phz* cells were grown in GMM + 100 mM MOPS until OD_{500} = 0.7-0.8, centrifuged, washed and re-suspended at OD_{500} = 2 in buffer (100 mM MOPS + 42.8 mM NaCl, pH = 7). Then, the different nutrients were added as indicated. Final concentrations for each nutrient were: carbon = 80 mM glucose; phosphorus = 50 mM KH_2PO_4/ K_2HPO_4 [pH 7]; sulfur = 1 mM $MgSO_4$. In all experiments, trace metals solution [70] at the same concentration as the one used for growth was added. During the survival experiments, the nitrogen source (NH_4Cl) was omitted in all treatments as a way to minimize growth (OD_{500} still increased during the first ~5h of the experiment, but shortly afterward cells stopped growing). Removing nitrogen from the medium did not sensitize the cells to PYO (Fig. 3A). To confirm that an increase in PI fluorescence indeed meant cell death, we plated cells for CFU counting after 50 hours of incubation (Fig. S2).

Finally, to further test the importance of carbon availability to survival against PYO, cells were grown in the presence or absence of PYO in GMM under different glucose concentrations (4 mM, 10 mM, 40 mM, 80 mM). For all survival and growth experiments, OD_{500} measurements

during inoculum preparation were performed using a Beckman Coulter DU 800 spectrophotometer. Measurements of pH using pH strips after the end of the experiments revealed no significant changes.

PYO toxicity under anaerobic conditions

To quantify poisoning and cell death caused by PYO under anaerobic conditions, Δ*phz* cells were grown aerobically exactly as described for the survival experiment above, but then were shifted to an anaerobic chamber, where cells were incubated for 4 hours before addition of PYO to minimize potential oxidative stress. Resazurin (1 μg/mL) was added to a control tube to monitor oxygen consumption. This control tube contained an aliquot culture derived from the experiment culture, but to avoid any potential interference of resazurin in the experiment, these cells were only used for monitoring of O_2 consumption. The 4 hours incubation resulted in a colorless resazurin in the control tube (indicating consumption of trace levels of O_2 in the medium, [74]. PYO was then added to cultures and cells were transferred to the plate reader present in the anaerobic chamber. PYO solution and 96-well plates used in this experiment had been acclimatized under anaerobic conditions for at least 3 days. Incubation conditions were the same as before, but fluorescence measurements were performed with a tungsten lamp using a red filter cube (excitation: 486/20, emission: 620/40; settings available for the anaerobic plate reader). Direct comparison of absolute fluorescence values between aerobic and anaerobic measurements are not possible due to the different plate readers used. Reduction of PYO by cells was monitored by two ways: (i) absorbance at OD_{310}, which is intense for oxidized PYO, but weak for reduced PYO [36]; (ii) fluorescence at ~500nm using a green filter cube (excitation: 360/40, emission: 460/40) which is intense for reduced PYO, but null for oxidized PYO [36].

ATP measurements and ATP synthesis inhibition

ATP measurements were performed using the BacTiter-Glo reagent (Promega) in 96-well opaque white microtiter plates as previously described [22]. In summary, aerobic survival experiments as described above were set up under high or low carbon concentrations (80 mM or 4 mM glucose, respectively). The expectation was that cells under low carbon availability would

starve for carbon first, resulting in ATP depletion and cell death. After incubation, cultures were sampled at 8, 18 and 26 hours for both ATP quantification and viability through CFUs counting. For ATP measurements, 20 µL aliquot of each culture was added to 180 µL of DMSO. This solution was diluted with 800 µL of 100 mM HEPES (pH 7.5) and stored at -80ºC until analysis (no more than 2 days). Thawed samples were mixed 1:1 BacTiter-Glo reagent and luminescence was measured at 30ºC using a plate reader (BioTek Synergy 4). For determining ATP concentrations in the sample, a standard curve with known concentrations of ATP was generated.

To test for a direct connection between ATP depletion and PYO toxicity, experiments using the molecule N,N-dicyclohexylcarbodiimide (DCCD) were performed. DCCD is classical inhibitor of the F_0F_1-ATP synthase [41], disrupting ATP synthesis. Aerobic survival experiments as described before were set up where cells had three different treatments: (i) low carbon (4 mM glucose) with no DCCD; (ii) high carbon (80 mM glucose) with no DCCD (i.e. normal ATP synthesis) or (iii) high carbon (80 mM glucose) + 200 µM DCCD (i.e. ATP inhibition). This concentration of the inhibitor was used because it did not seem to cause a negative impact on the negative control (No PYO treatment, Fig. 5B). OD_{500} and PI fluorescence were measured over a time course of 40 hours.

RNA extraction and quantitative reverse transcriptase PCR (qRT-PCR)

For RNA extraction, three independent cultures of Δ*phz* cells were grown in GMM and a survival experiment as described in Fig. 3A was performed, where cells were incubated under two treatments: (i) 100 µM PYO and (ii) No PYO. Under these conditions, cells were able to survive and had nutrients necessary to power defense mechanisms against PYO toxicity. For all three replicates, 750 µL of culture containing +/- PYO were split into five wells in a 96-well BRAND® microplate followed by incubation in the plate reader for 5h. Cells were then harvested from the wells, pelleted and re-suspended in 215 µL of TE buffer (30 mM Tris.Cl, 1 mM EDTA, pH 8.0) containing 15 mg/mL of lysozyme + 15 µL of proteinase K solution (20 mg/mL, Qiagen), and incubated for 8-10 min. Further lysis steps and RNA extraction were performed using an RNeasy kit (Qiagen) following the manufacturer's instructions. For further removal of contaminant genome DNA, additional treatment of the extracted RNA with TURBO DNA-free kit (Invitrogen)

was performed following the manufacturer's instructions. Finally, cDNA was synthesized from 1 µg of total RNA using iScript cDNA Synthesis kit (Bio-Rad) according to the manufacturer's protocol.

For qRT-PCR, iTaq Universal SYBR Green Supermix (Bio-Rad) was used. Reactions were performed in 20 µL volume containing 10 µL of the supermix, 5 µL of cDNA and 5 µL of forward and reverse primer solution (2 µM each). Primers are listed in Table S1. Reactions were run using a 7500 Fast Real-Time PCR System machine (Applied Biosystems). Standard curves for each primer pair using known concentrations of *Pa* PA14 genomic DNA were used to back calculate concentrations of cDNA for each gene of interest. Normalizations for a control gene were done using the house-keeping gene *oprI* [75]. Reactions with the additional gene *proC* were also run as a second negative control [76]. After normalization by *oprI*, data is displayed as a log2 fold change in expression (Fig. 6A).

Testing a "persister-like" phenotype upon PYO exposure

To test if the survival of a subpopulation of cells upon exposure to PYO under nutrient-limiting conditions happens (i) due to release of nutrients from dead cells or (ii) due to a "persister-like" phenotype, experiments followed the scheme presented in Fig. 7. First, a Δ*phz* culture was grown in SMM as described for experiments measuring phenazines toxicity, split in three different replicates, washed and shifted to MPB and exposed to 100 µM PYO for three days. The negative control did not contain PYO. Then, survivor cells were pelleted and washed twice to remove nutrients released from dead cells, followed by re-suspension in MPB and a second exposure to PYO for three days. Finally, after second exposure to PYO, survivors were grown again in SMM until OD_{500} = 1.0 and a third exposure to PYO (during six days) was performed to test if cells had become sensitive again. During all exposures to PYO, incubation was done under shaking conditions (250 rpm) at 37 ºC. PYO remained blue during the entire experiment, indicating that oxygenation was sufficient to maintain the phenazine in its oxidized state. Survival was assessed by plating and CFU counting.

Statistical analyses

All statistical analyses were performed using R (R Core Team, 2018). One-way ANOVA with post-hoc Tukey's HSD test for multiple comparisons was used in Fig. 2A-B. Unpaired t-tests were used for data presented in Fig. 5A and Fig. 7. Before performing the mentioned statistical tests, normality and homogeneity of variances were assessed using the Shapiro-Wilk test and Levene's test, respectively.

Acknowledgements

We thank all the members of the Newman lab for experimental advice and feedback on the manuscript; Megan Bergkessel was particularly generous with her time and intellectual support. We also thank Scott Saunders for helping with pyocyanin quantification. Grants to D.K.N. from the ARO (W911NF-17-1-0024) and NIH 341 (1R01AI127850-01A1) supported this research.

References

1. Flemming H-C, Wingender J, Szewzyk U, Steinberg P, Rice SA, Kjelleberg S. Biofilms: an emergent form of bacterial life. Nat Rev Microbiol. 2016;14: 563–575.
2. Olsen I. Biofilm-specific antibiotic tolerance and resistance. Eur J Clin Microbiol Infect Dis. 2015;34: 877–886.
3. Govan JR, Deretic V. Microbial pathogenesis in cystic fibrosis: mucoid *Pseudomonas aeruginosa* and *Burkholderia cepacia*. Microbiol Rev. 1996;60: 539–574.
4. Flemming H-C. EPS-then and now. Microorganisms. 2016;4.
5. Okshevsky M, Regina VR, Meyer RL. Extracellular DNA as a target for biofilm control. Curr Opin Biotechnol. 2015;33: 73–80.
6. Ibáñez de Aldecoa AL, Zafra O, González-Pastor JE. Mechanisms and regulation of extracellular DNA release and its biological roles in microbial communities. Front Microbiol. 2017;8: 1390.
7. Matsukawa M, Greenberg EP. Putative exopolysaccharide synthesis genes influence *Pseudomonas aeruginosa* biofilm development. J Bacteriol. 2004;186: 4449–4456.
8. Whitchurch CB, Tolker-Nielsen T, Ragas PC, Mattick JS. Extracellular DNA required for bacterial biofilm formation. Science. 2002;295: 1487.
9. Allesen-Holm M, Barken KB, Yang L, Klausen M, Webb JS, Kjelleberg S, et al. A characterization of DNA release in *Pseudomonas aeruginosa* cultures and biofilms. Mol Microbiol. 2006;59: 1114–1128.
10. Okshevsky M, Meyer RL. The role of extracellular DNA in the establishment, maintenance and perpetuation of bacterial biofilms. Crit Rev Microbiol. 2013;41: 341–352.
11. D'Argenio DA, Calfee MW, Rainey PB, Pesci EC. Autolysis and autoaggregation in *Pseudomonas aeruginosa* colony morphology mutants. J Bacteriol. 2002;184: 6481–6489.
12. Webb JS, Thompson LS, James S, Charlton T, Tolker-Nielsen T, Koch B, et al. Cell death in *Pseudomonas aeruginosa* biofilm development. J Bacteriol. 2003;185: 4585–4592.
13. Turnbull L, Toyofuku M, Hynen AL, Kurosawa M, Pessi G, Petty NK, et al. Explosive cell lysis as a mechanism for the biogenesis of bacterial membrane vesicles and biofilms. Nat Commun. 2016;7: 11220.
14. Hazan R, Que YA, Maura D, Strobel B, Majcherczyk PA, Hopper LR, et al. Auto poisoning of the respiratory chain by a quorum-sensing-regulated molecule favors biofilm formation and antibiotic tolerance. Curr Biol. 2016;26: 195–206.
15. Rice KC, Bayles KW. Molecular control of bacterial death and lysis. Microbiol Mol Biol Rev. 2008;72: 85–109, table of contents.
16. Bayles KW. Bacterial programmed cell death: making sense of a paradox. Nat Rev Microbiol. 2014;12: 63–69.
17. Mavrodi DV, Blankenfeldt W, Thomashow LS. Phenazine compounds in fluorescent *Pseudomonas* spp. biosynthesis and regulation. Annu Rev Phytopathol. 2006;44: 417–445.
18. Price-Whelan A, Dietrich LEP, Newman DK. Rethinking "secondary" metabolism: physiological roles for phenazine antibiotics. Nat Chem Biol. 2006;2: 71–78.
19. Laursen JB, Nielsen J. Phenazine natural products: biosynthesis, synthetic analogues, and biological activity. Chem Rev. 2004;104: 1663–1686.

20. Dietrich LE, Price-Whelan A, Petersen A, Whiteley M, Newman DK. The phenazine pyocyanin is a terminal signalling factor in the quorum sensing network of *Pseudomonas aeruginosa*. Mol Microbiol. 2006;61: 1308–1321.
21. Wang Y, Kern SE, Newman DK. Endogenous phenazine antibiotics promote anaerobic survival of *Pseudomonas aeruginosa* via extracellular electron transfer. J Bacteriol. 2010;192: 365–369.
22. Glasser NR, Kern SE, Newman DK. Phenazine redox cycling enhances anaerobic survival in *Pseudomonas aeruginosa* by facilitating generation of ATP and a proton-motive force. Mol Microbiol. 2014;92: 399–412.
23. Wang Y, Wilks JC, Danhorn T, Ramos I, Croal L, Newman DK. Phenazine-1-carboxylic acid promotes bacterial biofilm development via ferrous iron acquisition. J Bacteriol. 2011;193: 3606–3617.
24. Lau GW, Hassett DJ, Ran H, Kong F. The role of pyocyanin in *Pseudomonas aeruginosa* infection. Trends Mol Med. 2004;10: 599–606.
25. Muller M. Pyocyanin induces oxidative stress in human endothelial cells and modulates the glutathione redox cycle. Free Radic Biol Med. 2002;33: 1527–1533.
26. Rada B, Leto TL. Pyocyanin effects on respiratory epithelium: relevance in *Pseudomonas aeruginosa* airway infections. Trends Microbiol. 2013;21: 73–81.
27. Das T, Kutty SK, Tavallaie R, Ibugo AI, Panchompoo J, Sehar S, et al. Phenazine virulence factor binding to extracellular DNA is important for *Pseudomonas aeruginosa* biofilm formation. Sci Rep. 2015;5: 8398.
28. Ramos I, Dietrich LE, Price-Whelan A, Newman DK. Phenazines affect biofilm formation by *Pseudomonas aeruginosa* in similar ways at various scales. Res Microbiol. 2010;161: 187–191.
29. Das T, Manefield M. Pyocyanin promotes extracellular DNA release in *Pseudomonas aeruginosa*. PLoS One. 2012;7: e46718.
30. Costa KC, Glasser NR, Conway SJ, Newman DK. Pyocyanin degradation by a tautomerizing demethylase inhibits *Pseudomonas aeruginosa* biofilms. Science. 2017;355: 170–173.
31. Okegbe C, Fields BL, Cole SJ, Beierschmitt C, Morgan CJ, Price-Whelan A, et al. Electron-shuttling antibiotics structure bacterial communities by modulating cellular levels of c-di-GMP. Proc Natl Acad Sci USA. 2017;114: E5236–E5245.
32. Dietrich LEP, Okegbe C, Price-Whelan A, Sakhtah H, Hunter RC, Newman DK. Bacterial community morphogenesis is intimately linked to the intracellular redox state. J Bacteriol. 2013;195: 1371–1380.
33. Jo J, Cortez KL, Cornell WC, Price-Whelan A, Dietrich LE. An orphan cbb3-type cytochrome oxidase subunit supports *Pseudomonas aeruginosa* biofilm growth and virulence. Elife. 2017;6: e30205.
34. Okshevsky M, Meyer RL. Evaluation of fluorescent stains for visualizing extracellular DNA in biofilms. J Microbiol Methods. 2014;105: 102–104.
35. Sakhtah H, Koyama L, Zhang Y, Morales DK, Fields BL, Price-Whelan A, et al. The *Pseudomonas aeruginosa* efflux pump MexGHI-OpmD transports a natural phenazine that controls gene expression and biofilm development. Proc Natl Acad Sci USA. 2016;113: E3538-47.
36. Wang Y, Newman DK. Redox reactions of phenazine antibiotics with ferric (hydr)oxides and molecular oxygen. Environ Sci Technol. 2008;42: 2380–2386.

37. Sakhtah H, Price-Whelan A, Dietrich LE. Regulation of phenazine biosynthesis. Microbial Phenazines: Biosynthesis, Agriculture and Health. Springer; 2013.
38. Fagerbakke KM, Heldal M, Norland S. Content of carbon, nitrogen, oxygen, sulfur and phosphorus in native aquatic and cultured bacteria. Aquat Microb Ecol. 1996;10: 15–27.
39. Imlay JA. The molecular mechanisms and physiological consequences of oxidative stress: lessons from a model bacterium. Nat Rev Microbiol. 2013;11: 443–454.
40. Barakat R, Goubet I, Manon S, Berges T, Rosenfeld E. Unsuspected pyocyanin effect in yeast under anaerobiosis. Microbiologyopen. 2014;3: 1–14.
41. Sebald W, Machleidt W, Wachter E. N,N'-dicyclohexylcarbodiimide binds specifically to a single glutamyl residue of the proteolipid subunit of the mitochondrial adenosinetriphosphatases from *Neurospora crassa* and *Saccharomyces cerevisiae*. Proc Natl Acad Sci USA. 1980;77: 785–789.
42. Ochsner UA, Vasil ML, Alsabbagh E, Parvatiyar K, Hassett DJ. Role of the *Pseudomonas aeruginosa oxyR-recG* operon in oxidative stress defense and DNA repair: OxyR-dependent regulation of *katB-ankB*, *ahpB*, and *ahpC-ahpF*. J Bacteriol. 2000;182: 4533–4544.
43. Hishinuma S, Ohtsu I, Fujimura M, Fukumori F. OxyR is involved in the expression of thioredoxin reductase TrxB in *Pseudomonas putida*. FEMS Microbiol Lett. 2008;289: 138–145.
44. Panmanee W, Hassett DJ. Differential roles of OxyR-controlled antioxidant enzymes alkyl hydroperoxide reductase (AhpCF) and catalase (KatB) in the protection of *Pseudomonas aeruginosa* against hydrogen peroxide in biofilm vs. planktonic culture. FEMS Microbiol Lett. 2009;295: 238–244.
45. Hassett DJ, Charniga L, Bean K, Ohman DE, Cohen MS. Response of *Pseudomonas aeruginosa* to pyocyanin: mechanisms of resistance, antioxidant defenses, and demonstration of a manganese-cofactored superoxide dismutase. Infect Immun. 1992;60: 328–336.
46. Hassan HM, Fridovich I. Mechanism of the antibiotic action pyocyanine. J Bacteriol. 1980;141: 156–163.
47. Köhler T, Michéa-Hamzehpour M, Henze U, Gotoh N, Curty LK, Pechère JC. Characterization of MexE-MexF-OprN, a positively regulated multidrug efflux system of *Pseudomonas aeruginosa*. Mol Microbiol. 1997;23: 345–354.
48. Johnson DC, Dean DR, Smith AD, Johnson MK. Structure, function, and formation of biological iron-sulfur clusters. Annu Rev Biochem. 2005;74: 247–281.
49. Imlay JA. Iron-sulphur clusters and the problem with oxygen. Mol Microbiol. 2006;59: 1073–1082.
50. Gu M, Imlay JA. The SoxRS response of *Escherichia coli* is directly activated by redox-cycling drugs rather than by superoxide. Mol Microbiol. 2011;79: 1136–1150.
51. Djaman O, Outten FW, Imlay JA. Repair of oxidized iron-sulfur clusters in Escherichia coli. J Biol Chem. 2004;279: 44590–44599.
52. Romsang A, Duang-Nkern J, Leesukon P, Saninjuk K, Vattanaviboon P, Mongkolsuk S. The iron-sulphur cluster biosynthesis regulator IscR contributes to iron homeostasis and resistance to oxidants in *Pseudomonas aeruginosa*. PLoS One. 2014;9: e86763.
53. Lee SA, Gallagher LA, Thongdee M, Staudinger BJ, Lippman S, Singh PK, et al. General and condition-specific essential functions of *Pseudomonas aeruginosa*. Proc Natl Acad Sci USA. 2015;112: 5189–5194.

54. Van den Bergh B, Fauvart M, Michiels J. Formation, physiology, ecology, evolution and clinical importance of bacterial persisters. FEMS Microbiol Rev. 2017;41: 219–251.
55. Dietrich LEP, Teal TK, Price-Whelan A, Newman DK. Redox-active antibiotics control gene expression and community behavior in divergent bacteria. Science. 2008;321: 1203–1206.
56. Price-Whelan A, Dietrich LEP, Newman DK. Pyocyanin alters redox homeostasis and carbon flux through central metabolic pathways in *Pseudomonas aeruginosa* PA14. J Bacteriol. 2007;189: 6372–6381.
57. Glasser NR, Saunders SH, Newman DK. The colorful world of extracellular electron shuttles. Annu Rev Microbiol. 2017;71: 731–751.
58. Lin Y-C, Sekedat MD, Cornell WC, Silva GM, Okegbe C, Price-Whelan A, et al. Phenazines regulate Nap-dependent denitrification in *Pseudomonas aeruginosa* biofilms. J Bacteriol. 2018;200.
59. Muller M, Merrett ND. Pyocyanin production by *Pseudomonas aeruginosa* confers resistance to ionic silver. Antimicrob Agents Chemother. 2014;58: 5492–5499.
60. Rada B, Lekstrom K, Damian S, Dupuy C, Leto TL. The *Pseudomonas* toxin pyocyanin inhibits the dual oxidase-based antimicrobial system as it imposes oxidative stress on airway epithelial cells. J Immunol. 2008;181: 4883–4893.
61. Wang D, Yu JM, Dorosky RJ, Pierson LS, Pierson EA. The phenazine 2-hydroxy-phenazine-1-carboxylic acid promotes extracellular DNA release and has broad transcriptomic consequences in *Pseudomonas chlororaphis* 30-84. PLoS One. 2016;11: e0148003.
62. Gibson J, Sood A, Hogan DA. *Pseudomonas aeruginosa-Candida albicans* interactions: localization and fungal toxicity of a phenazine derivative. Appl Environ Microbiol. 2009;75: 504–513.
63. Voggu L, Schlag S, Biswas R, Rosenstein R, Rausch C, Götz F. Microevolution of cytochrome *bd* oxidase in Staphylococci and its implication in resistance to respiratory toxins released by *Pseudomonas*. J Bacteriol. 2006;188: 8079–8086.
64. Lu J, Holmgren A. The thioredoxin antioxidant system. Free Radic Biol Med. 2014;66: 75–87.
65. Hall S, McDermott C, Anoopkumar-Dukie S, McFarland AJ, Forbes A, Perkins AV, et al. Cellular effects of pyocyanin, a secreted virulence factor of *Pseudomonas aeruginosa*. Toxins (Basel). 2016;8.
66. Piddock LJV. Multidrug-resistance efflux pumps - not just for resistance. Nat Rev Microbiol. 2006;4: 629–636.
67. Hollstein U, Van Gemert RJ. Interaction of phenazines with polydeoxyribonucleotides. Biochemistry. 1971;10: 497–504.
68. DeAngelis DL, Mulholland PJ, Palumbo AV, Steinman AD, Huston MA, Elwood JW. Nutrient dynamics and food-web stability. Annu Rev Ecol Syst. 1989;20: 71–95.
69. Odum WE, Odum EP, Odum HT. Nature's pulsing paradigm. Estuaries. 1995;18: 547.
70. Widdel F, Pfennig N. Studies on dissimilatory sulfate-reducing bacteria that decompose fatty acids. Arch Microbiol. 1981;129: 395–400.
71. Paintdakhi A, Parry B, Campos M, Irnov I, Elf J, Surovtsev I, et al. Oufti: an integrated software package for high-accuracy, high-throughput quantitative microscopy analysis. Mol Microbiol. 2016;99: 767–777.

72. Cheluvappa R. Standardized chemical synthesis of *Pseudomonas aeruginosa* pyocyanin. MethodsX. 2014;1: 67–73.
73. Sullivan NL, Tzeranis DS, Wang Y, So PTC, Newman D. Quantifying the dynamics of bacterial secondary metabolites by spectral multiphoton microscopy. ACS Chem Biol. 2011;6: 893–899.
74. Bacic MK, Smith CJ. Laboratory maintenance and cultivation of bacteroides species. Curr Protoc Microbiol. 2008;Chapter 13: Unit 13C.1.
75. Babin BM, Bergkessel M, Sweredoski MJ, Moradian A, Hess S, Newman DK, et al. SutA is a bacterial transcription factor expressed during slow growth in *Pseudomonas aeruginosa*. Proc Natl Acad Sci USA. 2016;113: E597-605.
76. Heussler GE, Cady KC, Koeppen K, Bhuju S, Stanton BA, O'Toole GA. Clustered regularly interspaced short palindromic repeat-dependent, biofilm-specific death of *Pseudomonas aeruginosa* mediated by increased expression of phage-related genes. MBio. 2015;6: e00129-15.
77. Racki LR, Tocheva EI, Dieterle MG, Sullivan MC, Jensen GJ, Newman DK. Polyphosphate granule biogenesis is temporally and functionally tied to cell cycle exit during starvation in *Pseudomonas aeruginosa*. Proc Natl Acad Sci USA. 2017;114: E2440–E2449.
78. Malhotra S, Limoli DH, English AE, Parsek MR, Wozniak DJ. Mixed communities of mucoid and nonmucoid *Pseudomonas aeruginosa* exhibit enhanced resistance to host antimicrobials. MBio. 2018;9.

Supplementary information

Table S1. Strains and primers used in this study.

Strain or primer	Description or sequence			Reference
Strains				
P. aeruginosa PA14 DKN263	Wild-type *P. aeruginosa* strain, produces phenazines			
P. aeruginosa PA14 DKN330	Δ*phz P. aeruginosa* strain, does not produce phenazines (this strain had both *phz1* and *phz2* operons deleted)			[20]
P. aeruginosa PA14 DKN1338	Wild-type *P. aeruginosa* strain - constitutive YFP expression			[23]
Primers (qRT-PCR)		**Gene**	**Orientation**	
LAM-PRT0027-ahpC-F	TGATCTTCATGCCGGCTGCCTT	*ahpC*	forward	This study
LAM-PRT0028-ahpC-R	GAGGTTTCGTGCCAGACCTT	*ahpC*	reverse	This study
LAM-PRT0029-ahpF-F	CTGCAACGCAAGCTCTACAG	*ahpF*	forward	This study
LAM-PRT0030-ahpF-R	ACGAAGATGCCTTCCAGCTC	*ahpF*	reverse	This study
LAM-PRT0023-ahpB-F	ACTGGTCAACAAGCAAGCCC	*ahpB*	forward	This study
LAM-PRT0024-ahpB-R	TTGTGGGCGATGATTTCCGA	*ahpB*	reverse	This study
LAM-PRT0025-trxB2-F	TCTTCGACCACATCCATGCC	*trxB2*	forward	This study
LAM-PRT0033-trxB2-R	ATCAGTGCGTCGCAGGTGTA	*trxB2*	reverse	This study
LAM-PRT0037-katB-F	GCGAAGTGCACTACGTGAAG	*katB*	forward	This study
LAM-PRT0038-katB-R	TGGTCATGTGGCTGTAGTCG	*katB*	reverse	This study
LAM-PRT0049-trxA-F	ATCAGGGCAAGCTGAAGGTC	*trxA*	forward	This study
LAM-PRT0050-trxA-R	ATATTGGCGTCGAGGAAGGC	*trxA*	reverse	This study
LAM-PRT0019-mexG-F	AACTCGCTCGAAAGCAACTG	*mexG*	forward	[20]
LAM-PRT0020-mexG-R	GCTGGCCTGATAGTCGAACA	*mexG*	reverse	[20]
LAM-PRT0021-mexH-F	CACCTCGGCCAGTACCTC	*mexH*	forward	[20]
LAM-PRT0022-mexH-R	GACTGGTGCTTTCGTCCAG	*mexH*	reverse	[20]
LAM-PRT0045-mexE-F	CTGATCAAGGACGAAGCGGT	*mexE*	forward	This study
LAM-PRT0046-mexE-R	TTCGGTCCCATCTCGACAGT	*mexE*	reverse	This study
LAM-PRT0047-mexF-F	CAGTTGAAGGTGCGCAACAA	*mexF*	forward	This study
LAM-PRT0048-mexF-R	GTTGGGCAGTTCCTCCTTCA	*mexF*	reverse	This study
LAM-PRT0001-recA-F	GCCCTGGAAATCACCGACAT	*recA*	forward	[77]
LAM-PRT0002-recA-R	TTCGATCTCGGCCTTGGGTA	*recA*	reverse	[77]
LAM-PRT0003-lexA-F	CCAGGAACTCGGCTTCAAGT	*lexA*	forward	[77]
LAM-PRT0004-lexA-R	TGTTCTGTTCGGCGAGGATC	*lexA*	reverse	[77]
LAM-PRT0007-Ftail-F	GGAAGTTAGGCAAGAGTGGAAA	PA14_08300	forward	[76]
LAM-PRT0008-Ftail-R	CCAGTTGTTGTATCCGTCAAGTA	PA14_08300	reverse	[76]

LAM-PRT0031-lys-F	GAACCTCAATTACAGCGCCC	*lys*	forward	[78]
LAM-PRT0032-lys-R	GTAGGTGTTGTCGGCAATCG	*lys*	reverse	[78]
LAM-PRT0041-iscA-F	GGCTTGCCTATGTCCTCGAA	*iscA*	forward	This study
LAM-PRT0042-iscA-R	AAGCCTTCGTTGAGCCCTTC	*iscA*	reverse	This study
LAM-PRT0043-iscU-F	TCGACCACTACGAAAACCCG	*iscU*	forward	This study
LAM-PRT0044-iscU-R	TCTTGCCCTTCATCCACTCG	*iscU*	reverse	This study
LAM-PRT0039-fdx2-F	GATCGAGCATGCCTGTGAGA	*fxd2*	forward	This study
LAM-PRT0040-fdx2-R	CCAGCATGTCGTCTTCGAGT	*fxd2*	reverse	This study
LAM-PRT0035-oprI-F	AGCAGCCACTCCAAAGAAAC	*oprI*	forward	[75]
LAM-PRT0036-oprI-R	CAGAGCTTCGTCAGCCTTG	*oprI*	reverse	[75]
LAM-PRT0015-proC	GCTGCTGTCTGCGGTAGG	*proC*	forward	[76]
LAM-PRT0016-proC	CATCAGCAGGAAGAAATACGCC	*proC*	reverse	[76]

Table S2. Results of Tukey's HSD multiple-comparison test (95% confidence interval) for different phenazines performed in Fig. 2.

Time: 24 hrs		**Time: 48 hrs**	
Comparison (n = 4)	adjusted p-value	Comparison (n = 4)	adjusted p-value
PYO vs No phenazines	0.0000000	PYO vs No phenazines	0.0000000
1-OH-PHZ vs No phenazines	0.0000001	1-OH-PHZ vs No phenazines	0.0000000
PCN vs No phenazines	0.0001662	PCN vs No phenazines	0.0000000
PCA vs No phenazines	0.0098043	PCA vs No phenazines	0.0000048
1-OH-PHZ vs PYO	0.3851492	1-OH-PHZ vs PYO	0.0650415
PCN vs PYO	0.0000555	PCN vs PYO	0.0062471
PCA vs PYO	0.0000019	PCA vs PYO	0.0000023
PCN vs 1-OH-PHZ	0.0015297	PCN vs 1-OH-PHZ	0.7374776
PCA vs 1-OH-PHZ	0.0000322	PCA vs 1-OH-PHZ	0.0002683
PCA vs PCN	0.2413360	PCA vs PCN	0.0026315

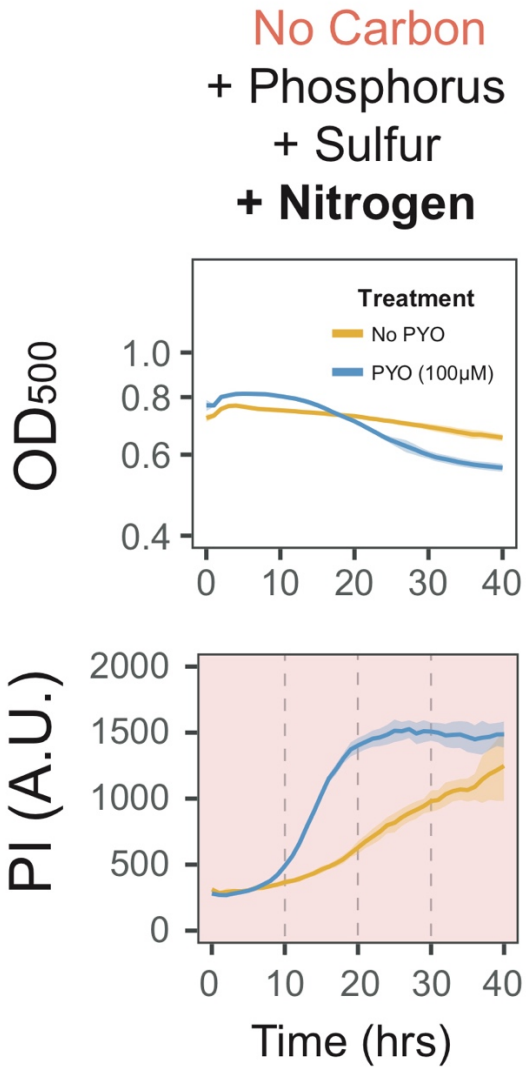

Figure S1. Addition of Nitrogen (NH_4Cl) back to the culture does not prevent PYO-mediated cell death. Experiment performed like in Fig. 3, but adding N back to the culture.

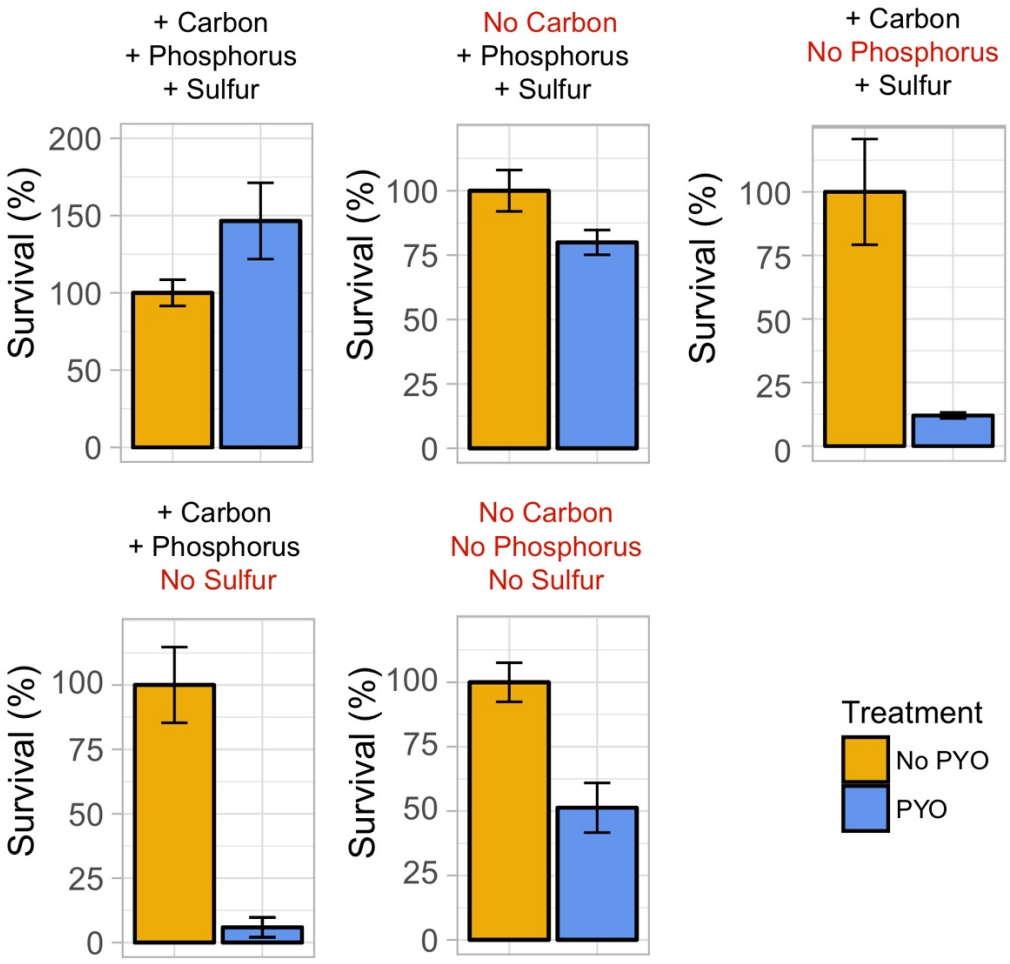

Figure S2. Nutrient starvation triggers PYO-mediated cell death in *Pa* PA14. Survival rates were obtained by CFU recovery after incubation for 50 hrs under the same conditions for the experiment displayed in Fig. 3. For each treatment, survival was normalized by the control (No PYO). For starvation conditions (Carbon, Phosphorus, Sulfur), PYO poisoned cells and caused cell death, confirming interpretation of the propidium iodide (PI) fluorescence signal as a marker for death in plate reader experiments.

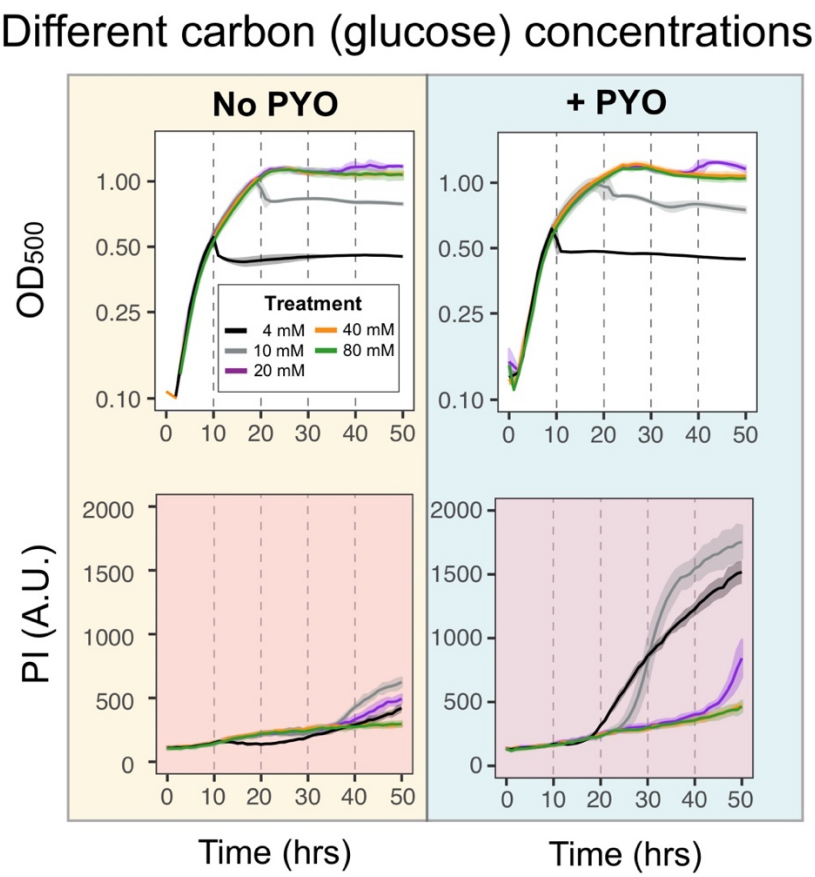

Figure S3. Toxic effects of PYO are coupled to the available reducing power levels. Carbon starvation in stationary phase is the cause of increased PYO-mediated cell death under normal growth conditions. Cell-death signal increase correlates with carbon limitation and higher levels of glucose (> 40 mM) inhibits cell death during the time span used for these experiments. Increase in cell death is PYO-stimulated (right), with the absence of PYO (left) always resulting in lower cell death levels. Data here presented for +PYO treatment is the same displayed in Fig. 3F.

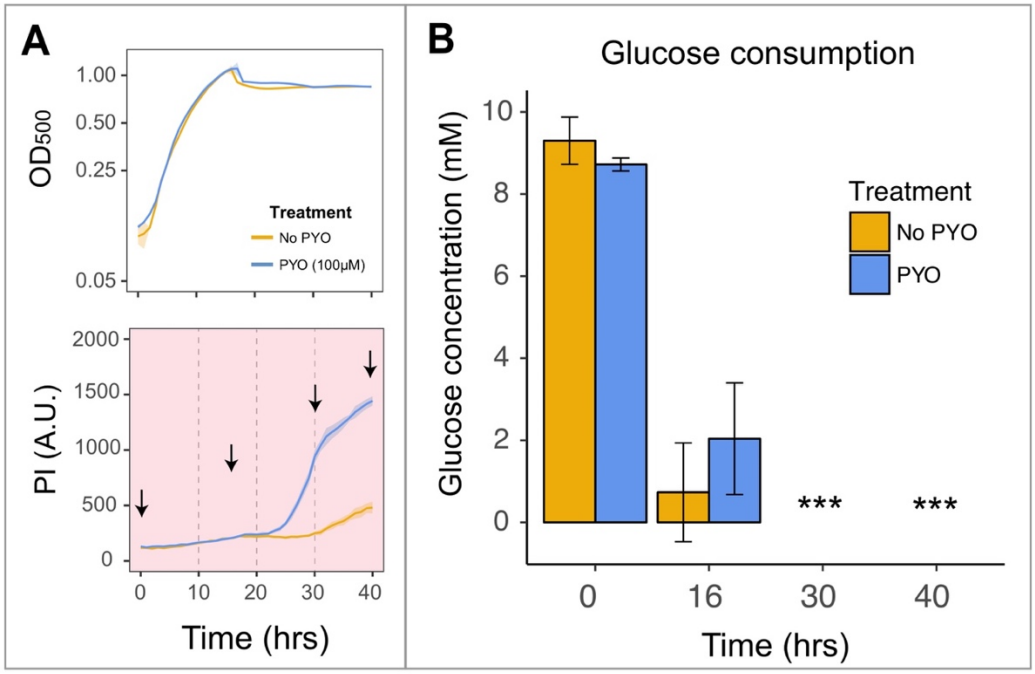

Figure S4. Glucose measurements over time during Δ*phz Pa* PA14 growth in 10 mM glucose. **A.** Growth and cell death levels over the course of batch growth. Arrows represent time points for which glucose levels were measured. Plotted lines represent averages of six replicates and shaded areas are SD. **B**. Glucose measurements over the course of batch growth. Cell death correlates with starvation of glucose. *** = undetectable glucose levels. Bar graphs represent averages of three replicates and error bars are SD. Glucose levels were measured using Glucose Colorimetric Detection Kit (Invitrogen) following manufacturer's instructions.

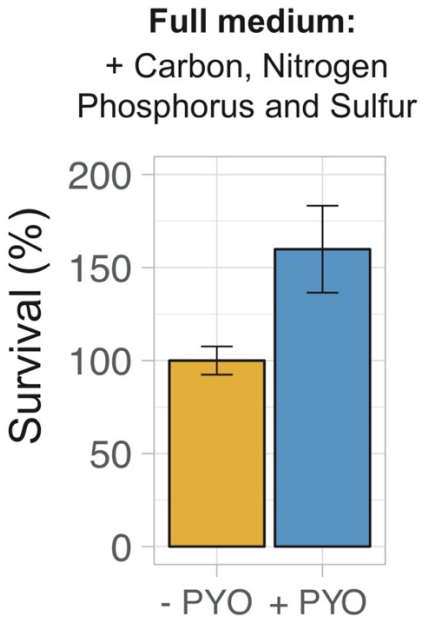

Figure S5. PYO causes beneficial effects under nutrient-replete conditions, resulting in increased cell density. Survival percentages were obtained by CFU recovery after 45 hrs of incubation in full medium and were normalized by the control (- PYO). Presence of PYO in the nutrient-replete medium resulted in increased CFU recovery. Cells were incubated in GMM + 100 mM MOPS, with 80 mM glucose as C source, as used for experiments shown in Fig. 3.

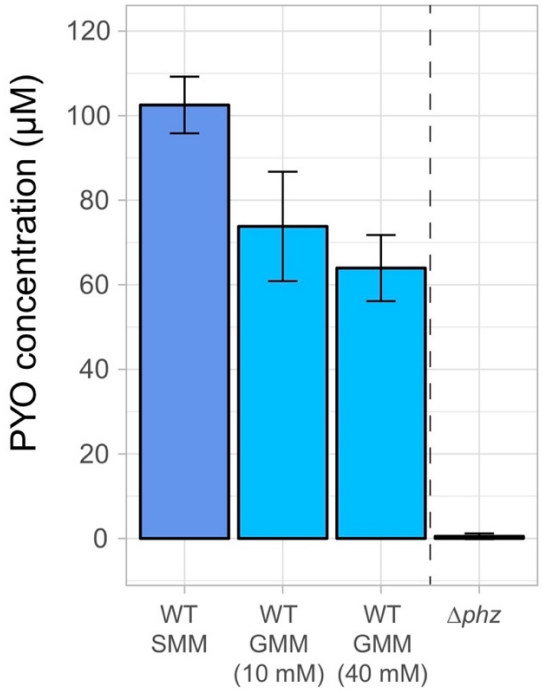

Figure S6. Concentrations of PYO in WT cultures for the different culture media used in this study. SMM = succinate minimal medium (with 40 mM sodium succinate), GMM = glucose minimal medium (with 10 or 40 mM of glucose). Δ*phz Pa* PA14 did not produce any PYO. Cultures were grown in 5 mL tubes for 18 hrs (following protocol described for Fig. 2A), and pyocyanin was measured by HPLC as previously described [30].

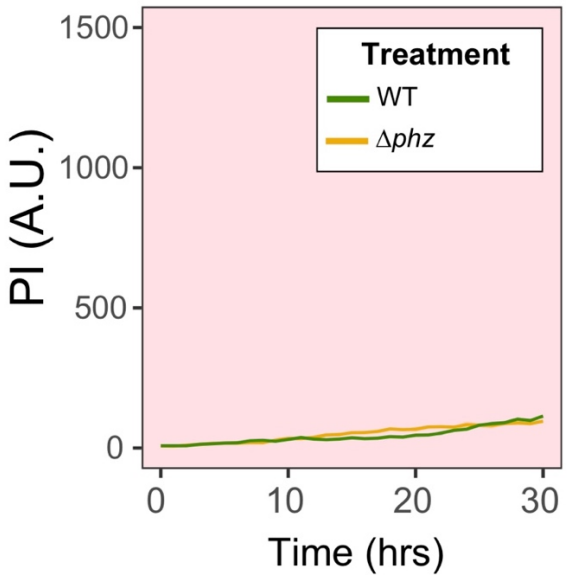

Figure S7. Cultures of WT and Δ*phz Pa* PA14 did not show background fluorescence at the excitation/emission wavelength used for measuring PI signal. Cultures grown in succinate minimal medium as done for Fig. 2.

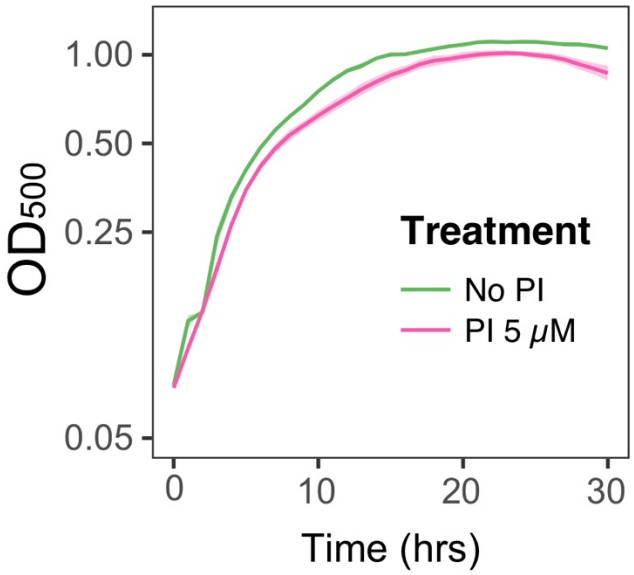

Figure S8. Propidium iodide (5 µM) only mildly impacted Δ*phz* growth. Cultures grown in succinate minimal medium as done for Fig. 2.

Chapter 4

WHAT DOESN'T KILL YOU MAKES YOU STRONGER:
Pyocyanin-mediated antibiotic resilience in opportunistic pathogens

This chapter is adapted from:

Meirelles, L.A.*, Perry, E.K.*, Bergkessel, M., and Newman, D.K. (2021) Bacterial defenses against a natural antibiotic promote collateral resilience to clinical antibiotics. *PLoS Biol* **19**: e3001093. https://doi.org/10.1371/journal.pbio.3001093

Abstract

Bacterial opportunistic human pathogens frequently exhibit intrinsic antibiotic tolerance and resistance, resulting in infections that can be nearly impossible to eradicate. We asked whether this recalcitrance could be driven by these organisms' evolutionary history as environmental microbes that engage in chemical warfare. Using *Pseudomonas aeruginosa* as a model, we demonstrate that the self-produced antibiotic pyocyanin activates defenses that confer collateral tolerance specifically to structurally-similar synthetic clinical antibiotics. Non-pyocyanin-producing opportunistic pathogens, such as members of the *Burkholderia cepacia* complex, likewise display elevated antibiotic tolerance when co-cultured with pyocyanin-producing strains. Furthermore, by widening the population bottleneck that occurs during antibiotic selection and promoting the establishment of a more diverse range of mutant lineages, pyocyanin increases apparent rates of mutation to antibiotic resistance to a degree that can rival clinically-relevant hypermutator strains. Together, these results reveal an overlooked mechanism by which opportunistic pathogens that produce natural toxins can dramatically modulate the efficacy of clinical antibiotics and the evolution of antibiotic resistance, both for themselves and other members of clinically-relevant polymicrobial communities.

Introduction

The emergence and spread of bacterial resistance to clinical antibiotics is a growing public health concern worldwide [1]. Moreover, it is increasingly appreciated that antibiotic tolerance can also contribute to the failure of treatments for infections [2] and that tolerance can lead to the evolution of resistance [3,4]. Yet bacterial resilience to antibiotics is anything but new: microbes in environments like soil have been producing natural antibiotics and evolving mechanisms of tolerance and resistance for millions of years [5,6]. Here, we define tolerance as the ability to survive a transient exposure to an otherwise lethal antibiotic concentration, and resistance as the ability to grow in the presence of an antibiotic, similar to recent recommendations [2,7,8].

Considering that most of the antibiotics used today are derived from microbially-produced molecules, we hypothesized that molecular defenses that originally evolved to protect cells from a natural antibiotic in the environment might also promote tolerance and/or resistance to structurally- or mechanistically-similar clinical drugs. Indeed, several clinical antibiotic resistance genes are thought to have originated in non-pathogenic soil bacteria, but it has often been assumed that intermediate steps of horizontal gene transfer are necessary in order for such genes to be acquired by human pathogens [6]. In this study, we asked whether there could be a direct link between production of natural antibiotics by an opportunistic human pathogen and its recalcitrance to clinical antibiotic treatment due to shared protective mechanisms. In addition, we sought to determine whether in the presence of such a natural antibiotic producer, recalcitrance to clinical antibiotics could also be observed in other opportunistic pathogens found together with it in polymicrobial infections. Given that many opportunistic pathogens share their natural environment (e.g. soil), we posited that the evolutionary legacy of natural-antibiotic-mediated ecological interactions between these microbial species could have important implications for antibiotic tolerance and resistance in the clinical context.

One organism that is well-suited to testing these hypotheses is the opportunistic pathogen *Pseudomonas aeruginosa*, which is notorious for causing chronic lung infections in cystic fibrosis (CF) patients, as well as other types of infections in immunocompromised hosts [9]. *P. aeruginosa* produces several redox-active, heterocyclic compounds known as phenazines [10]. Phenazines

have been shown to provide multiple benefits for their producers, including by: (i) serving as an alternative electron acceptor in the absence of oxygen, thereby promoting redox homeostasis and anaerobic survival [11], which is particularly relevant for oxidant-limited biofilms [12]; (ii) acting as signaling molecules [13]; (iii) promoting iron acquisition [14]; and (iv) killing competitor species [15]. In addition, despite possessing broad-spectrum antimicrobial activity [10], including against *P. aeruginosa* itself [16], phenazines have recently been shown to promote tolerance to clinical antibiotics under some circumstances, via mechanisms that have yet to be characterized [17,18]. Here, we sought to assess potential broader implications of this phenomenon by investigating whether phenazine-mediated tolerance to clinical antibiotics in *P. aeruginosa* is driven by cellular defenses that evolved to mitigate self-induced toxicity. We also tested whether phenazine production by *P. aeruginosa* could promote antibiotic tolerance in other clinically-relevant opportunistic pathogens from the *Burkholderia* and *Stenotrophomonas* genera. Finally, we explored the ramifications of phenazine-induced tolerance for the evolution of heritable antibiotic resistance, both in *P. aeruginosa* and in a clinical isolate from the *Burkholderia cepacia* complex.

Results

Mechanisms of tolerance to the self-produced natural antibiotic PYO in P. aeruginosa

We started by characterizing the defense mechanisms *P. aeruginosa* has evolved to tolerate its most toxic self-produced phenazine, pyocyanin (PYO) [10,16]. To do so in an unbiased fashion, we performed a genome-wide transposon sequencing (Tn-seq) screen in which the mutant library was exposed to PYO under starvation to maximize PYO toxicity [16], and tolerance of the pooled mutants to PYO was assessed following re-growth (Fig 1A). This revealed five broad categories of genes that significantly affect tolerance to PYO: (i) efflux system repressors, (ii) protein damage responses, (iii) membrane or cell wall biosynthesis, (iv) oxidative stress responses, and (v) carbon metabolism and transport (Fig 1B). We validated the screen results by constructing and testing chromosomal clean deletion mutants for four of these genes (Fig 1C).

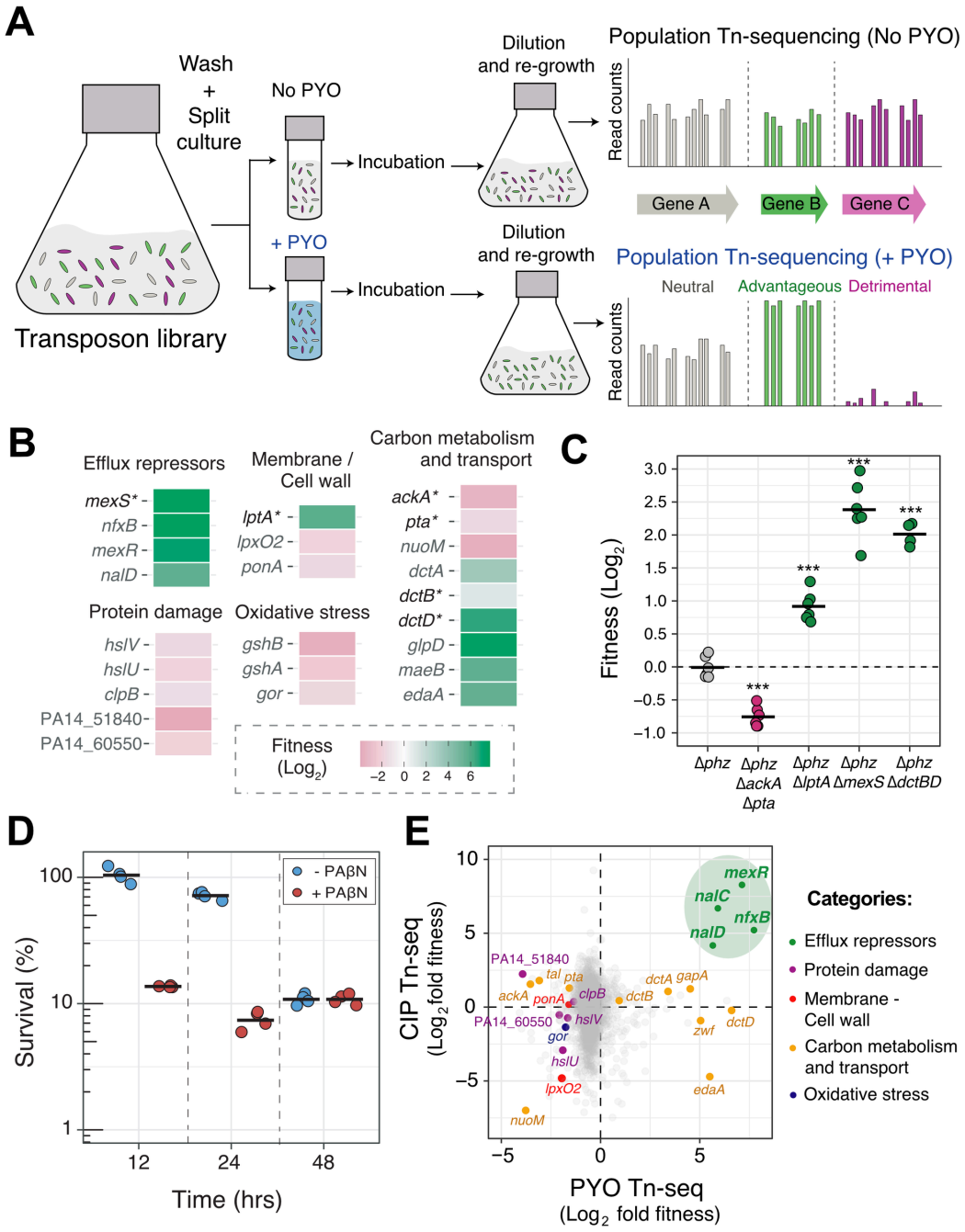

Figure 1. Mechanisms of tolerance to the self-produced natural antibiotic PYO in *P. aeruginosa*. A. Genome-wide transposon sequencing (Tn-seq) experimental design. Cells were incubated with and without PYO under nutrient starvation for maximum PYO toxicity [16] (see Methods for details). Bar graphs shown are hypothetical representations of the expected results for genes with different fitness effects and are not derived from the obtained data. **B.** Statistically-significant fitness effects of transposon insertions in different representative genes under conditions that maximize PYO toxicity (for full dataset, see S1 Table). See Methods for details on calculation of fitness. Asterisks show genes for which chromosomal clean deletion mutants were constructed and validated. **C.** Tn-

seq validations. Chromosomal clean deletion mutants were exposed to PYO under carbon starvation, similar to the conditions used for the Tn-seq experiment. Survival of each strain was measured by colony forming units (CFUs) and compared to the survival of the parent Δ*phz* strain for fitness calculation (see Methods for details). Statistical significance was calculated using one-way ANOVA with Tukey's HSD multiple-comparison test, with asterisks showing significant differences relative to Δ*phz* (*** $p < 0.001$). Data points represent independent replicates and black horizontal lines mark the mean fitness for each strain. **D.** Tolerance to PYO toxicity in the presence and absence of the efflux inhibitor PAβN. Each data point represents an independent biological replicate (n = 4), and the horizontal black lines mark the mean survival for each condition and time point. **E.** Fitness correlation analysis between PYO tolerance Tn-seq (this study) and CIP persistence Tn-seq [24]. Efflux repressors present in both datasets are highlighted in green. For full analysis, see S1 Table.

The fitness effects of different transposon insertions largely aligned with what is thought to be the primary mode of PYO toxicity, which is the generation of reactive oxygen species (ROS) [19,20]. For example, the fact that transposon insertions in different genes within the "carbon metabolism and transport" category had opposite effects on fitness likely reflects conflicting priorities for cells challenged with ROS-generating toxins: on one hand, limiting flux through the electron transport chain decreases the potential for ROS generation, but on the other hand, proton-motive force is required to pump the toxin out, and NADH is needed to power reductases involved in repair of oxidative damage. The need to counteract oxidative stress would also explain why transposon insertions in genes related to protein damage repair and glutathione synthesis or reduction led to decreased fitness in the presence of PYO (Fig 1B). Finally, for genes related to cell wall/membrane synthesis, the transposon insertions may have altered cellular permeability and thereby either increased or decreased PYO influx.

However, the strongest hits in our Tn-seq were transposon insertions in transcriptional repressors of resistance-nodulation-division (RND) efflux system genes (Fig 1B and S1 Table), which would cause overexpression of the downstream efflux pumps. These insertions dramatically increased fitness in the presence of PYO, suggesting that one of the most effective defenses against PYO toxicity is to decrease the intracellular concentration of the toxin. While transposon insertions in the genes encoding the efflux pump proteins themselves did not have strong effects in our screen (S1 Table), this is likely due to partial functional redundancy among the various efflux systems [21]. Indeed, when we challenged starved *P. aeruginosa* with PYO in the presence of the broad-spectrum RND efflux inhibitor phenylalanine-arginine β-naphthylamide (PAβN), cell death was accelerated, confirming that efflux pumps are necessary for minimizing PYO toxicity (Fig 1D).

Mutations in the efflux system repressors identified in our Tn-seq screen are commonly found in clinical isolates that are resistant to synthetic fluoroquinolone antibiotics, as the efflux systems regulated by these repressors efficiently export this class of drugs [22,23]. We therefore asked whether the mechanisms used by *P. aeruginosa* to tolerate PYO toxicity might overlap more broadly with those that confer tolerance to fluoroquinolones. To address this question, we compared our dataset to a recent Tn-seq study that screened for genes that affect *P. aeruginosa* survival in the presence of the broad-spectrum fluoroquinolone ciprofloxacin [24]. Across the two datasets, we observed similar fitness effects for insertions in a small number of genes within the "protein damage response," "membrane/cell wall," and "oxidative stress response" categories, but the most dramatic fitness increases in both experiments were caused by insertions in a shared set of efflux system repressors (Fig 1E and S1 Table). These results highlighted the potential for a conserved molecular route to increased tolerance against both a natural antibiotic, PYO, and a synthetic clinical antibiotic, ciprofloxacin.

PYO induces expression of specific efflux systems, conferring cross-tolerance to fluoroquinolones

Given that cellular processes involved in PYO tolerance have also been implicated in ciprofloxacin tolerance, we asked whether exposure to PYO could promote an increase in tolerance to ciprofloxacin and related clinical antibiotics, including other synthetic fluoroquinolones. Importantly, such an effect would require that PYO induces the expression of shared defense mechanisms. We have previously established that PYO upregulates expression of not only the oxidative stress response genes *ahpB* (a thiol-specific peroxidase) and *katB* (a catalase) [16], but also at least two efflux systems known to pump fluoroquinolones, *mexEF-oprN* and *mexGHI-opmD* [13,16]. We confirmed these expression patterns by performing qRT-PCR on the WT strain that produces PYO, a Δ*phz* mutant that does not produce PYO, and Δ*phz* treated with exogenous PYO (S1, S2 and S3 Figs). Notably, phenazines and fluoroquinolones both contain at least one aromatic ring, unlike other antibiotics that are not thought to be pumped by *mexEF-oprN* and *mexGHI-opmD*, such as aminoglycosides [21] (Fig 2A). Thus, structural similarities could account for why efflux pumps that likely evolved to export natural antibiotics such as PYO can also transport certain classes of synthetic antibiotics. To determine whether PYO also induces other

efflux systems known to pump clinical antibiotics besides fluoroquinolones, we performed qRT-PCR on representative genes from all 11 major RND efflux systems in the *P. aeruginosa* genome. These measurements confirmed that *mexEF-oprN* and *mexGHI-opmD* are the only two efflux systems significantly induced by PYO, and that the induction is PYO dose-dependent (Fig 2B and S2 and S3 Figs). The *mexGHI-opmD* system in particular reached expression levels comparable to the constitutively-expressed *mexAB-oprM* efflux system (Fig 2B and S2 Fig), which plays an important role in the intrinsic antibiotic tolerance and resistance of *P. aeruginosa* [21].

To assess whether the induction of efflux pumps and oxidative stress responses by PYO could increase the tolerance of *P. aeruginosa* to clinical drugs such as ciprofloxacin, we grew cultures with or without clinically-relevant concentrations of PYO [25] and performed a survival assay following treatment with different antibiotics. Importantly, we hypothesized that PYO would not be a universal antagonist to all clinical antibiotics. Instead, we expected tolerance to increase only for drugs affected by the defense mechanisms induced by PYO in the cells. Indeed, compared to the non-PYO-producing Δ*phz* mutant, the PYO-producing WT strain and PYO-treated Δ*phz* were more tolerant to both ciprofloxacin and another fluoroquinolone, levofloxacin (Fig 2C). On the other hand, PYO did not confer increased tolerance to: (i) aminoglycosides (Fig 2D and S4B Fig), which are not substrates for the efflux pumps upregulated by PYO [21]; or (ii) colistin (polymyxin E) (Fig 2C), an antimicrobial peptide that permeabilizes the outer membrane of the cell by interacting with the lipopolysaccharide and causing displacement of divalent cations [1]. Similar to aminoglycosides, colistin is not known to be pumped by the PYO-induced efflux systems [21]; moreover, efflux rarely impacts polymyxin efficacy [26]. PYO itself was not toxic under the experimental conditions used in our tolerance assays [16] (S4C Fig). Aside from PYO, 1-hydroxyphenazine was the only other phenazine made by *P. aeruginosa* that increased tolerance to ciprofloxacin under our conditions, albeit to a lesser extent than PYO (Fig 2E). We also tested whether the presence of PYO could affect the minimum inhibitory concentration (MIC) for ciprofloxacin, as the classical definition of antibiotic tolerance also stipulates that increased survival in the presence of an antibiotic is not accompanied by an increase in MIC [2,8]. When we determined the MIC for ciprofloxacin according to standard clinical protocols [27] for our *P. aeruginosa* strain in the presence or absence of PYO, we saw no consistent difference at a detection

limit of a two-fold increase in MIC (S7 Table), supporting the interpretation that the effect of PYO on *P. aeruginosa* is primarily an increase in antibiotic tolerance (i.e. survival without the ability to grow) rather than phenotypic resistance. Importantly, PYO also induced ciprofloxacin tolerance when *P. aeruginosa* was grown in synthetic cystic fibrosis sputum medium (SCFM) (Fig 2D), suggesting that PYO production could contribute to antibiotic tolerance of this bacterium in CF patients. Together, these results indicate that PYO preferentially induces tolerance to fluoroquinolones.

Under *in vitro* conditions, PYO is typically produced in early stationary phase [13]. However, the heterogeneous nature of physiological conditions in infections [28,29] could lead to intermixing of PYO-producing and -non-producing cells *in vivo*. We therefore tested whether exogenous PYO could increase the fluoroquinolone tolerance of cells harvested during log phase, which did not make PYO. To limit the growth of the no-antibiotic control, we exposed these cells to the antibiotics under nitrogen depletion. PYO still increased tolerance to both ciprofloxacin and levofloxacin under these conditions, suggesting that the induced tolerance phenotype does not depend on the previous growth phase of growth-arrested cells [16] (S4B Fig). Next, to visualize the recovery of cell growth after a transient exposure to ciprofloxacin, we performed a time-lapse microscopy assay (S4D Fig). Interestingly, WT *P. aeruginosa* and PYO-treated Δ*phz* exhibited a shorter lag phase compared to non-PYO-treated Δ*phz* following ciprofloxacin treatment (Fig 2F-G and S4E-F Fig and S1 Movie), suggesting that PYO-induced defenses may help minimize cellular damage during the antibiotic treatment. We also found that addition of PYO to Δ*phz* increased ciprofloxacin tolerance in a dose-dependent manner (Fig 2H), mirroring the dose-dependent induction of *mexEF-oprN* and *mexGHI-opmD* (Fig 2B).

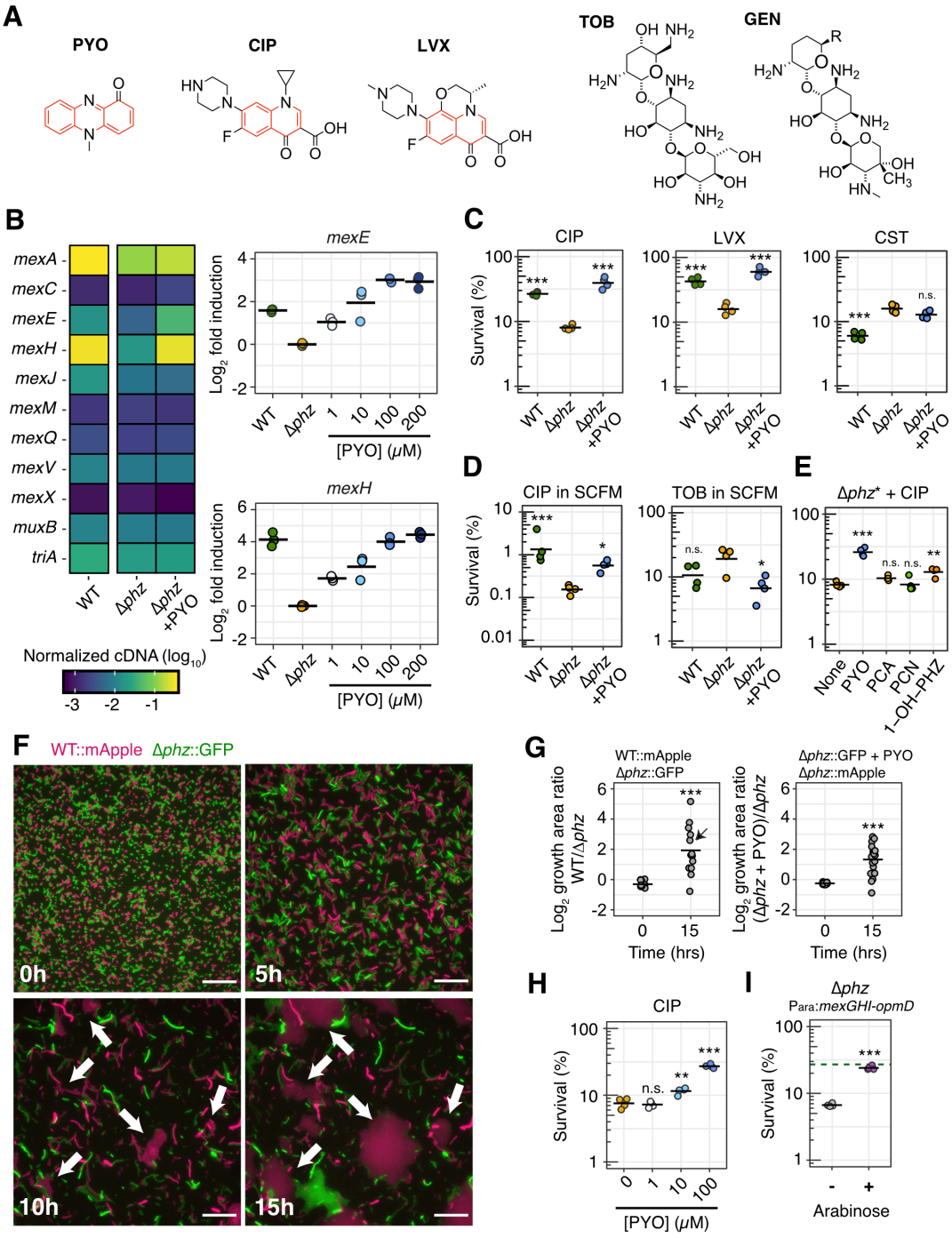

Figure 2. PYO induces expression of specific efflux systems, conferring cross-tolerance to fluoroquinolones. A. Structures of PYO, two representative fluoroquinolones (CIP = ciprofloxacin, LVX = levofloxacin) and two representative aminoglycosides (GEN = gentamicin, TOB = tobramycin). PYO and fluoroquinolones are pumped by MexEF-OprN and MexGHI-OpmD, while aminoglycosides are not [21,22]. Rings with an aromatic character are highlighted in red. **B.** Normalized cDNA levels for genes within operons coding for the 11 main RND efflux systems in *P. aeruginosa* (left; n = 3), and PYO-dose-dependent changes in expression of *mexEF-oprN* and *mexGHI-opmD* systems (right; n = 3). For full qRT-PCR dataset, see S1, S2 and S3 Figs. **C.** Effect of PYO on tolerance to CIP (1

μg/mL), LVX (1 μg/mL) and CST (colistin, 16 μg/mL) in glucose minimal medium (n = 4). **D.** Effect of PYO on tolerance to CIP (1 μg/mL) and TOB (40 μg/mL) in SCFM (n = 4). PYO itself was not toxic under the experimental conditions [16] (S4C Fig). WT made 50-80 μM PYO as measured by absorbance of the culture supernatant at 691 nm. See S5A Fig for experimental design. **E.** Effect on tolerance to CIP (1 μg/mL) caused by the presence of the four main phenazines produced by *P. aeruginosa* (PYO = pyocyanin, PCA = phenazine-1-carboxylic acid, PCN = phenazine-1-carboxamide and 1-OH-PHZ = 1-hydroxyphenazine) (n = 4). For this experiment, a Δ*phz** strain that cannot produce or modify any phenazine was used (see Methods). **F-G.** Effect of PYO on lag during outgrowth after exposure to CIP. A representative field of view over different time points (F; magenta = WT::mApple, green = Δ*phz*::GFP; see S1 Movie) is shown together with the quantification of growth area on the agarose pads at time 0 hrs and 15 hrs (G). For these experiments, a culture of each strain tested was grown and exposed to CIP (10 μg/mL) separately, then cells of both cultures were washed, mixed and placed together on a pad and imaged during outgrowth. The pads did not contain any PYO or CIP (see Methods and S5D Fig for details). White arrows in the displayed images point to regions with faster recovery of WT growth. The field of view displayed is marked with a black arrow in the quantification plot. The results for the experiment with swapped fluorescent proteins are shown in S4E Fig. See S4C Fig for complementary data about effects of PYO on lag. Scale bar: 20 μm. **H.** Tolerance of Δ*phz* to CIP (1 μg/mL) in stationary phase in the presence of different concentrations of PYO (n = 4). **G.** Tolerance of Δ*phz* to CIP (1 μg/mL) upon artificial induction of the *mexGHI-opmD* operon with arabinose (n = 4). The dashed green line marks the average survival of PYO-producing WT under similar conditions (without arabinose). Statistics: C, D, E, H – One-way ANOVA with Tukey's HSD multiple-comparison test, with asterisks showing significant differences relative to untreated Δ*phz* (no PYO); G, I – Welch's unpaired t-test (* $p < 0.05$, ** $p < 0.01$, *** $p < 0.001$, n.s. $p > 0.05$). In all panels with quantitative data, black horizontal lines mark the mean value for each condition. Individual data points represent independent biological replicates, except for in panel G, where the data points represent different fields of view.

Given that PYO-induced efflux pumps transport specific substrates [21], we asked if increased drug efflux could be the primary mechanism underlying PYO-mediated tolerance to fluoroquinolones. At high concentrations of ciprofloxacin, addition of the efflux inhibitor PAβN eliminated the survival advantage of PYO-treated cells, indicating that efflux pump activity is necessary for the PYO-mediated increase in antibiotic tolerance (S4G Fig). Next, we constructed a Δ*phz* strain with the *mexGHI-opmD* operon under the control of an arabinose-inducible promoter (P_{ara}:*mexGHI-opmD*). We verified that the transcription levels of *mexGHI-opmD* under arabinose induction were comparable to when PYO is present (S5 Fig). Indeed, arabinose induction of *mexGHI-opmD* expression increased ciprofloxacin tolerance to near-WT levels (Fig 2I), suggesting that induction of this efflux system is sufficient to confer the PYO-mediated increase in tolerance. On the other hand, arabinose induction of the oxidative stress response genes *ahpB* or *katB* did not significantly increase tolerance of Δ*phz* to ciprofloxacin (S6A-B Fig); however, the levels of induction achieved for these two genes with arabinose were lower than those observed in the presence of PYO (S1 and S5 Figs). Importantly, the clinical relevance of *mexGHI-opmD* was previously not well known, as to our knowledge, there have been no reports of clinical mutants with constitutive overexpression of this efflux system. Taken together, our results demonstrate that

PYO-mediated regulation of *mexGHI-opmD* expression modulates tolerance to a particular class of clinically used antibiotics in *P. aeruginosa*.

PYO promotes the evolution of antibiotic resistance in P. aeruginosa

Previous studies have demonstrated that mutations conferring antibiotic tolerance or persistence promote the evolution of antibiotic resistance [3,4]. Moreover, tolerance mutations can (i) interact synergistically with resistance mutations to increase bacterial survival during antibiotic treatment [30] and (ii) promote the establishment of resistance mutations during combination drug therapy [31]. To assess whether antibiotic tolerance induced by PYO could similarly promote the establishment of resistance mutations in populations of *P. aeruginosa* undergoing extended exposure to a clinical antibiotic, we next performed a series of fluctuation tests (Fig 3A). In clinical settings, antibiotic resistance is likely to result in treatment failure if a pathogen can grow at antibiotic concentrations above a threshold commonly referred to as a "breakpoint." We adopted this criterion by selecting mutants on antibiotic concentrations equal to or higher than the breakpoints defined by the European Committee on Antimicrobial Susceptibility Testing (EUCAST) [32]. Furthermore, we added PYO to our cultures either prior to the antibiotic selection step and/or concurrently with the antibiotic selection, in order to distinguish between the effects of preemptive versus continuous induction of PYO-regulated cellular defenses. Finally, while mutation rates inferred from fluctuation tests have sometimes been assumed to correlate with the per-base mutation rate across the genome [33,34], the results from these assays are also affected by the number of unique possible mutations that permit growth under the selection condition [35]. To encompass both possibilities in this study, we use the term μ_{app} (apparent rate of mutation) as a proxy for the likelihood of evolving antibiotic resistance. We calculated this parameter using standard methods for fluctuation test analysis (see Methods for details).

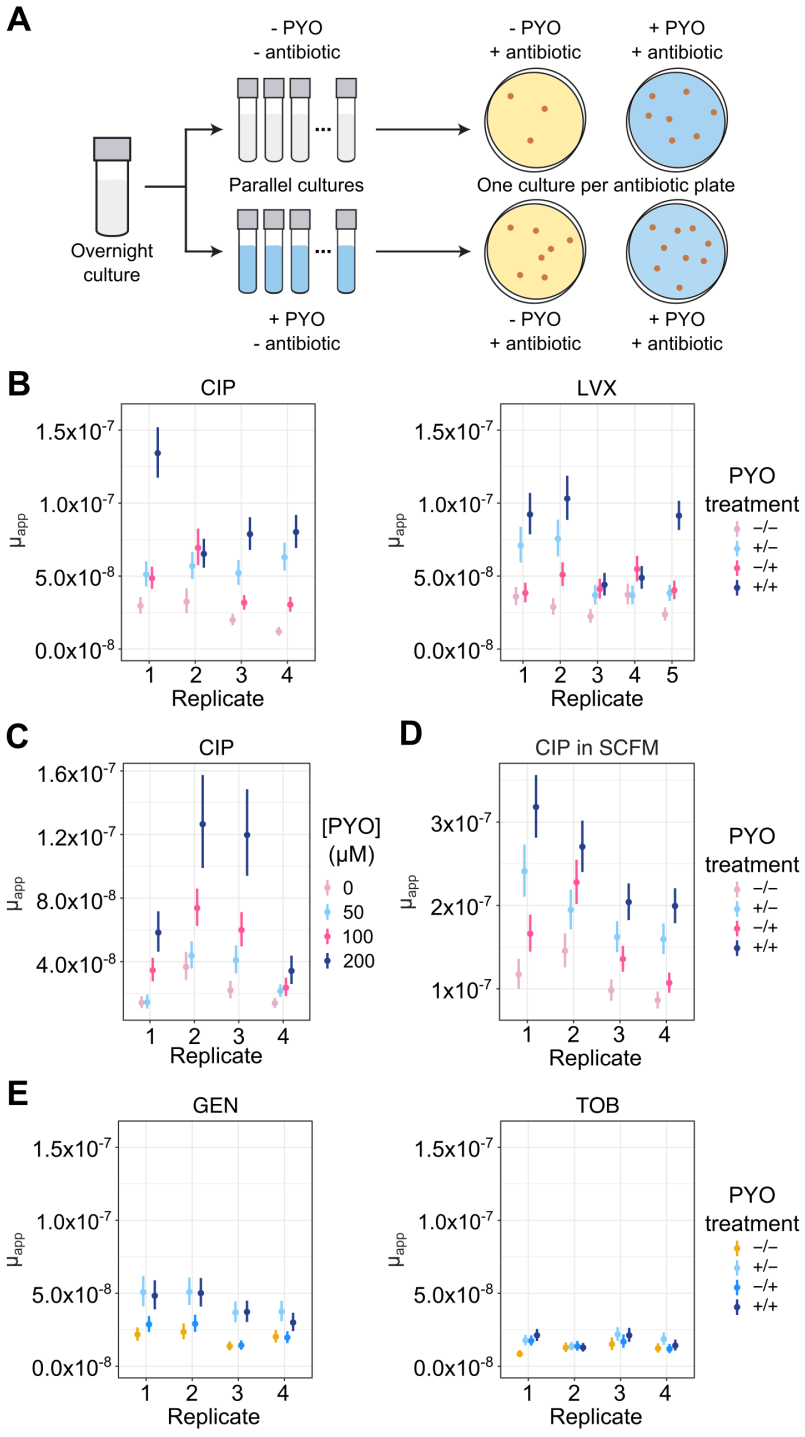

Figure 3. PYO increases the apparent rate of mutation to antibiotic resistance in *P. aeruginosa*. A. Experimental design for fluctuation tests to determine the effect of PYO (100 μM unless otherwise noted) on apparent mutation rates. For panels B-E, mutation rates were calculated using an established maximum likelihood-based method that accounts for the effects of plating a small proportion of the total culture volume (see Methods for details). Each data point in those panels represents a single biological replicate comprising 44 parallel cultures, and the vertical lines

represent the 84% confidence intervals. Lack of overlap in these confidence intervals corresponds to statistical significance at the $p < 0.05$ threshold [99]. For statistical significance as determined by a likelihood ratio test, see S2 Table. In B, D, and E, the PYO treatments correspond to the following: -/- denotes no PYO pre-treatment (in the liquid culture stage) or co-treatment (in the antibiotic agar plates), +/- denotes PYO pre-treatment but no co-treatment, -/+ denotes PYO co-treatment without pre-treatment, and +/+ denotes both PYO pre-treatment and co-treatment. **B.** Apparent mutation rates of log-phase Δ*phz* grown in glucose minimal medium and plated on MH agar containing ciprofloxacin (CIP, 0.5 μg/mL; n = 4) or levofloxacin (LVX, 1 μg/mL; n = 5), with or without pre- and/or co-exposure to PYO relative to the antibiotic selection step. **C.** The apparent rate of mutation to resistance for Δ*phz* cells that were pre-treated with different concentrations of PYO and plated onto CIP (0.5 μg/mL). **D.** Apparent mutation rates of log-phase Δ*phz* grown in SCFM and plated on SCFM agar containing CIP (1 μg/mL; n = 4) with or without pre- and/or co-exposure to PYO. **E.** Apparent mutation rates of log-phase Δ*phz* grown in glucose minimal medium and plated during onto MH agar containing gentamicin (GEN, 16 μg/mL; n = 4) or tobramycin (TOB, 4 μg/mL; n = 4), with or without pre- and/or co-exposure to PYO.

Regardless of whether PYO was added prior to or concurrently with the antibiotic selection, PYO significantly increased μ_{app} for resistance to ciprofloxacin in log-phase cultures (Fig 3B and S2 and S3 Tables). The same trends were also observed in stationary-phase cultures, albeit with smaller effect sizes (S7A Fig). These results indicate that pre-treatment with PYO is sufficient but not necessary to increase μ_{app} for ciprofloxacin resistance. Adding PYO at both stages of the fluctuation test generally resulted in an even greater increase in μ_{app} (Fig 3B, S7A Fig), and the increase in μ_{app} when PYO was added prior to antibiotic selection was dose-dependent (Fig 3C). Cultures that were selected on levofloxacin similarly displayed an increased μ_{app} upon PYO treatment, though the impact of pre-treatment vs. co-treatment with PYO varied across biological replicates (Fig 3B and S2 and S3 Tables). More importantly, PYO significantly increased μ_{app} for cultures that were grown in liquid SCFM and selected on SCFM plates containing ciprofloxacin (Fig 3D and S3 Table), suggesting that PYO produced by *P. aeruginosa* could promote mutation to antibiotic resistance in chronically infected lungs of CF patients [36].

Because PYO did not increase tolerance to aminoglycosides (Figs 2D and S4B Fig), we hypothesized that PYO would not promote mutation to aminoglycoside resistance if the induction of shared defense mechanisms was required for the observed increases in μ_{app}. On the other hand, if PYO affected μ_{app} primarily by acting as a mutagen, pre-treatment with PYO before antibiotic selection would be expected to increase μ_{app} by a similar proportion for resistance to all classes of antibiotics. To differentiate between these modes of action, we repeated the fluctuation tests using gentamicin and tobramycin, representative members of the aminoglycoside class that disrupt protein translation [1]. Cultures that were pre-exposed to PYO consistently exhibited significant

increases in μ_{app} for gentamicin resistance (Fig 3E and S2 and S3 Tables). For tobramycin resistance, on the other hand, pre-treatment with PYO only significantly increased μ_{app} in one out of four biological replicates (Fig 3E and S2 and S3 Tables). In addition, for both aminoglycosides, adding PYO to the antibiotic selection plates had no effect on μ_{app} in most replicates (Fig 3E and S2 and S3 Tables). These differing responses to PYO depending on the choice of clinical antibiotic suggested that the observed changes in μ_{app} were related to PYO-induced cellular defenses more so than a mutagenic effect of PYO. In fact, previous studies have suggested that gentamicin generates ROS more readily than tobramycin [37,38]. This could account for why the effect of pre-exposure to PYO on μ_{app} for resistance was greater for gentamicin than for tobramycin, given that PYO primes cells to detoxify ROS by inducing oxidative stress responses (S1 Fig). For resistance to fluoroquinolones, on the other hand, simultaneous induction of multiple defenses is likely necessary to recapitulate the increases in μ_{app} upon exposure to PYO. Overexpression of individual oxidative stress genes induced by PYO did not increase μ_{app} for ciprofloxacin resistance, while overexpression of the *mexGHI-opmD* efflux system only mildly increased μ_{app} in a subset of biological replicates (S7B Fig). Interestingly, the latter result contrasted with our finding that induction of *mexGHI-opmD* was sufficient to recapitulate PYO-mediated increases in fluoroquinolone tolerance. Together, our data suggest that while tolerance and resistance can be mechanistically interrelated, overcoming the barrier to growing in the presence of an antibiotic in some cases requires a different or broader set of defenses than is required for temporary survival under growth-arrested conditions. Nevertheless, PYO-induced defense mechanisms appear to contribute to both types of resilience to antibiotic treatment.

We envisioned at least three ways in which, under antibiotic selection, PYO-induced defense mechanisms could lead to the apparent increases in mutation rates: A) by enhancing the growth of pre-existing "partially-resistant" mutants during exposure to the antibiotic; B) by increasing the proportion of cells that survive and subsequently mutate to resistance while still in the presence of the antibiotic; or C) by a combination of A and B. To distinguish between these scenarios, we implemented a two-pronged approach. First, to explore the possibility of scenario A, we isolated and characterized several mutants from the fluctuation test plates containing ciprofloxacin. We re-grew the isolates under non-selective conditions both with and without PYO

treatment and calculated the percentage of CFUs that could subsequently be recovered on ciprofloxacin plates relative to non-selective plates, as a metric for each isolate's level of resistance. We defined as "partially-resistant" those isolates for which only a subset of the population could grow under the antibiotic selection without PYO treatment, as evidenced by lower CFU counts on antibiotic plates compared to non-selective plates. Second, to determine the relative likelihoods of scenario A and scenario B, we examined the fit of our fluctuation test data to different formulations of the theoretical Luria-Delbrück (LD) distribution. Specifically, we compared mathematical models that make different assumptions regarding whether mutants arise prior to or during the antibiotic selection.

We identified multiple partially-resistant mutants for which the percentage of CFUs recovered on ciprofloxacin plates following growth under non-selective conditions increased when the isolate was either pre-exposed or co-exposed to PYO (Fig 4A), although the trends were not always statistically significant. Importantly, CFUs for the Δ*phz* parent strain were below the level of detection on the ciprofloxacin plates even in the presence of PYO, confirming that PYO-induced defenses alone, in the absence of a resistance mutation, were insufficient to enable growth under the selection condition used for the fluctuation tests (Fig 4A). In addition, for all characterized partially-resistant mutants, the MIC for ciprofloxacin was higher than for the parent strain (S7 Table). For some of these mutants, the MIC determined according to standard clinical protocols [27] matched the ciprofloxacin concentration originally used for selection, even in the presence of PYO, but this is not surprising, as the relatively dilute inoculum (5×10^5 CFU/mL) and short incubation time (18 hrs) used for standard MIC assays can preclude detection of weak growth at a given antibiotic concentration. As a further validation of our assay for detection of partially-resistant mutants, we also tested isolates with distinct colony morphologies that were not enriched on the PYO-containing antibiotic plates relative to PYO-free antibiotic plates in the original fluctuation tests. As expected, these mutants were fully resistant to ciprofloxacin at the original selection concentration (S8A Fig), meaning that the same number of CFUs grew on both antibiotic plates and non-selective plates even in the absence of PYO. Interestingly, the effect of PYO on ciprofloxacin resistance varied across different partially-resistant isolates (Fig 4A). This suggests that PYO does not universally raise the level of resistance of the entire population, but rather

interacts synergistically with specific types of mutations conferring partial resistance. Such heterogeneity could account for why the effect of PYO in the fluctuation tests varied across biological replicates, as the degree of benefit conferred by PYO would depend on the specific mutations that randomly occurred in each replicate. We also repeated the stationary phase ciprofloxacin tolerance assay with the partially-resistant isolates and found that tolerance was likewise differentially affected by PYO (S8B Fig). Interestingly, the tolerance and resistance phenotypes shared no obvious underlying pattern, again suggesting that cellular processes that affect resistance do not always equally effect tolerance, and vice versa. Nevertheless, our results demonstrate that under antibiotic selection, a subset of partially-resistant mutants benefits from exposure to PYO.

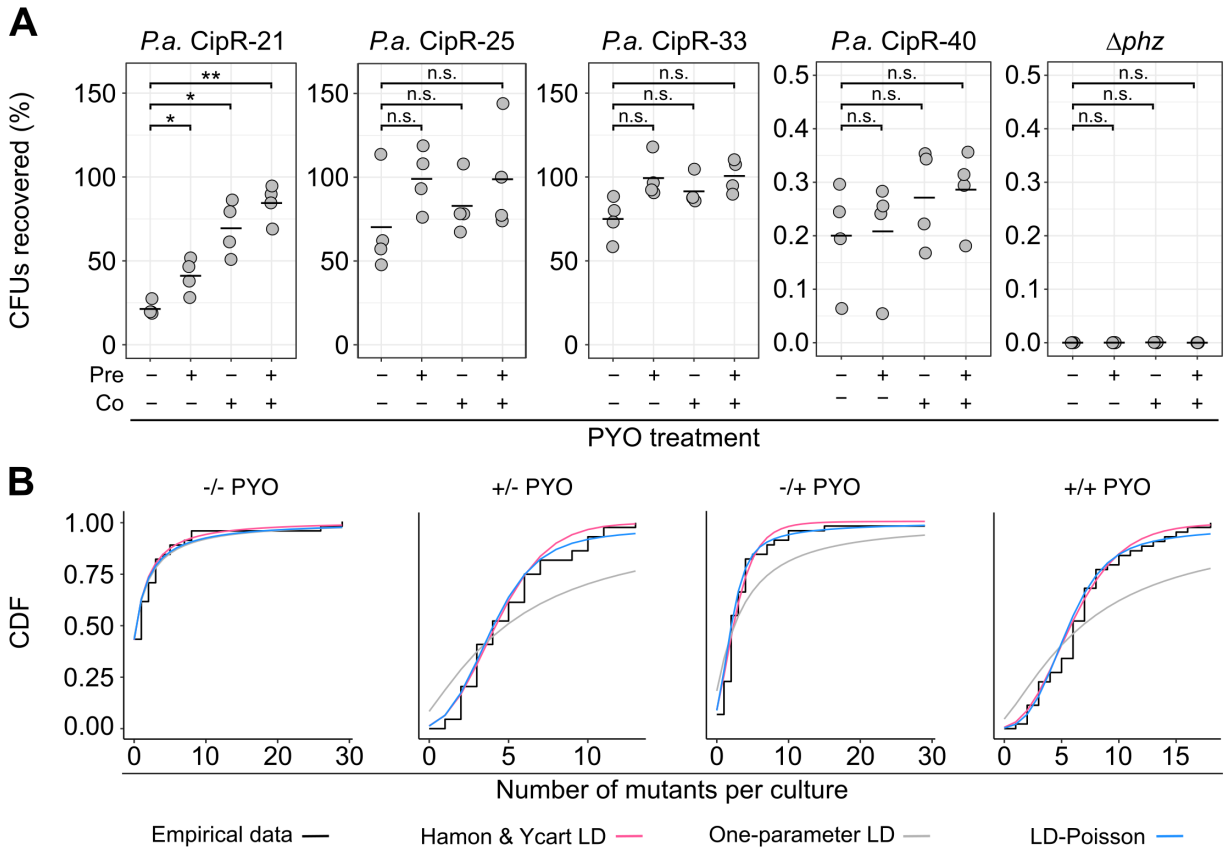

Figure 4. PYO promotes the growth of partially-resistant mutants and the occurrence of post-plating mutations. A. Putative ciprofloxacin-resistant mutants of *P. aeruginosa* (*P.a.*) isolated from fluctuation test plates were grown to mid-log phase in liquid glucose minimal medium with or without 100 μM PYO, before plating for CFUs on non-selective agar plates, plates containing ciprofloxacin alone (0.5 μg/mL), and plates containing ciprofloxacin and PYO. Plotted values represent the percentage of CFUs recovered on the ciprofloxacin plates,

calculated relative to total CFUs counted on non-selective plates. On the x-axis, "pre" denotes the presence of PYO in the liquid cultures and "co" denotes the presence of PYO in the agar plates. Data points represent independent biological cultures (n = 4). Black horizontal lines mark the mean values for each condition. **B.** Goodness-of-fit of different mathematical models for *P. aeruginosa* Δ*phz* fluctuation test data. Data from the fluctuation tests performed on ciprofloxacin are plotted for different combinations of PYO in liquid (pre-treatment) and PYO in agar (co-exposure to antibiotic selection). The empirical cumulative distribution functions of the data (black) are plotted against 1) a variation of the Luria-Delbrück model fit with two parameters, *m* (the expected number of mutations per culture) and *w* (the relative fitness of mutant cells vs. WT), as implemented by Hamon & Ycart [44] (pink); 2) a mixed Luria-Delbrück and Poisson distribution fit with two parameters, *m* and *d* (the number of generations that occur post-plating), allowing for the possibility of post-plating mutations, as implemented by Lang and Murray [45] (blue); 3) the basic Luria-Delbrück distribution model fit only with *m*, as implemented by Lang and Murray [45] (gray). In each condition, the plotted experimental data represent the biological replicate with the lowest chi-square goodness-of-fit *p*-value (i.e. least-good fit) for the Hamon & Ycart model, demonstrating that this model was still a reasonable fit for these samples. Statistics: A – Welch's unpaired t-tests with Benjamini-Hochberg correction for controlling false discovery rate (* $p < 0.05$, ** $p < 0.01$, *** $p < 0.001$, n.s. $p > 0.05$).

Whole-genome sequencing revealed that the partially-resistant isolates contained mutations either in the efflux pump repressors *nfxB* or *mexS,* or in genes that affected growth rate, such as a ribosomal protein, a C4-dicarboxylate transporter, and a cell-wall synthesis gene (S4 Table). Mutations in *nfxB* or *mexS* were also found in the fully-resistant isolates (S4 Table), albeit at different loci compared to the partially-resistant isolates. Notably, *nfxB* is considered a "pathoadaptive gene" in which mutations tend to accumulate during chronic infections [39,40]. Mutations in *mexS* are less common, but have also been detected in clinical isolates [41]. Slow-growing small colony variant mutants of *P. aeruginosa* have likewise been isolated from patients [42,43]. Thus, the growth benefits conferred by PYO-induced defenses during antibiotic selection could be relevant to a variety of clinically-adapted strains.

That PYO increases μ_{app} at least in part by promoting the growth of pre-existing partially-resistant mutants was further supported by the alternative approach of evaluating the fit of our data to different mathematical models. Specifically, Pearson's chi-square test indicated that our data closely fit the Hamon and Ycart model [44] (Fig 4B and S9 Fig and S3 Table), which allows for differential fitness of mutants compared to WT cells, but assumes that all mutants arise pre-plating. However, we could not unequivocally rule out the possibility that post-plating mutations contributed to the increases in μ_{app}, as a subset of our data also fit a mixed LD-Poisson model that assumes some mutations occurred during the antibiotic selection step [45] (Fig 4B and S9 Fig and S3 Table). We also performed growth curves under the culture conditions used in our fluctuation tests prior to the antibiotic selection step, with the addition of the live-cell-impermeable DNA-

binding dye propidium iodide as a marker for cell death. As expected from a previous study on PYO toxicity [16], cell death was undetectable prior to the sampling time point used in most of the fluctuation tests (S8D-E Fig). Thus, while increased population turnover due to stress can also lead to increases in μ_{app} [46], this is unlikely to underlie the effect of PYO on μ_{app}. Together, these results suggest that the most probable explanation for the PYO-mediated increases in apparent mutation rates is a combined effect of increased detection of partially-resistant mutants (the proposed scenario A) and increased occurrence of post-plating mutations resulting from elevated survival on the antibiotic plates (the proposed scenario B).

Importantly, previous studies based on *in vitro* evolution experiments have demonstrated that even modest increases in mutation rates, in the range of two- to five-fold, significantly affect the maximum achievable level of antibiotic resistance for diverse bacterial pathogens [47,48]. Moreover, it is well-established that partial resistance can rapidly lead to acquisition of full resistance via secondary mutations [49,50]. Indeed, several putative mutants appeared fully resistant to ciprofloxacin in our CFU-recovery assay despite having been enriched by exposure to PYO in the fluctuation tests (S8C Fig). This discrepancy could be a result of acquiring secondary mutations either during growth on the original fluctuation test plates or during the pre-growth for the CFU-recovery assay. Thus, our results suggest that PYO may significantly affect the rate at which high-level resistance emerges in populations of *P. aeruginosa* undergoing long-term antibiotic exposure.

PYO promotes antibiotic tolerance in other opportunistic pathogens

While the above experiments were performed with single-species cultures, *P. aeruginosa* is found in polymicrobial communities in both natural environments (e.g. soil) and clinical contexts (e.g. chronic infections) [51–54]. We hypothesized that microbes that frequently interact with *P. aeruginosa* would have evolved inducible defense mechanisms against PYO toxicity, and that production of PYO by *P. aeruginosa* might therefore also increase tolerance and resistance to clinical antibiotics in these community members. To test this hypothesis, we focused on the genera *Burkholderia* and *Stenotrophomonas*, both of which are (i) soil-born gram-negative opportunistic pathogens that are frequently refractory to clinical antibiotic treatments [55–57], and (ii) found in

co-infections with *P. aeruginosa*, e.g. in CF patients [58]. Specifically, we tested a soil-derived strain, *Burkholderia cepacia* ATCC 25416; a non-CF clinical isolate of *Stenotrophomonas*, *S. maltophilia* ATCC 13637; and several clinical isolates of the three most prevalent *Burkholderia* species found in CF patients [51]: *B. cenocepacia*, *B. multivorans*, and *B. gladioli* (for descriptions of these strains, see S5 Table).

We first assessed each strain's intrinsic resistance to PYO (Fig 5A), as we expected that strong defenses against PYO toxicity would be required in order to benefit from exposure to this natural antibiotic. Indeed, for *S. maltophilia*, which was sensitive to PYO (Fig 5A), the effects of PYO on antibiotic tolerance were complex: the presence of PYO was only beneficial when ciprofloxacin levels were low (1 μg/mL) (Fig 5B). At a higher concentration of ciprofloxacin (10 μg/mL), PYO was detrimental in a dose-dependent manner (Fig 5B), suggesting that the additional stress conferred by PYO outweighed any induction of defense mechanisms against ciprofloxacin. *S. maltophilia* also struggled to grow with *P. aeruginosa* in co-cultures (Fig 5C-D), indicating that the conditions under which this species could potentially benefit from PYO are very limited.

B. cepacia, *B. cenocepacia,* and *B. multivorans*, on the other hand, were highly resistant to PYO (Fig 5A). For these three species, exogenously-added PYO increased tolerance to ciprofloxacin (Fig 5E). Furthermore, for *B. cepacia*, we confirmed that this effect was PYO dose-dependent (Fig 5E). We therefore tested whether *P. aeruginosa* could induce tolerance to ciprofloxacin in co-cultures with these *Burkholderia* strains. Using liquid culture plates in which the two species were separated by a permeable membrane (Fig 5C), we found that PYO-producing *P. aeruginosa* strongly induced tolerance to ciprofloxacin in the *Burkholderia* species, and that the observed tolerance phenotypes were recapitulated by addition of exogenous PYO to co-cultures of *Burkholderia* and the *P. aeruginosa* Δ*phz* mutant, or to control cultures with *Burkholderia* alone in the same setup (Fig 5F). Notably, for *B. cenocepacia* and *B. multivorans*, increased ciprofloxacin tolerance was also observed in co-cultures with a PYO-producing strain isolated from a CF patient, *P. aeruginosa* PA 76-11 (Fig 5F). In addition, even when co-cultured with *Burkholderia,* the *P. aeruginosa* WT strain still showed elevated ciprofloxacin tolerance when compared to the non-PYO-producing Δ*phz* mutant (Fig 5G). This indicates that the presence of

Burkholderia did not alter *P. aeruginosa* tolerance patterns under our conditions. Finally, similar results were obtained for experiments performed in SCFM, where either the addition of exogenous PYO (Fig 5H) or co-culture with *P. aeruginosa* (Fig 5I) led to increased tolerance levels in *Burkholderia*. Together, these results suggest that PYO produced by *P. aeruginosa* in CF patients may decrease the efficacy of ciprofloxacin as a treatment for multispecies infections.

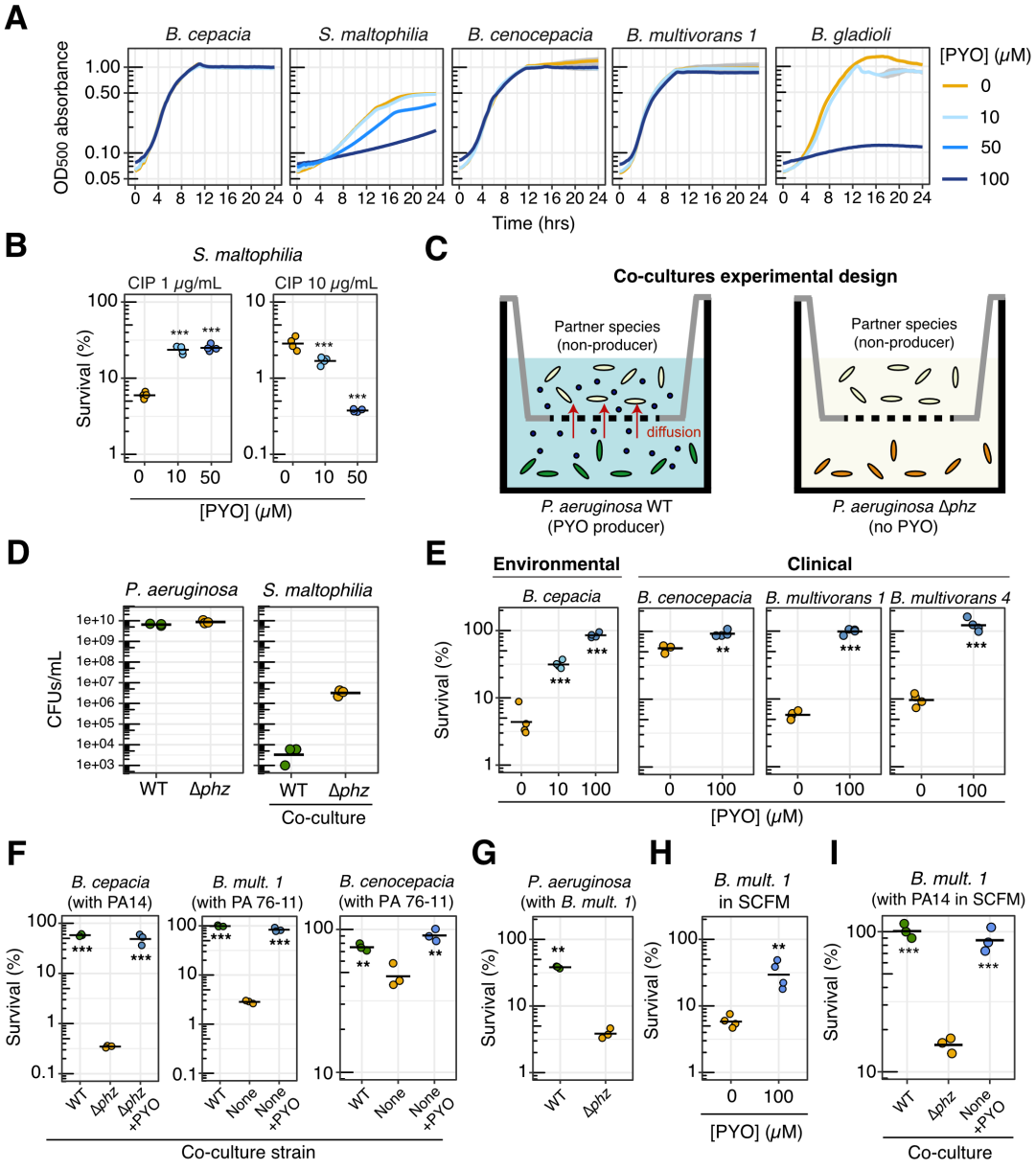

Figure 5. PYO promotes antibiotic tolerance in other opportunistic pathogens. A. Growth of several strains in the presence of different concentrations of PYO. Plotted lines represent averages of four to six replicates and shaded

areas in gray represent the standard deviation. *Burkholderia multivorans 1* = *B. multivorans* AU42096. For complete information on strains, see S5 Table. **B.** Tolerance of *S. maltophilia* to different concentrations of ciprofloxacin (CIP; 1 or 10 μg/mL) after growth in the presence of different concentrations of PYO (0, 10 or 50 μM) (n = 4). **C.** Schematic depicting the experimental design for co-culture antibiotic tolerance assays (see Methods for details). **D.** CFUs recovered from co-cultures of *P. aeruginosa* (PA14 WT and Δ*phz*) and *S. maltophilia* (n = 3), showing that the latter struggled to grow in the presence of *P. aeruginosa.* **E.** Effect of PYO on the tolerance to ciprofloxacin (10 μg/mL) of multiple *Burkholderia* species isolated from environmental and clinical samples (n = 4). **F.** Effect of PYO produced by *P. aeruginosa* in co-cultures on the tolerance of different *Burkholderia* species to ciprofloxacin (10 μg/mL). PA14 is our model laboratory strain of *P. aeruginosa*, while PA 76-11 is a PYO-producing strain of *P. aeruginosa* isolated from a CF patient. The *Burkholderia* strains were plated separately for CFUs to assess survival following treatment with ciprofloxacin in the co-cultures (n = 3). **G.** Tolerance of *P. aeruginosa* PA14 WT and Δ*phz* to ciprofloxacin (1 μg/mL) when grown in co-cultures with *B. multivorans 1* (n = 3). **H.** Effect of PYO on the tolerance to ciprofloxacin (10 μg/mL) of *B. multivorans 1* in SCFM (n = 4). **I.** Tolerance to ciprofloxacin (1 μg/mL) of *B. multivorans 1* grown in co-cultures with P. *aeruginosa* PA14 WT, Δ*phz* or alone with 100 μM PYO added exogenously (n = 3). Statistics: B, E, F, G, H, I – One-way ANOVA with Tukey's HSD multiple-comparison test for comparisons of three conditions or Welch's unpaired t-test for comparison of two conditions, with asterisks showing the statistical significance of comparisons with the untreated (no PYO or Δ*phz*) condition (* $p < 0.05$, ** $p < 0.01$, *** $p < 0.001$). In all panels, data points represent independent biological replicates, and black horizontal bars mark the mean values for each condition.

PYO promotes the evolution of antibiotic resistance in a co-occurring opportunistic pathogen

We next asked whether PYO could mediate an increase in apparent mutation rate for ciprofloxacin resistance in *Burkholderia* species. We chose *B. multivorans* AU42096 (*B. multivorans* 1 in Fig 5) as our model strain for these experiments because, among the clinical isolates, it displayed the strongest response to PYO in the ciprofloxacin tolerance assays. Remarkably, when selecting *B. multivorans* mutants on ciprofloxacin, we observed PYO-mediated increases in μ_{app} that were far more dramatic than for *P. aeruginosa*: pre-treatment with PYO increased μ_{app} for *B. multivorans* approximately 10-fold, while co-exposure to PYO in the antibiotic plate without pre-exposure increased μ_{app} approximately 40-fold, and the combination of pre- and co-exposure to PYO increased μ_{app} by 230-fold (Fig 6A and S3 Table). Notably, the magnitude of the latter effect is on par with observed differences between hypermutators, such as mutants deficient in the mismatch repair pathway, and their respective parent strains [59–61]. Moreover, hypermutators of *Burkholderia* isolated from CF infections are associated with clinical ciprofloxacin resistance [59]. In light of these observations, our results suggest that PYO could significantly affect clinical outcomes for co-infections of *P. aeruginosa* and *B. multivorans* treated with ciprofloxacin.

To verify that the *B. multivorans* colonies growing on ciprofloxacin in the presence of PYO were mutants, and to assess their responses to PYO, we isolated several putative mutants from the fluctuation test antibiotic plates and tested three in our CFU-recovery assay. All three displayed unique profiles of ciprofloxacin resistance in response to PYO treatment, as well as different maximal levels of resistance. However, all were more resistant than the WT parent strain in the presence of PYO, and none were noticeably resistant to ciprofloxacin in this assay without exposure to PYO (Fig 6B). MIC tests performed according to clinical standards revealed that the MIC of CipR-1 was indistinguishable from that of the parent strain, while the MIC of CipR-2 was two-fold higher than that of the parent strain in the absence of PYO but identical in the presence of PYO (S7 Table), reflecting the limitations of standard two-fold antibiotic dilution series for revealing mild increases in resistance. The MIC of CipR-7, on the other hand, was eight-fold higher than that of the parent strain, though in the absence of PYO, the MIC of this mutant was still below the ciprofloxacin concentration used in the fluctuation tests. Notably, for all tested *B. multivorans* isolates, including the WT parent, the addition of PYO to the standard MIC tests increased the MIC for ciprofloxacin by four- to eight-fold (S7 Table); however, even in the presence of PYO, the MIC for the parent strain was less than half of the ciprofloxacin concentration used in the tolerance assays, indicating that the observed tolerance phenotype for this strain cannot be fully explained by phenotypic resistance. Interestingly, the percentage of the parent strain population that could grow on ciprofloxacin in the presence of PYO (Fig 6B) was approximately equal to what would have been expected from the frequency of colonies detected in the fluctuation tests; moreover, when the CFU recovery assay was performed for the parent strain, the colonies that grew on ciprofloxacin in the presence of PYO exhibited diverse morphologies. This suggests that much of the parent strain growth on ciprofloxacin in the presence of PYO may have in fact reflected the growth of high-frequency spontaneous mutants, rather than background growth of the parent strain itself.

Whole-genome sequencing of the fluctuation test isolates revealed that *B. multivorans* CipR-1 possessed mutations in three uncharacterized regulatory genes (S6 Table). *B. multivorans* CipR-2 possessed mutations in two different homologs of the SpoT/RelA (p)ppGpp synthetase gene, which is known to affect antibiotic tolerance and resistance [62]. Finally, *B. multivorans*

CipR-7 possessed a point mutation in DNA gyrase A (S83R), along with a point mutation in a malto-oligosyltrehalose synthase. Given that DNA gyrase A is the target of ciprofloxacin and that the specific mutated residue is likely homologous to the T83 residue that was mutated in a study of fluoroquinolone-resistant mutants in *B. cepacia* [63], it is intriguing that this mutant was not able to grow on the original selection concentration of ciprofloxacin in the absence of PYO; however, the specific amino acid substitution in this strain may have resulted in only a mild disruption of ciprofloxacin binding.

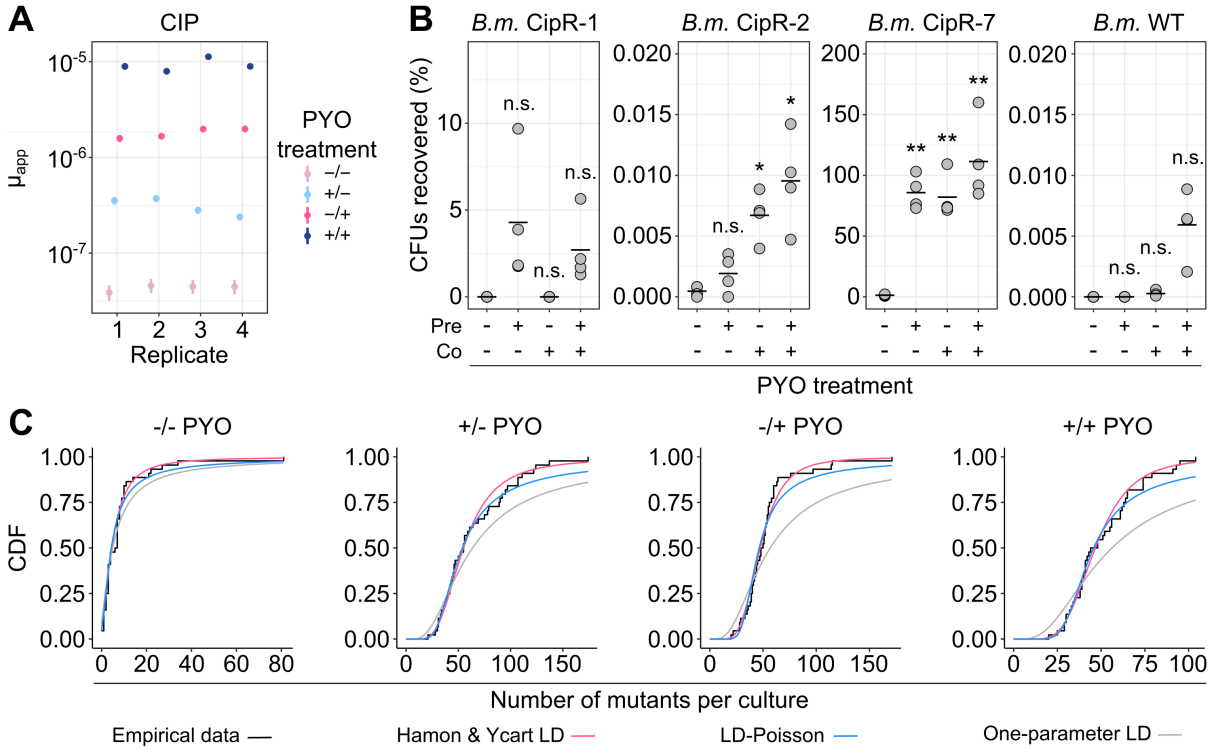

Figure 6. PYO promotes antibiotic resistance in *B. multivorans*. A. The apparent rate of mutation to resistance when log-phase *B. multivorans 1* cells were plated on MH agar containing ciprofloxacin (8 µg/mL), with or without pre- and/or co-exposure to 100 µM PYO relative to the antibiotic selection step. Each data point represents a biological replicate comprising 44 parallel cultures (n = 4). The vertical lines represent 84% confidence intervals, in which lack of overlap corresponds to statistical significance at the $p < 0.05$ level [99]. The PYO treatments correspond to the following: -/- denotes no PYO pre-treatment (in the liquid culture stage) or co-treatment (in the antibiotic agar plates), +/- denotes PYO pre-treatment but no co-treatment, -/+ denotes PYO co-treatment without pre-treatment, and +/+ denotes both PYO pre-treatment and co-treatment. **B.** The percentage of CFUs recovered on ciprofloxacin plates either with or without PYO in the agar, for exponential phase cultures of different partially-resistant *B. multivorans 1* (*B.m.*) mutants that were pre-grown with or without PYO in liquid cultures. Plotted values represent the percentage of CFUs recovered on the ciprofloxacin plates, calculated relative to total CFUs counted on non-selective plates. On the x-axis, "pre" denotes the presence of PYO in the liquid cultures and "co" denotes the presence of PYO in the agar plates. Data points represent independent biological replicates (n = 4), and black horizontal bars mark the mean values for each condition. **C.** Goodness-of-fit of different mathematical models for *B. multivorans 1* fluctuation test data. Data are plotted for different combinations of PYO in liquid (pre-treatment) and PYO in agar (co-exposure to antibiotic

selection). The empirical cumulative distribution functions of the data (black) are plotted against 1) a variation of the Luria-Delbrück model fit with two parameters, *m* (the expected number of mutations per culture) and *w* (the relative fitness of mutant cells vs. WT), as implemented by Hamon & Ycart [44] (pink); 2) a mixed Luria-Delbrück and Poisson distribution fit with two parameters, *m* and *d* (the number of generations that occur post-plating), allowing for the possibility of post-plating mutations, as implemented by Lang and Murray [45] (blue); 3) the basic Luria-Delbrück distribution model fit only with *m*, as implemented by Lang and Murray [45] (gray). In each condition, the plotted experimental data represent the biological replicate with the lowest chi-square goodness-of-fit *p*-value (i.e. least-good fit) for the Hamon & Ycart model. Statistics: B – Welch's unpaired t-tests with Benjamini-Hochberg correction for controlling false discovery rate (* $p < 0.05$, ** $p < 0.01$, *** $p < 0.001$).

Lastly, we asked whether the *B. multivorans* mutants we detected primarily arose prior to or during the antibiotic selection. In all cases, the distribution of mutants closely matched the Hamon and Ycart formulation of the theoretical LD distribution, suggesting that the detected mutants arose prior to the antibiotic exposure (Fig 6C and S3 Table). Interestingly, the Hamon and Ycart model also predicted the average relative fitness of mutants detected in PYO-treated samples to be significantly lower compared to mutants detected in non-PYO treated samples (S3 Table; $p < 0.05$ for all three comparisons between non-PYO-treated and PYO-treated sample groups, using Welch's paired t-test with Benjamini-Hochberg corrections for controlling the false discovery rate). In addition, unlike for *P. aeruginosa*, the mixed LD-Poisson distribution that allows for post-plating mutations was a poorer fit than the Hamon and Ycart model for all PYO-treated *B. multivorans* samples (Fig 6C and S3 Table). Together, these results suggest that in *B. multivorans*, PYO increases μ_{app} by promoting growth of a wider range of mutants that arise prior to antibiotic selection, including those with slower growth rates.

Discussion

Many clinical antibiotic resistance genes are thought to have originated in environmental microorganisms as responses to microbial chemical warfare, with subsequent mobilization into human pathogens via horizontal gene transfer [5,6,64]. Here, we have demonstrated that tolerance and resistance to clinically relevant concentrations of synthetic antibiotics can also arise as a collateral benefit of natural antibiotic production by an opportunistic pathogen. *P. aeruginosa* is a particularly relevant example of an opportunistic pathogen whose self-produced natural antibiotics can promote resilience to clinical antibiotics, given the large number of chronic infections caused by this bacterium worldwide [9] and the fact that PYO has been detected at concentrations up to 130 μM in lung infection sputum samples [25] and 0.31 mg/g in infected wound exudate [65].

Notably, treatments for infections caused by *P. aeruginosa* and other opportunistic pathogens often fail even when *in vitro* MIC tests indicate susceptibility to the chosen antibiotic [58]. Previous studies have attributed this discrepancy to metabolic and physiological changes within biofilms [66,67], which represent a major form of bacterial life within infections [68]. Our results suggest that cellular defenses induced by bacterially-produced natural antibiotics may also contribute to *in vitro* versus *in vivo* differences in antibiotic susceptibility, as standard MIC tests are inoculated at a low cell density [32], but *P. aeruginosa* typically does not make PYO *in vitro* until reaching a relatively high cell density [13]. Furthermore, the observation that PYO produced by *P. aeruginosa* strongly promotes antibiotic tolerance and resistance in *Burkholderia* species could hold important ramifications for the treatment of co-infections of these organisms in CF patients, for which clear best practices have yet to be established [58]. In particular, it could be prudent to avoid treating such infections with antibiotics for which PYO is likely to promote increased tolerance and resistance, such as fluoroquinolones, chloramphenicol, and trimethoprim/sulfamethoxazole—the latter two also being known substrates for efflux pumps that we have shown are upregulated by PYO [9,21].

Interestingly, our finding that PYO does not increase tolerance to aminoglycosides (Fig 2D and S4B Fig) contrasts with the conclusions of two previous studies on phenazine-mediated antibiotic tolerance, which claimed that phenazines broadly increase tolerance to all classes of antibiotics except cationic peptides [17,18]. Importantly, however, these studies did not explore whether or which molecular defense mechanisms are induced by the phenazines and how these defenses might interact with clinical antibiotics. Moreover, the studies were performed under very different experimental setups, including different media, which can profoundly impact the outcomes of antibiotic susceptibility assays. One study focused on colony biofilms of *P. aeruginosa* that produced only phenazine-1-carboxylic acid and phenazine-1-carboxamide [17], which are less toxic than PYO [16] and consequently may induce a different set of cellular responses. Alternatively, the observed increased tolerance to tobramycin in that study might not be related to molecular defenses induced by phenazines, but rather phenazine-mediated physiological differences under the studied conditions [17]. Phenazines are redox-active molecules that can promote metabolic activity under oxygen limitation, which occurs within biofilms

[12,17,69]; the specific details of how such metabolic activity might affect antibiotic tolerance merit further attention. The other previous study found that PYO increased planktonic culture cell densities in the presence of various antibiotics [18], but these experiments did not directly demonstrate an effect on antibiotic tolerance (i.e. the ability to survive an otherwise lethal antibiotic treatment) [2]. Notably, both studies found that phenazines actually increase sensitivity to cationic peptides, consistent with our observation that WT *P. aeruginosa* is less tolerant to colistin than the Δ*phz* strain. The mechanism of this synergistic lethality warrants further investigation. Our results highlight that identifying the cellular defenses induced by natural antibiotics, not only in the case of *P. aeruginosa* and phenazines, but also potentially other opportunistic pathogens and their endogenously-produced natural antibiotics, is essential for accurately predicting clinical antibiotic efficacy.

Our results furthermore suggest that by inducing cellular defenses against specific clinical antibiotics, PYO widens the population bottleneck that occurs during antibiotic selection. This effect occurs via a two-pronged mechanism (Fig 7). First, PYO increases the proportion of cells that survive short-term antibiotic treatments, which would inherently tend to preserve a greater range of genetic variation in the post-selection population. Second, PYO promotes the establishment of a broader range of resistant mutant lineages, which are likely primed to acquire further step-wise mutations to high-level resistance, yet may otherwise be lost during extended antibiotic treatment. Interestingly, a recent study demonstrated that lineages of spontaneous resistant mutants can be lost through stochastic cell death even at antibiotic concentrations well below the mutants' MICs [70]. Thus, besides boosting the growth of partially-resistant mutants whose MICs failed to exceed the antibiotic concentrations used in our fluctuation tests, it is possible that PYO-induced defenses (e.g. enhanced efflux and oxidative stress responses) also increased apparent mutation rates by decreasing the stochastic loss of individual spontaneous mutants with higher MICs. In addition, a recent study in *Staphylococcus aureus* highlighted the important role that pre-existing genetic diversity in the population can play in shaping the evolution of antibiotic resistance [71]. In particular, even small variations in efflux-mediated intrinsic resistance of parent strains significantly affected the probability that a population would evolve resistance under ciprofloxacin selection at the clinical breakpoint concentration [71].

Multiple studies have also demonstrated additive or synergistic interactions between increased drug efflux and classical ciprofloxacin resistance mutations [71–73]. We observed a similar phenomenon in our *B. multivorans* CipR-7 strain, which had acquired a mutation in the cellular target of ciprofloxacin (i.e. DNA gyrase A), yet still required exposure to PYO in order to grow at the ciprofloxacin concentration on which it was originally selected (Fig 6B). Together, these findings suggest that microbial production of natural antibiotics in the context of an infection could dynamically, and in some cases dramatically, affect the evolvability of opportunistic pathogens challenged with clinical drugs.

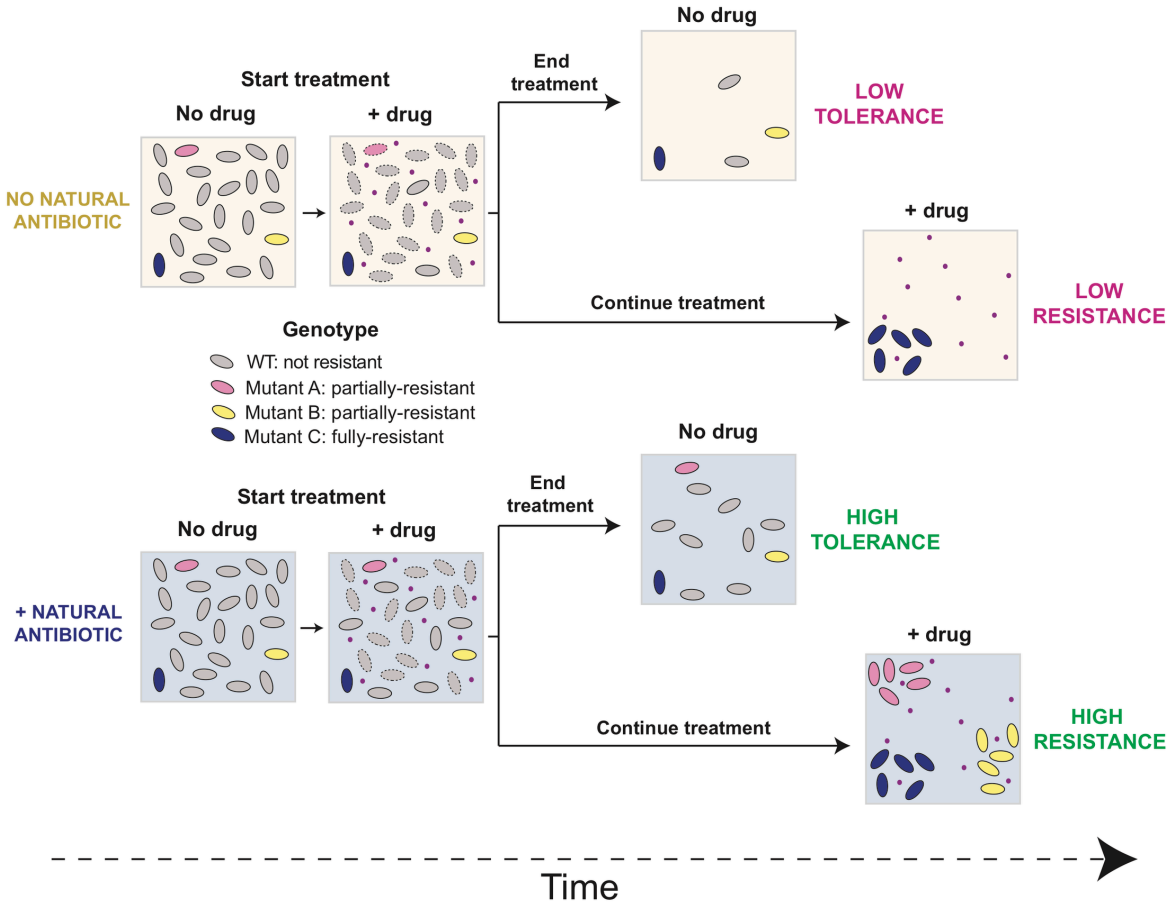

Fig 7. Proposed model for how natural antibiotics increase bacterial tolerance and resistance to clinical drugs. In the first scenario (tolerance), cells are exposed to the clinical drug (pink dots) for a short period of time. Surviving cells will eventually re-start growth after the drug is removed. The presence of the natural antibiotic (bottom) increases tolerance of both WT and partially-resistant mutants. In the second scenario (resistance), cells are constantly exposed to the drug for an extended period of time, and only mutants are maintained in the population. The presence of the natural antibiotic (bottom) widens the population bottleneck and allows partially-resistant mutants to grow under drug selection, preserving a greater range of genetic diversity in the population.

Beyond *P. aeruginosa* and PYO, our proposed model for collateral benefits of exposure to natural antibiotics (Fig 7) potentially represents a broader phenomenon among human pathogens than has previously been appreciated. Many opportunistic pathogens originate in environments like soil [55,74], where they have evolved in the presence of diverse natural antibiotics [5,6], and *P. aeruginosa* is not the only pathogen with the capacity to synthesize its own antibiotics. For example, *Burkholderia* species possess the biosynthetic capability to produce a variety of compounds with antibacterial activity, whose potential clinical significance has not been explored [75]. If a given natural antibiotic induces expression of a molecular defense, the only requirement for a consequent increase in tolerance to a clinically-relevant drug would be that the induced defense has some efficacy against the drug—e.g. due to structural similarities like those shared by PYO and fluoroquinolones. This inference is supported by recent evidence that certain food additives and synthetic drugs antagonize the efficacy of specific clinical antibiotics by triggering stress responses in cells, including the induction of efflux pumps [76], and that exposure to a clinical drug to which a strain is already resistant can collaterally affect its development of tolerance and resistance to other drugs [77]. In fact, bacterially-produced toxic metabolites that promote antibiotic tolerance and resistance in human pathogens need not be limited to the types of molecules traditionally thought of as natural antibiotics. For example, indole secretion by highly antibiotic-resistant spontaneous mutants of *Escherichia coli* enables partially-resistant mutants within the same species to grow at drug concentrations above their own MICs, in part by stimulating efflux pump expression [78]. Unlike PYO, indole is generally thought of as a signaling molecule rather than a natural antibiotic [79], though it can likewise be toxic to bacteria at high concentrations [79,80]. Efforts to identify and characterize additional examples of such metabolites produced by opportunistic human pathogens could lead to an improved understanding of the modes of antibiotic treatment failure in clinics, and ultimately inform the design of more effective and longer-lived therapies.

Methods

Culture media and incubation conditions

Different culture media were used for different experiments as indicated throughout the Methods. Succinate minimal medium (SMM) composition was: 40 mM sodium succinate (or 20 mM, if specified), 50 mM KH_2PO_4/K_2HPO_4 (pH 7), 42.8 mM NaCl, 1 mM $MgSO_4$, 9.35 mM NH_4Cl, and a trace elements solution [81]. Glucose minimal medium (GMM) was identical to SMM, except with 10 or 20 mM glucose (as specified for different experiments) instead of succinate. SMM and GMM were prepared by autoclaving all components together for 20 min at 121□C, except for the carbon source and the 1000x trace elements stock solution, which were filter-sterilized and added separately; interestingly, we found that autoclaving $MgSO_4$ with the other components was crucial for consistent PYO production by WT *Pseudomonas aeruginosa* UCBPP-PA14 in GMM. Luria-Bertani (LB) Miller broth (BD Biosciences) and BBL Cation-Adjusted Mueller-Hinton II (MH) broth (BD Biosciences) were prepared according to the manufacturer's instructions (notably with only a 10 min autoclave step for MH medium), with the addition of 1.5% Bacto agar (BD Biosciences) to make solid media. Synthetic cystic fibrosis sputum medium (SCFM) composition was prepared as described previously [36], with 1.355mM K_2SO_4 and no nitrate. In addition, 3.6 μM $FeSO_4.7H_2O$ and 0.3 mM N-acetyl-glucosamine were added [82]. All components except for the latter two were dissolved together, sterilized by filtration through a 0.22 μm membrane, and stored for up to two weeks; $FeSO_4.7H_2O$ and N-acetyl-glucosamine solutions were prepared fresh each time or stored at -20ºC, respectively, and added to SCFM on the day of use. For SCFM agar, a 2x solution of the medium components was prepared and added to a separately autoclaved 3% molten agar solution, for a final concentration of 1x SCFM and 1.5% agar.

Antibiotics were prepared in concentrated stock solutions (100x or greater) and stored at -20ºC. Ciprofloxacin was dissolved in 0.1 M or 20 mM HCl, while levofloxacin, gentamicin, tobramycin and colistin were dissolved in sterile deionized water. Phenylalanine-arginine β-naphthylamide (PAβN) dihydrochloride (MedChemExpress) was dissolved in sterile deionized water (50 mg/mL). Pyocyanin (PYO) was synthesized and purified as previously described [83,84]

and dissolved in 20 mM HCl to make 10 mM stock solutions. Experiments involving exogenous PYO always included negative controls to which an equivalent volume of 20 mM HCl was added. In addition, MH agar plates were buffered to pH 7 with 10 mM morpholinepropanesulfonic acid (MOPS) to avoid any pH changes upon addition of PYO or HCl; all other media used with exogenous PYO were already inherently buffered. Incubations were always done at 37ºC, with shaking for liquid cultures (250 rpm), unless mentioned otherwise.

Strain construction

In this study, we use PA14 as an abbreviation for UCBPP-PA14. *P. aeruginosa* PA14 was used for all experiments unless otherwise noted. For a full list of strains made in this study, see S5 Table. Three types of strains were made in different *P. aeruginosa* PA14 backgrounds: (i) unmarked deletions, used for Tn-seq validation experiments; (ii) fluorescent strains for time-lapse microscopy experiments; and (iii) strains overexpressing one of the following three systems: *mexGHI-opmD*, *ahpB* and *katB*. Established protocols were used for all these procedures [85].

Briefly, for unmarked deletions, ~1kb fragments immediately upstream and downstream of the target locus were cloned using Gibson assembly into the pMQ30 suicide vector [86,87]. Fragments amplified from *P. aeruginosa* PA14 genomic DNA (gDNA) and cleaned up using the Monarch PCR Purification kit (New England Biolabs) were used for Gibson assembly together with pMQ30 cut with SacI and HindIII. The assembled construct was then transformed into *Escherichia coli* DH10B, with transformants being selected in LB with 20 µg/mL gentamicin. All correctly-assembled plasmids were identified by colony PCR and verified by Sanger sequencing (Laragen). Next, for the insertion of the constructs into *P. aeruginosa* PA14 genome, tri-parental conjugation was performed following Choi and Schweizer [88]. All unmarked deletions were done in the *P. aeruginosa* PA14 Δ*phz* background (both *phzA-G1* and *phzA-G2* operons are deleted in this strain [13]), allowing clean experiments by addition of exogenous phenazines. Merodiploids containing the construct integrated into their genomes were selected on VBMM medium (3 g/L trisodium citrate, 2 g/L citric acid, 10 g/L K_2HPO_4, 3.5 g/L $NaNH_4PO_4{\cdot}4H_2O$, 1 mM $MgSO_4$, 100 µM $CaCL_2$, pH 7) with 100 µg/mL gentamicin following Choi and Schweizer [88]. Finally, merodiploids were then plated on LB lacking NaCl and containing 10% sucrose to select for

colonies resulting from homologous recombination. Colonies missing the target locus (unmarked deletions) were identified by PCR. For all primers used, see S5 Table.

Fluorescent strains used in time-lapse microscopy were made using previously published plasmids [85,89]. Constructs containing GFP and mApple florescent proteins under the control of the ribosomal *rpsG* gene were inserted in the *att*Tn7 site of *P. aeruginosa* PA14 Δ*phz* chromosome by tetra-parental conjugation, followed with selection on VBMM with 100 μg/mL gentamicin [88].

Finally, overexpressing strains were made as previously described [85]. The previously-made overexpression construct (pUC18T-miniTn7T-GmR vector containing the arabinose-inducible promoter P_{ara} [85]) and the three different targets (*mexGHI-opmD*, *ahpB* and *katB*) were all amplified by PCR. Next, using Gibson assembly, the targets were cloned downstream of P_{ara} in the pUC18T-miniTn7T-GmR vector, resulting in the three different overexpression constructs: P_{ara}*:mexGHI-opmD*, P_{ara}*:ahpB*, and P_{ara}*:katB*. The final constructs were introduced into the *att*Tn7 of the *P. aeruginosa* PA14 Δ*phz* background strain by tetraparental conjugation [88].

Transposon-sequencing (Tn-seq) experiment

The Tn-seq experiment was performed following the design presented in Fig 1A. Two aliquots of the *P. aeruginosa* PA14 transposon library previously prepared [89] were thawed on ice for 15 min, diluted to a starting optical density (OD_{500}) of 0.05 in 50 mL of SMM, and grown aerobically under shaking conditions (250 rpm) at 37ºC for ~ 4-5 generations to an OD_{500} of 0.8-1. These growing conditions were used for all the stages of the experiment. After growth in SMM, each aliquot was considered an independent replicate. Cells from each replicate were pelleted, washed and resuspended (5 mL in 18 x 150 mm glass tubes, OD_{500} = 2) in minimal phosphate buffer (MPB - 50 mM KH_2PO_4/ K_2HPO_4[pH 7], 42.8 mM NaCl) with and without 100 μM PYO. Cells were then incubated for 26 hrs under shaking conditions at 37ºC. Therefore, the experiment consisted of four different samples that were later sequenced: (i) “R1 No PYO,” (ii) “R1 + PYO,” (iii) “R2 No PYO,” and (iv) “R2 + PYO.” After the incubation, cultures from all treatments were pelleted, washed again to remove PYO, and resuspended in fresh SMM. Immediately, an aliquot of each sample was diluted to a starting OD_{500} of ~0.05 in 25 mL SMM, followed by outgrowth

for ~4-5 generations to an OD_{500} of 0.8-1. After outgrowth, 2.5 mL of each sample was pelleted and stored at -80ºC.

Genomic DNA was extracted from the pelleted samples using the DNeasy Blood & Tissue kit (Qiagen). All the steps for sequencing library preparation followed exactly the protocol used by Basta *et al*. [89], including (i) DNA shearing by sonication (to produce 200-500 bp fragments), (ii) end-repair, (iii) addition of poly(C) tail and (iv) enrichment of transposon-genome junctions and addition of adapter for Illumina sequencing by PCR [89,90]. The resulting amplified DNA samples were sequenced using 100 bp single-end reads on the Illumina HiSeq 2500 platform at the Millard and Muriel Jacobs Genetics and Genomics Laboratory at Caltech. Data analysis also followed Basta *et al*. [89]. In summary, sequences were mapped to the *P. aeruginosa* UCBPP-PA14 genome sequence using Bowtie 2 [91] and were analyzed in MATLAB using the ARTIST Tn-seq analysis pipeline [92], with non-overlapping windows of 100 bp across the genome [89,92]. Using the Mann-Whitney U statistical test, the total reads mapping for each gene in the "+PYO" samples were compared to the corresponding reads in the "No PYO" control for each replicate independently [89,92]. Next, the read ratio for each replicate was calculated within ARTIST for each gene and then $\log_2$-transformed. Finally, the *p*-values for both replicates were combined using the Fisher's combined probability test as done in Basta *et al.* [89], and the average of the $\log_2$-ratios of the two replicates are also shown. For the $\log_2$-ratios and *p*-values for all PA14 genes, see S1 Table. For heatmaps shown in Fig 1A, the average $\log_2$-ratios (fitness) for the selected genes were plotted using the *geom_tile()* function from the ggplot2 package in R [93,94].

Tn-seq datasets correlation analysis

To compare the results of this Tn-seq analysis with a previously published study [24] analyzing fitness determinants for survival during ciprofloxacin treatment in the *P. aeruginosa* PAO1 strain background (Fig 1E and S1 Table), the data from that study's supplemental Table S1 were used. The normalized average ratio of reads in the treated sample compared to reads in the input sample for each gene (geometric mean of 3 replicates) was $\log_2$-transformed for comparison to the Tn-seq data described above. The list of genes was filtered to include only genes for which ratios were reported in both our PYO Tn-seq experiment and the ciprofloxacin Tn-seq study, and

for which there are clear orthologs in both strains (n = 4209 genes). Orthologs were determined using the "pseudomonas.com" database [95].

Tn-seq validation experiments

To validate the Tn-seq results (Fig 1C), experiments were performed by comparing the survival of four different mutants (Δ*phz*Δ*ackA*Δ*pta*, Δ*phz*Δ*lptA*, Δ*phz*Δ*mexS,* and Δ*phz*Δ*dctBD*) to the survival of the Δ*phz* strain upon exposure to PYO. The experimental design was very similar to the one used in for the Tn-seq, with minor adaptations. An overnight culture (5 mL) of each strain was grown in SMM (40 mM succinate) from LB plates. Cells were washed and re-suspended at an OD_{500} of 0.1 (or 0.25 for Δ*phz*Δ*dctBD*) in the same medium to start the new cultures (5 mL), which were grown to OD_{500} ~0.8-1, pelleted, washed, and re-suspended in the same minimal medium without succinate (no carbon source) at OD_{500} of 1. For each strain, the culture was split across 8-12 wells (150 µL cultures) in a 96-well plate, with 100 µM PYO added to half of the cultures. 70 µL of mineral oil was added to the top of the wells to prevent evaporation. Propidium iodide (PI) at 5 µM was also added to the cultures to monitor cell death [16]. The plate was then moved to a BioTek Synergy 4 plate reader and incubated under shaking conditions at 37ºC for 24 hrs. After incubation, cultures were serially diluted in buffer and plated for colony forming units (CFUs) on LB agar, and survival in the presence of PYO was compared to the no-PYO control. Plates were incubated at room temperature (RT) and CFUs were counted after 36-48 hrs. In this study, a stereoscope was always used to count the CFUs. Survival levels were calculated for each mutant (i.e. for each replicate, the % survival for "+PYO" was calculated based on CFUs for "No PYO"). Then, the survival levels for each mutant were normalized by the survival levels of the Δ*phz* parent strain (i.e. % survival for "+PYO" for each mutant was divided by the average % survival for "+PYO" of the Δ*phz* strain); these "fitness" values were $\log_2$-transformed for plotting.

PYO tolerance with efflux inhibitor

Survival assays with efflux inhibition were performed to test the importance of efflux systems in *P. aeruginosa* for tolerance against PYO toxicity. From a Δ*phz* overnight culture pre-grown in SMM (20 mM succinate), a new 7 mL culture was started in fresh SMM at an OD_{500} of

0.05 and was incubated for around 10 hrs (enough to reach stationary phase). Cells were then pelleted, washed and re-suspended in MPB at an OD_{500} of 1 (10 mL of culture was prepared). The culture was then split into four different treatments: (i) no PYO, no PAβN; (ii) 100 μM PYO, no PAβN; (iii) no PYO, with PAβN (50 μg/mL), and (iv) 100 μM PYO, with PAβN. Each of the treatments were split across 12 wells containing 150 μL of culture + 70 μL of mineral oil in a 96-well plate. The plate was incubated at 37ºC under shaking conditions using a BioTek Synergy 4 plate reader. Samples were serially diluted in MPB and plated for CFUs on LB agar after 12, 24, and 48 hrs. Survival for treatments containing PYO were calculated based on the CFUs counted for the negative control without PYO (Fig 1D). At each time point, four wells were sampled, with each well considered an independent replicate. The experiment was repeated twice with similar results.

Antibiotic tolerance experiments using P. aeruginosa

Tolerance assay for WT, Δ*phz*, and Δ*phz* + PYO. For most antibiotic tolerance assays (except for tolerance using cells harvested during log-phase, see below), the experimental design shown in S4A Fig was followed. WT and Δ*phz* cells were grown from a plate into overnight cultures in GMM with 20 mM glucose. Next, WT and Δ*phz* cells were pelleted, washed and re-suspended at an OD_{500} of 0.05 in four independent new cultures (replicates) in GMM (10 mM glucose) per treatment. Three treatments were prepared: WT, Δ*phz* (no PYO), and Δ*phz* + 100 μM PYO, with four independent biological replicates for each. Each of the four individual cultures (replicates) were incubated for around 20 hrs, reaching stationary phase, in 7 mL cultures (18 x 150 mm glass tubes). Each individual culture (replicate) was then split into a negative control (no antibiotic) or antibiotic treatment (2 mL of culture per each treatment, using plastic Falcon tubes, VWR Cat. No. 352059). After addition of the antibiotic from concentrated stocks, cultures were incubated for four hours, serially diluted in MPB and then plated for CFUs on LB agar. Unless stated otherwise, cells were not washed before plating. We observed that washing the cells did not make any difference in the outcome of the experiments. In addition, washing was not feasible for the tolerance assays using smaller volumes (i.e. in 96-well plates). The only two experiments where washing was performed are described below ("Tolerance assay with PAβN" and "Tolerance

assay to measure the lag in CFUs appearance"). In these cases, cells were washed because (i) the ciprofloxacin concentrations were higher (10 μg/mL) and more likely to affect *P. aeruginosa* cells on the plate, and (ii) for the case of the PAβN experiment, we wanted to avoid having cells be in contact with the inhibitor while growing on the plate. Antibiotics were used at the concentrations mentioned in figure legends. Plates were incubated at RT and CFUs were counted after 36-48 hrs. Plates were always checked again after seven days to count any late-arising CFUs. Importantly, for all tolerance experiments performed in this study (including this and all experiments described below), each experiment was repeated at least twice on different days, with similar results.

The same protocol was followed for the experiment testing different concentrations of PYO (Fig 2H) and for the experiment testing how PYO impacts tolerance of different *P. aeruginosa* mutants with partial resistance to ciprofloxacin (CipR-21, 25, 33, and 40; S7E Fig). For the experiment testing tolerance after exposure to different phenazines (Fig 2E), all the phenazines were dissolved in a common solvent (DMSO), which was used as the negative control; these experiments were performed in a Δ*phz** mutant lacking not only the *phzA-G1* and *phzA-G2* operons but also all phenazine modification genes, to prevent the transformation of phenazine 1-carboxylic acid (PCA) into the other phenazines (see S5 Table). For experiments performed in synthetic cystic fibrosis sputum medium SCFM (Fig 2D), the same experimental design was followed, with the exception that SCFM was used instead of GMM.

Tolerance assay for strains with arabinose-inducible constructs. For these experiments (Fig 2I and S6B Fig), the 20 hr cultures of each strain (Δ*phz* P_{ara}*:mexGHI-opmD,* Δ*phz* P_{ara}*:ahpB*, and Δ*phz* P_{ara}*:katB*) were grown with and without 20 mM arabinose for induction of the controlled systems, and then exposed to ciprofloxacin the same way described above. To rule out any non-specific interference of the inducer, negative controls with and without 20 mM arabinose using the parent Δ*phz* strain (without the insertions in the *att*Tn7 site) were also done. Adding arabinose to the Δ*phz* strain did not impact tolerance levels (S6 Fig).

Tolerance assay with PAβN. Experiments using the efflux inhibitor PAβN (S4G Fig) were also performed similarly to the way as described above. The only differences were that after the 20 hrs incubation and before the addition of the antibiotic, PAβN was added to the cultures at a

final concentration of 50 μg/mL. Cultures were incubated for 15 min and then ciprofloxacin was added, followed by a four-hour incubation. For these experiments, instead of plating cells directly on LB, 1 mL of culture of each replicate/treatment was pelleted (12500 rpm for 2 min), washed in MPB for removal of ciprofloxacin and PAβN, and only then serially diluted in MPB and plated on LB for CFU counting.

Tolerance assay to measure the lag in CFUs appearance. This experiment (S4F Fig) followed the same general protocol described above (using 10 μg/mL of ciprofloxacin). The difference was that the reported CFUs were counted after incubation of LB plates for two days and seven days, whereas otherwise only the final counts from the seventh day were reported. This was done to quantify lag in the CFUs' growth under the studied conditions. Similar to the tolerance assays with PAβN and ciprofloxacin described above, cells were pelleted and washed before plating on LB for CFU counting.

Tolerance assay for cells harvested during log-phase. Δ*phz* cells were grown in overnight cultures in GMM (20 mM glucose). Next, cells were pelleted, washed, and re-suspended into two new cultures, one with PYO (100 μM) and one without PYO, at an OD_{500} of 0.05 in GMM (10 mM glucose, 7 mL cultures). Cultures were grown until OD_{500} = 0.5 (around 5-6 hrs). Cells were then washed and re-suspended in the same medium at an OD_{500} of 0.5, but without the nitrogen source (i.e. no NH_4Cl). PYO was re-added after washes to the culture that was pre-grown with PYO. The cultures, one with and one without PYO, were then split into different treatments: negative control (no antibiotic), ciprofloxacin (0.5 μg/mL), levofloxacin (1 μg/mL), gentamicin (16 μg/mL) and tobramycin (4 μg/mL). Then, they were all transferred to wells in a 96-well plate (three to four wells per treatment, with each well being considered an independent replicate). Cultures within wells contained 150 μL with an additional 70 μL of mineral oil on top to prevent evaporation. The depletion of nitrogen prevented growth in the negative control, which limited overestimation of the antibiotic killing effect (because survival rates were calculated relative to the negative control). The plates were incubated for four hours at 37ºC under shaking conditions (175 rpm) using a benchtop incubator (VWR incubator orbital shaker). The 96-well plate was kept inside an airtight plastic container with several wet paper towels to maintain high humidity

attached to the shaker. After incubation, cells were serially diluted and plated on LB agar for CFU counting (S4B Fig). A similar experiment was also performed with the strains containing arabinose-inducible constructs (Δ*phz* P_{ara}*:mexGHI-opmD,* Δ*phz* P_{ara}*:ahpB* and Δ*phz* P_{ara}*:katB*) and the Δ*phz* background control (S6A Fig), for which tolerance to ciprofloxacin (0.5 μg/mL) was tested. The experiment followed the same protocol described above, with the difference that, instead of presence or absence of PYO, strains were incubated in the presence or absence of 20 mM arabinose.

Time-lapse microscopy experiment and quantification

Fluorescently tagged strains of WT or Δ*phz* were grown in GMM and tolerance experiments were performed as shown in S4D Fig using ciprofloxacin (10 μg/mL). After the four-hour incubation with the antibiotic, cells were washed and re-suspended in GMM. The two different strains were then mixed and placed on an agarose pad containing GMM (no ciprofloxacin or PYO was added to the pad). Agarose pads were placed into a PELCO Clear Wall Glass Bottom Dish (Cat. No. 14023-20), and the dish was used for imaging within the microscope incubation chamber. Outgrowth was visualized using a Nikon Ti2E microscope with Perfect Focus System 4. Incubation proceeded for 12.5 to 15 hrs at 37ºC, with imaging every 15 min in bright field (phase contrast), green and red fluorescence channels (50 ms exposure with 470 nm LED lamp and a green-FITC filter [ex = 465-495nm, em = 515-555nm] for GFP; 50 ms exposure with 555 nm LED lamp and a quad band filter [red ex = 543-566nm, red em = 580-611nm] for mApple).

For image analysis, a Fiji macro was used. Briefly, fluorescent channels (GFP/mApple) of the first and last time points were segmented using the "Auto Threshold" function and "Default" setting. The area of the segmented cells was then recorded using the "Analyze Particles" function in Fiji [96]. This allowed for quantification of the total area covered by cells within each channel, with each field of view being processed separately. After that, for each field of view, the total area covered by WT cells (or Δ*phz* + 100 μM PYO, depending on the experiment) was divided by the area covered by Δ*phz* cells to obtain the relative "growth area ratios." This was done for first and last time points. Three experiments were performed, with different fluorescent protein/strain combinations: (i) WT::mApple/Δ*phz*::GFP (n = 13 fields of view, Fig 2F-G, S1 Movie); (ii)

Δ*phz*::GFP+PYO /Δ*phz*::mApple (n = 19, Fig 2G); and (iii) WT::GFP/Δ*phz*::mApple (n = 16, S4E Fig). GFP/mApple were controlled by the *rpsG* promoter for all of the strains (S5 Table).

RNA extraction and quantitative reverse transcriptase PCR (qRT-PCR)

Experiment 1 – measurement of PYO-induced gene expression. Six different treatments were prepared for this qRT-PCR experiment: (i) WT PA14, (ii) Δ*phz*, (iii) Δ*phz* + 1 μM PYO, (iv) Δ*phz* + 10 μM PYO, (v) Δ*phz* + 100 μM PYO and (vi) Δ*phz* + 200 μM PYO. Cultures of WT or Δ*phz* were grown overnight in GMM (20 mM glucose), then cells were washed and resuspended at an OD_{500} of 0.05 (three replicates) in fresh GMM (5 mL in culture tubes). Different concentrations of PYO were added to Δ*phz* cultures as mentioned and all cultures were incubated for around 8.5 hrs (until early stationary phase). This was enough time for WT to make PYO (around 50-70 μM, measured by absorbance at OD_{691} [97]). After incubation, cells were pelleted, immediately frozen using liquid nitrogen and stored at -80ºC.

Experiment 2 – measuring arabinose induction of *mexGHI-opmD*, *ahpB* and *katB*. Eight different treatments were prepared for this qRT-PCR experiment, in which each of the four tested strains (Δ*phz*, Δ*phz* P_{ara}:*mexGHI-opmD*, Δ*phz* P_{ara}:*ahpB* and Δ*phz* P_{ara}:*katB*) were incubated with and without 20 mM arabinose for artificial induction of the constructs. Cultures of the four strains were grown overnight in GMM (20 mM glucose), then cells were washed and resuspended at an OD_{500} of 0.05 (three replicates) in the same medium (5 mL in culture tubes), with and without 20 mM arabinose (for conditions without arabinose, the respective amount of water was added). Cultures were incubated for around 8.5 hrs, then pelleted, immediately frozen using liquid nitrogen and stored at -80ºC.

For RNA extraction, previously published protocols were followed [16,85]. Briefly, samples were thawed in ice for 10 min and re-suspended in 215 μL of TE buffer (30 mM Tris.Cl, 1 mM EDTA, pH 8.0) containing 15 mg/mL of lysozyme + 15 μL of proteinase K solution (20 mg/mL, Qiagen), and then incubated for 8–10 min. For lysis steps and RNA extraction the RNeasy kit (Qiagen) was used. Samples were then treated with TURBO DNA-free kit (Invitrogen) for removal of any contaminant gDNA. Next, cDNA was synthesized using iScript cDNA Synthesis

kit (Bio-Rad) (1 μg of total RNA was used). For these kits, the manufacturer's instructions were followed. qRT-PCR reactions were performed using iTaq Universal SYBR Green Supermix (Bio-Rad) in 20 μL reactions using a 7500 Fast Real-Time PCR System machine (Applied Biosystems) following published protocols [16]. Standard curves for each primer pair were prepared using *P. aeruginosa* gDNA and were used for calculation of cDNA for each gene studied. The house-keeping gene *oprI* was used as a control gene for normalizations [85].

Data showing total *oprI*-normalized cDNA levels (i.e. cDNA measured for a certain gene in a certain sample, divided by the respective cDNA measured for *oprI* in the same sample) and the $\log_2$-fold change in expression are shown in Figs 2B and S1, S2, S3, and S5 Figs. Fold changes were calculated relative to the mean value for Δ*phz* samples without added PYO (Fig 2B and S1B and S3 Figs) or the mean value of samples from the same strain without added arabinose (S5B Fig). cDNA values for replicates within each efflux gene/treatment (shown in S2 Fig) were averaged and used with the *geom_tile()* function in R [93,94] for generation of the heatmap shown in Fig 2B.

Stenotrophomonas *and* Burkholderia *growth curves and antibiotic tolerance assays*

Stenotrophomonas maltophilia ATCC 13637, *Burkholderia cepacia* ATCC 25416, *B. cenocepacia* AU42085, *B. multivorans* AU42096 (*B. multivorans 1)*, and *B. gladioli* AU42104 were used in the growth experiments shown in Fig 5A (for strain details, see S5 Table). Each strain was grown overnight in GMM (20 mM glucose, 5 mL culture tubes) supplemented with 1x MEM amino acids (AA) (Sigma, Cat. No. M5550). Cells were pelleted, washed and re-suspended in new cultures at an OD_{500} of 0.05 in the same medium. Cultures were then split, different concentrations of PYO were added (0, 10, 50 or 100 μM for *S. maltophilia*; 0, 10 or 100 μM for all others), and moved to a 96-well plate (4 to 6 wells per treatment, with each well being considered an independent replicate). Cultures within wells contained 150 μL with an additional 70 μL of mineral oil on top to prevent evaporation. The plates were incubated at 37ºC under shaking conditions using a BioTek Synergy 4 plate reader with OD_{500} measurements every 15 min for 24 hrs to measure growth. Assays for tolerance to ciprofloxacin with or without exogenous PYO were performed for *S. maltophilia* (sensitive to PYO) and for four *Burkholderia* strains (all resistant to

PYO): *B. cepacia*, *B. cenocepacia*, *B. multivorans 1* and *B. multivorans* AU18358 (*B. multivorans 4*). The experiments followed exactly what was done for *P. aeruginosa* (S4A Fig), except that cultures were grown in GMM + AA, and are shown in Figs 4B and 4E. Finally, a tolerance assay in SCFM with and without PYO was performed for *B. multivorans 1* (Fig 5H) and followed what was described for the SCFM experiments in *P. aeruginosa* (with the only difference being the ciprofloxacin concentrations, always mentioned in the legends).

Co-culture antibiotic tolerance experiments

To test how PYO produced by *P. aeruginosa* impacts tolerance to ciprofloxacin in other species, co-culture experiments were performed using membrane-separated 12-well tissue plate cultures containing 0.1 μm pore PET membranes (VWR Cat. No. 10769-226). Briefly, overnight cultures of the *P. aeruginosa* strain (WT/Δ*phz* PA14 or PA 76-11) and the respective other species tested (*S. maltophilia*, *B. cepacia*, *B. cenocepacia* or *B. multivorans 1*) were prepared in GMM (20 mM glucose) + AA. Cells were pelleted, washed and re-suspended to different ODs as follows: (i) for any *P. aeruginosa-Burkholderia* assay, *P. aeruginosa* starting OD_{500} = 0.05 and *Burkholderia* starting OD_{500} = 0.025; (ii) for the *P. aeruginosa-S. maltophilia* assay, *P. aeruginosa* starting OD_{500} = 0.01 and *S. maltophilia* starting OD_{500} = 0.1. *P. aeruginosa* was cultured in the bottom part of the well (600 μL), while the other species was cultured in the upper part of the well (100 μL), as shown in Fig 5C. *B. cepacia* and *S. maltophilia* were cultured either with WT or Δ*phz P. aeruginosa* PA14 (with and without 100 μM PYO exogenously added).

B. cenocepacia and *B. multivorans 1* were cultured either with PA 76-11 (a *P. aeruginosa* strain isolated from CF sputum that produced 50-100 μM PYO in these assays) or alone in the presence or absence of 100 μM PYO. For cases where *Burkholderia* was grown alone, the strain tested was grown in both the bottom and top parts of the membrane-separated wells. In all experiments, co-cultures were grown for around 20 hrs at 37 ºC under shaking conditions (175 rpm) using a benchtop incubator, followed by addition of ciprofloxacin (concentrations were either 1 or 10 μg/mL, as specified in the figure legends) and incubation for four hours. The membrane-separated plates were kept inside an airtight plastic container with several wet paper towels to maintain high humidity attached to the shaker. For every co-culture combination in the membrane-

separated plate, three wells were used as a negative control (no antibiotic) and three wells were used for ciprofloxacin treatment; each well was considered an independent replicate. After incubation with ciprofloxacin, cells were serially diluted in MPB and plated for CFUs on LB. In most cases, only *Burkholderia* cells were plated (Fig 5F). However, to test if our *P. aeruginosa* WT strain was still more tolerant than the Δ*phz* strain when both were grown in the presence of a *Burkholderia* species, we performed an experiment with *P. aeruginosa* PA14 and *Burkholderia multivorans 1* where we treated the co-cultures with ciprofloxacin 1 μg/mL and plated *P. aeruginosa* (Fig 5G). Finally, we also performed a co-culture experiment in SCFM (*P. aeruginosa* PA14 WT/Δ*phz* with *B. multivorans 1*) to test if PYO produced by PA14 WT increases tolerance in *Burkholderia* in this medium (Fig 5I). This experiment in SCFM followed the same overall experimental design used before, except for using SCFM instead of GMM in all steps.

Determination of minimum inhibitory concentrations

The antibiotic concentrations used for selecting *de novo* antibiotic-resistant mutants in the fluctuation tests were chosen based on the results of a modified agar dilution MIC assay. Overnight cultures were grown for each strain in GMM (with 10 mM glucose) or GMM (10 mM glucose) + AA, respectively, then diluted to an OD_{500} of 0.5, from which 3 μL was spotted onto MH agar containing a 2-fold dilution series of the antibiotic. After the spots dried, the antibiotic plates were incubated upside down for 48 hrs at 37ºC before assessing the spots for growth. We considered the MIC to be the first concentration at which there was neither a lawn of background growth, nor dozens of overlapping colonies visible without magnification. We generally used 2x this MIC as the selection condition for fluctuation tests; for *P. aeruginosa*, this corresponded to the EUCAST [27] resistance breakpoints for ciprofloxacin and levofloxacin, while our chosen concentrations of gentamicin and tobramycin were two-fold higher than the EUCAST breakpoints [32]. EUCAST breakpoints are not available for *Stenotrophomonas* spp. or the *Burkholderia cepacia* complex. The appropriateness of the selection condition was additionally verified by performing a fluctuation test, as described below, and choosing the antibiotic concentration that reliably yielded a countable number of colonies (zero to several dozen, with at least several non-zero counts per 44 parallel cultures) in each well.

Ciprofloxacin MICs for parent strains and isolated mutants from the fluctuation tests were determined according to standard clinical methods for broth microdilution assays [27]. In brief, cells from either overnight cultures in MH broth or fresh streaks on LB agar (14-16 hrs old) were resuspended to a density of 3-7 x 10^5 CFUs/mL in a two-fold dilution series of ciprofloxacin in MH broth, with or without 100 μM PYO. The dilution series were set up in a final volume of 100 μL per well in 96-well microtiter plates, with appropriate no-antibiotic and cell-free controls. Three biological replicates (independent overnight cultures or cell suspensions) were prepared for each tested strain. Following inoculation, the microtiter plates were sealed with a plastic film to prevent evaporation and incubated in a single layer at 37ºC, without shaking. The wells were assessed for growth (turbidity) visible to the naked eye after 18 hrs of incubation.

Fluctuation tests, calculation of mutation rates, and model fitting

For all tested strains and conditions, fluctuation tests were performed by inoculating 200 μL cultures in parallel in a flat-bottomed 96-well plate. All reported fluctuation test data for *P. aeruginosa* are from experiments using the Δ*phz* strain. We also performed fluctuation tests using the *P. aeruginosa* PA14 WT strain, and performed phenotypic and genotypic characterization of partially-resistant mutants detected in those experiments (see below); however, the effect of PYO on apparent mutation rates in WT was difficult to interpret due to inconsistent PYO production in the 96-well plates. For cultures that were grown with PYO (or arabinose in the case of strains with arabinose-inducible constructs), the PYO (or 20 mM arabinose) was added to the medium before inoculation. The cultures were inoculated with a 10^{-6} dilution of a single overnight culture (representing a biological replicate) that had first been diluted to a standard OD_{500} of 1.0, corresponding to an initial cell density of approximately 2000-2500 CFUs/mL (400-500 cells/culture). Each treatment condition consisted of 44 such parallel cultures.

The 96-well plates were placed inside an airtight plastic container with several wet paper towels to maintain high humidity, then incubated at 37ºC with shaking at 250 rpm. For plating during log-phase, the cultures were incubated until reaching approximately half-maximal density (OD_{500} of 0.4-0.7 for *P. aeruginosa* in GMM with 10 mM glucose, or 0.9-1.2 for *P. aeruginosa* in SCFM or *B. multivorans* in GMM + AA). For plating during stationary phase, the cultures were

incubated for 24 hrs. The cultures were then plated by spotting 40-50 μL per culture into single wells of 24-well plates (for any given experiment, the same volume was spotted for all parallel cultures); each well contained 1 mL of MH agar or SFCM agar plus an antibiotic, with or without 100 μM PYO (or 20 mM arabinose for strains with arabinose-inducible constructs). In the case of *B. multivorans* cultures that were spotted onto antibiotic plates containing 100 μM PYO, the cultures were first diluted 1:10 (if not pre-treated with 100 μM PYO) or 1:100 (if pre-treated with 100 μM PYO).

At the same time as plating onto the antibiotic plates, six representative cultures from each treatment were serially diluted and plated on LB agar plates to assess total CFUs. The antibiotic plates were incubated upside down, in stacks of no more than eight, at 37ºC for 16-24 hrs for *P. aeruginosa* (except for gentamicin plates, which were incubated for 40-48 hrs) or 40-48 hrs for *B. multivorans*. Subsequently, colonies were counted under a stereoscope at the highest magnification for which the field of view still encompassed an entire well; occasionally, a well contained too many colonies to count (a so-called "jackpot" culture [98]), in which case that culture was discarded from further analysis. The LB agar plates for total CFU counts were incubated for 30-36 hrs at RT before counting colonies at the same magnification.

Mutation rates reported in the figures were calculated using the function newton.LD.plating from the R package rSalvador [99] to estimate *m*, the expected number of mutations per culture. This is a maximum likelihood-based method for inferring mutation rates from fluctuation test colony counts, based on the classic Luria-Delbrück (LD) distribution with a correction to account for the effects of partial plating (i.e. plating a portion of each culture rather than the total volume) [99]. We chose this method because it has been shown to be the most accurate estimator of *m* when partial plating is involved [99,100]. To get μ_{app} (apparent mutation rate per generation) from *m*, we divided *m* by the total number of cells per parallel culture [99], as estimated from the mean number of CFUs counted for the six representative cultures.

To compare the fits of different formulations of the LD distribution to our data, we generated theoretical cumulative distributions using the parameter values estimated for our data. Specifically, for the Hamon and Ycart version of the LD model [44], we estimated *m* and *w*

(relative fitness of mutants compared to the parent strain in the non-selective pre-plating liquid growth medium) using the function GF.est from the R script available at http://ljk.imag.fr/membres/Bernard.Ycart/LD/ (version 1.0; note that in the script, *m* is called alpha and 1/*w* is called rho); then, we used the function pLD from the same script to generate the theoretical distribution. For the mixed LD-Poisson and basic LD models, we wrote and used an R translation of the MATLAB code written by Lang *et al.* [45]; the original code is available at https://github.com/AWMurrayLab/FluctuationTest_GregLang. The basic LD model used by Lang *et al.* [45] is equivalent to that available in the rSalvador package (using the function newton.LD), except without the correction for partial plating; the latter is only important when using the estimate of *m* to infer the mutation rate, not when comparing the fits of different models to the empirical cumulative distribution of the raw colony counts.

Plots of the empirical cumulative distributions of our data against the theoretical models showed that the Hamon and Ycart model was a visually good fit in all cases (see Figs 4B, 6C, and S9 Fig for examples). To further assess goodness-of-fit of the Hamon and Ycart model, we performed Pearson's chi-square test in R after binning the data and theoretical distribution such that the expected number of cultures in each bin of mutant counts was at least five [101]. To compare the goodness-of-fit of the Hamon and Ycart model to the basic LD model, we calculated the negative log-likelihood for each model and performed the likelihood ratio test. To compare the Hamon and Ycart model to the mixed LD-Poisson model, we simply compared the negative log-likelihoods (smaller values indicate a better fit); the likelihood ratio test was not applicable as these two models contain the same number of parameters. Note that although the Hamon and Ycart (or in some cases, LD-Poisson) models were often better fits than the basic LD model, we still used the basic LD model for statistical comparison of mutation rates between conditions, because an accurate method to account for partial plating has not yet been developed for the cases of post-plating mutations or differential fitness between mutants and parent strains [99]. Nevertheless, similar patterns in mutation rates were observed when using an older method of accounting for partial plating to derive μ_{app} from the Hamon and Ycart model [102]; the Pearson correlation coefficient was 0.98 for mutation rates calculated with the newton.LD.plating function in rSalvador versus the partial-plating-corrected Hamon and Ycart method (S3 Table). We also

separately performed non-parametric statistical analysis of the raw mutant frequencies (i.e. mutant colony counts divided by the number of cells per parallel culture), as such analysis is agnostic to any assumptions about the biological processes underlying the data. The statistical significance of this analysis generally corresponded with the statistical significance of a likelihood ratio test based on the newton.LD.plating model of mutation rates, indicating that the effects of PYO were robust to different mathematical approaches to analyzing the fluctuation test data (S2 Table).

Characterization of antibiotic resistance phenotypes

We defined putative ciprofloxacin-resistant mutants as "enriched" by PYO in the fluctuation tests if colonies with a given morphology were at least 2x more numerous on the PYO-containing ciprofloxacin plate than the respective non-PYO-containing ciprofloxacin plate derived from the same 200 µL culture. These putative mutants could be either from the PYO pre-treated or non-PYO pre-treated branches of the fluctuation test. Putative mutants that were seemingly enriched by PYO were restreaked for purity on PYO-containing agar plates at the same ciprofloxacin concentration on which they were selected in the fluctuation test (0.5 µg/mL for *PA*, 8 µg/mL for *B. multivorans*). Putative mutants that were not enriched by PYO were restreaked on ciprofloxacin agar plates without PYO. Frozen stocks of each restreaked, visually pure isolate were prepared by inoculating cultures with single colonies in 5 mL of liquid LB, incubating to stationary phase, mixing 1:1 with 50% glycerol, and storing at -80ºC.

The levels of ciprofloxacin resistance of selected isolates, as well as the parent strains, were assessed using a CFU recovery assay as follows. For each isolate, four 5 mL cultures in GMM (for *P. aeruginosa*) or GMM + AA (for *B. multivorans*) were inoculated directly from the frozen stock, to minimize the number of generations in which secondary mutations could be acquired. The cultures were grown to stationary phase overnight, then subcultured to an OD_{500} of 0.05 in 5 mL of fresh GMM (for *P. aeruginosa*) or GMM + AA (for *B. multivorans*), with or without 100 µM PYO. The new cultures were grown to mid log-phase, then serially diluted in GMM or GMM + AA (+/- 100 µM PYO as appropriate) and plated for CFUs (10 µL per dilution step) on 1) plain MH agar, 2) MH agar + ciprofloxacin, and 3) MH agar + ciprofloxacin + 100 µM PYO. The lowest plated dilution was 10^{-1}, making the limit of detection approximately 1000 CFUs/mL.

Identification of mutations by whole-genome sequencing

Genomic DNA was isolated from selected putative mutants and the parent strains using the DNeasy Blood & Tissue kit (Qiagen). Library preparation and 2x150 bp paired-end Illumina sequencing was performed by the Microbial Genome Sequencing Center (Pittsburgh, PA), with a minimum of 300 Mb sequencing output per sample (~50x coverage). Forward and reverse sequencing reads were concatenated into a single file for each isolate and quality control was performed using Trimmomatic (version 0.39) [103] with the following settings: LEADING:27 TRAILING:27 SLIDINGWINDOW:4:27 MINLEN:35. Mutations were then identified using breseq (version 0.34.1) [104]. The annotated reference genome for *P. aeruginosa* UCBPP-PA14 was obtained from BioProject accession number PRJNA38507. For *B. multivorans* AU42096, no reference genome was available from NCBI. Therefore, a genome scaffold was assembled from the paired-end sequencing data for the parent strain using SPAdes (version 3.14.0) with default parameters [105]. This scaffold was then used as the reference for breseq. Differences between the parent strain and isolates were identified using the gdtools utility that comes with breseq to compare the respective breseq outputs. All sequenced *P. aeruginosa* mutants were derived from the Δ*phz* strain except for CipR-33 and CipR-40, which were derived from the WT strain. In the case of *B. multivorans*, several dozen putative mutations were identified that were common to all three sequenced putative mutants. We assumed that these represented assembly errors in the parent strain genome scaffold, but even if they were genuine mutations, these would not account for the phenotypic differences between the isolates; therefore, S6 Table reports only mutations that were unique to each isolate. The genomic loci containing each putative mutation for the *B. multivorans* isolates were identified by retrieving the surrounding 200 bp from the parent genome scaffold and using the nucleotide BLAST tool on the MicroScope platform [106] to find the closest match in the *B. multivorans* ATCC 17616 genome.

Growth curves with propidium iodide

To verify that PYO did not increase the population turnover rate (i.e. cell death) in our log-phase fluctuation tests prior to the antibiotic selection step, we performed growth curves in the presence of different concentrations of PYO, with the addition of propidium iodide (PI) as a

fluorescent marker for cell death. The use of PI as a marker for PYO-induced cell death has previously been validated under similar conditions (Meirelles and Newman, 2018). The growth curves were performed in GMM and SCFM for *P. aeruginosa* Δ*phz*, and GMM + AA for *B. multivorans 1*. The cultures were prepared and incubated in the same manner as the fluctuation tests, except that 5 μM PI was added at the beginning of the experiment, and measurements for OD_{500} and PI fluorescence (ex = 535 nm, em = 617 nm) were taken periodically using a Spark 10M plate reader (Tecan). Importantly, PI stock concentration (5 mM, 1000x) was prepared in DMSO, and the final concentration of DMSO in the cultures did not exceed 0.1%. In addition, black 96-well plates with clear bottoms were used to minimize the effects of adjacent wells on fluorescence readings.

Statistical analyses

All statistical analyses were performed using R [94]. Welch's unpaired t-tests or one-way ANOVA with post-hoc Tukey's HSD test for multiple comparisons were used for tolerance assay data. The likelihood ratio test as implemented by the rSalvador function LRT.LD.plating was used to compare mutation rates, alongside the alternative criterion of non-overlapping 84% confidence intervals as a proxy for the $p < 0.05$ threshold for statistical significance. The Mann-Whitney U test was used to compare the distributions of mutant frequencies. Welch's unpaired t-tests were used for comparisons of CFU recovery on ciprofloxacin plates under different PYO treatments. Benjamini-Hochberg corrections were used in all cases to control false discovery rates, except where Tukey's HSD test was performed. For all antibiotic tolerance assays measured by CFUs, survival data were $\log_{10}$-transformed before statistical analyses.

Acknowledgments

We thank members of the Newman lab and Shashank Gandhi for constructive feedback throughout the project and on the manuscript. We also thank Steven Wilbert for assistance with image analysis, David Basta for providing the plasmid used for *lptA* deletion, and The Millard and Muriel Jacobs Genetics and Genomics Laboratory at Caltech and Igor Antoshechkin for support during library preparation and sequencing of the Tn-seq samples. Finally, we thank John LiPuma

(CFF *Burkholderia cepacia* Research Laboratory and Repository at the University of Michigan) for providing clinical *Burkholderia* strains and Justin Bois for constructive feedback on our statistical approach.

Data availability

Tn-seq data have been deposited at GEO under accession number GSE148769. Whole genome sequencing data for the parent strains and ciprofloxacin-resistant mutants of *P. aeruginosa* and *B. multivorans* AU42096 have been deposited at NCBI under accession number PRJNA625945. Due to their size/format, supplementary tables mentioned in this chapter were not included in this document. These tables are linked to this thesis and available through CaltechTHESIS. All strains/plasmids used in this study are available from the corresponding author upon request.

References

1. Fair RJ, Tor Y. Antibiotics and bacterial resistance in the 21st century. Perspect Medicin Chem. 2014;6: 25–64.
2. Brauner A, Fridman O, Gefen O, Balaban NQ. Distinguishing between resistance, tolerance and persistence to antibiotic treatment. Nat Rev Microbiol. 2016;14: 320–330.
3. Levin-Reisman I, Ronin I, Gefen O, Braniss I, Shoresh N, Balaban NQ. Antibiotic tolerance facilitates the evolution of resistance. Science. 2017;355: 826–830.
4. Windels EM, Michiels JE, Fauvart M, Wenseleers T, Van den Bergh B, Michiels J. Bacterial persistence promotes the evolution of antibiotic resistance by increasing survival and mutation rates. ISME J. 2019;13: 1239–1251.
5. Martinez JL. The role of natural environments in the evolution of resistance traits in pathogenic bacteria. Proc Biol Sci. 2009;276: 2521–2530.
6. Davies J, Davies D. Origins and evolution of antibiotic resistance. Microbiol Mol Biol Rev. 2010;74: 417–433.
7. Kester JC, Fortune SM. Persisters and beyond: mechanisms of phenotypic drug resistance and drug tolerance in bacteria. Crit Rev Biochem Mol Biol. 2014;49: 91–101.
8. Balaban NQ, Helaine S, Lewis K, Ackermann M, Aldridge B, Andersson DI, et al. Definitions and guidelines for research on antibiotic persistence. Nat Rev Microbiol. 2019;17: 441–448.
9. Driscoll JA, Brody SL, Kollef MH. The epidemiology, pathogenesis and treatment of *Pseudomonas aeruginosa* infections. Drugs. 2007;67: 351–368.
10. Laursen JB, Nielsen J. Phenazine natural products: biosynthesis, synthetic analogues, and biological activity. Chem Rev. 2004;104: 1663–1686.
11. Glasser NR, Kern SE, Newman DK. Phenazine redox cycling enhances anaerobic survival in *Pseudomonas aeruginosa* by facilitating generation of ATP and a proton-motive force. Mol Microbiol. 2014;92: 399–412.
12. Saunders SH, Tse ECM, Yates MD, Otero FJ, Trammell SA, Stemp EDA, et al. Extracellular DNA Promotes Efficient Extracellular Electron Transfer by Pyocyanin in *Pseudomonas aeruginosa* Biofilms. Cell. 2020;182: 919–932.e19.
13. Dietrich LE, Price-Whelan A, Petersen A, Whiteley M, Newman DK. The phenazine pyocyanin is a terminal signalling factor in the quorum sensing network of *Pseudomonas aeruginosa*. Mol Microbiol. 2006;61: 1308–1321.
14. Wang Y, Wilks JC, Danhorn T, Ramos I, Croal L, Newman DK. Phenazine-1-carboxylic acid promotes bacterial biofilm development via ferrous iron acquisition. J Bacteriol. 2011;193: 3606–3617.
15. Korgaonkar A, Trivedi U, Rumbaugh KP, Whiteley M. Community surveillance enhances *Pseudomonas aeruginosa* virulence during polymicrobial infection. Proc Natl Acad Sci USA. 2013;110: 1059–1064.
16. Meirelles LA, Newman DK. Both toxic and beneficial effects of pyocyanin contribute to the lifecycle of *Pseudomonas aeruginosa*. Mol Microbiol. 2018;110: 995–1010.
17. Schiessl KT, Hu F, Jo J, Nazia SZ, Wang B, Price-Whelan A, et al. Phenazine production promotes antibiotic tolerance and metabolic heterogeneity in *Pseudomonas aeruginosa* biofilms. Nat Commun. 2019;10: 762.

18. Zhu K, Chen S, Sysoeva TA, You L. Universal antibiotic tolerance arising from antibiotic-triggered accumulation of pyocyanin in *Pseudomonas aeruginosa.* PLoS Biol. 2019;17: e3000573.
19. Muller M. Pyocyanin induces oxidative stress in human endothelial cells and modulates the glutathione redox cycle. Free Radic Biol Med. 2002;33: 1527–1533.
20. Rada B, Leto TL. Pyocyanin effects on respiratory epithelium: relevance in *Pseudomonas aeruginosa* airway infections. Trends Microbiol. 2013;21: 73–81.
21. Lister PD, Wolter DJ, Hanson ND. Antibacterial-resistant *Pseudomonas aeruginosa*: clinical impact and complex regulation of chromosomally encoded resistance mechanisms. Clin Microbiol Rev. 2009;22: 582–610.
22. Llanes C, Hocquet D, Vogne C, Benali-Baitich D, Neuwirth C, Plésiat P. Clinical strains of *Pseudomonas aeruginosa* overproducing MexAB-OprM and MexXY efflux pumps simultaneously. Antimicrob Agents Chemother. 2004;48: 1797–1802.
23. Sobel ML, Neshat S, Poole K. Mutations in PA2491 (*mexS*) promote MexT-dependent *mexEF-oprN* expression and multidrug resistance in a clinical strain of *Pseudomonas aeruginosa*. J Bacteriol. 2005;187: 1246–1253.
24. Cameron DR, Shan Y, Zalis EA, Isabella V, Lewis K. A genetic determinant of persister cell formation in bacterial pathogens. J Bacteriol. 2018;200.
25. Wilson R, Sykes DA, Watson D, Rutman A, Taylor GW, Cole PJ. Measurement of *Pseudomonas aeruginosa* phenazine pigments in sputum and assessment of their contribution to sputum sol toxicity for respiratory epithelium. Infect Immun. 1988;56: 2515–2517.
26. Olaitan AO, Morand S, Rolain J-M. Mechanisms of polymyxin resistance: acquired and intrinsic resistance in bacteria. Front Microbiol. 2014;5: 643. doi:10.3389/fmicb.2014.00643
27. The European Committee on Antimicrobial Susceptibility Testing (EUCAST). Determination of minimum inhibitory concentrations (MICs) of antibacterial agents by broth dilution. Clin Microbiol Infect. 2003;9: ix–xv.
28. Kopf SH, Sessions AL, Cowley ES, Reyes C, Van Sambeek L, Hu Y, et al. Trace incorporation of heavy water reveals slow and heterogeneous pathogen growth rates in cystic fibrosis sputum. Proc Natl Acad Sci USA. 2016;113: E110-6.
29. Winstanley C, O'Brien S, Brockhurst MA. *Pseudomonas aeruginosa* evolutionary adaptation and diversification in cystic fibrosis chronic lung infections. Trends Microbiol. 2016;24: 327–337.
30. Levin-Reisman I, Brauner A, Ronin I, Balaban NQ. Epistasis between antibiotic tolerance, persistence, and resistance mutations. Proc Natl Acad Sci USA. 2019;116: 14734–14739.
31. Liu J, Gefen O, Ronin I, Bar-Meir M, Balaban NQ. Effect of tolerance on the evolution of antibiotic resistance under drug combinations. Science. 2020;367: 200–204.
32. The European Committee on Antimicrobial Susceptibility Testing (EUCAST). Breakpoint tables for interpretation of MICs and zone diameters. Version 10.0. 2020. Available: http://www.eucast.org
33. Kohanski MA, DePristo MA, Collins JJ. Sublethal antibiotic treatment leads to multidrug resistance via radical-induced mutagenesis. Mol Cell. 2010;37: 311–320.
34. Bridges BA. The fluctuation test. Arch Toxicol. 1980;46: 41–44.
35. Luria SE, Delbrück M. Mutations of bacteria from virus sensitivity to virus resistance.

Genetics. 1943;28: 491–511.
36. Palmer KL, Aye LM, Whiteley M. Nutritional cues control *Pseudomonas aeruginosa* multicellular behavior in cystic fibrosis sputum. J Bacteriol. 2007;189: 8079–8087.
37. Smith CR, Lipsky JJ, Laskin OL, Hellmann DB, Mellits ED, Longstreth J, et al. Double-blind comparison of the nephrotoxicity and auditory toxicity of gentamicin and tobramycin. N Engl J Med. 1980;302: 1106–1109.
38. Prayle A, Watson A, Fortnum H, Smyth A. Side effects of aminoglycosides on the kidney, ear and balance in cystic fibrosis. Thorax. 2010;65: 654–658.
39. Marvig RL, Sommer LM, Molin S, Johansen HK. Convergent evolution and adaptation of *Pseudomonas aeruginosa* within patients with cystic fibrosis. Nat Genet. 2015;47: 57–64.
40. Marvig RL, Dolce D, Sommer LM, Petersen B, Ciofu O, Campana S, et al. Within-host microevolution of *Pseudomonas aeruginosa* in Italian cystic fibrosis patients. BMC Microbiol. 2015;15: 218.
41. Richardot C, Juarez P, Jeannot K, Patry I, Plésiat P, Llanes C. Amino acid substitutions account for most MexS alterations in clinical *nfxC* mutants of *Pseudomonas aeruginosa*. Antimicrob Agents Chemother. 2016;60: 2302–2310.
42. Häussler S, Tümmler B, Weissbrodt H, Rohde M, Steinmetz I. Small-colony variants of *Pseudomonas aeruginosa* in cystic fibrosis. Clin Infect Dis. 1999;29: 621–625.
43. Malone JG, Jaeger T, Spangler C, Ritz D, Spang A, Arrieumerlou C, et al. YfiBNR mediates cyclic di-GMP dependent small colony variant formation and persistence in *Pseudomonas aeruginosa*. PLoS Pathog. 2010;6: e1000804.
44. Hamon A, Ycart B. Statistics for the Luria-Delbrück distribution. Electron J Stat. 2012;6: 1251–1272.
45. Lang GI, Murray AW. Estimating the per-base-pair mutation rate in the yeast *Saccharomyces cerevisiae*. Genetics. 2008;178: 67–82.
46. Frenoy A, Bonhoeffer S. Death and population dynamics affect mutation rate estimates and evolvability under stress in bacteria. PLoS Biol. 2018;16: e2005056.
47. Orlén H, Hughes D. Weak mutators can drive the evolution of fluoroquinolone resistance in *Escherichia coli*. Antimicrob Agents Chemother. 2006;50: 3454–3456.
48. Ragheb MN, Thomason MK, Hsu C, Nugent P, Gage J, Samadpour AN, et al. Inhibiting the evolution of antibiotic resistance. Mol Cell. 2019;73: 157–165.e5.
49. Baym M, Lieberman TD, Kelsic ED, Chait R, Gross R, Yelin I, et al. Spatiotemporal microbial evolution on antibiotic landscapes. Science. 2016;353: 1147–1151.
50. Toprak E, Veres A, Michel J-B, Chait R, Hartl DL, Kishony R. Evolutionary paths to antibiotic resistance under dynamically sustained drug selection. Nat Genet. 2011;44: 101–105.
51. Lipuma JJ. The changing microbial epidemiology in cystic fibrosis. Clin Microbiol Rev. 2010;23: 299–323.
52. Green SK, Schroth MN, Cho JJ, Kominos SK, Vitanza-Jack VB. Agricultural plants and soil as a reservoir for *Pseudomonas aeruginosa*. Appl Microbiol. 1974;28: 987–991.
53. Fierer N, Jackson RB. The diversity and biogeography of soil bacterial communities. Proc Natl Acad Sci USA. 2006;103: 626–631.
54. Stressmann FA, Rogers GB, van der Gast CJ, Marsh P, Vermeer LS, Carroll MP, et al. Long-term cultivation-independent microbial diversity analysis demonstrates that bacterial communities infecting the adult cystic fibrosis lung show stability and resilience. Thorax.

2012;67: 867–873.
55. Berg G, Eberl L, Hartmann A. The rhizosphere as a reservoir for opportunistic human pathogenic bacteria. Environ Microbiol. 2005;7: 1673–1685.
56. Rhodes KA, Schweizer HP. Antibiotic resistance in *Burkholderia* species. Drug Resist Updat. 2016;28: 82–90.
57. Adegoke AA, Stenström TA, Okoh AI. *Stenotrophomonas maltophilia* as an emerging ubiquitous pathogen: looking beyond contemporary antibiotic therapy. Front Microbiol. 2017;8: 2276.
58. Chmiel JF, Aksamit TR, Chotirmall SH, Dasenbrook EC, Elborn JS, LiPuma JJ, et al. Antibiotic management of lung infections in cystic fibrosis. I. The microbiome, methicillin-resistant *Staphylococcus aureus*, gram-negative bacteria, and multiple infections. Annals of the American Thoracic Society. 2014;11: 1120–1129.
59. Martina P, Feliziani S, Juan C, Bettiol M, Gatti B, Yantorno O, et al. Hypermutation in *Burkholderia cepacia* complex is mediated by DNA mismatch repair inactivation and is highly prevalent in cystic fibrosis chronic respiratory infection. Int J Med Microbiol. 2014;304: 1182–1191.
60. Lee H, Popodi E, Tang H, Foster PL. Rate and molecular spectrum of spontaneous mutations in the bacterium *Escherichia coli* as determined by whole-genome sequencing. Proc Natl Acad Sci USA. 2012;109: E2774-83.
61. Nunvar J, Capek V, Fiser K, Fila L, Drevinek P. What matters in chronic *Burkholderia cenocepacia* infection in cystic fibrosis: Insights from comparative genomics. PLoS Pathog. 2017;13: e1006762.
62. Hobbs JK, Boraston AB. (p)ppGpp and the stringent response: an emerging threat to antibiotic therapy. ACS Infect Dis. 2019;5: 1505–1517.
63. Pope CF, Gillespie SH, Pratten JR, McHugh TD. Fluoroquinolone-resistant mutants of *Burkholderia cepacia*. Antimicrob Agents Chemother. 2008;52: 1201–1203.
64. Granato ET, Meiller-Legrand TA, Foster KR. The evolution and ecology of bacterial warfare. Curr Biol. 2019;29: R521–R537.
65. Cruickshank CN, Lowbury EJ. The effect of pyocyanin on human skin cells and leucocytes. Br J Exp Pathol. 1953;34: 583–587.
66. Walters MC, Roe F, Bugnicourt A, Franklin MJ, Stewart PS. Contributions of antibiotic penetration, oxygen limitation, and low metabolic activity to tolerance of *Pseudomonas aeruginosa* biofilms to ciprofloxacin and tobramycin. Antimicrob Agents Chemother. 2003;47: 317–323.
67. Olsen I. Biofilm-specific antibiotic tolerance and resistance. Eur J Clin Microbiol Infect Dis. 2015;34: 877–886.
68. Costerton JW, Stewart PS, Greenberg EP. Bacterial biofilms: a common cause of persistent infections. Science. 1999;284: 1318–1322.
69. Dietrich LEP, Okegbe C, Price-Whelan A, Sakhtah H, Hunter RC, Newman DK. Bacterial community morphogenesis is intimately linked to the intracellular redox state. J Bacteriol. 2013;195: 1371–1380.
70. Alexander HK, MacLean RC. Stochastic bacterial population dynamics restrict the establishment of antibiotic resistance from single cells. Proc Natl Acad Sci USA. 2020;117: 19455–19464.
71. Papkou A, Hedge J, Kapel N, Young B, MacLean RC. Efflux pump activity potentiates the

evolution of antibiotic resistance across *S. aureus* isolates. Nat Commun. 2020;11: 3970.
72. Oethinger M, Kern WV, Jellen-Ritter AS, McMurry LM, Levy SB. Ineffectiveness of topoisomerase mutations in mediating clinically significant fluoroquinolone resistance in *Escherichia coli* in the absence of the AcrAB efflux pump. Antimicrob Agents Chemother. 2000;44: 10–13.
73. Bruchmann S, Dötsch A, Nouri B, Chaberny IF, Häussler S. Quantitative contributions of target alteration and decreased drug accumulation to *Pseudomonas aeruginosa* fluoroquinolone resistance. Antimicrob Agents Chemother. 2013;57: 1361–1368.
74. LiPuma JJ, Spilker T, Coenye T, Gonzalez CF. An epidemic *Burkholderia cepacia* complex strain identified in soil. Lancet. 2002;359: 2002–2003.
75. Depoorter E, Bull MJ, Peeters C, Coenye T, Vandamme P, Mahenthiralingam E. *Burkholderia*: an update on taxonomy and biotechnological potential as antibiotic producers. Appl Microbiol Biotechnol. 2016;100: 5215–5229.
76. Brochado AR, Telzerow A, Bobonis J, Banzhaf M, Mateus A, Selkrig J, et al. Species-specific activity of antibacterial drug combinations. Nature. 2018;559: 259–263.
77. Imamovic L, Ellabaan MMH, Dantas Machado AM, Citterio L, Wulff T, Molin S, et al. Drug-driven phenotypic convergence supports rational treatment strategies of chronic infections. Cell. 2018;172: 121–134.e14.
78. Lee HH, Molla MN, Cantor CR, Collins JJ. Bacterial charity work leads to population-wide resistance. Nature. 2010;467: 82–85.
79. Kumar A, Sperandio V. Indole signaling at the host-microbiota-pathogen interface. MBio. 2019;10.
80. Garbe TR, Kobayashi M, Yukawa H. Indole-inducible proteins in bacteria suggest membrane and oxidant toxicity. Arch Microbiol. 2000;173: 78–82.
81. Widdel F, Pfennig N. Studies on dissimilatory sulfate-reducing bacteria that decompose fatty acids. Arch Microbiol. 1981;129: 395–400.
82. Turner KH, Wessel AK, Palmer GC, Murray JL, Whiteley M. Essential genome of *Pseudomonas aeruginosa* in cystic fibrosis sputum. Proc Natl Acad Sci USA. 2015;112: 4110–4115.
83. Cheluvappa R. Standardized chemical synthesis of *Pseudomonas aeruginosa* pyocyanin. MethodsX. 2014;1: 67–73.
84. Costa KC, Glasser NR, Conway SJ, Newman DK. Pyocyanin degradation by a tautomerizing demethylase inhibits *Pseudomonas aeruginosa* biofilms. Science. 2017;355: 170–173.
85. Babin BM, Bergkessel M, Sweredoski MJ, Moradian A, Hess S, Newman DK, et al. SutA is a bacterial transcription factor expressed during slow growth in *Pseudomonas aeruginosa*. Proc Natl Acad Sci USA. 2016;113: E597-605.
86. Shanks RMQ, Caiazza NC, Hinsa SM, Toutain CM, O'Toole GA. *Saccharomyces cerevisiae*-based molecular tool kit for manipulation of genes from gram-negative bacteria. Appl Environ Microbiol. 2006;72: 5027–5036.
87. Gibson DG, Young L, Chuang R-Y, Venter JC, Hutchison CA, Smith HO. Enzymatic assembly of DNA molecules up to several hundred kilobases. Nat Methods. 2009;6: 343–345.
88. Choi K-H, Schweizer HP. mini-Tn7 insertion in bacteria with single *att*Tn7 sites: example *Pseudomonas aeruginosa*. Nat Protoc. 2006;1: 153–161.

89. Basta DW, Bergkessel M, Newman DK. Identification of fitness determinants during energy-limited growth arrest in *Pseudomonas aeruginosa*. MBio. 2017;8: e01170-17.
90. van Opijnen T, Lazinski DW, Camilli A. Genome-wide fitness and genetic interactions determined by Tn-seq, a high-throughput massively parallel sequencing method for microorganisms. Curr Protoc Mol Biol. 2014;106: 7.16.1-24.
91. Langmead B, Salzberg SL. Fast gapped-read alignment with Bowtie 2. Nat Methods. 2012;9: 357–359.
92. Pritchard JR, Chao MC, Abel S, Davis BM, Baranowski C, Zhang YJ, et al. ARTIST: high-resolution genome-wide assessment of fitness using transposon-insertion sequencing. PLoS Genet. 2014;10: e1004782.
93. Wickham H. ggplot2 - Elegant Graphics for Data Analysis. New York, NY: Springer-Verlag New York; 2016.
94. R Core Team. R: A language and Environment for Statistical Computing 2018. Vienna: R Foundation for Statistical Computing. Available at: https://www.R-project.org/.
95. Winsor GL, Griffiths EJ, Lo R, Dhillon BK, Shay JA, Brinkman FSL. Enhanced annotations and features for comparing thousands of *Pseudomonas* genomes in the *Pseudomonas* genome database. Nucleic Acids Res. 2016;44: D646-53.
96. Schindelin J, Arganda-Carreras I, Frise E, Kaynig V, Longair M, Pietzsch T, et al. Fiji: an open-source platform for biological-image analysis. Nat Methods. 2012;9: 676–682.
97. Reszka KJ, O'Malley Y, McCormick ML, Denning GM, Britigan BE. Oxidation of pyocyanin, a cytotoxic product from *Pseudomonas aeruginosa*, by microperoxidase 11 and hydrogen peroxide. Free Radic Biol Med. 2004;36: 1448–1459.
98. Rosche WA, Foster PL. Determining mutation rates in bacterial populations. Methods. 2000;20: 4–17.
99. Zheng Q. rSalvador: An R package for the fluctuation experiment. G3 (Bethesda). 2017;7: 3849–3856.
100. Zheng Q. A new practical guide to the Luria-Delbrück protocol. Mutat Res. 2015;781: 7–13.
101. Boe L, Tolker-Nielsen T, Eegholm KM, Spliid H, Vrang A. Fluctuation analysis of mutations to nalidixic acid resistance in *Escherichia coli.* J Bacteriol. 1994;176: 2781–2787.
102. Gillet-Markowska A, Louvel G, Fischer G. bz-rates: A web tool to estimate mutation rates from fluctuation analysis. G3 (Bethesda). 2015;5: 2323–2327.
103. Bolger AM, Lohse M, Usadel B. Trimmomatic: a flexible trimmer for Illumina sequence data. Bioinformatics. 2014;30: 2114–2120.
104. Deatherage DE, Barrick JE. Identification of mutations in laboratory-evolved microbes from next-generation sequencing data using breseq. Methods Mol Biol. 2014;1151: 165–188.
105. Bankevich A, Nurk S, Antipov D, Gurevich AA, Dvorkin M, Kulikov AS, et al. SPAdes: a new genome assembly algorithm and its applications to single-cell sequencing. J Comput Biol. 2012;19: 455–477.
106. Vallenet D, Calteau A, Dubois M, Amours P, Bazin A, Beuvin M, et al. MicroScope: an integrated platform for the annotation and exploration of microbial gene functions through genomic, pangenomic and metabolic comparative analysis. Nucleic Acids Res. 2020;48: D579–D589.

Supporting information

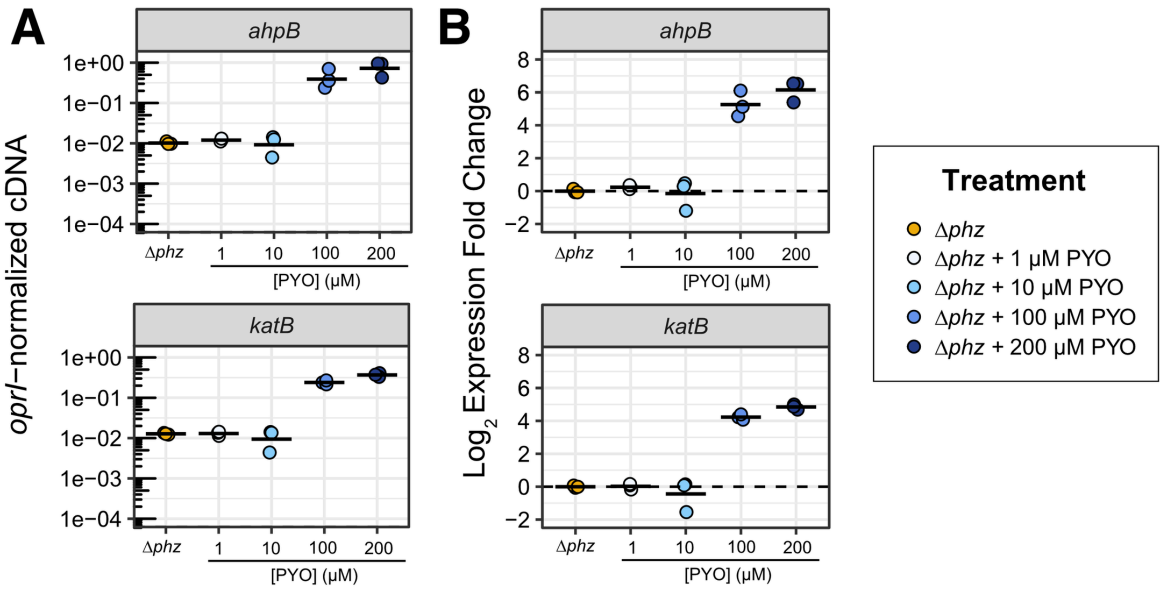

S1 Figure. Effects of different concentrations of PYO on the expression of the *P. aeruginosa* oxidative stress response genes *ahpB* and *katB*. A. Normalized cDNA levels measured by qRT-PCR. cDNA measurements were normalized by levels of the housekeeping gene *oprI* (see Methods). **B.** Fold change in expression upon PYO treatment, relative to the measurements in untreated Δ*phz*. *ahpB*: alkyl hydroperoxide reductase B; *katB*: catalase B. Black horizontal lines mark the mean value for independent biological cultures (n = 3).

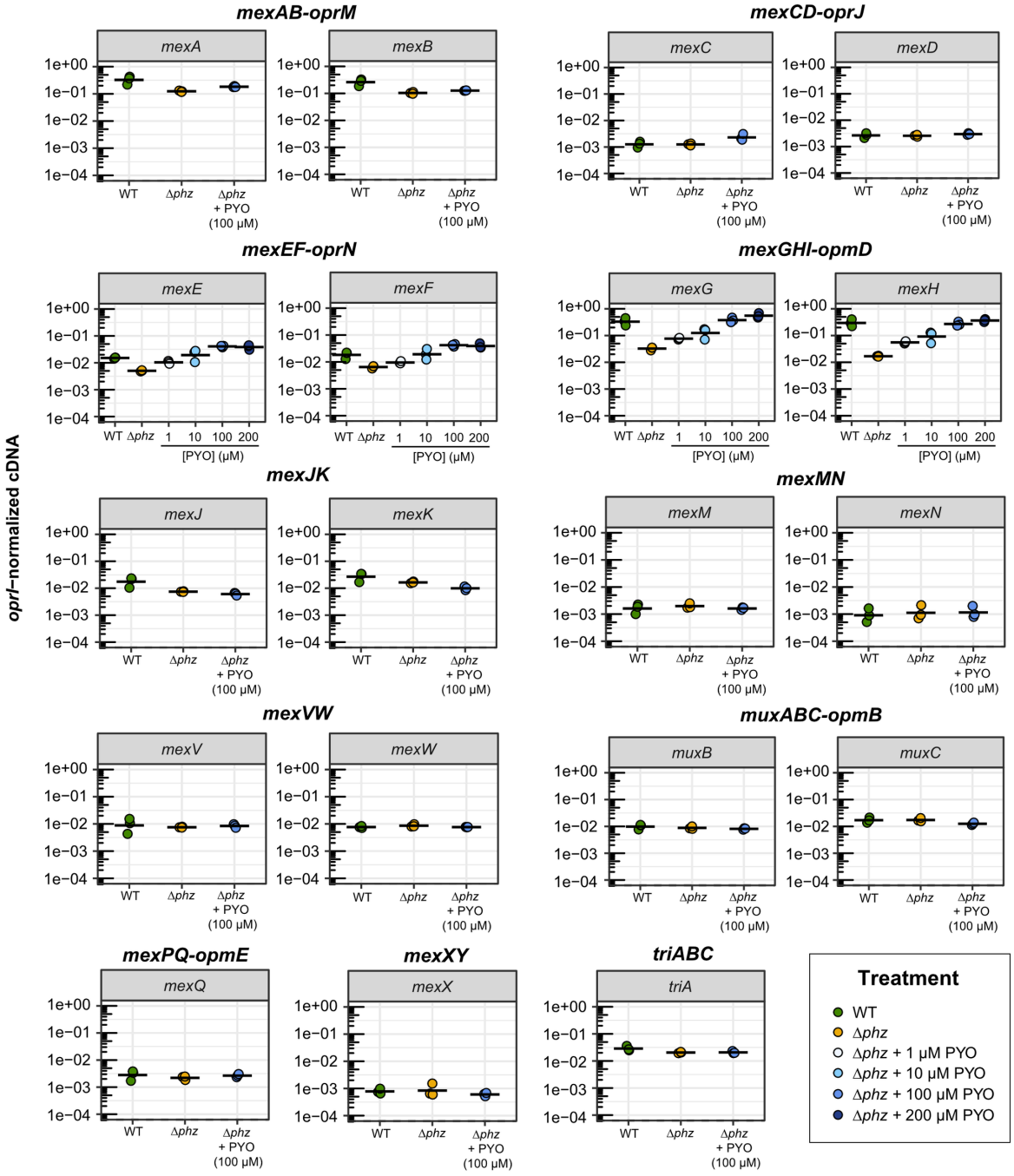

S2 Figure. Effects of PYO on the expression of *P. aeruginosa* RND efflux systems (normalized cDNA levels). The normalized cDNA levels for genes within operons coding for the 11 main RND efflux systems in *P. aeruginosa* are shown. cDNA levels for each gene were measured by qRT-PCR during early stationary phase and normalized by the levels of the housekeeping gene *oprI* (see Methods). This dataset was used to make the heatmap presented in Fig 2B. Black horizontal lines mark the mean value for independent biological cultures (n = 3).

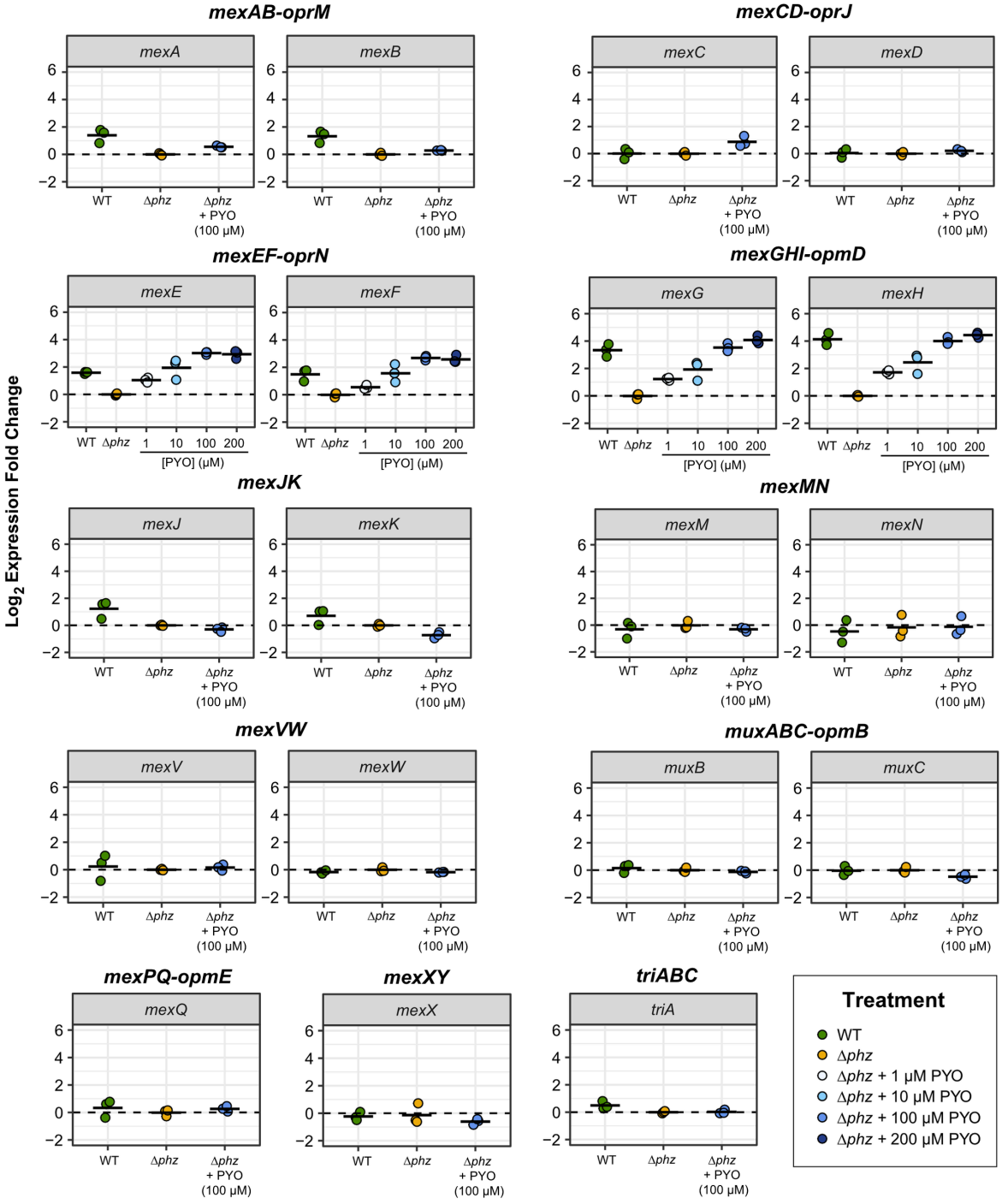

S3 Figure. Effects of PYO on the expression of *P. aeruginosa* RND efflux systems (fold change). The PYO-induced changes in expression for genes within operons coding for the 11 main RND efflux systems in *P. aeruginosa* are shown. These plots are derived from the normalized cDNA dataset shown in S2 Fig. Here, the values for Δ*phz* were used as the basis for calculation of changes of expression (shown as $\log_2$ fold change). Black horizontal lines mark the mean value for independent biological cultures (n = 3).

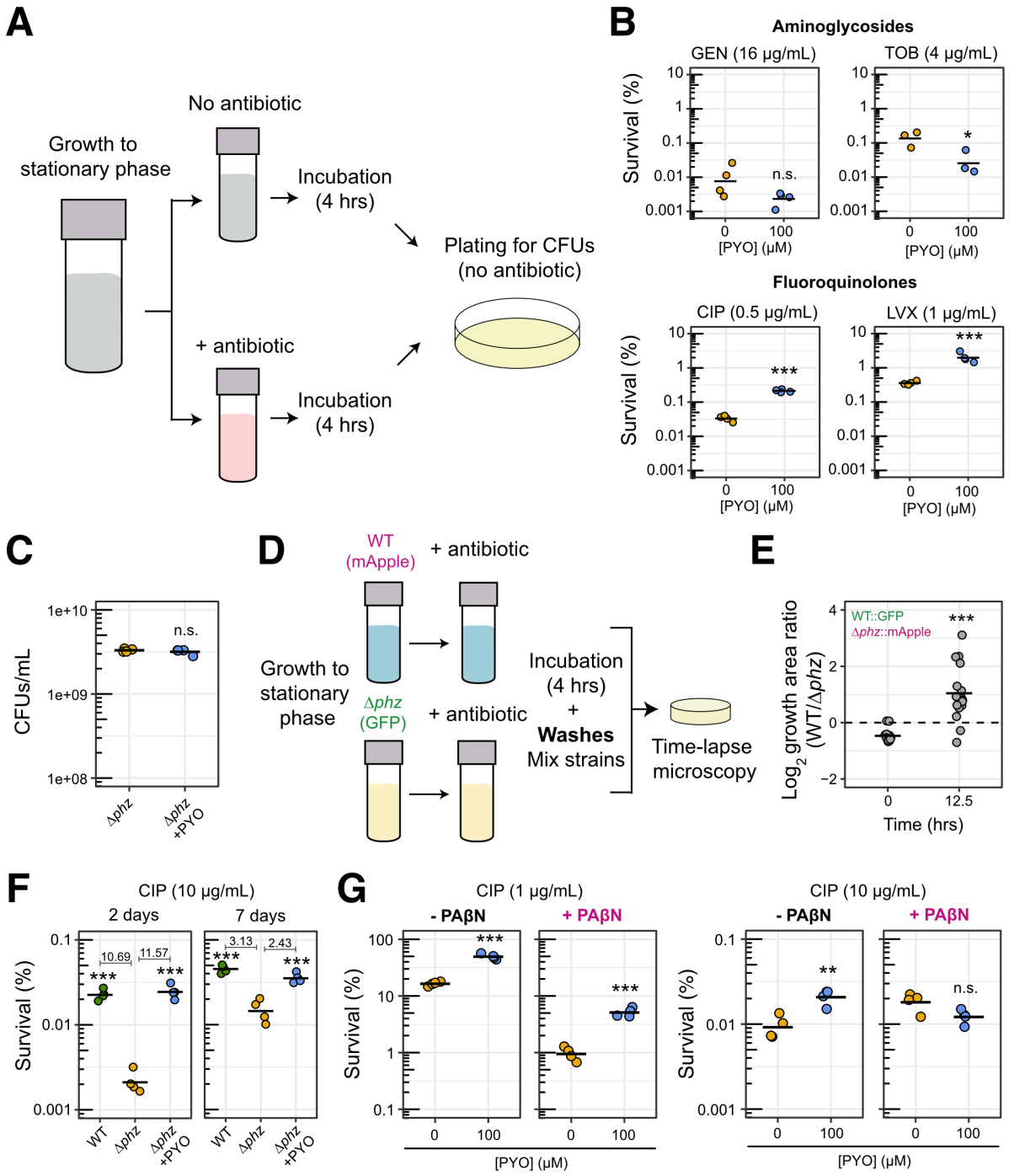

S4 Figure. Effects of PYO on *P. aeruginosa* tolerance to different antibiotics. A. Experimental design for survival assay to measure tolerance to clinical antibiotics. In conditions with exogenous PYO, the PYO was added when cultures were inoculated. PYO itself was not lethal under these experimental conditions (see panel C in this Fig). **B.** Tolerance levels of Δ*phz* cells harvested in log phase, following growth in the presence or absence of PYO (100 µM), to different aminoglycosides and fluoroquinolones (GEN = gentamicin, TOB = tobramycin, CIP = ciprofloxacin, and LVX = levofloxacin). Data points represent replicates (n = 4 for all except tobramycin, for which n = 3). Stationary phase tolerance experiments are not shown for the aminoglycosides (gentamicin and tobramycin), as treatment with

tobramycin in stationary phase under our conditions at this clinically-relevant concentration [32] did not result in cell death, regardless of the presence of PYO. However, for experiments performed with stationary phase cells in SCFM, killing did happen (see Fig 2D). **C.** Representative data showing CFUs counted for Δ*phz* grown for 20 hrs (glucose minimal medium, see Methods) in the presence and absence of PYO in our tolerance assays, showing that PYO itself was not toxic under the studied conditions (n = 4). These are the CFUs for the negative control (no antibiotic) for the experiment performed with CIP in Fig 2C. **D.** Experimental design for time-lapse microscopy experiments, in which cells were grown on agarose pads after exposure to CIP (10 μg/mL). The strain/fluorescent protein examples shown (i.e. WT::mApple, Δ*phz*::GFP) are the ones used in the images of Fig 2F and S1 Movie. **E.** Quantification of microscopy data as done in Fig 2G, but for the experiment with swapped fluorescent proteins. **F.** Experiment quantifying how PYO affects lag for CFUs appearing after treatment with CIP (10 μg/mL, see Methods). Treating *P. aeruginosa* cells with 10 μg/mL resulted in high killing levels (see panel G), and we observed an increased lag in the absence of PYO (this supports microscopy data presented in Figs 2F-G and S4E Fig). The survival levels were calculated for CFUs counted after two days (too early, since more CFUs appeared later, changing the calculated survival levels) and seven days (no CFUs appeared after this time point; correct survival rate) of the LB plates incubation. Few new CFUs arose for WT and Δ*phz*+PYO treatments after two days, while several appeared for Δ*phz*. Numbers represent the mean survival ratio of WT/Δ*phz* and Δ*phz*+PYO/Δ*phz*. For survival calculated after two days, PYO's presence gave the impression of a ~10-fold higher survival rate. However, this was mostly due to lag of Δ*phz*, and the real survival difference was around ~2-3-fold (calculated after seven days) (n = 4). **G.** Effects of the efflux inhibitor PAβN on tolerance levels to CIP of Δ*phz* cells grown in the presence or absence of PYO (100 μM). Cultures were treated with low (left) and high (right) CIP concentrations. Experiments for all the conditions were done in parallel (see Methods for full protocol) (n = 4). Statistics: B, C, E, G – Welch's unpaired t-tests. F – One-way ANOVA with Tukey's HSD multiple-comparison test, with asterisks showing the statistical significance of comparisons with the Δ*phz* (no PYO) (* $p < 0.05$, ** $p < 0.01$, *** $p < 0.001$, n.s. $p > 0.05$). Black horizontal lines mark the mean value for independent cultures (or fields of view, for E).

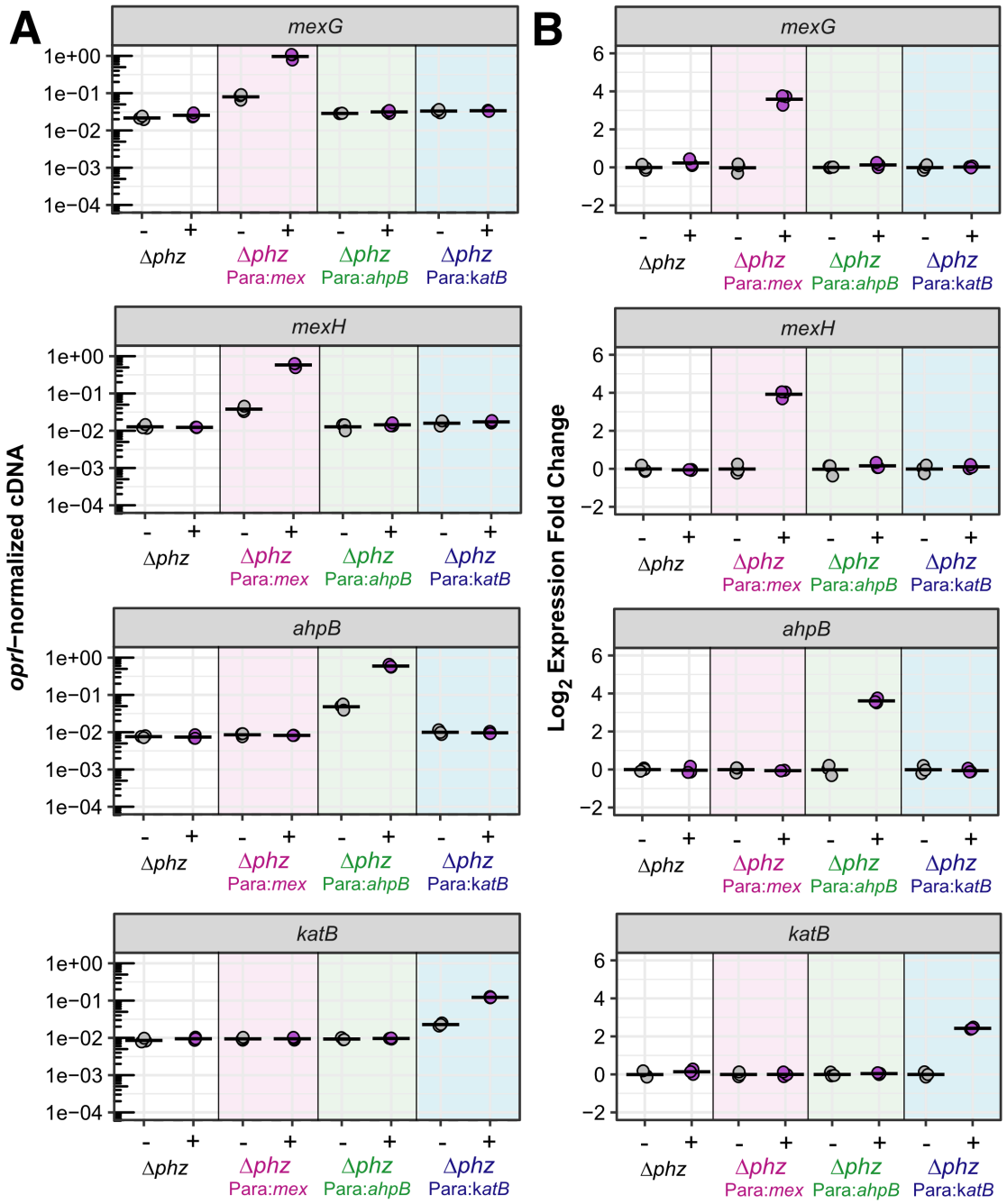

S5 Figure. Artificial induction of *mexGHI-opmD*, *ahpB* and *katB*. A. Normalized cDNA levels measured by qRT-PCR. cDNA levels were normalized by the housekeeping gene *oprI*. **B.** Fold change in expression upon arabinose induction. This dataset can be compared to the PYO-mediated induction of the same genes as shown in Figs. 2B, and S1, S2 and S3 Figs. The four strains shown are: 1) the parent Δ*phz* (white background), 2) Δ*phz* P_{ara}:*mexGHI-opmD* (magenta background), 3) Δ*phz* P_{ara}:*ahpB* (green background) and 4) Δ*phz* P_{ara}:*katB* (blue background). +/- represent addition or not of 20 mM arabinose to the cultures for the artificial induction of expression. For additional experimental details and strain information, see Methods and S5 Table. Black horizontal lines mark the mean value for independent biological cultures (n = 3).

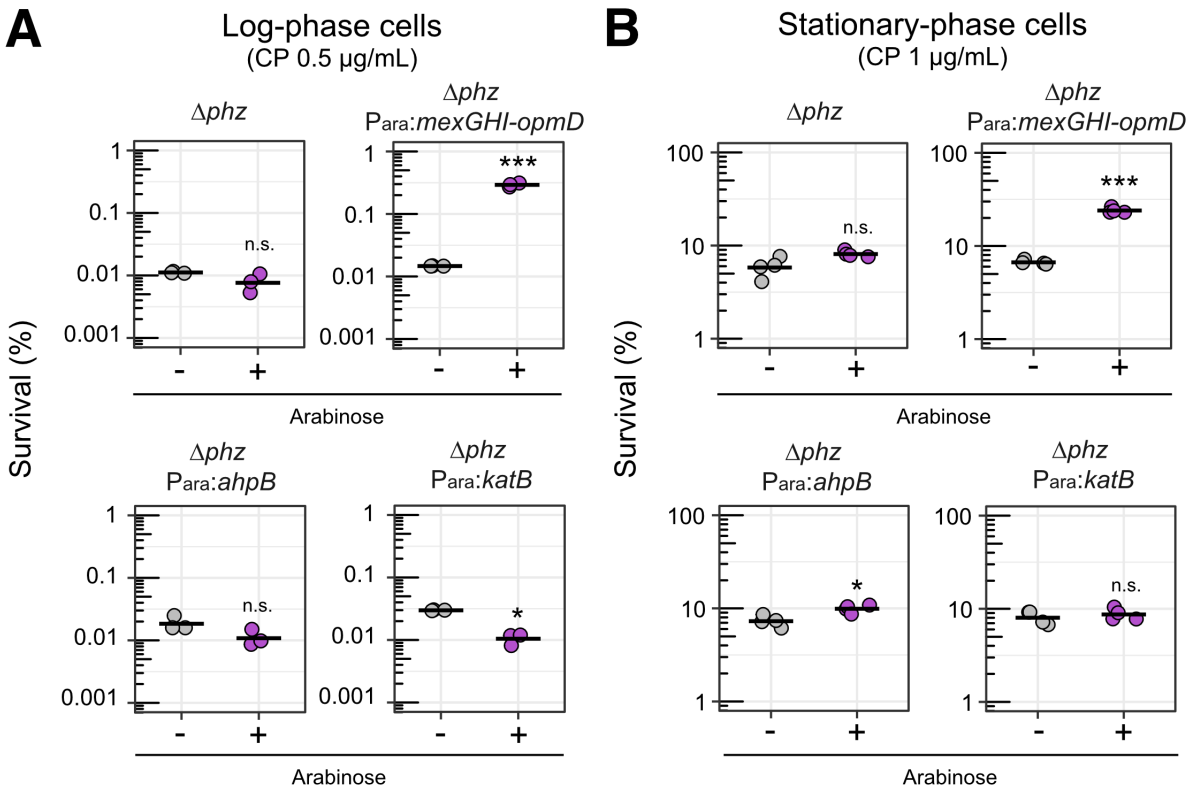

S6 Figure. Effect of artificial induction of PYO-induced genes on tolerance to ciprofloxacin. Survival relative to the no-antibiotic control is shown for the parent Δ*phz* strain and the three arabinose-inducible strains (in which the PYO-inducible genes *mexGHI-opmD, ahpB,* or *katB* are under control of an arabinose-inducible promoter) grown in the presence or absence of 20 mM arabinose, without exposure to PYO. The tolerance experiments were performed for cultures in both log phase (A, n = 3) and stationary phase (B, n = 4). In B, the experiment for *mexGHI-opmD* is the same as in Fig 2I, but is also shown here for ease of comparison. Statistics: Welch's unpaired t-tests (* $p < 0.05$, ** $p < 0.01$, *** $p < 0.001$, n.s. $p > 0.05$). Black horizontal lines mark the mean value for independent cultures.

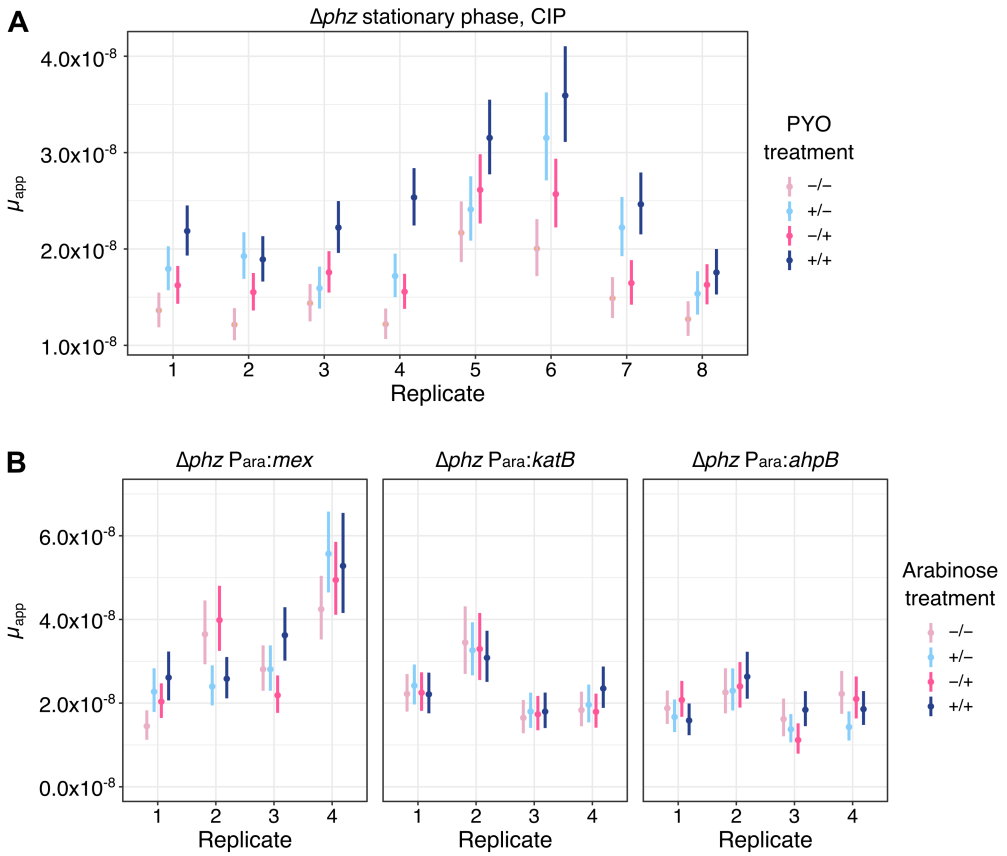

S7 Figure. Effect of PYO or PYO-induced genes on apparent mutation rates in *P. aeruginosa*. A. Apparent mutation rates of stationary-phase Δ*phz* grown in liquid minimal medium and plated onto MH agar containing ciprofloxacin (CIP, 0.5 μg/mL), with or without pre- and/or co-exposure to 100 μM PYO relative to the antibiotic selection step (n = 8). **B.** Apparent mutation rates of log-phase cells grown in glucose minimal medium and plated onto MH agar containing CIP (0.5 μg/mL), with or without pre- and/or co-exposure to 20 mM arabinose relative to the antibiotic selection step. Data are shown for Δ*phz* P_{ara}:*mexGHI-opmD* (B, left, n = 4), Δ*phz* P_{ara}:*katB* (B, center, n = 4), and Δ*phz* P_{ara}:*ahpB* (B, right, n = 4). In all panels, each data point represents 44 parallel cultures from a single biological replicate, and the vertical lines represent 84% confidence intervals, for which lack of overlap corresponds to statistical significance at the $p < 0.05$ level [99]. The PYO treatments correspond to the following: -/- denotes no PYO pre-treatment (in the liquid culture stage) or co-treatment (in the antibiotic agar plates), +/- denotes PYO pre-treatment but no co-treatment, -/+ denotes PYO co-treatment without pre-treatment, and +/+ denotes both PYO pre-treatment and co-treatment.

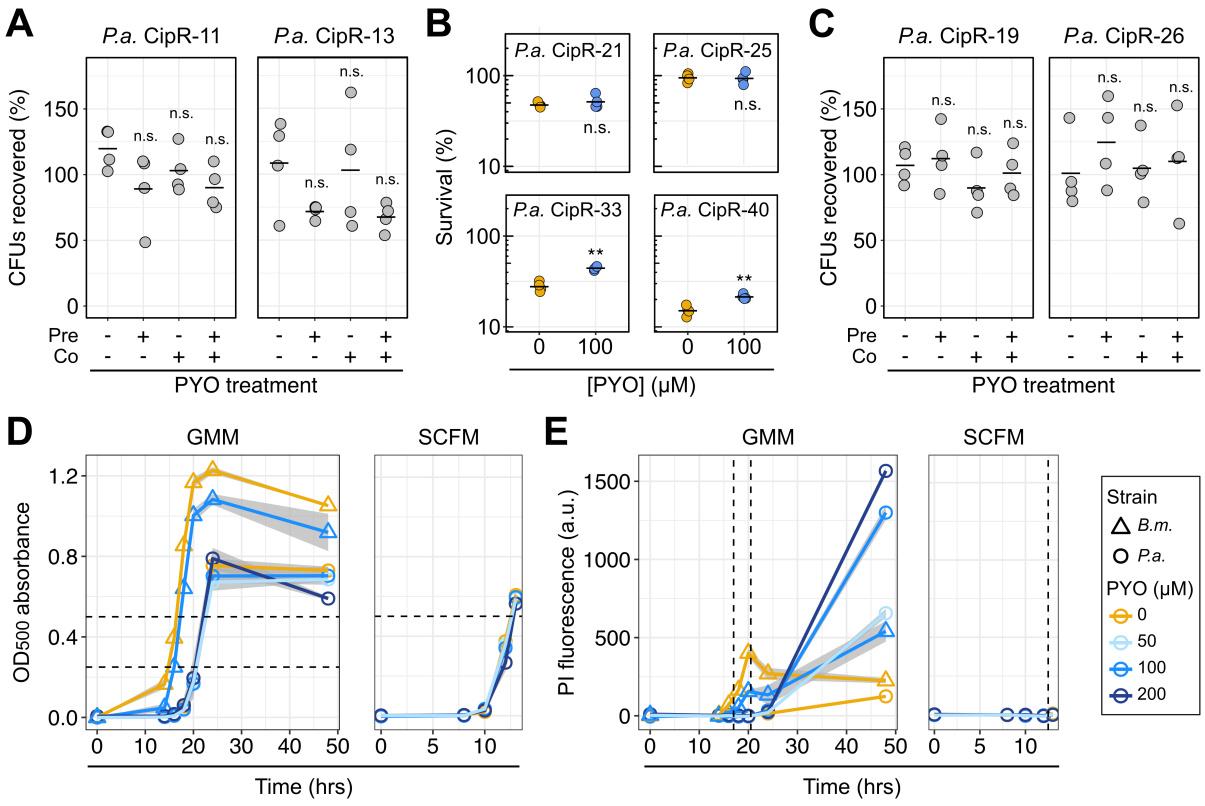

S8 Figure. Effect of PYO on resistance phenotypes and antibiotic tolerance of *P. aeruginosa* mutants. A. The percentage of CFUs recovered on CIP (0.5 μg/mL) either with or without 100 μM PYO in the agar, for log-phase cultures of representative resistant mutants of *P. aeruginosa* (*P.a.*) that were not enriched by exposure to PYO in the fluctuation tests. The mutants were pre-grown with or without 100 μM PYO in glucose minimal medium before plating. On the x-axis, "pre" denotes the presence of PYO in the liquid cultures and "co" denotes the presence of PYO in the agar plates. Percentage recovery was calculated relative to total CFUs counted on non-selective plates (n = 4). **B.** Tolerance to CIP (1 μg/mL) of partially-resistant mutants grown in glucose minimal medium to stationary phase with or without 100 μM PYO (n = 4). Experiments were performed as shown in S5A Fig. **C.** The percentage of CFUs recovered on CIP (0.5 μg/mL) for log-phase cultures of representative resistant mutants that were enriched by exposure to PYO in the fluctuation tests (n = 4). Experiments were performed in the same way as in panel A. **D-E.** Growth curves performed for *P. aeruginosa* Δ*phz* (*P.a.*) and *B. multivorans 1* (*B.m.*) in glucose minimal medium (with the addition of amino acids for *B. multivorans*; see Methods) or SCFM, with different concentrations of PYO in the presence of 5 μM propidium iodide (PI), which is a fluorescent marker for cell death. OD_{500} (cell density) is plotted in G, while PI fluorescence is plotted in H. Gray shaded regions represent the standard deviation of four biological replicates. In G, the dashed horizontal lines mark the cell density at which *P. aeruginosa* (lower line in left panel) or *B. multivorans* (upper line in left panel) would have been plated in our fluctuation tests. Note that these OD_{500} values differ from those reported in the Methods section for fluctuation tests due to the use of a microtiter plate reader in this experiment, whereas a different spectrophotometer was used in the fluctuation tests. In H, the vertical dashed lines mark the time at which the cultures would have been plated in the fluctuation tests (in the left panel, left line = *B.m.* sampling time, right line = *P.a.* sampling time). The increase in fluorescence seen for *B. multivorans* prior to stationary phase likely reflects the production of a fluorescent metabolite rather than early cell death, as fluorescence was initially higher for the cultures not treated with PYO and the exponential phase growth rates were identical regardless of PYO treatment. Statistics: A-C – Welch's unpaired t-tests (* $p < 0.05$, ** $p < 0.01$, *** $p < 0.001$, n.s. $p > 0.05$). Unless indicated otherwise with brackets, statistical significance is shown for the comparison with the untreated (no PYO) condition. In A-C, data points represent independent biological cultures, with horizontal black lines marking the mean value for each condition.

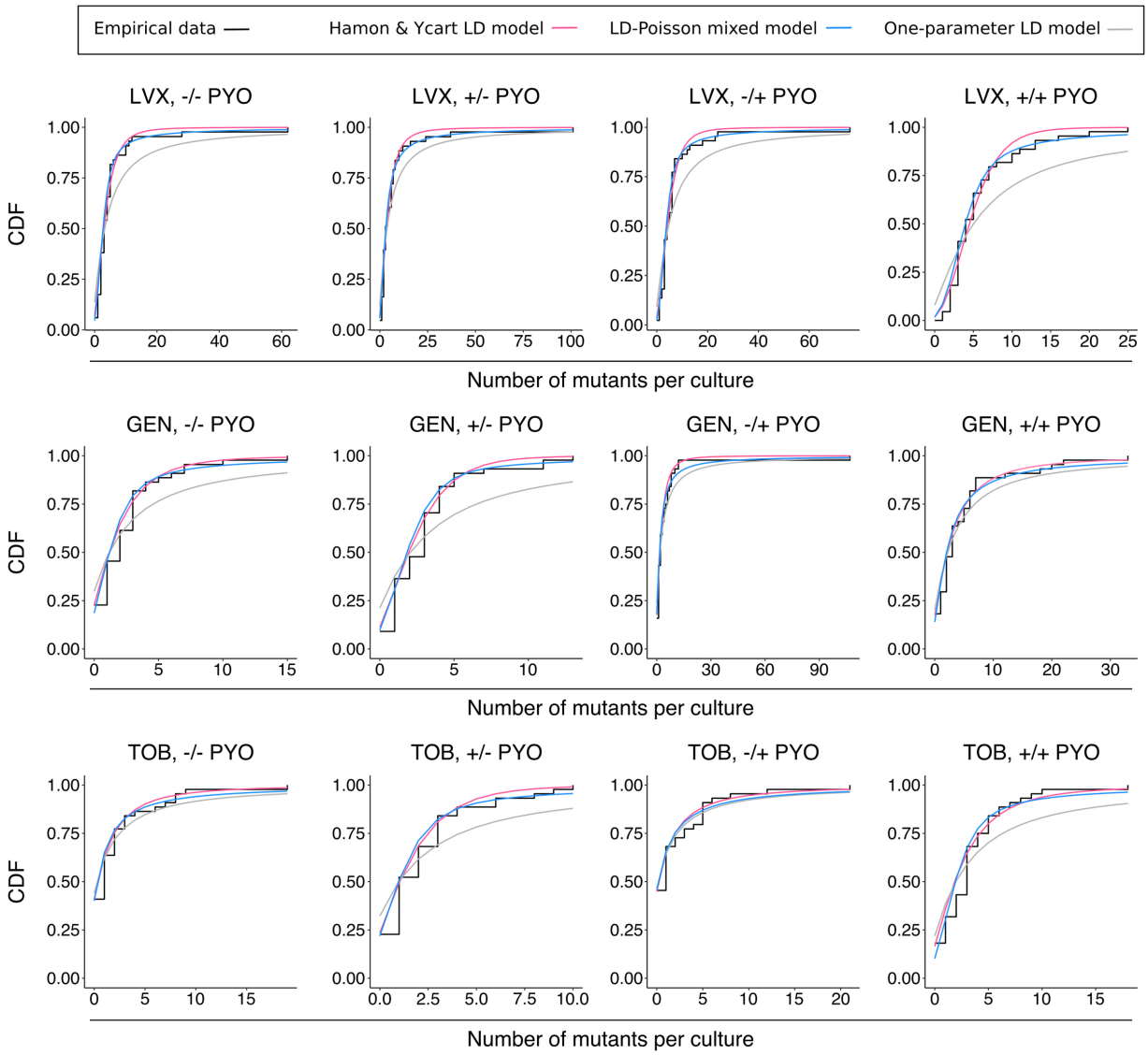

S9 Figure. Goodness-of-fit of different mathematical models for *P. aeruginosa* Δ*phz* fluctuation test data. Data are plotted for different combinations of PYO in liquid (pre-treatment) and PYO in agar (co-exposure to antibiotic selection). LVX = levofloxacin, GEN = gentamicin, and TOB = tobramycin. The empirical cumulative distribution functions of the data (black) are plotted against 1) a variation of the Luria-Delbrück model fit with two parameters, *m* (the expected number of mutations per culture) and *w* (the relative fitness of mutant cells vs. WT), as implemented by Hamon & Ycart [44] (pink); 2) a mixed Luria-Delbrück and Poisson distribution fit with two parameters, *m* and *d* (the number of generations that occur post-plating), allowing for the possibility of post-plating mutations, as implemented by Lang *et al.* [45] (blue); 3) the basic Luria-Delbrück distribution model fit only with *m*, as implemented by Lang *et al*. [45] (gray). In each condition, the plotted data represent the biological replicate with the lowest chi-square goodness-of-fit *p*-value (i.e. least-good fit) for the Hamon & Ycart model.

S1 Table. Read ratios for each gene (PA14 genome) in the PYO tolerance Tn-seq experiment. Analysis was done using ARTIST software (see Methods). Ratios = reads + PYO conditions / reads no PYO condition (log2-transformed), where high ratio values = increased fitness, and low ratio values = decreased fitness. Ciprofloxacin Tn-seq values are from: Cameron *et al*. [24] (see Methods). NA = not applicable. NR = not reported, meaning that there were no reads from the gene/locus within the replicate (or in at least one of the replicates, when displayed in the "average log2-tranformed ratio" column).

S2 Table. Statistical significance of comparisons of mutation rates and mutant frequencies. Mutation rates reported in this table were calculated using the rSalvador function newton.LD.plating and were compared using the LRT.LD.plating function to determine statistical significance. Mutant frequencies were compared using the Mann-Whitney U test. Reported *p*-values were adjusted with the Benjamini-Hochberg correction to control the false discovery rate.

S3 Table. Fluctuation test analysis results for all log-phase experiments conducted in minimal medium. Model parameters: μ = apparent mutation rate per generation; m = expected number of mutational events per cultures; w = fitness ratio of mutants/WT; d = number of post-plating generations. Abbreviations: HY = Hamon & Ycart; LD = Luria-Delbrück; score = negative log likelihood; LRT = likelihood ratio test; CIP = ciprofloxacin; LVX = levofloxacin; GEN = gentamicin; TOB = tobramycin. See Methods for details on the different mathematical models.

S4 Table. Mutations detected in ciprofloxacin-resistant isolates of *Pseudomonas aeruginosa* PA14. Mutations were detected using breseq, with the reference set as the *P. aeruginosa* UCBPP-PA14 genome obtained from BioProject accession number PRJNA38507. Pseudogenes and synonymous substitution mutations were omitted from the table.

S5 Table. Strains, plasmids, and primers used in this study. This table contains a list of the strains, plasmids, and primers used in this study.

S6 Table. Mutations detected in partially ciprofloxacin-resistant isolates of *Burkholderia multivorans* AU42096. Mutations were detected using breseq, with a draft assembly of the genome for *B. multivorans* AU42096 as the reference. Only mutations unique to each isolate are included.

S7 Table. Ciprofloxacin MICs for fluctuation test isolates and parent strains. MICs were determined in a microbroth dilution assay according to standard clinical methods (see Methods). Where a range of values is presented, this indicates that the observed MIC sometimes varied depending on the initial cell density of the inoculum, even within the clinically-acceptable range of 3-7 x 10^5 CFUs/mL.

Note about tables: Due to their size/format, supplementary tables mentioned in this chapter were not included in this document. These tables are linked to this thesis and available through CaltechTHESIS.

Chapter 5

THE CONSEQUENCES OF BEING IN A COMMUNITY: Redox-active metabolites as interspecies modulators of antibiotic resilience

This chapter has been posted on *bioRxiv* and has been submitted for peer review as:

Meirelles, L.A., and Newman, D.K. (2021) Redox-active secondary metabolites act as interspecies modulators of antibiotic resilience. *bioRxiv*.
https://doi.org/10.1101/2021.12.01.470848

Abstract

Bacterial opportunistic pathogens make a wide range of secondary metabolites both in the natural environment and when causing infections, yet how these molecules mediate microbial interactions and their consequences for antibiotic treatment are still poorly understood. Here, we explore the role of two redox-active secondary metabolites, pyocyanin and toxoflavin, as interspecies modulators of antibiotic resilience. We find that these molecules dramatically change susceptibility levels of diverse bacteria to clinical antibiotics. Pyocyanin is made by *Pseudomonas aeruginosa*, while toxoflavin is made by *Burkholderia gladioli*, organisms that infect cystic fibrosis and other immunocompromised patients. Both molecules alter the susceptibility profile of pathogenic species within the "*Burkholderia cepacia* complex" to different antibiotics, either antagonizing or potentiating their effects, depending on the drug's class. Defense responses regulated by the redox-sensitive transcription factor SoxR potentiate the antagonistic effects these metabolites have against fluoroquinolones, and the presence of genes encoding SoxR and the efflux systems it regulates can be used to predict how these metabolites will affect antibiotic susceptibility of different bacteria. Finally, we demonstrate that inclusion of secondary metabolites in standard protocols used to assess antibiotic resistance can dramatically alter the results, motivating the development of new tests for more accurate clinical assessment.

Introduction

The use of antibiotics revolutionized medicine in the 20th century, but the evasion of antibiotic treatment by pathogens is a pressing health concern in the 21st century [1–3]. Without new approaches, it is estimated that by 2050 our ability to treat infections with antibiotics will dramatically decrease, resulting in up to 10 million deaths per year [4]. Bacteria can withstand antibiotic treatment in many ways, including by acquiring resistance mutations and/or by developing physiological tolerance, which together enable antibiotic resilience [5–8]. Following recent terminology guidelines [9–11], we define (i) ***antibiotic resistance*** as "the ability to grow in the presence of an antibiotic at a given concentration"; (ii) ***antibiotic tolerance*** as "the ability to survive transient antibiotic exposure"; and (iii) ***antibiotic resilience*** as "the ability of a bacterial population to be refractory to antibiotic treatment" [12]. When physicians face situations where treatments do not work in the clinic, this is typically caused due to increased tolerance and/or resistance levels [7].

One important and underappreciated factor that promotes both resistance and tolerance is the production of secondary metabolites [12]. These are a broad category of molecules generally produced under slow-growth conditions (i.e., "stationary phase" in the laboratory batch cultures) that are secreted extracellularly or kept inside the cell [13,14]. When secreted, secondary metabolites have the potential to affect their surroundings, including other microbes [13,15]. Even though it is well known that microbes can influence each other through secondary metabolite production [15], only recently has this concept been considered in the context of antibiotic susceptibility [12,16,17]. Secondary metabolites typically affect antibiotic susceptibility by (i) inducing efflux systems or (ii) modulating redox homeostasis or oxidative stress responses [12,17]. It stands to reason that they might significantly affect our ability to treat polymicrobial infections.

Certain secondary metabolites are redox-active molecules that promote multifaceted benefits for their producers, from acquiring nutrients to controlling redox homeostasis and promoting anaerobic survival [14,18,19]. Because they readily react with oxygen (leading to reactive oxygen species generation) and with Fe-S clusters inside the cells (directly oxidizing proteins), redox-active secondary metabolites also display high toxicity levels [20–23]. For this

reason, they are often called “natural antibiotics.” Their toxicity puts selective pressure on producers and other microbes that are commonly found together with producing species to develop defense mechanisms against their toxic effects [24–26]. We have recently proposed that, through the induction of such defense mechanisms, redox-active metabolites can promote collateral resilience to certain clinical drugs [17]. This is particularly relevant when the redox-active metabolite shares structural similarities to the drug used [17]. It is still unclear, however, how broad this phenomenon is when considering distinct redox-active secondary metabolites, the molecular mechanisms involved, and the drugs affected.

Here, we explore the role of two redox-active secondary metabolites as modulators of antibiotic resilience. We focus on pyocyanin and toxoflavin, structurally similar compounds made by diverse opportunistic pathogens, including *Pseudomonas aeruginosa* and *Burkholderia* species. Our mechanistic investigation of representatives of strains that are commonly co-isolated from clinical infections reveals that the production of these metabolites and conserved machinery that senses them can affect the antibiotic susceptibility levels of neighboring species in a significant and predictable fashion. Our findings motivate the development of new approaches to improve the accuracy of antibiotic resistance diagnostics, which is necessary to optimize the use of available drugs.

Results

Pyocyanin produced by Pseudomonas aeruginosa *induces complex defense responses in* Burkholderia

To investigate how redox-active secondary metabolite producers might affect antibiotic susceptivity levels in polymicrobial infections, we started by exploring interactions between two opportunistic pathogens relevant to the cystic fibrosis (CF) lung environment: *Pseudomonas aeruginosa* and *Burkholderia multivorans*. *P. aeruginosa* is a global opportunist pathogen that causes serious infections in patients with CF, chronic wounds, and compromised immune systems [27]. *B. multivorans* is part of the *Burkholderia cepacia* complex (Bcc). Species in this group can cause severe chronic infections and are associated with dire prognoses in patients with CF [28,29].

Even though *P. aeruginosa* and Bcc species already display high levels of antibiotic resistance [27,30], recent evidence indicated that the production of pyocyanin (PYO) by *P. aeruginosa* can modulate susceptibility levels to fluoroquinolone antibiotics in Bcc [17] (Fig. 1A), but the mechanisms involved in this process were unknown. PYO is part of a diverse group of molecules classified as phenazines, which are important virulence factors during *P. aeruginosa* infections and have been detected in patients [31–33].

To screen PYO-mediated molecular responses induced in *B. multivorans*, we first performed RNA-seq experiments either by (i) exposing the cells to exogenously added PYO or (ii) by co-culturing *B. multivorans* with *P. aeruginosa* (Fig. 1B-left). Control treatments involved sequencing RNA of *B. multivorans* alone or in co-culture with a *P. aeruginosa* strain that cannot make phenazines (Δ*phz*), including PYO. We used the *B. multivorans* strain AU42096 (referred to here as *B. multivorans* 1, see Table S1 for details). Notably, when in the presence PYO-producing *P. aeruginosa*, *B. multivorans* 1 is highly tolerant of fluoroquinolones such as ciprofloxacin (Fig. 1B-right). We found that PYO, either when added directly or when produced by *P. aeruginosa*, induces a set of responses in *B. multivorans* 1 (Table S2) that can be grouped into two broad classes: (i) induction of specific efflux systems, including a resistance-nodulation-division (RND) efflux system and a potential major facility superfamily (MFS) transporter, and (ii) oxidative stress responses, including alkyl hydroperoxide reductases (Fig. 1C). These results were confirmed by qRT-PCR (Fig. 1C-D). Not surprisingly, exposing *B. multivorans* to *P. aeruginosa* lead to more complex transcriptional responses than exposure to PYO alone, likely due to the wide variety of molecules secreted by *P. aeruginosa* [34].

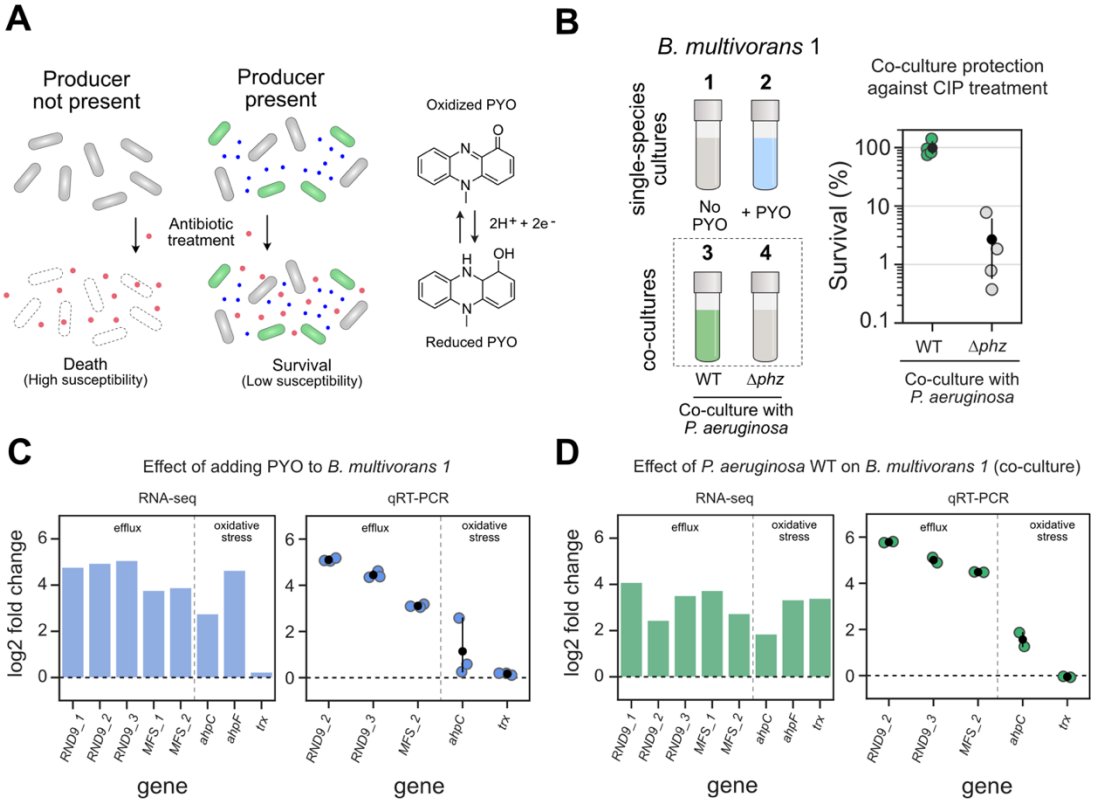

Figure 1. PYO produced by *P. aeruginosa* induces complex defense responses in *B. multivorans*. A. Left: Model of secondary metabolite-mediated induction of survival against antibiotics in microbial populations. Blue dots represent secondary metabolites made by producer species (green cells); red dots represent the antibiotic. Right: one example of such metabolites is PYO, a redox-active molecule produced by *P. aeruginosa*. **B.** Left: Conditions used during RNA-seq and qRT-PCR experiments (1 to 4). In all cases, responses were measured using *B. multivorans* 1 WT (see Materials and Methods). The strain was either grown as a single-species culture and exposed or not to PYO (conditions 1 and 2), or co-cultured with *P. aeruginosa* that can (WT) or cannot (Δ*phz*) make the phenazine (conditions 3 and 4). Right: *B. multivorans* 1 tolerance against ciprofloxacin (CIP, 10 µg/mL) when in co-culture with WT or Δ*phz* *P. aeruginosa* (n = 4). **C-D.** Representative genes highlighting the responses induced by exogenously added PYO (C) or by co-culturing with PYO-producing *P. aeruginosa* (D). RNA-seq and qRT-PCR results are shown as bar (left) and strip (right) plots, respectively. Genes are displayed in two categories (efflux and oxidative stress) and named accordingly to their draft annotation or to their respective homolog in the *P. aeruginosa* genome. For qRT-PCR data, n = 3 in panel C, and n = 2 in panel D (see "experiment 1" in the Material and Methods). For full dataset for each comparison that includes transcriptional changes across *B. multivorans* genome and their respective loci tags, see Table S2. For additional qRT-PCR results, see Fig. S1.

Despite the complexity of the *B. multivorans* transcriptomic responses, the induction of one operon called our attention: an efflux system commonly known as RND-9 [35]. All the genes of this operon (Bmul_3930, Bmul_3931, and Bmul_3932) were induced in the presence of PYO, either when added exogenously or via production by co-cultured *P. aeruginosa* WT (Figs. 1C-D, Fig. S1, Table S2). Given the importance of RND efflux systems in antibiotic tolerance and resistance [36], especially when these systems are induced by PYO [17], we were motivated to

investigate whether the RND-9 efflux system in *B. multivorans* and other *Burkholderia* species is required to confer antibiotic tolerance in the presence of PYO.

Redox-regulated efflux mediates Burkholderia *susceptibility to pyocyanin and its collateral effects on antibiotic resilience*

The PYO-mediated induction of RND-9 in *Burkholderia multivorans* seen in our RNA-seq and qRT-PCR experiments led us to investigate this efflux system more carefully. When searching the genomic region where RND-9 is present, we noticed a flanking gene annotated as a "MerR family transcriptional regulator" (Bmul_3929, Fig. 2A). BLASTing the Bmul_3929 protein sequence from our *B. multivorans* 1 strain against proteins encoded in the *P. aeruginosa* PA14 and *P. aeruginosa* PAO1 genomes [37] resulted in their respective SoxR as first hits (gene locus tags PA2273 and PA14_35170, respectively, Table S3). SoxR is primarily studied in *P. aeruginosa* and *E. coli*; in both cases, the transcription factor contains a Fe-S cluster that can be directly oxidized by redox-active molecules, such as PYO (Fig. 2A) [22,38]. This results in an induction of stress responses, including efflux systems [17,38,39]. However, the role of SoxR in other organisms is much less understood.

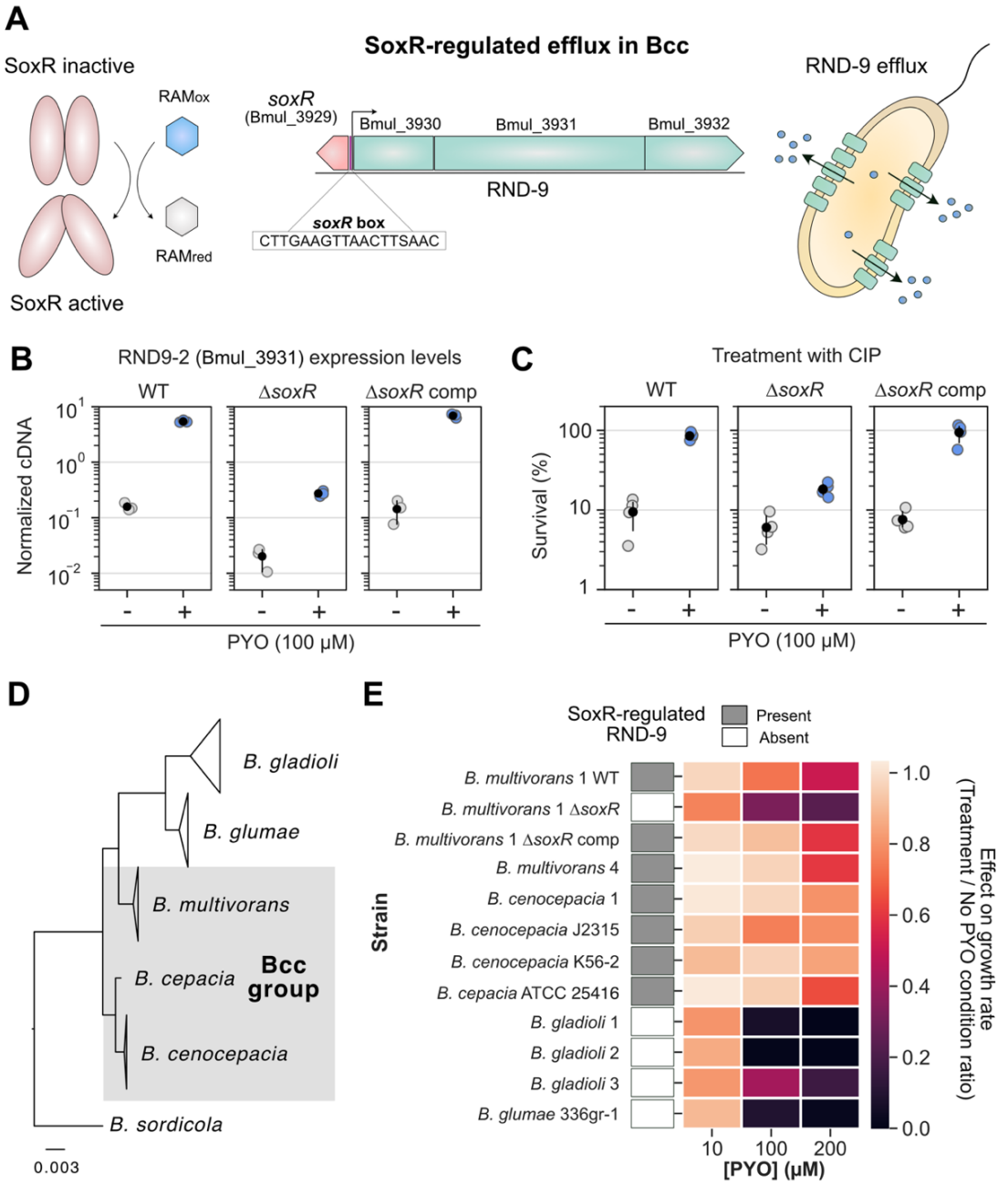

Figure 2. Redox-regulated efflux mediates *Burkholderia* susceptibility to PYO and its collateral effects on antibiotic resilience. A. SoxR-mediated regulation of RND-9 in Bcc. The example is based on the *B. multivorans* ATCC 17616 genome locus structure and orientation. SoxR is oxidized by redox active metabolites (RAMs), triggering its activation (left) [12,20,40]. In Bcc, SoxR is commonly found adjacent to the RND-9 efflux system; the SoxR box [40] is found upstream to RND-9 genes, and the sequence displayed is the consensus found in this genomic region for the Bcc strains studied (center). Following other examples of RND efflux systems, proteins derived from Bmul_3930 and Bmul_3931 are likely associated with the inner membrane, while the one from Bmul_3932 is likely an outer membrane protein [41]. SoxR-mediated induction of the system allows efflux of toxic molecules by the

bacterial cell (right). **B.** Expression levels of the second gene in the RND-9 operon (Bmul_3931) measured by qRT-PCR in different *B. multivorans* strains in the presence or absence of PYO (n = 3). Δ*soxR* comp means complementation of Δ*soxR*. Data is shown as normalized cDNA (see Materials and Methods). For additional qRT-PCR results, see Fig S2. **C**. Effect of PYO on tolerance to ciprofloxacin (CIP, 10 μg/mL) in the same three *B. multivorans* strains (n = 4). **D**. Phylogenetic relationship between the *Burkholderia* species used in this study (gray shading highlights species within the Bcc group). For full tree detailing different strains, see Fig. S4. For broader phylogenetic placement of these species within the *Burkholderia* genus, see ref. [42]. **E.** PYO effect on growth rates of distinct strains of the different *Burkholderia* species studied. Data for three different concentrations are shown (10, 100 and 200 μM). The results are shown as a ratio of the growth rates for each strain under different PYO concentrations by their growth rates in the "No PYO" condition (i.e. values close to 1 mean no inhibition, while values close to 0 mean severe growth inhibition by PYO). Presence or absence of the genomic locus containing SoxR and RND-9 in these strains is indicated by the grey or white boxes, respectively. Growth rates were estimated based on growth curves under the different conditions (Fig. S5). In panels B and C, the black dots mark the means and error bars represent 95% confidence intervals.

First, we hypothesized that, by sensing redox-active metabolites such as PYO, SoxR might regulate the expression of RND-9, which is then used to export them. We confirmed that in our model Bcc strain, *B. multivorans* 1, the RND-9 promoter region has a SoxR box (Fig. 2A). The SoxR box has been shown to be a strong predictor for the operon's regulation by SoxR [40], suggesting that SoxR regulates RND-9 expression in *B. multivorans*. To confirm that SoxR is necessary for PYO-mediated increase in RND-9 expression in *B. multivorans* 1, we made a Δ*soxR* deletion mutant. As predicted, PYO did not increase RND-9 expression in the Δ*soxR* strain to the extent it did in the WT, and overall expression levels were significantly lower and comparable to background levels (i.e., no PYO in the WT) (Fig. 2B, Fig. S2). Complementation of the *soxR* gene restored PYO-mediated activation of RND-9 (Fig. 2B, Fig. S2).

We hypothesized that the PYO-mediated increase in resilience against fluoroquinolones in *B. multivorans* was mediated by SoxR-induction of RND-9. Supporting our hypothesis, the Δ*soxR* strain was much less tolerant to ciprofloxacin in the presence of PYO than the WT (Fig. 2C). Even though there was an apparent slight increase in the survival percentage for Δ*soxR* when PYO is present, we attribute this to a normalization artifact: because PYO affected the growth of Δ*soxR*, the strain reached a lower cell density when PYO was present, causing the normalization (i.e., % survival) to be calculated by a smaller CFU number. Raw CFU values showed that PYO only mildly increased the number of surviving cells upon treatment with ciprofloxacin in the Δ*soxR* strain, while the effect was significantly higher in the WT strain (Fig. S3). Complementation of *soxR* in the mutant restored WT levels of tolerance (Fig. 2C and Fig. S3).

Because PYO significantly increased the expression of RND-9 in *B. multivorans*, we decided to investigate the importance of this system for PYO resistance in other *Burkholderia* species. Specifically, we hypothesized that the presence of the SoxR-regulated RND-9 efflux system might be used to predict how well different *Burkholderia* species can manage PYO toxicity. Export is crucial for handling PYO's toxic effects [17,38,39]. In this scenario, *Burkholderia* species containing SoxR-mediated RND-9 would sense the presence of PYO secreted by *P. aeruginosa* and quickly induce the efflux system, increasing their fitness in the presence of the molecule. We searched the *Burkholderia* Genome Database (www.burkholderia.com) [43] for species commonly found in CF patients as well as in the environment (e.g., plant-associated strains). These included species within the Bcc (such as *B. multivorans*, *B. cepacia*, *B. cenocepacia*) and non-Bcc species (such as *B. glumae* and *B. gladioli*). We obtained several strains within these species, many of which are clinical isolates from lung respiratory infections (see Table S1), compared their phylogenetic relationship (Fig. 2D, Fig. S4), and assessed whether the SoxR-regulated RND-9 efflux system was present (Fig. 2E). The system's presence was determined by (i) directly inspecting the genome (available in databases or through whole-genome sequencing), by (ii) PCR-amplifying a fragment containing part of the SoxR/RND-9 genome locus, or by (iii) by inference based on the genomic content of closely-related strains within the same species in genome databases, such as the *Burkholderia* Genome Database [43] and Integrated Microbial Genomes and Microbiomes IMG/M [44,45] (see Materials and Methods for details). In parallel, we measured the growth rates of these strains in the presence of different concentrations of PYO (Fig. 2E and Fig. S5). We saw a strong correlation between the presence of SoxR/RND-9 locus and the strain's ability to handle PYO toxicity. The system was present in all Bcc species tested, and growth of these strains was only mildly affected by PYO, even at concentrations as high as 200 μM (Fig. 2E and Fig. S5). However, growth of strains lacking the regulator/efflux system (*B. glumae*, different *B. gladioli* strains, and the *B. multivorans* Δ*soxR*) was dramatically inhibited by PYO (Fig. 2E and Fig. S5). This indicates that SoxR-regulated efflux plays a conserved role in how well *Burkholderia* species can tolerate PYO, potentially affecting their ability to inhibit habitats where *P. aeruginosa* is present. Moreover, this system also modulates *P. aeruginosa*'s impact on *Burkholderia* susceptibility to antibiotics because the *P. aeruginosa*-mediated increase in antibiotic tolerance on *B. multivorans* is SoxR dependent (Fig. S6).

Overall, these results highlight the importance of SoxR and its redox-regulated efflux systems during interspecies interactions mediated by redox-active secondary metabolites, demonstrating their antagonistic effect on fluoroquinolone susceptibility.

Redox-active secondary metabolites as interspecies modulators of antibiotic susceptibility: the toxoflavin example

Our results with PYO motivated us to ask whether other redox-active secondary metabolites might similarly be capable of modulating antibiotic susceptibility in polymicrobial infections [12]. Accordingly, we searched for other potential candidate molecules known to be made by pathogens that have been found infecting CF patients. We found that phenazine-1-carboxylic acid (PCA), another phenazine made by *P. aeruginosa*, also dramatically increased *B. multivorans* tolerance against ciprofloxacin in a SoxR-dependent manner (Fig. S7). But to test the generality of the phenomenon, we looked for non-phenazine molecules made by species other than *Pseudomonas*. One example we found was toxoflavin (TOX) (Fig. 3A). TOX is made by different *Burkholderia* species, including *B. glumae* and *B. gladioli*, and has been proposed to increase the fitness and virulence of its producers when infecting plants [46–48]. *B. glumae* is a plant pathogen, while *B. gladioli* can cause disease in plants and humans [28,49,50]. In fact, *B. gladioli* is among the most prevalent *Burkholderia* species in CF patients [28]. Though TOX detection in CF sputum has not been attempted to our knowledge, clinical *B. gladioli* strains commonly produce TOX *in vitro* [50]. TOX is redox-active and thought to induce efflux and oxidative stress response in bacteria (Fig. 3A-B) [51,52]. Therefore, TOX is a potentially clinically-relevant molecule and a good candidate for testing the hypothesis that redox-active secondary metabolites have broad potential to modulate antibiotic resilience.

We started by determining whether TOX can increase ciprofloxacin tolerance in the producing species *B. glumae,* just like PYO does in *P. aeruginosa* [17,53]. TOX induces the efflux system ToxFGHI in *B. glumae* [54], and we confirmed that the WT strain makes TOX under the studied conditions (Fig. S8). However, when comparing WT ciprofloxacin survival levels to a Δ*toxA* strain that cannot make TOX [55], we did not see a significant increase in tolerance (Figs. 3C); similarly, adding TOX exogenously to Δ*toxA* did not significantly increase tolerance (Fig.

3C). Although we observed a slight tolerance increase trend when TOX was present, the magnitude of the effect is much smaller than what PYO provides to *P. aeruginosa* [17], revealing that ToxFGHI and the overall responses induced by TOX in *B. glumae* do not confer ciprofloxacin tolerance to this strain.

Even though TOX does not provide significant protection against ciprofloxacin in *B. glumae*, we reasoned that it might act as an interspecies modulator of antibiotic resilience in another organism. For example, *B. gladioli* strains (potentially TOX producers) [50,56] can infect CF patients together with other Bcc pathogens [57]. We thus decided to test if Bcc species might benefit from the presence of TOX when treated with ciprofloxacin. Tolerance assays using our Bcc model organism, *B. multivorans* 1, showed that TOX increased its survival against ciprofloxacin in a concentration-dependent manner (Fig. 3D). Levels of 50 μM or above made the strain completely tolerant to the antibiotic treatment (Fig. 3D). Importantly, concentrations of TOX within the 10-100 μM range are physiologically relevant since they fall within the amounts produced by *B. gladioli* and *B. glumae* under the studied conditions (Fig. S8). We next hypothesized that this tolerance phenotype is mediated by the SoxR-regulated RND-9 efflux system, like it is for PYO. Consistent with this prediction, the TOX-mediated increase in tolerance against ciprofloxacin disappeared in the Δ*soxR* strain, but was restored in the SoxR-complemented strain (Fig. 3E). Moreover, using qRT-PCR to quantify the expression of RND-9 in *B. multivorans* 1, we observed that TOX increased transcription of RND-9 in *B. multivorans* 1 and its induction disappeared in the Δ*soxR* mutant, but was restored in the SoxR-complemented strain (Fig. 3F, Fig. S9). This indicates that SoxR in *B. multivorans* 1 works as a broader sensor for a wide range of redox-active molecules, with direct consequences for antibiotic efficacy.

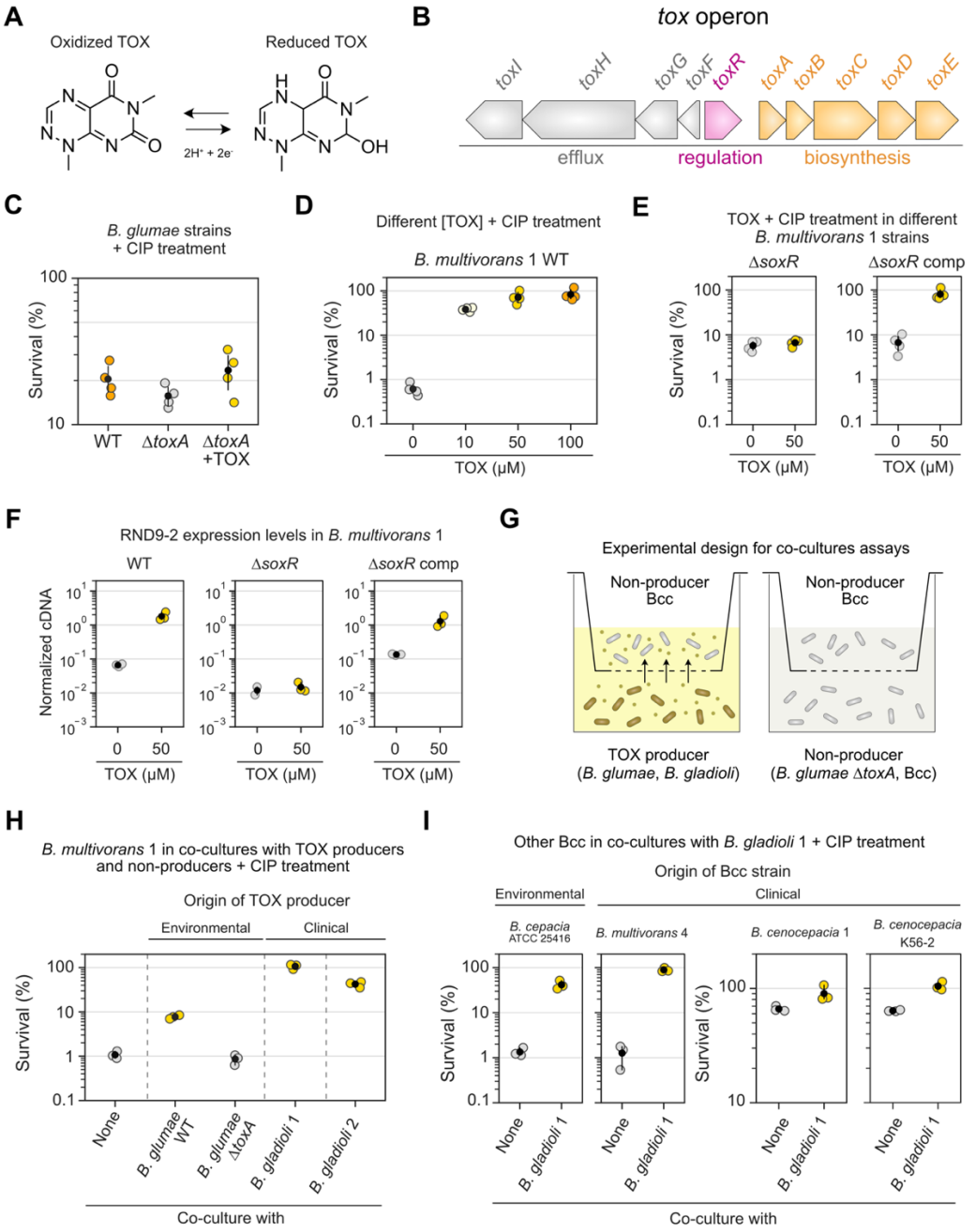

Figure 3. TOX increases tolerance against ciprofloxacin in Bcc. A. TOX molecule and its redox states. **B.** Genomic structure of the *tox* operon present in the TOX producer *B. glumae* [47,54]. Similar genomic context is found in other TOX producers [50]. **C.** Effect of TOX on tolerance to ciprofloxacin (CIP, 1 μg/mL) in different *B. glumae* strains (n = 4). TOX was either produced endogenously by the WT strain or added exogenously (50 μM) to the Δ*toxA* mutant. **D.** Effect of different TOX concentrations on tolerance to CIP (10 μg/mL) in the *B. multivorans* 1 WT strain (n = 4). **E.** Effect of TOX on tolerance to CIP (10 μg/mL) in the *B. multivorans* 1 Δ*soxR* or Δ*soxR* comp strains (n = 4). This experiment was performed separately from that shown in panel D. **F.** Expression levels of the second gene in the RND-9 operon (Bmul_3931) measured by qRT-PCR in different *B. multivorans* strains in the presence or absence of TOX (n = 3 for all except "Δ*soxR* + 0 μM TOX," where n = 2). Data is shown as normalized cDNA (see Materials and Methods). Also, see Figs. S9 additional qRT-PCR data. **G.** Experimental design used during the co-culture

antibiotic assays (see Materials and Methods for details). **H.** Effect of TOX produced by different producer species (*B. glumae* WT, and several *B. gladioli* strains) on the tolerance of *B. multivorans* 1 to CIP (10 μg/mL). Conditions where TOX was not produced were: "none" (i.e. only *B. multivorans* 1 is present) or co-culture with the *B. glumae* Δ*toxA* strain that cannot make TOX. *B. glumae* was originally isolated from environmental sample [47], while *B. gladioli* strains are derived from CF patients (see Table S1). Only the top part of the co-culture plate (i.e. containing *B. multivorans* 1) was plated for CFUs for survival assessment (n = 3). **I.** Effect of TOX produced by *B. gladioli* 1 on the tolerance of multiple Bcc species (isolated from environmental and clinical samples) to CIP (10 μg/mL, n = 3). Note that the scales on the two plots assessing tolerance in *B. cenocepacia* (two on the right) are different from the ones on the left, since the background tolerance levels in these strains are much higher than the ones in *B. cepacia* or *B. multivorans* 4 (left). In panels C-F and H-I, the black dots mark the means and error bars represent 95% confidence intervals. Panel G was adapted from [17], CC BY 4.0 (https://creativecommons.org/licenses/by/4.0/).

We next evaluated the effect of TOX in co-culture assays (Fig. 3G). First, we tested if *B. multivorans* 1 becomes more tolerant to ciprofloxacin when grown with environmental or clinical TOX producers (Fig. 3H). Co-culture with *B. glumae* WT (i.e., TOX present) increased *B. multivorans* 1 tolerance to ciprofloxacin. The phenotype disappeared when the strain was co-cultured with the *B. glumae* Δ*toxA* (i.e., no TOX). Notably, co-culture with two different clinical strains of *B. gladioli* isolated from CF patients dramatically increased tolerance against ciprofloxacin by *B. multivorans* 1 (Fig. 3H). These two clinical strains produce TOX (Fig. S8), and the molecule was present in the co-cultures, evident by its yellow pigmentation. To evaluate the generality of these results, we compared the ciprofloxacin tolerance of multiple Bcc strains from different species (*B. cepacia*, *B. multivorans*, and *B. cenocepacia*) to that seen when they were co-cultured with a TOX-producing clinical strain of *B. gladioli*. These Bcc strains were derived either from environmental samples or from patients. In all cases, co-culture with *B. gladioli* increased ciprofloxacin tolerance levels in the Bcc species (Fig. 3I). All co-cultures were yellow, indicating TOX was present. The effect was dramatic for *B. cepacia* and *B. multivorans*, increasing tolerance levels more than an order of magnitude; although *B. cenocepacia* strains showed higher background tolerance levels when grown alone in the absence of TOX, co-culturing these strains with TOX-producing *B. gladioli* still made them more tolerant of ciprofloxacin (Fig. 3I).

Overall, our results show that phenazines made by *P. aeruginosa* are not the only redox-active secondary metabolites that can modulate antibiotic resilience. TOX, a redox-active molecule produced by different *Burkholderia* species, can do the same, suggesting generality for the phenomenon.

Assessing the effects of redox-active secondary metabolites on antimicrobial susceptibility testing

These mechanistically-oriented laboratory results raised an important practical question: how might redox-active secondary metabolites impact standard clinical antibiotic susceptibility testing (AST)? Current AST methods are blind to potential modulating effects of redox-active secondary metabolites. This happens because the synthesis of these metabolites is usually controlled by quorum sensing, being made only at cells densities that are much higher than what is used for typical AST inocula [13,58]. However, redox-active secondary metabolites have been detected in infections [32,33] and presumably could dramatically change the performance of certain drugs during treatment [12]. To take this into account, we modified the protocol of a traditional AST assay that determines the minimum inhibitory concentration (MIC) for specific drugs. Using PYO and TOX as examples, we tested how these metabolites affect susceptibility to several antibiotics from different classes.

Our experimental design is shown in Fig. 4A and Fig. S10A. In brief, MIC assays following the EUCAST guidelines (see Materials and Methods) were performed in the absence or presence of exogenously added PYO or TOX. For these assays, we used our model organism, *B. multivorans* 1. We tested several different (sub)classes of drugs, including fluoroquinolones (ciprofloxacin and levofloxacin), tetracyclines (tetracycline and doxycycline), amphenicols (chloramphenicol), sulfonamides (sulfamethoxazole in combination with trimethoprim), aminoglycosides (tobramycin), carbapenems (meropenem), cephalosporins (ceftazidime), and polymyxins (colistin). PYO and TOX altered the MIC of *B. multivorans* for several types of drugs. Both PYO and TOX had overall antagonistic effects on fluoroquinolones, tetracyclines, and chloramphenicol, increasing their MICs (Figs. 4B-C). In some cases, although not enough to change the MIC, PYO and TOX had drug-antagonistic effects that could be measured by an increase in optical density at the pre-MIC concentration (see antibiotics marked with "+" in Figs. 4B-D). Examples include exposure to PYO together with tetracycline or sulfamethoxazole/trimethoprim (Fig. 4D). Similar antagonistic effects were observed for cells exposed to TOX and levofloxacin (Fig. 4D). On the other hand, PYO and TOX acted synergistically with other drugs, potentiating their toxicity, resulting in lower MICs or lower optical densities at the pre-MIC concentrations when the

metabolites were present. This was the case for tobramycin and meropenem in the presence of PYO (Figs. 4B, 4D), and for sulfamethoxazole/trimethoprim, tobramycin, meropenem, and ceftazidime in the presence of TOX (Figs. 4C-D). Cases where the synergistic effect was only visible at the pre-MIC concentrations are marked as "-" in Figs. 4B-D. We also tested the effect of PYO and TOX on colistin susceptibility, with both enhancing its toxicity. In the absence of these metabolites, *B. multivorans* 1 was completely resistant to colistin at all the concentrations tested (MIC > 4.096 mg/mL, Table S4), and therefore colistin is not included in Figs. 4B-C. However, addition of PYO caused a decrease in optical density (Fig. S11C), and TOX caused a dramatic drop in the MIC (Table S4), indicating that these metabolites can act synergistically with polymyxins [17,53,59]. Overall, these results show that the effects of redox-active secondary metabolites on antibiotic susceptibility can be dramatic and are distinct for different classes of drugs.

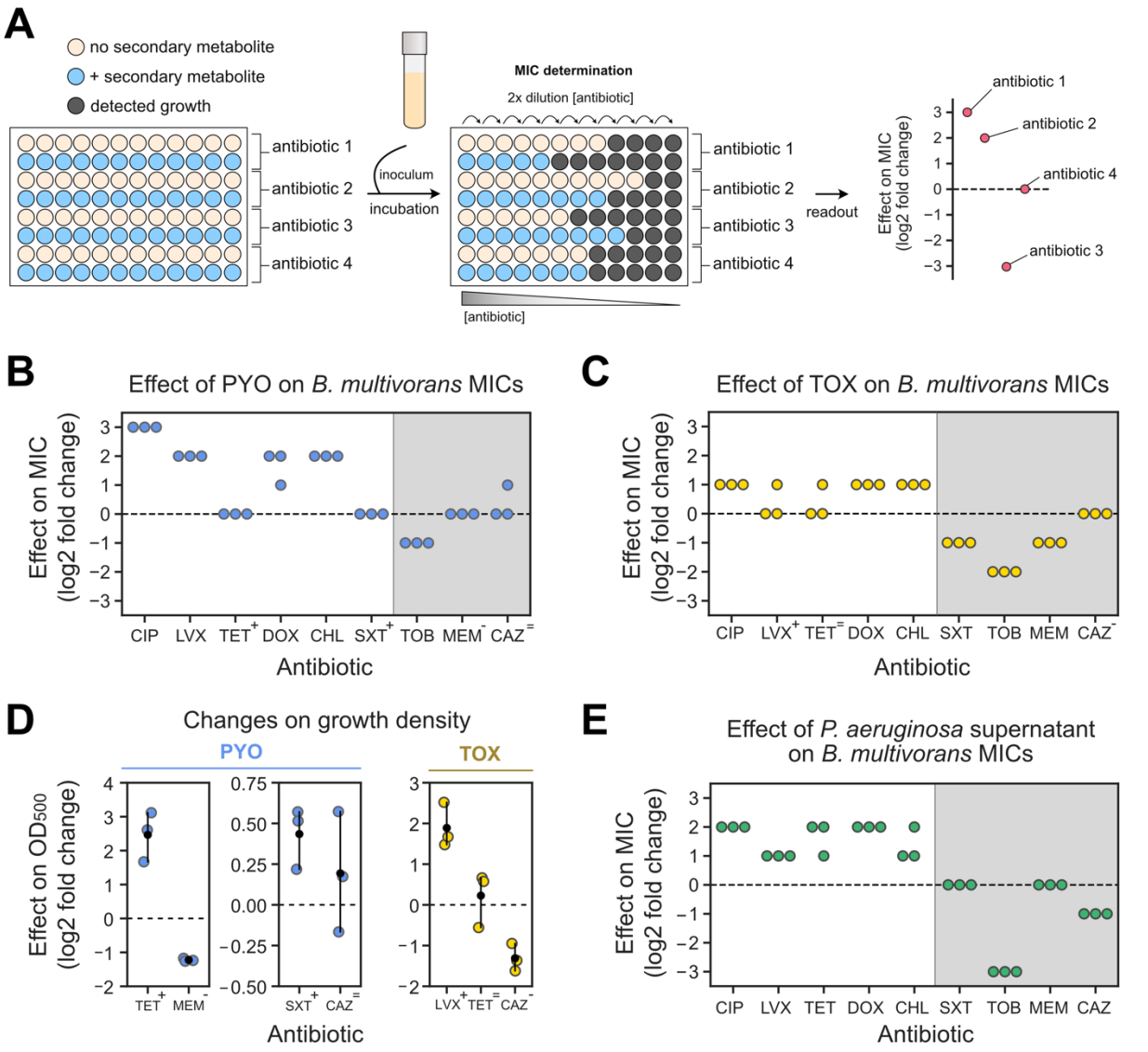

Figure 4. Assessing the effects of secondary metabolites on antimicrobial susceptibility testing. A. Experimental design used during MIC tests that account for the effect of secondary metabolites on resistance levels. **B.** Effects of PYO (100 µM) on *B. multivorans* 1 MICs (for each antibiotic, n = 3). **C.** Effects of TOX (50 µM) on *B. multivorans* 1 MICs (for each antibiotic, n = 3). In B and C, symbols above the antibiotic names represent effects of PYO and TOX on growth density displayed in D ("+" represents increase in density, "-" represents decrease in density, and "=" represents no consistent change in density). **D.** Effects of PYO (two plots on the left) and TOX (right) on the growth density at the pre-MIC antibiotic concentrations during MIC assays. Antibiotics shown are the ones previously highlighted by the symbols in panels B and C. Note that scales are different for each plot. For normalized absorbance values, see Fig. S11A-B. **E.** Effects of *P. aeruginosa* WT supernatant (i.e. PYO present) on *B. multivorans* 1 MICs (for each antibiotic, n = 3). For experimental design, see Fig. S10B. Grey shading in B, C and E represent antibiotics for which metabolite-mediated increase in resilience was not observed under the studied conditions. In panels D, the black dots mark the means and error bars represent 95% confidence intervals. CIP, ciprofloxacin; LVX, levofloxacin; TET, tetracycline, DOX, doxycycline, CHL, chloramphenicol, SXT, sulfamethoxazole/trimethoprim; TOB, tobramycin; MEM, meropenem; CAZ, ceftazidime.

Recognizing that these effects might be generalizable for a wide range of unknown molecules for which purified compounds are unavailable, we sought to determine whether modified MIC protocols could be agnostic to any specific metabolite secreted by a pathogen. Accordingly, we used spent media from grown cultures (i.e., containing secondary metabolites) mixed with fresh media (Fig. S10B and Materials and Methods for experimental design) to modify the traditional MIC assay. As proof of principle, we tested the susceptibility of our model organism, *B. multivorans* 1, to all the drugs mentioned above, using spent medium from *P. aeruginosa* WT (Fig. 4E). We predicted that the phenazine-producing *P. aeruginosa* cultures would change the MIC like exogenously added PYO did in the previous experiments. As expected, *P. aeruginosa* spent medium increased the MIC of *B. multivorans* against fluoroquinolones, tetracyclines, and chloramphenicol (Fig. 4E). We did not see changes in MIC against sulfamethoxazole/trimethoprim (Fig. 4E), likely because our experimental design led to a four-fold dilution of the active metabolite(s) from its initial concentration in the spent medium. For instance, the PYO concentration was ~80-100 μM in the original culture from which the spent medium was taken, but only ~20-25 μM in the final assay (see Materials and Methods). Because the impact of exogenously adding 100 μM PYO was already small (Fig. 4D), it is not surprising that we observed no effect using the diluted spent media. Still, in agreement with our experiments using purified PYO, *P. aeruginosa* spent medium potentiated the efficacy of tobramycin, reducing the MIC (Fig. 4E). On the other hand, unlike our findings with purified PYO, *P. aeruginosa* spent medium decreased the MIC against ceftazidime (Fig. 4E). To evaluate if the results observed for *P. aeruginosa* spent medium were caused by phenazines, we also tested spent medium from the *P. aeruginosa* Δ*phz* mutant (Fig. S11D). We saw no significant increase in the *B. multivorans* MICs when Δ*phz* spent medium was used (Fig. S11D), suggesting that the antagonistic effects against these drugs were due to phenazines. Finally, we also tested the impact of spent medium from *B. multivorans* on its own MICs (Fig. S11E). We saw no effect on MICs for fluoroquinolones or sulfamethoxazole/trimethoprim, but we did see changes for the other drugs: *B. multivorans* spent medium increased MICs against tetracyclines, chloramphenicol, and meropenem but decreased MICs against tobramycin and ceftazidime (Fig. S11E). Altogether, our results suggest that metabolites secreted by opportunistic pathogens can substantially alter MIC levels in ways that are overlooked by current protocols.

Discussion

Redox-active secondary metabolites, produced by organisms throughout the tree of life [60], are of particular interest due to their multifaceted and nuanced effects, which depend on the environmental and physiological conditions experienced by the cells when exposed to them [39,61]. Within the clinical context, their dynamic functions range from the support of biofilm development to serving as virulence factors that are toxic to host cells [31,62–65]. In this study, we found that these molecules can also modulate antibiotic resilience, altering susceptibility levels to drugs commonly used to treat infections. Together with recent evidence demonstrating that these molecules can increase mutation rates to antibiotic resistance against certain drugs [17], our results point towards the production of redox-active secondary metabolites by opportunistic pathogens as an underappreciated route for the evolution of antimicrobial resistance.

To better predict contexts where redox-active secondary metabolites might affect antimicrobial susceptibility, it is necessary to understand the molecular mechanisms involved in the process. Our results support the role of SoxR as a broad redox sensor in nature [40]. This transcription factor has been primarily studied in enteric bacteria (*E. coli* and *Salmonella* sp.) and in *P. aeruginosa*, where it senses redox-active molecules through oxidation of its Fe-S cluster [22,23,38,66,67]. However, SoxR is widely distributed throughout the bacterial domain, with homologs enriched in the *Actinobacteria* and *Proteobacteria* [61]. Many of these organisms include well-established or emerging opportunistic pathogens, such as species within the genus *Mycobacterium*, *Nocardia*, *Burkholderia* (including the Bcc species studied here), *Ralstonia*, *Acinetobacter*, and *Stenotrophomonas*, among others [40,61]. However, we know little about the redox-active molecules SoxR might sense and the responses it might control in these organisms. Our work demonstrates that, if focused on antibiotic susceptibility, special attention should be given to SoxR-regulated efflux systems and to the drugs these systems might be able to transport. SoxR homologs in other pathogens might control the transport of yet-to-be-discovered redox-active secondary metabolites that affect antibiotic susceptibility, whether the metabolite is produced endogenously or by a neighbor species.

While we have shown that certain secondary metabolites can dramatically modulate antibiotic susceptibility *in vitro*, it is important to recognize that these effects have yet to be confirmed *in vivo*. Testing the relevance of this phenomenon in the host context is an essential next step, and we hope our study will stimulate future work on this topic. Moreover, there is still a long path ahead when considering interspecies interactions during infections, mostly due to our still limited understanding of the colonization dynamics in polymicrobial infections. This is true even for CF, a well-studied infection context. Although we know certain species can be found infecting patients at the same time, our understanding of the frequency of these interactions is much less clear. For example, *P. aeruginosa* can be found with *Staphylococcus* or Bcc [28,68–70], but the prevalence of such co-infections among patients is not well documented. Similarly, *B. gladioli* is among the most common *Burkholderia* species isolated from CF sputum [28], but we do not know which other microbes typically co-reside with this species. Moreover, how these organisms co-exist within infections is poorly constrained due to very limited data on their spatial distribution within patients, though methods for accessing this are improving [71–74]. While our study suggests that redox-active metabolites such as PYO and TOX may be broad modulators of antibiotic susceptibility, to accurately predict how/which neighboring species might be affected by such molecules, future work must characterize community dynamics and spatial proximity between co-infecting organisms within individual patients.

Our results also highlight the need for redesign of antimicrobial susceptibility tests to make them more accurately mimic the context of infections. While there is room for improvement across a range of parameters, inclusion of secondary metabolites from spent supernatants of infecting strains in AST protocols could be a simple and constructive first step, even without knowledge of the identity of the metabolite(s) that impact the results. Because the vast majority of secondary metabolites are still uncharacterized [75], it is important to use phenotypic screens to identify the existence of an unknown whose identity can later be determined through follow-up research. Our case study using PYO and TOX as models for evaluating the impact of redox-active secondary metabolites on antibiotic resilience serves as a proof of principle that awareness and understanding of these interactions has the potential to inform drug selection for more effective treatment. For example, our results suggest that when in the presence of *P. aeruginosa*, treating Bcc with

fluoroquinolones, tetracyclines, chloramphenicol, or sulfamethoxazole/trimethoprim would likely be less effective, increasing the chances of the evolution of resistance [17]. For these situations, drugs like meropenem or ceftazidime would possibly be more appropriate. TOX-producing *B. gladioli* might also significantly impact Bcc susceptibility to antibiotics, mainly decreasing the efficacy of fluoroquinolones. Finally, *B. multivorans* appears to produce unknown metabolites that reduce its susceptibility to certain drugs, such as tetracyclines, chloramphenicol, and meropenem, which could be investigated in more detail in the future.

More generally, we end by observing that approaches that have been employed to identify polymicrobial and/or microbe-host interactions mediated by secondary metabolites in the context of the gut microbiome [76,77] can and should be leveraged more strongly in the context of infectious disease. While some studies have begun to light the way [78,79], there remains tremendous potential for discovery of secondary metabolite-mediated effects that shape clinical outcomes. To identify endogenously produced molecules that impact antimicrobial susceptibility, we must ask: Who is there? What are they making? What are the responses induced in the community by the presence of specific molecules? And, finally, which drugs are affected by these responses? High-throughput methods combined with various "systems approaches" used for studying how drugs interact with the gut microbiome [80–83] could be adapted to study how metabolites produced by pathogens in different infection contexts might affect their interactions with each other and their susceptibility to antibiotics. We anticipate that our findings with PYO and TOX are likely just the tip of the iceberg, and we hope growing awareness of the potential ubiquity of these type of interactions will enhance our understanding of and ability to control polymicrobial infections.

Materials and methods

Media and incubation conditions

Most of the media and conditions used followed previous descriptions [17]. The defined medium mostly used in this work was the glucose minimal medium (GMM), comprising 20 mM glucose (or 10 mM, if specified), 50 mM KH_2PO_4/K_2HPO_4 (pH 7.2), 42.8 mM NaCl, 9.35 mM

NH_4Cl, 1 mM $MgSO_4$, 1x MEM Amino Acids (AA) solution (MilliporeSigma, Cat. No. M5550), and a trace elements solution [84]. As described previously [17], the medium was prepared by autoclaving all the components together, except for the glucose and the 1,000x trace elements stock solution, which were sterilized through filtration and added after the autoclave step. Autoclave step proceeded for 20 minutes at 121°C. As previously noted [17], autoclaving $MgSO_4$ together with other media components is essential for consistent production of PYO by our WT *P. aeruginosa* UCBPP-PA14 strain in this medium. Two other media were used: Luria–Bertani (LB) Miller broth (BD Biosciences) and BBL cation-adjusted Mueller–Hinton II (MH) broth (BD Biosciences). Their preparation followed the manufacturer's instructions. Importantly, for the MH broth medium, the autoclave step was 10 min. 1.5% Bacto agar (BD Biosciences) was used for solid media unless mentioned otherwise (see strains construction section below). Pyocyanin (PYO) was synthesized and purified following published protocols [85,86], and 10 mM stock solutions were prepared using 20 mM HCl and stored at −20°C. Toxoflavin (TOX) (MedChemExpress) was dissolved in dimethyl sulfoxide (DMSO) to make 10 mM stock solutions that were prepared on the same day of the experiment. Phenazine-1-carboxylic acid (PCA) (Princeton Bio) was dissolved in 20 mM NaOH and stored at −20°C. Finally, experiments using PYO, TOX or PCA always had negative controls with equivalent volumes of the solvents used (20 mM HCl, DMSO, or 20 mM NaOH, respectively). Unless otherwise specified, incubations were performed at 37°C, with shaking for liquid cultures at 250 rpm.

Strain construction

We performed genetics in the *B. multivorans* AU42096 strain, our model Bcc organism. We refer to this strain as *B. multivorans* 1 [17] (Table S1). An unmarked deletion of the Bmul_3929 gene (*soxR* homolog) was made through homologous recombination using the pEX18Tc plasmid [87,88]. Briefly, ~800 bp fragments upstream and downstream of the gene were amplified and cloned into the pEX18Tc suicide vector using Gibson assembly [89]. Amplifications were done using *B. multivorans* 1 genomic DNA (gDNA, extracted with DNeasy Blood & Tissue Kit, Qiagen), cleaned up using the Monarch PCR Purification kit (New England Biolabs), and used in a Gibson assembly reaction (New England Biolabs) together with a PCR-amplified fragment

containing the entire pEX18Tc sequence. The assembled construct was transformed into *E. coli* S17 [90], with selection in LB with 10 µg/mL tetracycline and incubation at 30ºC. The assembled plasmid was identified by colony PCA, verified by Sanger sequencing (Laragen), and inserted into *B. multivorans* 1 genome by biparental conjugation using a modified version of previously published protocols [91,92]. Briefly, *E. coli* S17 (containing the pEX18Tc-based deletion plasmid) and the *B. multivorans* 1 WT strain were grown overnight in LB (with 10 µg/mL tetracycline for the *E. coli* strain) and then diluted in the same medium to OD_{600} of 0.05 and 0.025, respectively. Cultures were grown until OD_{600} of ~0.5; if one of the cultures reached the final OD earlier, this culture was moved to a non-shaking incubator (also 37ºC) until the other was ready for the next steps. When ready, 400 µL of each culture were mixed into a Falcon tube and left stand (non-shaking) for 1 hour. Next, 100-200 µL of the mixed cultures were plated on top of polycarbonate membranes (MilliporeSigma, Cat. No. WHA10417006) on LB plates, followed by an incubation step of ~15 hours at 37ºC. Next, cells were scrapped from the filters, resuspended in 0.9% NaCl, plated on to VBMM agar plates (3 g/L trisodium citrate, 2 g/L citric acid, 10 g/L K_2HPO_4, 3.5 g/L $NaNH_4PO_4{\cdot}4H_2O$, 1 mM $MgSO_4$, 100 µM $CaCl_2$, pH 7) containing 100 µg/mL of tetracycline [92], and incubated for 24-48 hours at 30ºC. This resulted in colonies of *B. multivorans* 1 that were merodiploids containing the construct integrated in their genomes, which were then plated on to LB containing 10% sucrose. Importantly, LB plates lacked NaCl and contained only 1.05% agar. This was relevant because we noticed that even though pEX18Tc contains a *sacB* cassette, the *sacB* counter selection was not effective in our *B. multivorans* 1 strain, as has been observed for other *Burkholderia* strains [93]. However, these conditions still allowed the screening of colonies that lost the integrated plasmid. We noticed that such colonies presented a spreading "flat" morphology under these conditions, while the merodiploids were round "thick" colonies (Fig. S12). The flat colonies were rare (roughly 1 in ~200 colonies) and, as expected, ~50% of them were WT genotype and ~50% were unmarked deletions. These were screened by PCR and verified by both Sanger sequencing and whole-genome sequencing.

Complementation of the Δ*soxR* mutant was also done through homologous recombination with the re-insertion of the gene in its native site following the same protocols described above. The only difference was that, in this case, a unique fragment from ~800 bp fragments upstream to

~800 downstream region of *soxR* (i.e., containing the *soxR* gene) was amplified from *B. multivorans* 1 WT gDNA and cloned into the pEX18Tc. This was then inserted in the Δ*soxR* mutant through homologous recombination was described above, with PCR and whole-genome sequencing verifications. Information on all primers and strains used is available in Table S1.

Whole-genome sequencing and draft genome assembly and annotation

Genomic DNA (gDNA) was extracted from the following strains using the DNeasy Blood & Tissue kit (Qiagen): *B. multivorans* 1 WT; *B. multivorans* 1 Δ*soxR*; *B. multivorans* 1 Δ*soxR* comp (complementation of *soxR* in the Δ*soxR* background). Library preparation was performed by the Microbial Genome Sequencing Center (MiGS) (Pittsburgh, Pennsylvania, USA) and included (i) 2 x 150 bp paired-end Illumina sequencing for all these strains (minimum of 400-Mb sequencing output per sample, with approximately 50-60x coverage), and (ii) an additional Nanopore sequencing for the *B. multivorans* 1 WT strain (minimum of 300 Mb Long Reads) for draft genome assembly and annotation of this strain.

Draft genome assembly and annotation of the *B. multivorans* 1 WT strain was performed by the MiGS analysis pipeline, and included: (i) quality control and adapter trimming performed using bcl2fastq (for Illumina reads) and porechop (for Nanopore reads, available at: https://github.com/rrwick/Porechop); (ii) assembly (using both Illumina and Nanopore reads) performed using Unicycler [94]; (iii) assembly statistics assessed using QUAST [95]; and (iv) draft assembly annotation performed using Prokka [96].

To check for the Δ*soxR* and Δ*soxR* comp strains, quality control was performed using Trimmomatic (version 0.39) [97] with the following settings: LEADING:27 TRAILING:27 SLIDINGWINDOW:4:20 MINLEN:35. Mutations were then identified using breseq (version 0.35.7) [98] using the draft annotation we described above. This was important because we observed dozens of potential non-related mutations that appeared in the genome during the process of making these strains. This was not surprising since *B. multivorans* 1 is a clinical strain that has not been extensively used in the laboratory, with the exception of our previous work that did not include genetic manipulation [17]. Despite these additional potential mutations, we were able to

confirm the correct *soxR* deletion and complementation, which resulted in the phenotypes described in our results. Whole-genome sequence data for the strains studied was submitted to the NCBI Sequence Read Archive under the accession number TBD.

Assessment of the presence of SoxR/RND-9 locus in the studied strains

The SoxR/RND-9 locus presence was determined by three complementary methods. First, we directly inspected the genomes of the *Burkholderia* species studied that are available at the *Burkholderia* Genome Database (BGD) [43] and Integrated Microbial Genomes and Microbiomes IMG/M [44,45]. These included *B. cenocepacia* J2315, *B. cenocepacia* K56-2, *B. cepacia* ATCC 25416, and *B. glumae* 336gr-1. We also inspected the draft genomes for the strains we performed whole-genome sequencing, which included all the genotypes of our *B. multivorans* 1 strain. Second, we performed PCR amplification attempts for a fragment containing part of the SoxR/RND-9 genome locus in all strains. Primers were designed using consensus sequences of the region known from the available genomes (see primers in Table S1). As positive controls for this screen, we used primers for 16S rRNA amplification. For all PCRs, overnight cultures for all strains were grown in LB and 1 μL of the cultures were used during amplification attempts. Finally, we also checked annotated genome of closely-related strains available at the BGD or IMG/M. We could not find strains of *B. glumae* or *B. gladioli* that had the SoxR/RND-9 genome locus.

Phylogenetically analyses

Phylogenetic analysis included 15 *Burkholderia* strains for which 16S sequences were either generated by Sanger sequencing (Laragen; primers available in Table S1) or retrieved from the BGD database or GenBank. For generated sequences, contigs were prepared using MacVector (version 18.2.0). Sequences were aligned with MAFFT (version 7.490, alignment available in the supplementary material) [99,100], and phylogeny was reconstructed through Bayesian inference using MrBayes (version 3.2.7) [101]. Briefly, GTR was used as initial model for two independent analyses, each consisting of three heated chains and one cold chain. Markov Chain Monte Carlo sampling ran for one million generations (additional parameters: diagnfreq=1000; samplefreq=100; relburnin=yes; and burninfrac=0.25), which was enough to reach convergency

(i.e. average standard deviation of split frequencies < 0.01). The final tree was edited in FigTree (version 1.4.4, software available at: https://github.com/rambaut/figtree/releases) and polished in Affinity Designer (Serif, version 1.10.4).

RNA-seq experiment and data analysis

Four different conditions were prepared for the RNA-seq experiment: (i) *B. multivorans* (no PYO added); (ii) *B. multivorans* + 100 μM PYO; (iii) *B. multivorans* + *P. aeruginosa* WT (co-culture, PYO and other phenazines produced); and (iv) *B. multivorans* + *P. aeruginosa* Δ*phz* (co-culture, no PYO or phenazines produced). For these experiments, we used our *B. multivorans* 1 WT strain. From freshly streaked LB plates (< 2 days old), overnight cultures of *B. multivorans*, *P. aeruginosa* WT and *P. aeruginosa* Δ*phz* were grown in GMM (20 mM glucose) + AA. Cells were washed (12500 rpm for 2 min) and resuspended in the same medium. OD_{500} values were measured and adjusted for the start of the experiment. Due to growth differences, the conditions involving co-cultures started with four times more *Burkholderia* cells than *Pseudomonas* cell. ODs used were as follows: conditions (i) and (ii) had initial OD_{500} = 0.04 (only *Burkholderia* was present); conditions (iii) and (iv) had final OD_{500} = 0.05, composed from 0.04 of *Burkholderia* cells and 0.01 of *Pseudomonas* cells. Cultures were prepared in 7 mL media using GMM (20 mM glucose) + AA, with either 100 μM PYO (used in condition 2) or the respective amount of HCl added to the cultures. The four tubes were incubated for ~9 hours, and then collected for RNA extraction. For this, 0.7 mL of cultures were spun down (14000 rpm for 2 min), supernatants were removed, and the pellets were immediately frozen using liquid nitrogen and stored at -80ºC. At this same time, PYO concentration produced by the co-culture containing the WT *P. aeruginosa* was measured from the supernatant using absorbance at OD_{691} [102], and ~ 60 μM was detected at the time of sampling.

Next, RNA extraction was performed using the RNeasy kit (Qiagen) following the manufacturer's instructions. Samples were thawed on ice and resuspended in TE buffer (30 mM Tris.Cl, 1 mM EDTA, pH 8.0) containing 15 mg/mL of lysozyme and proteinase K solution (20 mg/mL, Qiagen), followed by an incubation with vortex and lysis steps described in the kit. Purified RNA was then sent for sequencing at the MiGS Center as done for whole-genome

sequencing. The facility pipeline included: (i) DNase treatment (RNAse free) (Invitrogen); (ii) library preparation using Qiagen FastSelect and Library Prep kits (Qiagen) and Ribo-Zero Plus kit (Illumina); (iii) sequencing using a NextSeq500, with 1 x 75 bp reads for the four conditions, with a minimum of 16M reads for conditions 1 and 2 (single *Burkholderia* cultures), or 24M reads for conditions 3 and 4 (co-cultures); (iv) demultiplexing and adaptors trimming using bcl2fastq (version 2.20.0.422). Next, low-quality bases were removed using Trimmomatic (version 0.39) with the following settings: LEADING: 27 TRAILING: 27 SLIDINGWINDOW: 4:20 MINLEN: 35 [97]. Genome mapping and calculation of number of reads per gene was performed through Rockhopper (version 2.03) [103] using the *Burkholderia multivorans* ATCC 17616 genome available in the software as reference. Mapping was done against all three chromosomes (NC_010084; NC_010086; NC_010087), as well as against the pBMUL01 and pTGL1 plasmids (NC_010070 and NC_010802, respectively). Settings within the software were: 0.15 for allowed mismatches; 0.33 for minimum seed length; 500 for max bases between paired reads; 0.5 for minimum expression of UTRs and ncRNAs; and the "strand specific" option was unmarked. Even though the library preparation pipeline included an rRNA depletion step, we retrieved a large amount of rRNA sequences, which were manually deleted from the read-count table exported by Rockhopper. Data exploration and analysis were performed using the online Degust tool [104]. With Degust, counts per million (CPM) for each gene were used for sequencing depth normalization and $\log_2$ fold changes are presented for two different comparison. In comparison 1, condition 1 (*B. multivorans* - no PYO added) was used as a baseline control during fold-changes calculation detected for condition 2 (*B. multivorans* + 100 μM PYO). In comparison 2, condition 4 (*B. multivorans* + *P. aeruginosa* Δ*phz*) was used as baseline control during fold-changes calculation detected for condition 3 (*B. multivorans* + *P. aeruginosa* WT). See Table S2 for the full results. Because our samples consisted of one replicate, no statistical tests were performed. Instead, we used this RNA-seq data as a screen where specific genes of interest (particularly related to efflux) were next explored by qRT-PCR experiments. RNA-seq sequence data was submitted to the NCBI Sequence Read Archive under the accession number TBD.

Quantitative reverse transcription PCR (qRT-PCR)

Experiment 1: validation of RNA-seq. The set up for this experiment was exactly the same as the RNA-seq described above, with the exception that three independent replicates were prepared. For each strain used in this experiment (*B. multivorans* 1, *P. aeruginosa* WT, *P. aeruginosa* Δ*phz*), three independent overnight cultures were grown in GMM (20 mM glucose) + AA. Each of overnights were inoculated from three different spots from the freshly streaked LB plates of each strain. Next, each one of these overnight cultures was used in the inoculum preparation of the four different conditions, as described in the RNA-seq section. Again, the conditions were: (i) *B. multivorans* (no PYO); (ii) *B. multivorans* + 100 μM PYO; (iii) *B. multivorans* + *P. aeruginosa* WT (co-culture, PYO and other phenazines produced); and (iv) *B. multivorans* + *P. aeruginosa* Δ*phz* (co-culture, no PYO or phenazines produced). A total of 12 tubes were prepared (three for each conditions). These were grown for ~9 hours, after which the pellets were collected (from 0.7 mL of culture), immediately frozen using liquid nitrogen, and stored at -80ºC for later RNA extraction.

Experiment 2: measuring the SoxR effect on PYO-mediated induction of RND-9. Four different conditions were prepared for this qRT-PCR experiment: (i) *B. multivorans* Δ*soxR*; (ii) *B. multivorans* Δ*soxR* + 100 μM PYO; (iii) *B. multivorans* Δ*soxR* comp; (iii) *B. multivorans* Δ*soxR* comp + 100 μM PYO. Three independent overnight cultures of each strain were grown in GMM (20 mM glucose) + AA, cells were then washed and resuspended at an OD_{500} of 0.04 in fresh GMM (20 mM glucose, 7 mL culture). Three replicates were prepared for each condition, with a total of 12 samples. Depending on the condition, either 100 μM PYO or the respective amount of HCl was added to the cultures. Cultures were then incubated for ~10 hours, after which the pellets were collected (from 0.7-1 mL of culture), immediately frozen using liquid nitrogen, and stored at -80ºC for later RNA extraction.

Experiment 3: measuring the SoxR effect on TOX-mediated induction of RND-9: Six different conditions were prepared for this qRT-PCR experiment. Each of the three tested strains (*B. multivorans* WT, Δ*soxR* and Δ*soxR* comp) were grown with and without 50 μM TOX. Three independent overnight cultures of each strain were grown in GMM (20 mM glucose) + AA, cells

were then washed and resuspended at an OD_{500} of 0.05 in fresh GMM + AA (20 mM glucose, 5 mL culture). Again, three replicates were prepared for each condition, with a total of 18 samples. Either 50 μM TOX or the respective amount of DMSO was added to the cultures. These cultures were incubated for ~20 hours, cells were pelleted (from 0.7 mL of culture), immediately frozen using liquid nitrogen, and stored at -80ºC for later RNA extraction.

For the next steps, we followed previously published protocols [17,39,105]. RNA extraction was performed as described in these studies and in the RNA-seq experiment using the RNeasy kit (Qiagen). Contaminant gDNA was removed using TURBO DNA-free kit (Invitrogen, Waltham, Massachusetts, USA), and cDNA was synthesized using the iScript cDNA Synthesis kit (Bio-Rad, Hercules, California, USA) (a total of 0.8 μg of total RNA was used), following the manufacturer's instructions. Then, qRT-PCR reactions were performed using iTaq Universal SYBR Green Supermix (Bio-Rad) (total of 20 μL per reaction) using a 7500 Fast Real-Time PCR System machine (Applied Biosystems, Waltham, Massachusetts, USA). For additional details on the protocol, see [39]. Finally, within each run, standard curves for each primer pair were prepared using known concentration of *B. multivorans* WT gDNA to calculate amounts of cDNA for each of the target genes. The gene Bmul_2161 (annotated as *uvrC*, coding for excinuclease ABC subunit C) was used as housekeeping gene during normalizations. As an additional control, we also ran reactions with the housekeeping gene Bmul_1456 (annotated as *rumA* gene, coding for the 23S rRNA 5-methyluridine methyltransferase) [106]. Primer pairs sequences are available in Table S1.

Data showing total *uvrC*-normalized cDNA levels and/or the $\log_2$ fold change in expression are shown in Fig. 1C-D, Fig. 2B, Fig. 3F, Fig. S1, Fig S2, and Fig. S9. Normalizations for cDNA measurement followed what we have previously described for *oprI*-normalized cDNA in *P. aeruginosa* [17], but using the *uvrC* gene instead. In brief, the cDNA estimated for a certain gene in a certain sample was divided by the respective cDNA estimated for *uvrC* in the same sample [17]. In some occasions, we also present the data as fold changes. These were calculated for each replicate relative to the mean cDNA value of the replicates within the negative control. The "no treatment" samples (i.e. "no PYO" or "no TOX") were used as negative controls for conditions where *B. multivorans* was in single-species cultures (in experiments 1, 2 and 3); meanwhile, the

"*B. multivorans* + *P. aeruginosa* Δ*phz*" samples was used as negative control for the "*B. multivorans* + *P. aeruginosa* WT" condition (in experiment 1). Importantly, we noticed the one replicate for three following conditions had significantly lower amounts of cDNA by the end of our qRT-PCR protocol: "*B. multivorans* + *P. aeruginosa* WT" and "*B. multivorans* + *P. aeruginosa* Δ*phz*" within experiment 1, and "Δ*soxR* no TOX" in experiment 3. These were removed from the analysis as noted in the legends of figures where this data is displayed.

Antibiotics used for tolerance and resistance assays

The following antibiotics were used in this study: ciprofloxacin (Fluka), levofloxacin (Sigma-Aldrich), tetracycline (tetracycline hydrochloride, Sigma-Aldrich), doxycycline (doxycycline hyclate, Sigma-Aldrich), tobramycin (TCI), colistin (colistin sulfate salt, Sigma-Aldrich), ceftazidime (TCI, containing ca. 10% Na_2CO_3), chloramphenicol (Sigma-Aldrich), meropenem (meropenem trihydrate, Sigma-Aldrich), trimethoprim (Sigma-Aldrich), and sulfamethoxazole (Sigma-Aldrich). Stock solutions of the antibiotics used were prepared in different solvents. Ciprofloxacin was dissolved in 20 mM HCl; levofloxacin, tetracycline, doxycycline, tobramycin, colistin and ceftazidime were dissolved in deionized water; chloramphenicol, meropenem and trimethoprim-sulfamethoxazole (mixed at 1:1 ratio) were dissolved in DMSO. Stock concentrations used were of 1 mg/mL for ciprofloxacin and levofloxacin, and 10 mg/mL for all other antibiotics.

Antibiotic tolerance assays with single species

A growth curve assay was used to measure resistance levels to PYO, following a previously described protocol [17]. Briefly, cells of the respective strain used were grown from a fresh plate into overnight cultures in GMM + AA with 20 mM glucose. Cells were then pelleted, washed, and resuspended in four independent cultures per treatment at an OD_{500} of 0.05 in GMM + AA, with 10 mM glucose. Treatments involved addition or not of the redox-active secondary metabolite (PYO, PCA or TOX, at the respective concentration displayed in the figures). These four independent replicates were prepared in 7 mL (for PYO and PCA) or 5 mL cultures (for TOX), always using 18 × 150 mm glass tubes, and incubated for around 20 hours. This was enough for

cells to reach stationary phase. Next, each individual culture was then split into a "no antibiotic" negative control, or an "+ antibiotic" treatment as done before [17], using 2 mL of culture per treatment in plastic Falcon tubes (VWR, Cat. No. 352059). After antibiotic treatment was added, cultures were then incubated for four hours under shaking conditions. Finally, cultures were serially diluted using Minimum Phosphate Buffer (50 mM KH_2PO_4/K_2HPO_4, 42.8 mM NaCl, pH 7.2) and plated for CFUs using LB agar plates. These plates were then incubated at room temperature, with CFUs counted after 36-48 hours. To check for slow-growing/late-arising colonies, plates were also checked after 5-7 days. This protocol was used for all the strains mentioned in the figures containing antibiotic assays with single species cultures. These included: *B. multivorans* 1 (WT, Δ*soxR* or Δ*soxR* comp strains), and *B. glumae* (WT and Δ*toxA* strains). The antibiotic used was ciprofloxacin (at 10 µg/mL), as indicated in the figure legends.

Growth curves for measuring resistance to PYO and data analysis

A growth curves assay was used to measure resistance levels to PYO, following conditions previously described [17]. Briefly, the several *Burkholderia* strains listed in Figs 2E and S4 (also see Table S1 for additional details) were used in this experiment. Each strain was grown overnight from a fresh plate in GMM with 20 mM glucose + AA. Cells were then pelleted, washed, and resuspended at an OD_{500} = 0.05 using the same medium (this was the initial OD used in the experiment). The experiment was set up in 96-well plates, with different concentration of PYO being used (0, 10, 100, or 200 µM). Three wells were prepared for each treatment, and each well was considered an independent replicate. The total volume within each well contained 150 µL of culture and 70 µL of mineral on top (used for evaporation prevention). Incubation proceeded for 24 hours at 37ºC under shaking conditions. A Spark 10M plate reader was used (Tecan), with absorbance readings at an OD_{500} every 15 minutes.

Data analysis was performed using a custom Python software containing tools for data processing/analysis/visualization designed for the datasets exported from our plate readers (available at: https://github.com/jciemniecki/dknlab_tools, version 1.1.0). Growth curves for all the strains and treatments can be seen in Fig. S5. Next, growth rates were determined using linear fits of the linear range of these growth curves (time range used: 3-8 hours for all strains except the

slow growers *B. cenocepacia* J2315 and *B. gladioli* 3; for which a range of 3-15 hours was used). This was done using a linear regression function (also available at the same GitHub repository). Means of the growth rates were calculated for each strain/treatment based on the data from the three replicates. Finally, for each strain, these growth rate means obtained for treatments containing the different concentrations of PYO (10, 100 and 200 μM) were normalized (i.e. divided by) the growth rate means obtained for the "No PYO" control to calculate the "growth rate ratio" displayed in Fig. 2E.

Antibiotic tolerance assays with co-cultures

Antibiotic tolerance assays using co-cultures were performed using a membrane-separated 12-well tissue plate cultures containing 0.1 μm pore PET membranes (VWR, Cat. No. 10769–226), following previously protocols [17]. These were used (i) to study how *P. aeruginosa* can have affect antibiotic tolerance levels of different strains *B. multivorans* 1; (ii) to study how multiple TOX producers (*B. glumae* and *B. gladioli* strains) can affect antibiotic tolerance levels of several Bcc species. Overnight cultures were grown for each strain in GMM (20 mM glucose) + AA, cells were pelleted, washed, and resuspended in the same medium at different OD_{500}: 0.05 for redox-active metabolites producers; and 0.025 for the Bcc species (in which antibiotic susceptibility was evaluated). Producers (*P. aeruginosa*, *B. glumae* and *B. gladioli* strains) were cultured in the bottom part of the well using a volume of 600 μL, while Bcc were cultured in the upper part of the well using a volume of 100 μL. The experimental design can be seen in Fig. 3G. When grown alone (i.e., no producer), the Bcc strain was added to both bottom and upper part of the well. Cells were grown under shaking conditions (175 rpm) for ~20 hours at 37ºC, with the plates placed within airtight plastic container. Several wet paper towels were used to maintain humidity. Next, ciprofloxacin was then added (10 μg/mL), and cultures were incubated for additional four hours. Within each plate, three replicates (wells) were used for "no antibiotic" (negative control) and three replicates for "+ ciprofloxacin" treatment. After incubation, the upper part of the co-cultures (containing the Bcc cells) was plated for CFUs on LB agar plates using serial dilution as described above.

In addition to the co-cultures grown on the membrane-separated 12-well tissue plate, we also performed a co-culture assay using 18 x 150 mm glass tubes (Fig. 1B, right). Here, *B. multivorans* 1 WT was grown together with *P. aeruginosa* WT or Δ*phz* in 7 mL cultures with a total starting OD_{500} of 0.05 (0.025 for each species). Four independent replicates were prepared, cultures were grown for 20 hours, treated with ciprofloxacin (10 μg/mL), and plated for CFUs as described before. Differently from the membrane-separated plates used before, the two species were mixed in this assay. However, *P. aeruginosa* and *B. multivorans* colonies display different morphologies and growth rates, allowing for visual distinction in the "no antibiotic" control treatment. Moreover, *P. aeruginosa* is orders of magnitude more susceptible to the drug than *B. multivorans* under the concentration used (10 μg/mL), allowing for easy counting of the *B. multivorans* colonies in the "+ ciprofloxacin" treatments (Fig. 1B).

Determination of minimum inhibitory concentrations (MICs)

MIC assays using pure redox-active molecules: MICs were determined following the EUCAST standard clinical methods suggested for broth microdilution assays [107], with modifications to account for the effects of redox-active molecules (e.g., PYO or TOX). Briefly, *B. multivorans* 1 cultures was grown from a fresh LB plate into MH broth, and were then diluted 1:100 into three independent replicates (5 mL) and grown for 14-18 hours until stationary phase. These three independent replicates were individually resuspended and used as inocula in 2-fold dilution series assays using 96-well microtiter plates, the 10 antibiotics mentioned before, and the redox-active molecules. The final concentrations used for PYO and TOX were 100 μM and 50 μM, respectively; controls involved adding the equivalent amount of the solvents used to solubilize these molecules (20 mM HCl for PYO, or DMSO for TOX). One antibiotic was used per plate, and the plate design can be seen in Fig. S10A, with each well having a final volume of 100 μL. Appropriate "no antibiotic" and "no cells" controls were always prepared (Fig. S10A). After inoculation, the microtiter plates were sealed with a plastic film (to avoid evaporation), wrapped in aluminum foil, and incubated without shaking at 37ºC for 18 hours. Microtiter plates were always incubated in a single layer. After incubation, the wells were assessed for growth (turbidity) using a BioTek Synergy 4 plate reader (BioTek) or a Spark 10M plate reader (Tecan). Growth

assessment was also done by naked eye as suggested by the reading guide for broth microdilutions by EUCAST (version 3.0, January 1st, 2021), and used for the OD_{500} thresholding (see the data analysis section below).

MIC assays using spent media from pathogens' cultures: these assays followed the same design described above, with the exception that instead of using pure redox-active molecules, a filtered-sterilized spent media from stationary cultures was mixed to fresh media and used during 2-fold dilution series assays. In summary, cultures of the strains in which spent media were analyzed (*P. aeruginosa* WT, *P. aeruginosa* Δ*phz*, and *B. multivorans* WT) were grown in MH broth, diluted back 1:100 into 50 mL cultures (initial OD_{500} = ~0.05), and grown for around 12 hours for metabolite production. Cells were then spun down (5000 rpm for 10 minutes, twice), and the supernatant containing the spent media was collected and filter-sterilized through a large bottle top filter (Millipore, Cat. No. SCGPS02RE). The filtered spent media samples were plated on LB agar for contamination verification. Then, spent media samples were mixed with fresh MH broth (1/4 of the final volume was spent media) during 2-fold dilution series assays using the antibiotics indicated in Fig. 4E and Fig. S11D-E. Importantly, spent medium from *P. aeruginosa* WT contained ~80-100 μM PYO measured by absorbance at 691 nm, meaning that the final PYO concentration on microtiter plates were around 20-25 μM. Incubation and growth assessment protocol followed what was described above.

Data analysis: after turbidity measurements by OD_{500} absorbance and inspection by naked eye, we adopted OD_{500} = 0.11 as a threshold value for the indication of growth in the microtiter plates. This means that this was the lowest absorbance where growth could be detected by naked eye; any reading value lower than this was determined "no growth." This threshold was applied to the raw absorbance values, and no normalizations by the "no cells" controls wells were done at this stage. MIC values for each treatment tested are available in Table S4. Next, calculation of the molecules' "Effect on MIC (log_2 fold change)" in Figs. 4B-C were performed as follows: for each antibiotic, MIC values detected for treatments containing PYO or TOX were divided by the MIC detected in respective negative controls (where HCl or DMSO were added, respectively). The plate design was always the same, and individual ratios were calculated within each replicate (for each

antibiotic, all replicates were prepared in parallel on the same day and plate – see Fig. S10A for design). These ratios were then log_2-transformed and are shown in Figs. 4B-C. Finally, for MICs detected in experiments containing spent media (from the *P. aeruginosa* strains or from *B. multivorans*), the plates were prepared on different days from the original experiments with the pure molecules. However, because MIC values were consistent (i.e. HCl or DMSO did not seem to affect the MICs measured at the amounts used), the same negative controls used for ratios' calculation in the experiments with pure molecules were also used for the ratios' calculation in experiments with spent media. Specifically, the "No PYO" controls (i.e. where HCl was added) were used for this purpose. Again, these ratios were log_2-transformed and are shown in Fig. 4E and Fig. S11D-E.

Finally, we realized that sometimes, even though the MIC detected itself did not change, treatments could alter the growth detected at the pre-MIC concentrations. For this reason, we have also included plots with the OD_{500} absorbance measurements and the log_2 fold change for OD_{500} absorbances between different treatment. For this, the absorbances measurements were normalized by their respective "no cells" control wells within the same plate. Then, as done for the MICs values, the fold changes were determined by calculating the ratio for each treatment (PYO or TOX) by their respective negative control within each replicate (e.g. absorbance for condition "+PYO replicate 1 in TET" divided by "+HCl replicate 1 in TET"), and these values were log_2 transformed. This was only done for experiments using pure molecules, since these were performed in parallel (i.e. same day) with their respective solvent control. Both OD_{500} normalized absorbance measurements and their log_2 fold change are shown (Fig. S11A-B and Fig. 4D, respectively).

Measurements of PYO and TOX concentrations

PYO concentrations in cultures containing *P. aeruginosa* WT were estimated by absorbance of the culture supernatant at 691 nm [102] using standard curves with the pure molecule. A similar approach was used for estimation of TOX concentrations within cultures containing *B. glumae* and *B. gladioli*. UV-Vis spectra (200-800 nm) were recorded using a spectrophotometer (Beckman Coulter DU 800) for solutions containing pure TOX (100, 50, 25 μM), and supernatants of overnight cultures (grown GMM, 20 mM glucose + AA) of the following

strains: *B. glumae* WT, B. *gladioli* 1 and *B. gladioli* 2. Moreover, supernatants of *B. glumae* Δ*toxA* and *B. multivorans* 1 strains grown in the same medium were used as negative controls since these strains cannot make TOX. Concentrations estimations were done for each sample based on characteristic absorbance of the molecule at 393 nm [47,54], calibrated by the absorbance values obtained for the standards using the pure molecule. Because only oxidized TOX absorbs at 393 nm, after being taken out of the shaking incubator, cultures were immediately spun down for supernatant collection. Absorbance spectra within the 300-500 nm range for these samples are shown in Fig. S8.

Data wrangling, analysis, and visualization

Data wrangling and analysis involved a combination of processing in (i) Python (version 3.8), using the Pandas (version 1.3.1) [108,109] and NumPy (version 1.20.3) [110] libraries; or in (ii) Microsoft Excel (version 16.39), as described throughout the Materials and Methods section. All the visualization presented in the manuscript was performed using Matplotlib (version 3.4.2) [111] and Seaborn (version 0.11.1) [112]. 95% confidence intervals presented in the figures were estimated with Seaborn while plotting the respective data using 10,000 bootstraps. Plots legends and their display organization within each figure were adjusted using Affinity Designer (Serif, version 1.10.4). The same software was used for drawing all the illustrations shown in the manuscript.

Acknowledgements

We thank Newman lab members for feedback and advice throughout the development of this project. In particular, we thank Megan Bergkessel for assistance and discussions about the RNA-seq, John Ciemniecki for developing and sharing the "dknlab_tools" package used during plate reader data analysis, John LiPuma (University of Michigan, CFF *Burkholderia cepacia* Research Laboratory and Repository) for providing the clinical *Burkholderia* strains, and the Microbial Genome Sequencing Center (MiGS) at Pittsburgh for sequencing of the samples. Finally, we thank Jong Ham and Inderjit Barphagha (Louisiana State University) for providing the *B. glumae* 336gr-1 strains (WT and Δ*toxA*), and Joanna Goldberg (Emory University) for

providing the pEX18Tc plasmid. This work was supported by grants to D.K.N from the NIH (1R01AI127850-01A1, 1R01HL152190-01) and the Doren Family Foundation.

References

1. Fair RJ, Tor Y. Antibiotics and bacterial resistance in the 21st century. Perspect Medicin Chem. 2014;6: 25–64.
2. MacLean RC, San Millan A. The evolution of antibiotic resistance. Science. 2019;365: 1082–1083.
3. Hutchings MI, Truman AW, Wilkinson B. Antibiotics: past, present and future. Curr Opin Microbiol. 2019;51: 72–80.
4. O'Neill J. Tackling drug-resistant infections globally: final report and recommendations. 2016.
5. Levin-Reisman I, Ronin I, Gefen O, Braniss I, Shoresh N, Balaban NQ. Antibiotic tolerance facilitates the evolution of resistance. Science. 2017;355: 826–830.
6. Blair JMA, Webber MA, Baylay AJ, Ogbolu DO, Piddock LJV. Molecular mechanisms of antibiotic resistance. Nat Rev Microbiol. 2015;13: 42–51.
7. Windels EM, Michiels JE, Van den Bergh B, Fauvart M, Michiels J. Antibiotics: combatting tolerance to stop resistance. MBio. 2019;10.
8. Windels EM, Michiels JE, Fauvart M, Wenseleers T, Van den Bergh B, Michiels J. Bacterial persistence promotes the evolution of antibiotic resistance by increasing survival and mutation rates. ISME J. 2019;13: 1239–1251.
9. Kester JC, Fortune SM. Persisters and beyond: mechanisms of phenotypic drug resistance and drug tolerance in bacteria. Crit Rev Biochem Mol Biol. 2014;49: 91–101.
10. Brauner A, Fridman O, Gefen O, Balaban NQ. Distinguishing between resistance, tolerance and persistence to antibiotic treatment. Nat Rev Microbiol. 2016;14: 320–330.
11. Balaban NQ, Helaine S, Lewis K, Ackermann M, Aldridge B, Andersson DI, et al. Definitions and guidelines for research on antibiotic persistence. Nat Rev Microbiol. 2019;17: 441–448.
12. Perry EK, Meirelles LA, Newman DK. From the soil to the clinic: the impact of microbial secondary metabolites on antibiotic tolerance and resistance. Nat Rev Microbiol. 2021;
13. Davies J. Specialized microbial metabolites: functions and origins. J Antibiot. 2013;66: 361–364.
14. Price-Whelan A, Dietrich LEP, Newman DK. Rethinking "secondary" metabolism: physiological roles for phenazine antibiotics. Nat Chem Biol. 2006;2: 71–78.
15. Tyc O, Song C, Dickschat JS, Vos M, Garbeva P. The ecological role of volatile and soluble secondary metabolites produced by soil bacteria. Trends Microbiol. 2017;25: 280–292.
16. Radlinski L, Rowe SE, Kartchner LB, Maile R, Cairns BA, Vitko NP, et al. *Pseudomonas aeruginosa* exoproducts determine antibiotic efficacy against *Staphylococcus aureus*. PLoS Biol. 2017;15: e2003981.
17. Meirelles LA, Perry EK, Bergkessel M, Newman DK. Bacterial defenses against a natural antibiotic promote collateral resilience to clinical antibiotics. PLoS Biol. 2021;19: e3001093.
18. Jo J, Cortez KL, Cornell WC, Price-Whelan A, Dietrich LE. An orphan cbb3-type cytochrome oxidase subunit supports *Pseudomonas aeruginosa* biofilm growth and virulence. Elife. 2017;6: e30205.

19. Glasser NR, Kern SE, Newman DK. Phenazine redox cycling enhances anaerobic survival in *Pseudomonas aeruginosa* by facilitating generation of ATP and a proton-motive force. Mol Microbiol. 2014;92: 399–412.
20. Imlay JA. The molecular mechanisms and physiological consequences of oxidative stress: lessons from a model bacterium. Nat Rev Microbiol. 2013;11: 443–454.
21. Laursen JB, Nielsen J. Phenazine natural products: biosynthesis, synthetic analogues, and biological activity. Chem Rev. 2004;104: 1663–1686.
22. Gu M, Imlay JA. The SoxRS response of *Escherichia coli* is directly activated by redox-cycling drugs rather than by superoxide. Mol Microbiol. 2011;79: 1136–1150.
23. Singh AK, Shin J-H, Lee K-L, Imlay JA, Roe J-H. Comparative study of SoxR activation by redox-active compounds. Mol Microbiol. 2013;90: 983–996.
24. Davies J, Davies D. Origins and evolution of antibiotic resistance. Microbiol Mol Biol Rev. 2010;74: 417–433.
25. Martinez JL. The role of natural environments in the evolution of resistance traits in pathogenic bacteria. Proc Biol Sci. 2009;276: 2521–2530.
26. Waglechner N, McArthur AG, Wright GD. Phylogenetic reconciliation reveals the natural history of glycopeptide antibiotic biosynthesis and resistance. Nat Microbiol. 2019;4: 1862–1871.
27. Driscoll JA, Brody SL, Kollef MH. The epidemiology, pathogenesis and treatment of *Pseudomonas aeruginosa* infections. Drugs. 2007;67: 351–368.
28. Lipuma JJ. The changing microbial epidemiology in cystic fibrosis. Clin Microbiol Rev. 2010;23: 299–323.
29. Coutinho CP, Dos Santos SC, Madeira A, Mira NP, Moreira AS, Sá-Correia I. Long-term colonization of the cystic fibrosis lung by *Burkholderia cepacia* complex bacteria: epidemiology, clonal variation, and genome-wide expression alterations. Front Cell Infect Microbiol. 2011;1: 12.
30. Rhodes KA, Schweizer HP. Antibiotic resistance in *Burkholderia* species. Drug Resist Updat. 2016;28: 82–90.
31. Lau GW, Hassett DJ, Ran H, Kong F. The role of pyocyanin in *Pseudomonas aeruginosa* infection. Trends Mol Med. 2004;10: 599–606.
32. Wilson R, Sykes DA, Watson D, Rutman A, Taylor GW, Cole PJ. Measurement of *Pseudomonas aeruginosa* phenazine pigments in sputum and assessment of their contribution to sputum sol toxicity for respiratory epithelium. Infect Immun. 1988;56: 2515–2517.
33. Cruickshank CN, Lowbury EJ. The effect of pyocyanin on human skin cells and leucocytes. Br J Exp Pathol. 1953;34: 583–587.
34. Bartell JA, Blazier AS, Yen P, Thøgersen JC, Jelsbak L, Goldberg JB, et al. Reconstruction of the metabolic network of *Pseudomonas aeruginosa* to interrogate virulence factor synthesis. Nat Commun. 2017;8: 14631.
35. Podnecky NL, Rhodes KA, Schweizer HP. Efflux pump-mediated drug resistance in *Burkholderia*. Front Microbiol. 2015;6: 305.
36. Li X-Z, Plésiat P, Nikaido H. The challenge of efflux-mediated antibiotic resistance in Gram-negative bacteria. Clin Microbiol Rev. 2015;28: 337–418.

37. Winsor GL, Griffiths EJ, Lo R, Dhillon BK, Shay JA, Brinkman FSL. Enhanced annotations and features for comparing thousands of *Pseudomonas* genomes in the *Pseudomonas* genome database. Nucleic Acids Res. 2016;44: D646-53.
38. Dietrich LE, Price-Whelan A, Petersen A, Whiteley M, Newman DK. The phenazine pyocyanin is a terminal signalling factor in the quorum sensing network of *Pseudomonas aeruginosa*. Mol Microbiol. 2006;61: 1308–1321.
39. Meirelles LA, Newman DK. Both toxic and beneficial effects of pyocyanin contribute to the lifecycle of *Pseudomonas aeruginosa*. Mol Microbiol. 2018;110: 995–1010.
40. Dietrich LEP, Teal TK, Price-Whelan A, Newman DK. Redox-active antibiotics control gene expression and community behavior in divergent bacteria. Science. 2008;321: 1203–1206.
41. Du D, Wang-Kan X, Neuberger A, van Veen HW, Pos KM, Piddock LJV, et al. Multidrug efflux pumps: structure, function and regulation. Nat Rev Microbiol. 2018;16: 523–539.
42. Depoorter E, Bull MJ, Peeters C, Coenye T, Vandamme P, Mahenthiralingam E. *Burkholderia*: an update on taxonomy and biotechnological potential as antibiotic producers. Appl Microbiol Biotechnol. 2016;100: 5215–5229.
43. Winsor GL, Khaira B, Van Rossum T, Lo R, Whiteside MD, Brinkman FSL. The *Burkholderia* Genome Database: facilitating flexible queries and comparative analyses. Bioinformatics. 2008;24: 2803–2804.
44. Chen I-MA, Chu K, Palaniappan K, Ratner A, Huang J, Huntemann M, et al. The IMG/M data management and analysis system v.6.0: new tools and advanced capabilities. Nucleic Acids Res. 2021;49: D751–D763.
45. Mukherjee S, Stamatis D, Bertsch J, Ovchinnikova G, Sundaramurthi JC, Lee J, et al. Genomes OnLine Database (GOLD) v.8: overview and updates. Nucleic Acids Res. 2021;49: D723–D733.
46. Jeong Y, Kim J, Kim S, Kang Y, Nagamatsu T, Hwang I. Toxoflavin produced by *Burkholderia glumae* causing rice grain rot is responsible for inducing bacterial wilt in many field crops. Plant Dis. 2003;87: 890–895.
47. Chen R, Barphagha IK, Karki HS, Ham JH. Dissection of quorum-sensing genes in *Burkholderia glumae* reveals non-canonical regulation and the new regulatory gene *tofM* for toxoflavin production. PLoS One. 2012;7: e52150.
48. Lee J, Park J, Kim S, Park I, Seo Y-S. Differential regulation of toxoflavin production and its role in the enhanced virulence of *Burkholderia gladioli*. Mol Plant Pathol. 2016;17: 65–76.
49. Ham JH, Melanson RA, Rush MC. *Burkholderia glumae*: next major pathogen of rice? Mol Plant Pathol. 2011;12: 329–339.
50. Jones C, Webster G, Mullins AJ, Jenner M, Bull MJ, Dashti Y, et al. Kill and cure: genomic phylogeny and bioactivity of *Burkholderia gladioli* bacteria capable of pathogenic and beneficial lifestyles. Microb Genom. 2021;7.
51. Stern KG. Oxidation-reduction potentials of toxoflavin. Biochem J. 1935;29: 500–508.
52. Latuasan HE, Berends W. On the origin of the toxicity of toxoflavin. Biochim Biophys Acta. 1961;52: 502–508.
53. Schiessl KT, Hu F, Jo J, Nazia SZ, Wang B, Price-Whelan A, et al. Phenazine production promotes antibiotic tolerance and metabolic heterogeneity in *Pseudomonas aeruginosa* biofilms. Nat Commun. 2019;10: 762.

54. Kim J, Kim J-G, Kang Y, Jang JY, Jog GJ, Lim JY, et al. Quorum sensing and the LysR-type transcriptional activator ToxR regulate toxoflavin biosynthesis and transport in Burkholderia glumae. Mol Microbiol. 2004;54: 921–934.
55. Lelis T, Peng J, Barphagha I, Chen R, Ham JH. The virulence function and regulation of the metalloprotease gene *prtA* in the plant-pathogenic bacterium *Burkholderia glumae*. Mol Plant Microbe Interact. 2019;32: 841–852.
56. Graves M, Robin T, Chipman AM, Wong J, Khashe S, Janda JM. Four additional cases of *Burkholderia gladioli* infection with microbiological correlates and review. Clin Infect Dis. 1997;25: 838–842.
57. Kennedy MP, Coakley RD, Donaldson SH, Aris RM, Hohneker K, Wedd JP, et al. *Burkholderia gladioli*: five year experience in a cystic fibrosis and lung transplantation center. J Cyst Fibros. 2007;6: 267–273.
58. Jorgensen JH, Ferraro MJ. Antimicrobial susceptibility testing: a review of general principles and contemporary practices. Clin Infect Dis. 2009;49: 1749–1755.
59. Zhu K, Chen S, Sysoeva TA, You L. Universal antibiotic tolerance arising from antibiotic-triggered accumulation of pyocyanin in *Pseudomonas aeruginosa.* PLoS Biol. 2019;17: e3000573.
60. Jacob C, Jamier V, Ba LA. Redox active secondary metabolites. Curr Opin Chem Biol. 2011;15: 149–155.
61. Glasser NR, Saunders SH, Newman DK. The colorful world of extracellular electron shuttles. Annu Rev Microbiol. 2017;71: 731–751.
62. Saunders SH, Tse ECM, Yates MD, Otero FJ, Trammell SA, Stemp EDA, et al. Extracellular DNA promotes efficient extracellular electron transfer by pyocyanin in *Pseudomonas aeruginosa* biofilms. Cell. 2020;182: 919–932.e19.
63. Liu GY, Nizet V. Color me bad: microbial pigments as virulence factors. Trends Microbiol. 2009;17: 406–413.
64. Dietrich LEP, Okegbe C, Price-Whelan A, Sakhtah H, Hunter RC, Newman DK. Bacterial community morphogenesis is intimately linked to the intracellular redox state. J Bacteriol. 2013;195: 1371–1380.
65. Ramos I, Dietrich LE, Price-Whelan A, Newman DK. Phenazines affect biofilm formation by *Pseudomonas aeruginosa* in similar ways at various scales. Res Microbiol. 2010;161: 187–191.
66. Sheplock R, Recinos DA, Mackow N, Dietrich LEP, Chander M. Species-specific residues calibrate SoxR sensitivity to redox-active molecules. Mol Microbiol. 2013;87: 368–381.
67. Lee K-L, Singh AK, Heo L, Seok C, Roe J-H. Factors affecting redox potential and differential sensitivity of SoxR to redox-active compounds. Mol Microbiol. 2015;97: 808–821.
68. Schwab U, Abdullah LH, Perlmutt OS, Albert D, Davis CW, Arnold RR, et al. Localization of *Burkholderia cepacia* complex bacteria in cystic fibrosis lungs and interactions with *Pseudomonas aeruginosa* in hypoxic mucus. Infect Immun. 2014;82: 4729–4745.
69. Chmiel JF, Aksamit TR, Chotirmall SH, Dasenbrook EC, Elborn JS, LiPuma JJ, et al. Antibiotic management of lung infections in cystic fibrosis. I. The microbiome, methicillin-resistant *Staphylococcus aureus*, gram-negative bacteria, and multiple infections. Annals of the American Thoracic Society. 2014;11: 1120–1129.

70. Folescu TW, da Costa CH, Cohen RWF, da Conceição Neto OC, Albano RM, Marques EA. *Burkholderia cepacia* complex: clinical course in cystic fibrosis patients. BMC Pulm Med. 2015;15: 158.
71. Wilbert SA, Mark Welch JL, Borisy GG. Spatial ecology of the human tongue dorsum microbiome. Cell Rep. 2020;30: 4003–4015.e3.
72. DePas WH, Starwalt-Lee R, Van Sambeek L, Ravindra Kumar S, Gradinaru V, Newman DK. Exposing the three-dimensional biogeography and metabolic states of pathogens in cystic fibrosis sputum via hydrogel embedding, clearing, and rRNA labeling. MBio. 2016;7: e00796-16.
73. Earle KA, Billings G, Sigal M, Lichtman JS, Hansson GC, Elias JE, et al. Quantitative imaging of gut microbiota spatial organization. Cell Host Microbe. 2015;18: 478–488.
74. Shi H, Shi Q, Grodner B, Lenz JS, Zipfel WR, Brito IL, et al. Highly multiplexed spatial mapping of microbial communities. Nature. 2020;588: 676–681.
75. Skinnider MA, Johnston CW, Gunabalasingam M, Merwin NJ, Kieliszek AM, MacLellan RJ, et al. Comprehensive prediction of secondary metabolite structure and biological activity from microbial genome sequences. Nat Commun. 2020;11: 6058.
76. Vernocchi P, Del Chierico F, Putignani L. Gut microbiota profiling: metabolomics based approach to unravel compounds affecting human health. Front Microbiol. 2016;7: 1144.
77. Agus A, Clément K, Sokol H. Gut microbiota-derived metabolites as central regulators in metabolic disorders. Gut. 2021;70: 1174–1182.
78. Garg N, Wang M, Hyde E, da Silva RR, Melnik AV, Protsyuk I, et al. Three-dimensional microbiome and metabolome cartography of a diseased human lung. Cell Host Microbe. 2017;22: 705–716.e4.
79. Bauermeister A, Mannochio-Russo H, Costa-Lotufo LV, Jarmusch AK, Dorrestein PC. Mass spectrometry-based metabolomics in microbiome investigations. Nat Rev Microbiol. 2021.
80. Zimmermann M, Patil KR, Typas A, Maier L. Towards a mechanistic understanding of reciprocal drug-microbiome interactions. Mol Syst Biol. 2021;17: e10116.
81. Maier L, Pruteanu M, Kuhn M, Zeller G, Telzerow A, Anderson EE, et al. Extensive impact of non-antibiotic drugs on human gut bacteria. Nature. 2018;555: 623–628.
82. Maier L, Goemans CV, Wirbel J, Kuhn M, Eberl C, Pruteanu M, et al. Unravelling the collateral damage of antibiotics on gut bacteria. Nature. 2021;599: 120–124.
83. Brochado AR, Telzerow A, Bobonis J, Banzhaf M, Mateus A, Selkrig J, et al. Species-specific activity of antibacterial drug combinations. Nature. 2018;559: 259–263.
84. Widdel F, Pfennig N. Studies on dissimilatory sulfate-reducing bacteria that decompose fatty acids. Arch Microbiol. 1981;129: 395–400.
85. Cheluvappa R. Standardized chemical synthesis of *Pseudomonas aeruginosa* pyocyanin. MethodsX. 2014;1: 67–73.
86. Costa KC, Glasser NR, Conway SJ, Newman DK. Pyocyanin degradation by a tautomerizing demethylase inhibits *Pseudomonas aeruginosa* biofilms. Science. 2017;355: 170–173.
87. Hoang TT, Karkhoff-Schweizer RR, Kutchma AJ, Schweizer HP. A broad-host-range Flp-FRT recombination system for site-specific excision of chromosomally-located DNA sequences: application for isolation of unmarked *Pseudomonas aeruginosa* mutants. Gene. 1998;212: 77–86.

88. Huang W, Wilks A. A rapid seamless method for gene knockout in *Pseudomonas aeruginosa*. BMC Microbiol. 2017;17: 199.
89. Gibson DG, Young L, Chuang R-Y, Venter JC, Hutchison CA, Smith HO. Enzymatic assembly of DNA molecules up to several hundred kilobases. Nat Methods. 2009;6: 343–345.
90. Simon R, Priefer U, Pühler A. A broad host range mobilization system for *in vivo* genetic engineering: transposon mutagenesis in gram negative bacteria. Nat Biotechnol. 1983;1: 784–791.
91. Dubarry N, Du W, Lane D, Pasta F. Improved electrotransformation and decreased antibiotic resistance of the cystic fibrosis pathogen *Burkholderia cenocepacia* strain J2315. Appl Environ Microbiol. 2010;76: 1095–1102.
92. Choi K-H, Schweizer HP. mini-Tn7 insertion in bacteria with single *att*Tn7 sites: example *Pseudomonas aeruginosa*. Nat Protoc. 2006;1: 153–161.
93. Barrett AR, Kang Y, Inamasu KS, Son MS, Vukovich JM, Hoang TT. Genetic tools for allelic replacement in *Burkholderia* species. Appl Environ Microbiol. 2008;74: 4498–4508.
94. Wick RR, Judd LM, Gorrie CL, Holt KE. Unicycler: Resolving bacterial genome assemblies from short and long sequencing reads. PLoS Comput Biol. 2017;13: e1005595.
95. Gurevich A, Saveliev V, Vyahhi N, Tesler G. QUAST: quality assessment tool for genome assemblies. Bioinformatics. 2013;29: 1072–1075.
96. Seemann T. Prokka: rapid prokaryotic genome annotation. Bioinformatics. 2014;30: 2068–2069.
97. Bolger AM, Lohse M, Usadel B. Trimmomatic: a flexible trimmer for Illumina sequence data. Bioinformatics. 2014;30: 2114–2120.
98. Deatherage DE, Barrick JE. Identification of mutations in laboratory-evolved microbes from next-generation sequencing data using breseq. Methods Mol Biol. 2014;1151: 165–188.
99. Katoh K, Standley DM. MAFFT multiple sequence alignment software version 7: improvements in performance and usability. Mol Biol Evol. 2013;30: 772–780.
100. Katoh K, Misawa K, Kuma K, Miyata T. MAFFT: a novel method for rapid multiple sequence alignment based on fast Fourier transform. Nucleic Acids Res. 2002;30: 3059–3066.
101. Ronquist F, Teslenko M, van der Mark P, Ayres DL, Darling A, Höhna S, et al. MrBayes 3.2: efficient Bayesian phylogenetic inference and model choice across a large model space. Syst Biol. 2012;61: 539–542.
102. Reszka KJ, O'Malley Y, McCormick ML, Denning GM, Britigan BE. Oxidation of pyocyanin, a cytotoxic product from *Pseudomonas aeruginosa*, by microperoxidase 11 and hydrogen peroxide. Free Radic Biol Med. 2004;36: 1448–1459.
103. Tjaden B. De novo assembly of bacterial transcriptomes from RNA-seq data. Genome Biol. 2015;16: 1.
104. Powell DR. Degust: interactive RNA-seq analysis. Zenodo. 2015.
105. Babin BM, Bergkessel M, Sweredoski MJ, Moradian A, Hess S, Newman DK, et al. SutA is a bacterial transcription factor expressed during slow growth in *Pseudomonas aeruginosa*. Proc Natl Acad Sci USA. 2016;113: E597-605.

106. Schnetterle M, Gorgé O, Nolent F, Boughammoura A, Sarilar V, Vigier C, et al. Genomic and RT-qPCR analysis of trimethoprim-sulfamethoxazole and meropenem resistance in *Burkholderia pseudomallei* clinical isolates. PLoS Negl Trop Dis. 2021;15: e0008913.
107. EUCAST EC for AST. Determination of minimum inhibitory concentrations (MICs) of antibacterial agents by broth dilution. Clin Microbiol Infect. 2003;9: ix–xv.
108. McKinney W. Data structures for statistical computing in python. Proceedings of the 9th Python in Science Conference. SciPy; 2010. pp. 56–61.
109. The pandas development team. pandas-dev/pandas: Pandas 1.0.3. Zenodo. 2020;
110. Harris CR, Millman KJ, van der Walt SJ, Gommers R, Virtanen P, Cournapeau D, et al. Array programming with NumPy. Nature. 2020;585: 357–362.
111. Hunter JD. Matplotlib: A 2D Graphics Environment. Comput Sci Eng. 2007;9: 90–95.
112. Waskom M. seaborn: statistical data visualization. JOSS. 2021;6: 3021.

Supplementary information

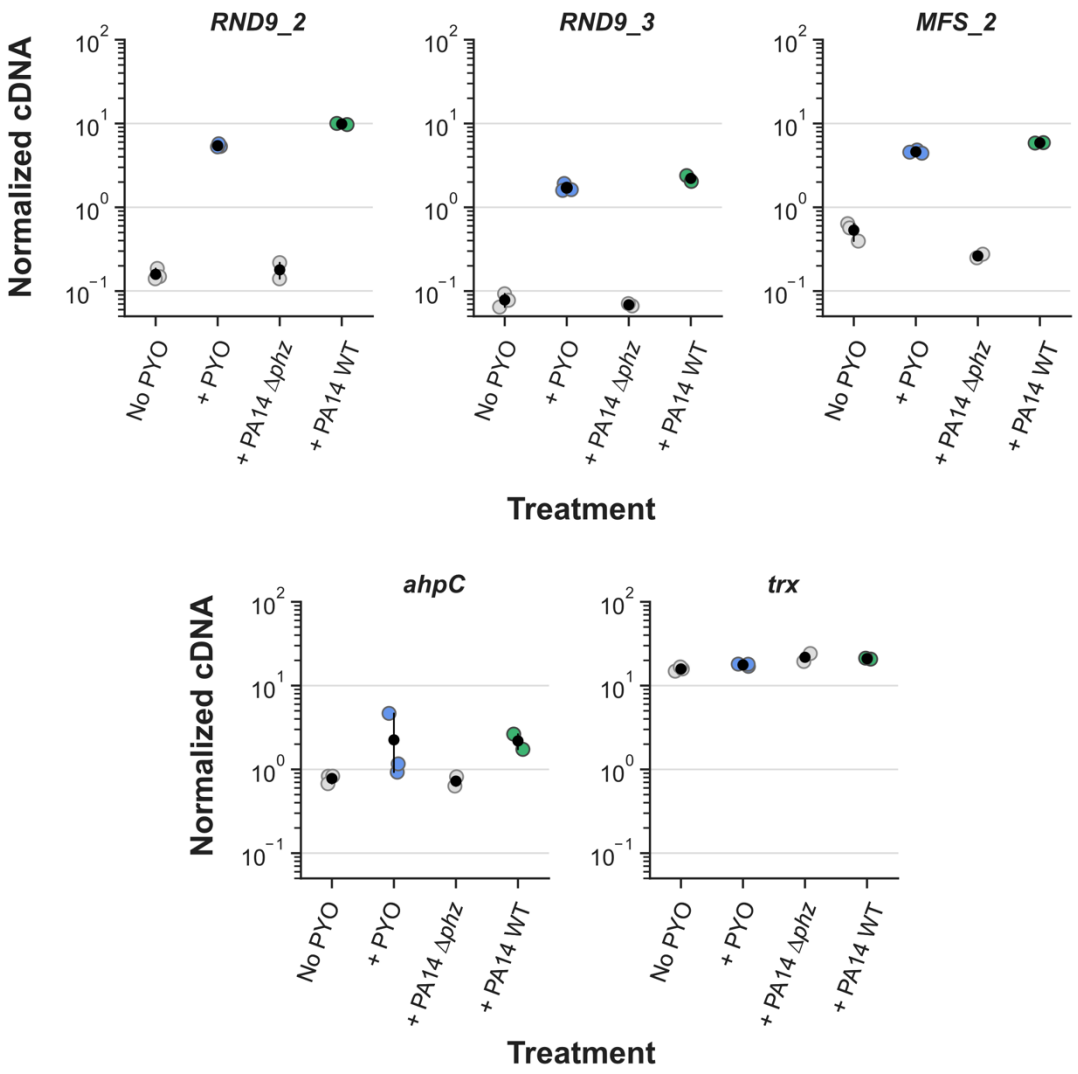

Figure S1. Results for qRT-PCR experiment 1 (normalized cDNA levels). Data for each gene show in Fig. 1C-D, displayed as normalized cDNA for comparison. Normalizations were done by the housekeeping gene *uvrC* (see Materials and Methods). Data for genes RND9_2 and RND9_3 (only for *B. multivorans* treatments with and without PYO) is also shown in Fig. 2B and Fig. S2, respectively, for comparison with other *B. multivorans* strains. Black dots mark the means and error bars represent 95% confidence intervals.

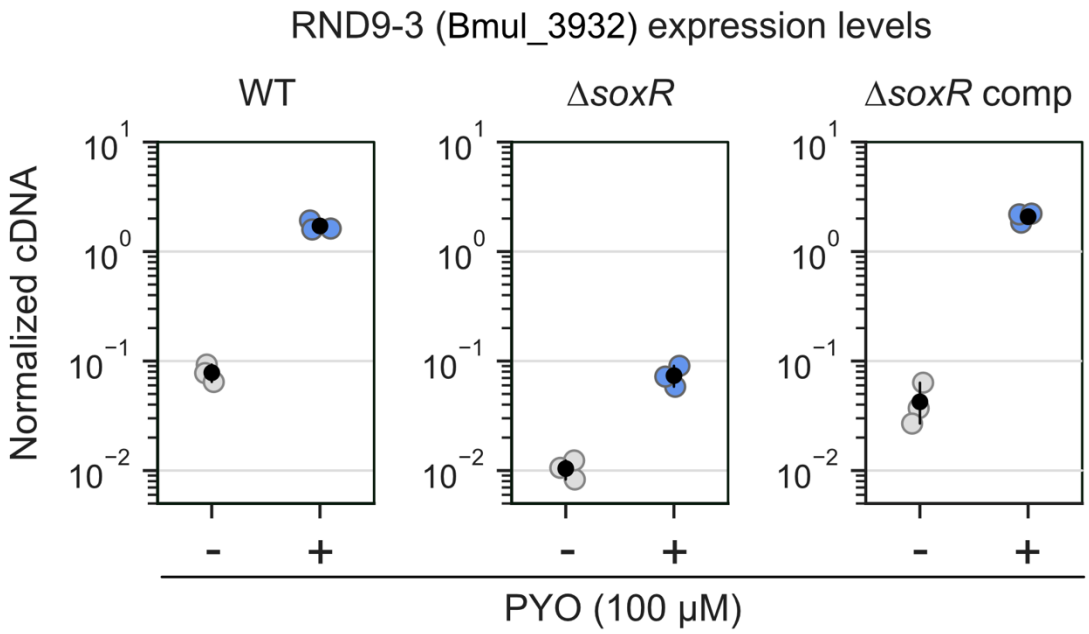

Figure S2. Expression levels of the third gene in the RND-9 operon (Bmul_3932) in the presence or absence of PYO. Values measured by qRT-PCR in different *B. multivorans* strains (n = 3). Δ*soxR* comp means complementation of Δ*soxR*. Data is shown as normalized cDNA. Normalizations were done by the housekeeping gene *uvrC* (see Materials and Methods). Data for the *B. multivoran*s WT strain is the same as in the experiment displayed in Fig. S1, but is shown here for comparison. Black dots mark the means and error bars represent 95% confidence intervals.

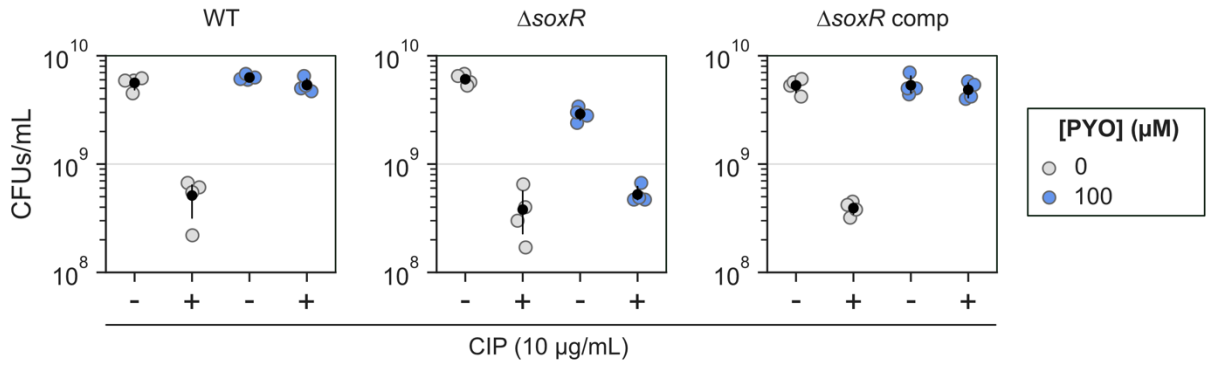

Figure S3. Raw colony forming unit (CFU) numbers during ciprofloxacin (CIP) tolerance experiments with WT, Δ*soxR* and Δ*soxR* comp strains. In these experiments, the No CIP controls ("-") were used as the baseline for calculation of survival rates displayed in Fig. 2C (n = 4). Notice that the Δ*soxR* strain was more sensitive to PYO than the other strains, visible by its lower CFUs in the "No CIP control + PYO." This resulted in the apparent PYO-mediated slight increase in tolerance for this strain shown for this strain in Fig. 2C. However, comparisons of the raw CFUs after treatment with CIP ("+") show that PYO did not have a meaningful effect on the CIP tolerance of this strain. Black dots mark the means and error bars represent 95% confidence intervals.

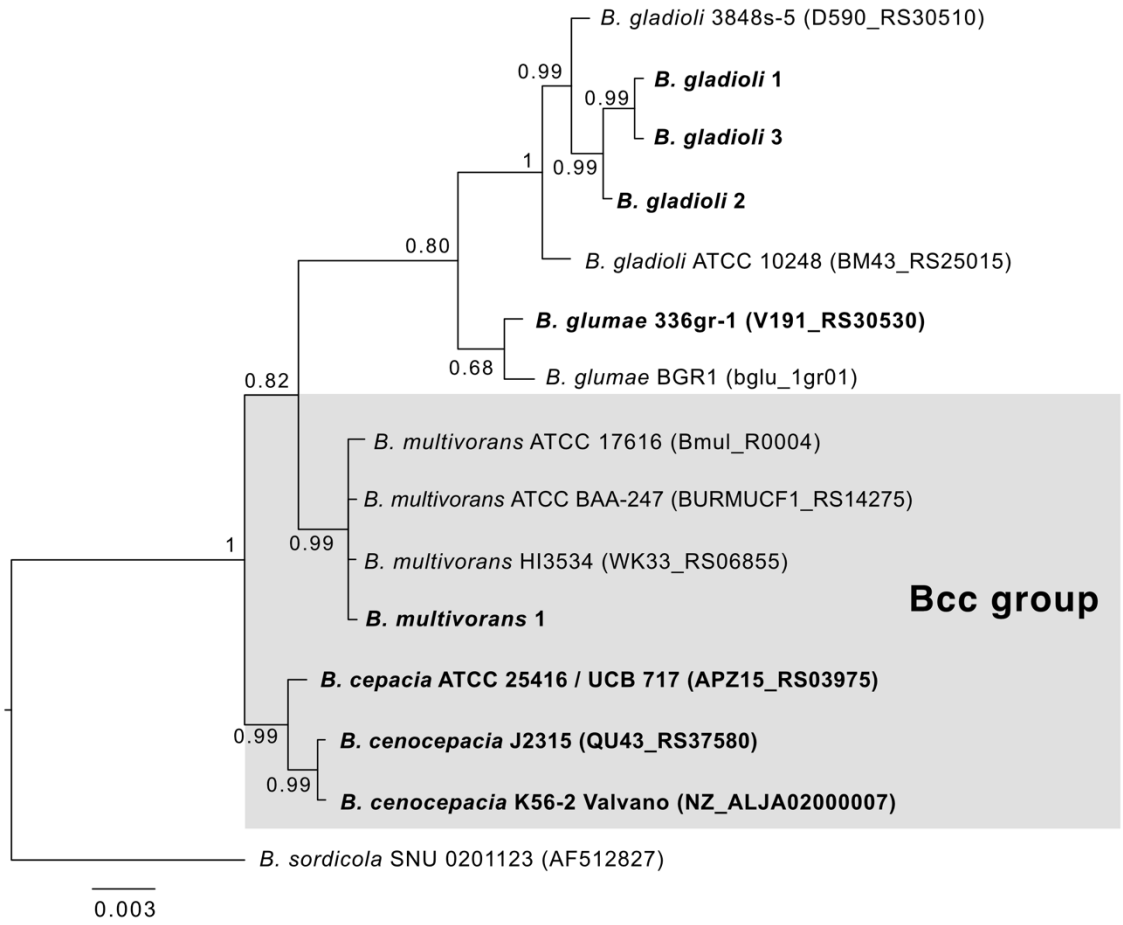

Figure S4. Full phylogenetic tree of *Burkholderia* species used in the study. Phylogeny is based on 16S rRNA sequences. Strains highlighted in bold were used in experiments throughout the study, and gray shading highlights species within the Bcc group. Posterior probabilities of Bayesian analysis are shown in the nodes. For sequences retrieved from the BGD database, the respective locus tag is given in parenthesis. *B. sordicula*, a *Burkholderia* species from the "*B. gathei* group" [42], was used as an outgroup (for this sequence, the number in parenthesis corresponds to its GenBank accession number). The alignment used during the phylogenetic analysis is available as supplementary material.

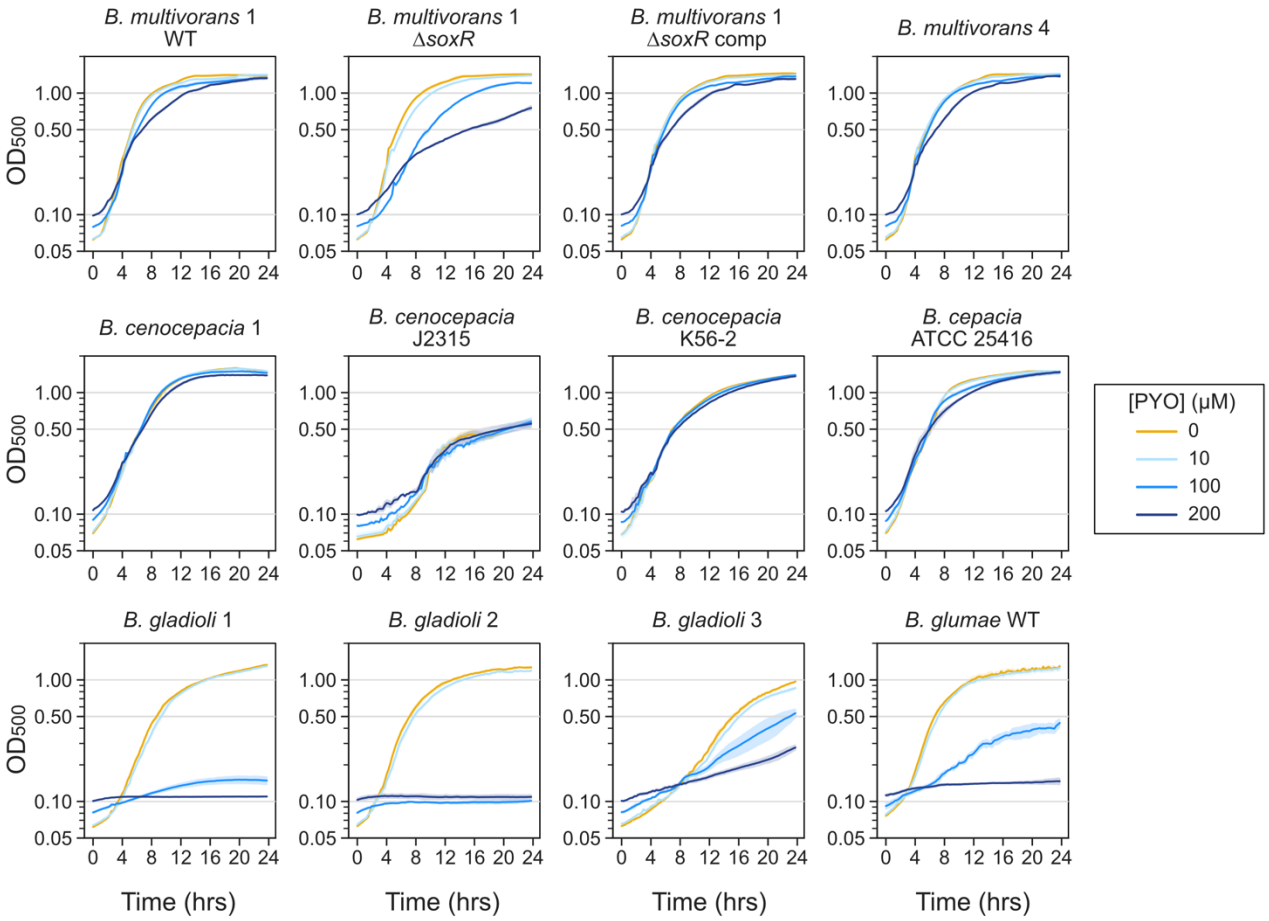

Figure S5. Growth curves for different *Burkholderia* species (all strains studied are included) under different concentrations of PYO. Notice accentuated growth defects for *B. gladioli*, *B. glumae* and *B. multivorans* 1 Δ*soxR* under high concentrations of PYO (100 μM or higher). Plotted lines represent means of three replicates, and shaded areas represent the standard deviations. This dataset was used to calculate the growth rates used in Fig. 2E.

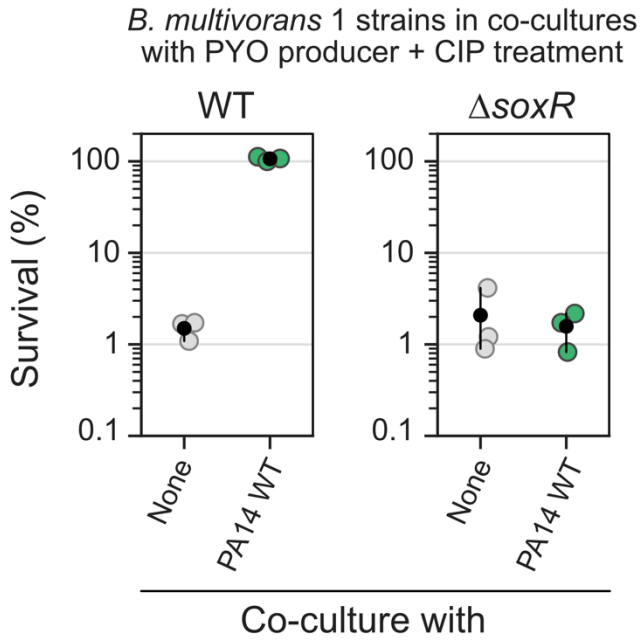

Figure S6. Tolerance of *B. multivorans* WT and Δ*soxR* when alone or in co-cultures with *P. aeruginosa*. PA14 = *P. aeruginosa* PA14 (PYO producer). PYO produced by *P. aeruginosa* induced tolerance to CIP (10 µg/mL) in *B. multivorans* 1 WT, but not in *B. multivorans* 1 Δ*soxR* (n = 3). Black dots mark the means and error bars represent 95% confidence intervals.

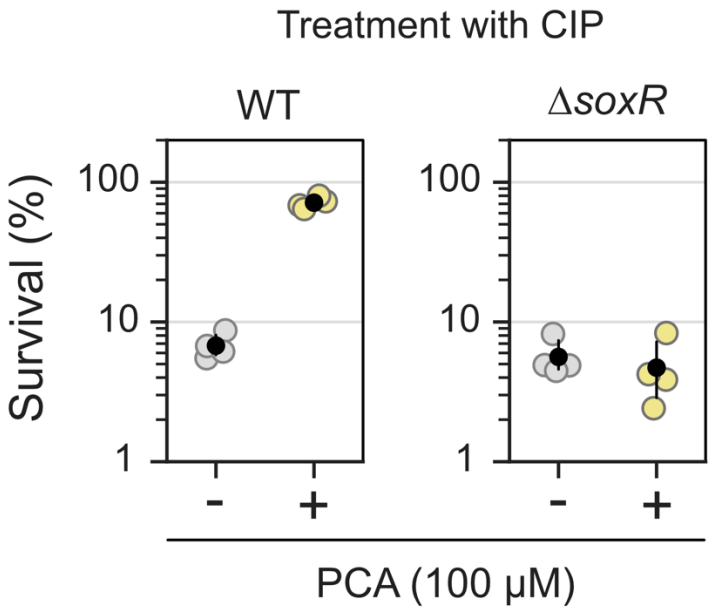

Figure S7. Effect of phenazine-1-carboxylic acid (PCA) on tolerance in *B. multivorans* 1. Results for WT and Δ*soxR* strains are shown (n = 4) after exposure to ciprofloxacin (CIP, 10 µg/mL). Black dots mark the means and error bars represent 95% confidence intervals.

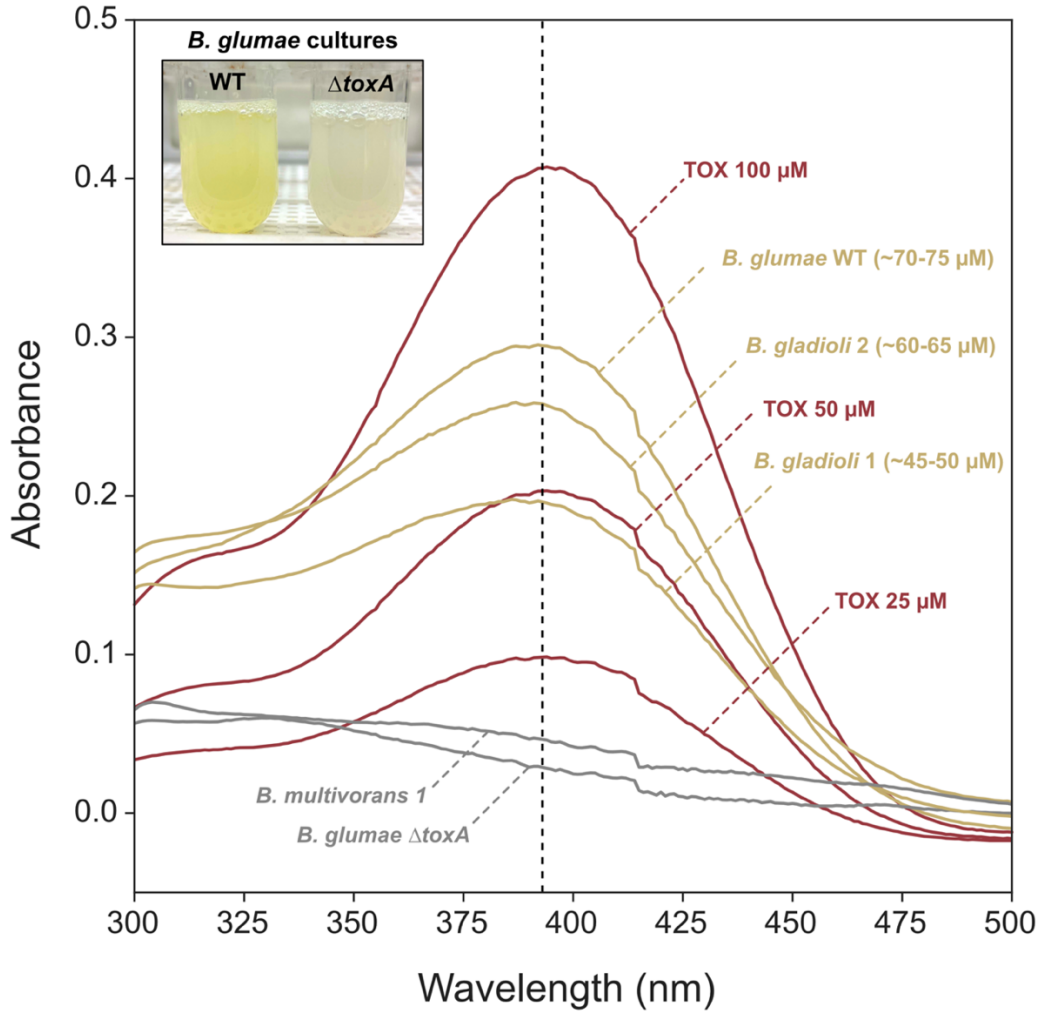

Figure S8. Toxoflavin (TOX) production by the *B. glumae* and *B. gladioli* species studied. Absorbance spectra for wavelengths between 300-500 nm are shown for culture supernatants of *Burkholderia* strains together with different standard concentrations of pure TOX. Absorbance at 393 nm (dashed line) is commonly used for TOX quantification [47,54]. Concentrations for cultures are estimations based on standards using the pure molecule. *B. glumae* WT is a validated TOX producer, and the *B. glumae* Δ*toxA* strain cannot make the metabolite [55]. Tube pictures on the top left show yellow pigmentation produced by the *B. glumae* WT strain culture in comparison to the Δ*toxA*. Cultures shown in the picture were not the same used during UV-Vis spectra collection. Picture saturation was increased for better visualization of the yellow pigmentation in the tubes.

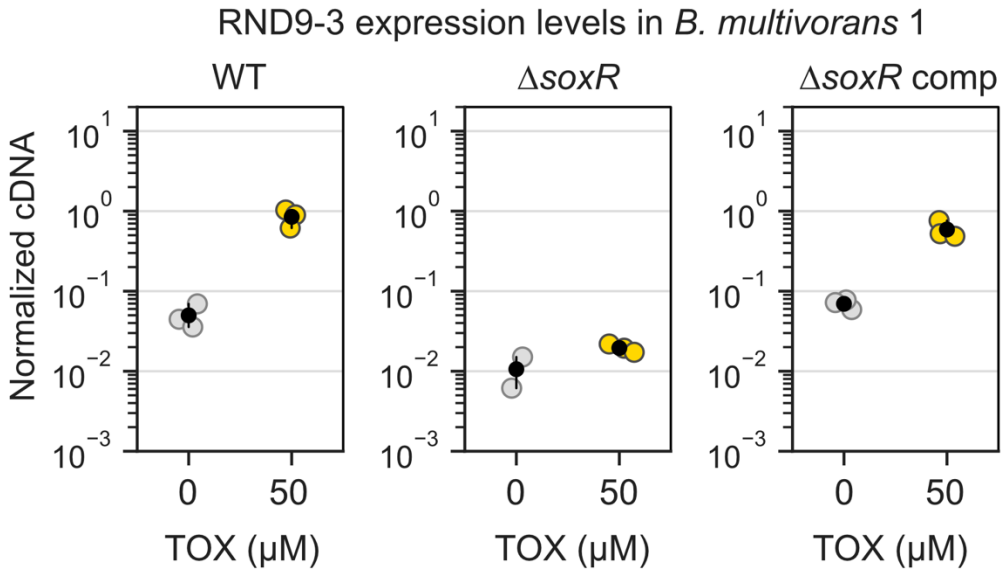

Figure S9. Expression levels of the third gene in the RND-9 operon (Bmul_3932) in the presence or absence of TOX. Values measured by qRT-PCR in different *B. multivorans* strains (n = 3 for all except "Δ*soxR* + 0 μM TOX," where n = 2). Δ*soxR* comp means complementation of Δ*soxR*. Data is shown as normalized cDNA. Normalizations were done by the housekeeping gene *uvrC* (see Materials and Methods). Black dots mark the means and error bars represent 95% confidence intervals.

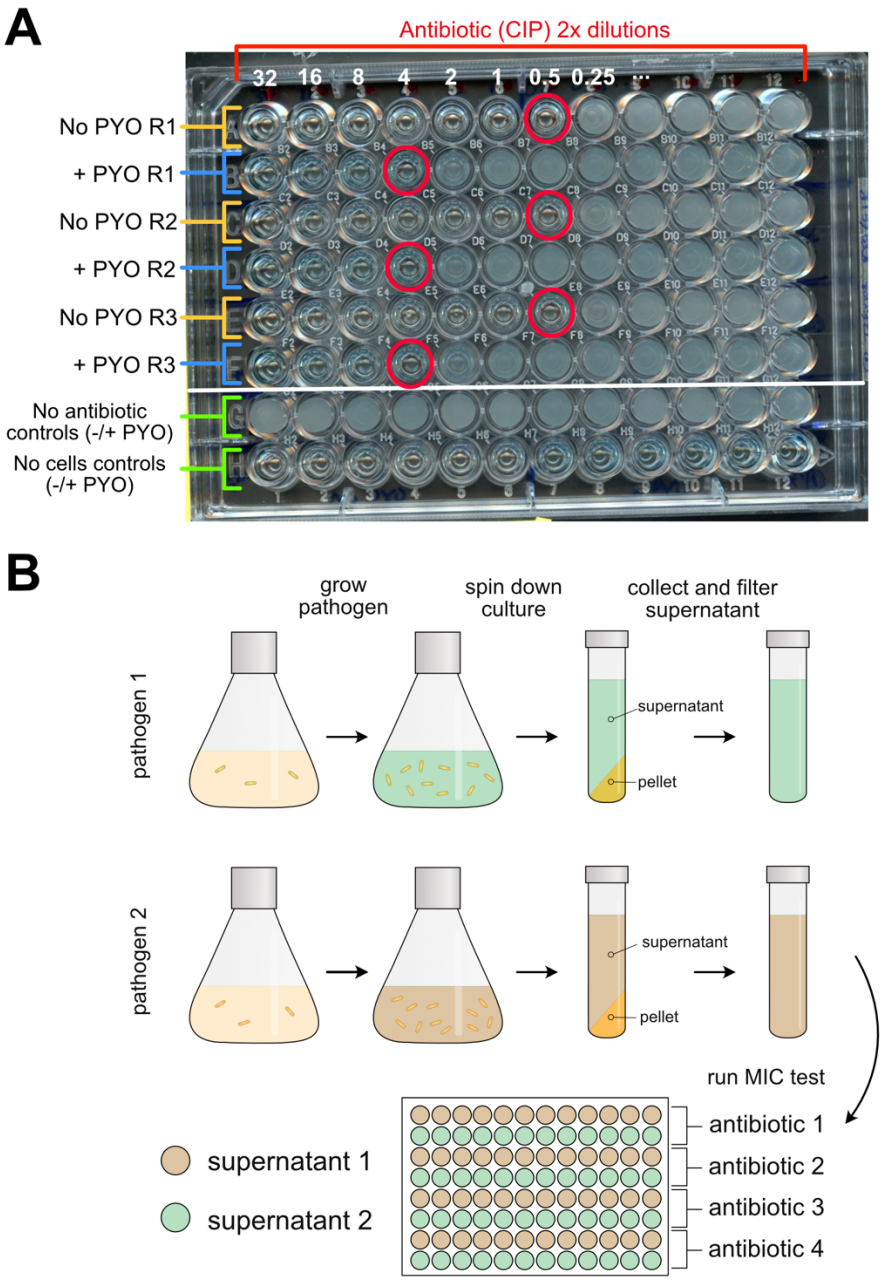

Figure S10. Additional information on experimental design during MIC assays. A. Example of experimental plate testing the effect of PYO on *B. multivorans* 1 WT resistance to MIC ciprofloxacin (CIP). Three replicates were prepared (R1-R3), with and without PYO added to the fresh medium. Cells always grew in the "no antibiotic" controls, independently of the presence of PYO (or other secondary metabolite tested). No growth was observed in the "no cells" controls. Red circles marks MICs detected based on analysis as described in the Materials and Methods. **B.** Cartoon describing the protocol for MIC experiments using spent media. Spent media were four-fold diluted into fresh media before the experiments (see Materials and Methods).

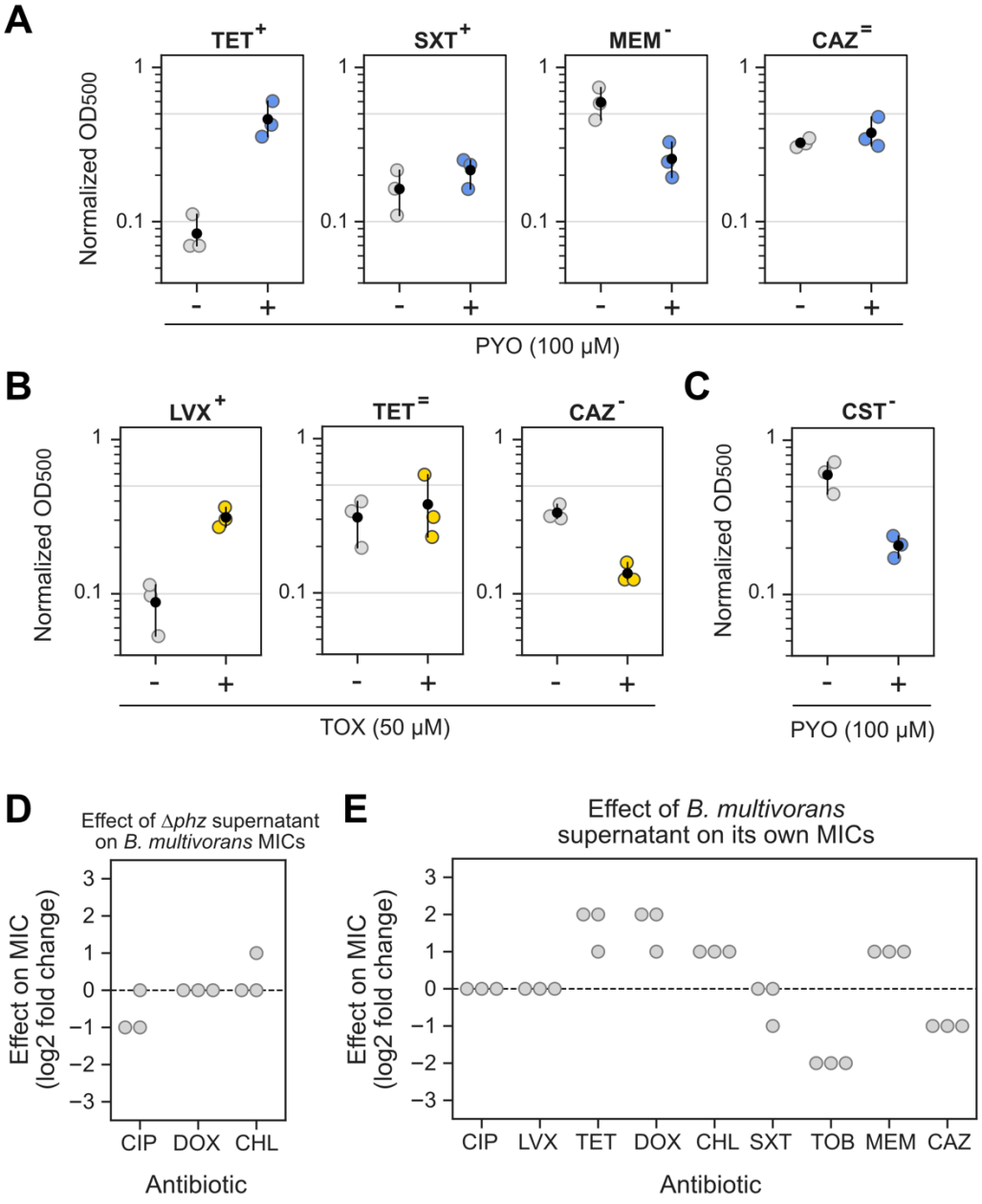

Figure S11. Additional MIC results. A-B. Normalized absorbance measurements (OD_{500}) used for the calculation of the fold changes on growth density caused by addition of PYO (A) or TOX (B) displayed in Figs. 4D. **C.** Effects of PYO on growth in the presence of colistin (CST, 4,096 µg/mL, a concentration still not enough to completely inhibit growth under these conditions). **D.** Effects of *P. aeruginosa* Δ*phz* supernatant (i.e. no PYO present) on *B. multivorans* 1 MICs for three antibiotics where PYO had increased MICs (for each antibiotic, n = 3). **E.** Effects of *B. multivorans* 1 supernatant on its own MICs (for each antibiotic, n = 3). In panels A-C, the black dots mark the means and error bars represent 95% confidence intervals.
CIP, ciprofloxacin; LVX, levofloxacin; TET, tetracycline, DOX, doxycycline, CHL, chloramphenicol, SXT, sulfamethoxazole/trimethoprim; TOB, tobramycin; MEM, meropenem; CAZ, ceftazidime; CST, colistin.

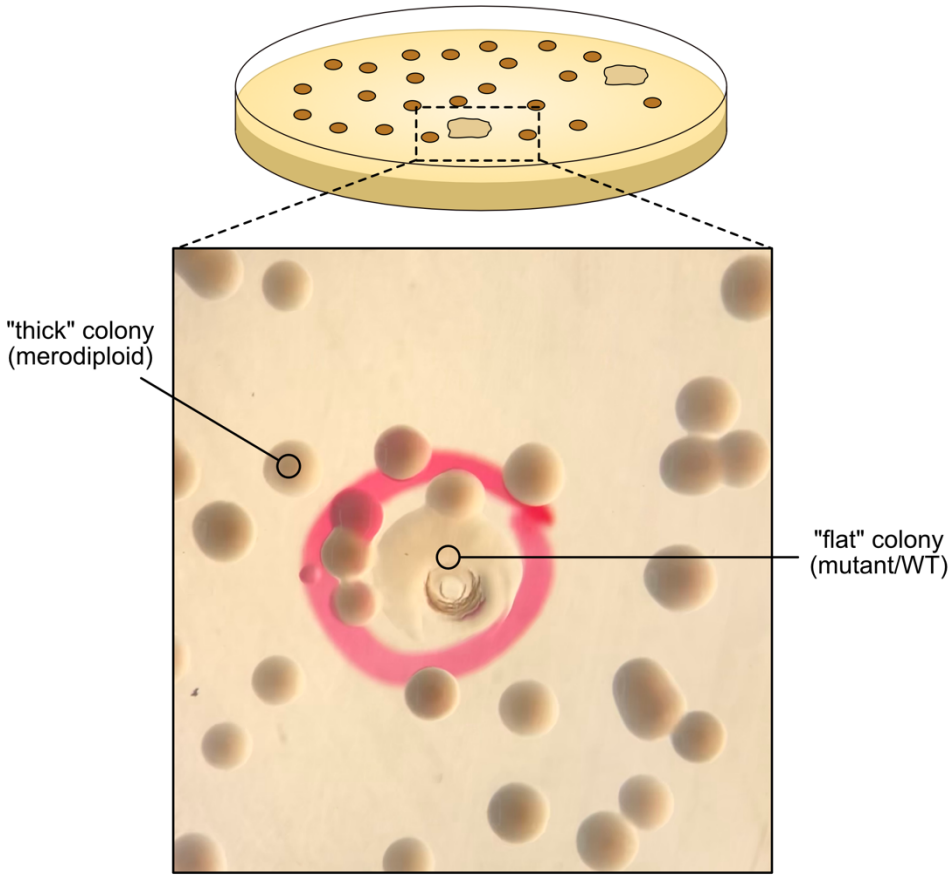

Figure S12. Colony screen in *B. multivorans* 1 during strains construction. The desired "flat" colonies were rare (the picture in the bottom part shows one that had been picked for later analysis). These "flat" colonies had lost the construct originally inserted during homologous recombination and had either the mutant or WT genotype, screened by PCR. Abundant "thick" colonies were merodiploids still containing the construct with tetracycline resistance marker integrated in the genome. While we do not know why merodiploids present as round, but "cured" strains present as flat, this phenotype is convenient for mutant identification. This screen was done using LB plates (no NaCl) containing only 1.05% agar (see Material and Methods).

Table S1. Strains, plasmids, and primers used in this study.

Table S2. Full results of the RNA-seq experiment. See information within each tab for distinct comparisons between treatments. A tab is also included with the information about the loci tags and gene names used in Fig. 1.

Table S3. BLASTP results for the protein sequence of Bmul_3929 (SoxR) from *B. multivorans* 1 against *Pseudomonas aeruginosa* PA14 and PAO1 database of protein sequences.

Table S4. MIC values measured in *B. multivorans* 1 for all the antibiotics and conditions tested in the study.

Note about tables: Due to their size/format, supplementary tables mentioned in this chapter were not included in this document. These tables are linked to this thesis and available through CaltechTHESIS.

Chapter 6

CONCLUSIONS

Summary

In this thesis, I have explored the multifaceted and nuanced effects that redox-active secondary metabolites produced by bacteria can have on the physiology of these organisms, with a particular focus on the role of these molecules as modulators of susceptibility to antibiotics. The consequences of exposure to these metabolites are complex, which often leads to different (apparently contradictory) conclusions based on the specific conditions studied. One of the main messages from this thesis is that *the conditions matter*, and understanding the nuances posed by the particular conditions studied is essential for interpreting how the results fit into a broader and more relevant biological context. As discussed in Chapter 3, the production of redox-active metabolites can have profoundly distinct physiological effects on the producers and other organisms exposed to them within the microbial community, ranging from "beneficial" (i.e., support of biofilm development, nutrient acquisition, competitive advantage) to "detrimental" (i.e., self-poisoning). Moreover, their effects on the susceptibility to clinical antibiotics are also complex and depend on the specific drug and conditions studied. Although apparently contradictory, these distinct outcomes make complete sense within the dynamic biological context that these molecules exist. The beauty of these molecules is in the complexity of their effects. Microbial populations are heterogeneous, and redox-active metabolites will affect distinct groups of cells in different ways. Understanding such effects at the molecular level is critical for accurate predictions of how these molecules act in contexts relevant for humans, from agriculture to health.

Within the human health context, Chapters 2, 4, and 5 explore the consequences of redox-active secondary metabolites on opportunistic pathogen's susceptibility to clinical antibiotics. Metabolites such as pyocyanin (PYO) and toxoflavin (TOX), made by *Pseudomonas aeruginosa* and *Burkholderia gladioli*, can modulate resilience levels to commonly used drugs. Specifically, the production of PYO by *P. aeruginosa* not only increases the organism's tolerance and resistance to fluoroquinolones, but also affects how susceptible other microbes found in the vicinity are to these drugs. For instance, PYO production by *P. aeruginosa* dramatically increases

fluoroquinolone resilience in species within the *Burkholderia cepacia* complex (Bcc) group. Similar effects happen when Bcc is exposed to TOX, another metabolite that antagonizes fluoroquinolone efficacy. In both cases, the mechanism mainly involves the induction of redox-regulated efflux systems. These transport systems, which likely evolved as a mechanism to avoid toxicity by metabolites such as PYO and TOX, can also transport certain drugs (e.g., fluoroquinolones), making treatment less effective. This brings another main message from this thesis: *understanding the defenses evolved by opportunistic pathogens to handle the toxicity of their "natural antibiotics" could help us manage antibiotic resistance in the clinic*. PYO and TOX are just two examples of molecules made by opportunistic pathogens in natural environments, such as the soil, that display toxicity to their producers and to microbes found in their vicinity. The soil is also the source of many of the clinical antibiotics used to treat infections, and some of these drugs share structural similarities to microbial metabolites such as PYO and TOX. Perhaps not surprisingly, these are the drugs against which the defenses induced by the redox-active metabolites seem to provide more effective protection. Yet, the implications of this phenomenon for drug efficacy and the evolution of resistance in the clinic remains mainly overlooked. My work suggests that redox-active metabolites and other yet-to-discover natural antibiotics made by pathogens might affect treatment efficacy during infections. A better understanding of the generality of this phenomenon could ultimately lead to more effective treatment strategies.

Future directions

- *Searching for other secondary metabolites with implications for antibiotic susceptibility*. We have reasons to believe that the examples studied here (PYO and TOX) are only the tip of the iceberg. Because most secondary metabolites are still uncharacterized, it would not be surprising to discover that other metabolites made by pathogens during infections could have consequences for their susceptibility levels against antibiotics. Notably, one might leverage recent tools developed by the gut microbiome research field when searching for new candidate molecules. As discussed at the end of Chapter 5, we believe there is an enormous potential for applying these approaches in the context of infectious disease. For example, metabolomics coupled with high-throughput methods for phenotypic characterization of microbial community's susceptibility profile could unravel relevant candidate metabolites. In combination with careful profiling of species/strains that are

clinically relevant (see below), these tools could be used to identify and develop synthetic communities that better capture polymicrobial infections found in patients. These synthetic communities could then be used as a model system to study the effect of interspecies interactions on drug efficacy at the molecular level.

- *Investigating the relevance of redox-active metabolite-mediated antibiotic resilience* in vivo. A critical limitation of the work I present here is that all the results are from assays *in vitro*. Although these are essential when studying complex molecular mechanisms, a natural next step is to investigate if metabolites such as PYO and TOX modulate resilience to clinical antibiotics *in vivo*. One option is to use animal models, such as mice, for this purpose. In addition, as mentioned above, the results presented throughout Chapters 4 and 5 point towards an immediate need for a better characterization of the community dynamics during the development of infections within individual patients. A relevant example in this scenario is chronic lung infections. Some unanswered questions are: what pathogens commonly co-occur within individual patients, and what is the prevalence of such co-infections among patients? Also, how are these pathogens spatially distributed within the infected tissue? As a specific example within this thesis context, we can ask: which species are more commonly found with *P. aeruginosa* and *B. gladioli* within infections? How often metabolites such as PYO/TOX are produced, and which species (based on spatial distribution) are affected by them *in vivo*? These same questions would be appropriate for any infection context where the goal is to investigate how metabolites might alter antibiotic susceptibility. Answering these questions would require extensive collaboration with clinicians and close monitoring of the infection development in patients. Constant isolations (or monitoring through sequencing) of relevant strains from different species within these communities combined with high-resolution tissue imaging would provide important colonization dynamics that would be foundational for our understanding of *in vivo* polymicrobial communities. Such information could later be leveraged in experiments using animal models.

- *Optimizing antimicrobial susceptibility testing (AST)*. Chapter 1 provides ideas for using recent evidence of secondary metabolite-mediated modulation of antibiotic susceptibility to optimize AST in the clinic. Chapter 5 includes a proof-of-principle for some of these

ideas, using PYO and TOX as examples. However, this is only an initial step towards optimizing such tests to better account for the complexity found during infections. Future work should develop high throughput AST that incorporates secondary metabolites into the protocol. Such an approach would be directly applicable to the characterization of infection dynamics proposed above.

- *Investigating the broader role of SoxR in pathogens*. Results from Chapters 4 and 5 indicate that SoxR may play a relevant clinical role in additional opportunistic pathogens. Through redox sensing, this transcription factor regulates efflux both in *P. aeruginosa* and in Bcc. Surprisingly, efflux-mediated increase in antibiotic resilience is remarkably higher in Bcc than in *P. aeruginosa*. As discussed in Chapter 5, several other pathogens have a *soxR* homolog in their genome, but the defenses controlled by these homologs and their consequences for antibiotic resilience are uncharacterized. Moreover, there also seems to be significant differences in the specificity of the redox sensor. For example, in *P. aeruginosa*, SoxR is thought to only be activated by methylated phenazines such as PYO or 5-methylphenazine-1-carboxylate (5-Me-PCA). Non-methylated phenazines such as phenazine-1-carboxylic acid (PCA) do not oxidize the sensor. However, in Bcc, SoxR seems to be more promiscuous and susceptible to oxidation by a broader range of molecules. These differences are probably due to dissimilarities in the protein structure, affecting reactivity with molecules from different redox potentials. This observation raises an interesting hypothesis: is the specificity or generality of SoxR linked to its biological role? For example, Bcc does not seem to make metabolites that activate SoxR (at least under the studied conditions), but its SoxR is reactive to a broader range of molecules. In contrast, SoxR in *P. aeruginosa* seems to be more specialized to respond to specific toxins that this bacterium makes (PYO and 5-Me-PCA are the more toxic phenazines made by this organism). Does the transcription factor work as a broader stress response in organisms that cannot make redox-active metabolites themselves, but specialize in controlling the defenses against specific molecules in redox-active metabolites producers? This is purely speculation at this point, but I believe there is a lot to learn on how SoxR (and the efflux systems it controls) works in a wider range of organisms. Focus on pathogens could unravel new mechanisms affecting susceptibility and the evolution of resistance to clinical drugs.

- *Using toxoflavin (TOX) as a complementary model to study the physiological effects of redox-active metabolites.* A significant part of the work done in the Newman Lab involves using phenazines, such as PYO, as models for redox-active metabolites and their consequences for their producers. Phenazines have been model systems for the study of, for example, energy conservation, extracellular electron shuttling, and their implications for biofilm development. However, we still lack complementary model systems to assess the generality of the effects caused by this class of molecules. I believe TOX could be an ideal molecule for such case because: (i) there is significant work done on its biological effects for one of its producers, the plant pathogen *Burkholderia glumae*; (ii) the producer is genetically tractable and easy to grow in the lab; (iii) the pure molecule is commercially available and could also be chemically synthesized in the lab. Future work should test to which extent the physiological effects found for phenazines apply to TOX. Examples of questions that could be explored are: can TOX promote energy conservation under anoxic conditions as phenazines do? Is the production of TOX also a "double-edged sword," with the molecule causing self-poisoning and extracellular DNA release during biofilm formation? Can TOX sustain metabolism within anaerobic regions of biofilms? Answering these and other related questions will help us draw a complete picture of the role of this class of molecules in bacterial physiology.